JURNAL ECOTIPE

ISSN 2355-5058
e-ISSN 2622-4852

Electronic, Control, Telecommunication, Information, and Power Engineering

https://ecotipe.ubb.ac.id/

Volume 13, Issue 1, April 2026

Electrical Engineering Department
Bangka Belitung University

JURNAL ECOTIPE
Electronic, Control, Telecommunication, Information, and Power Engineering

ISSN 2355-5068
e-ISSN 2622-4852

Volume 13, Issue 1, April 2026
DOI : 10.33019/jurnalecotipe.v13i1

Editorial Board

Preface

Jurnal Ecotipe (Electronics, Control, Telecommunication, Information, and Power Engineering), published by the Department of Electrical Engineering at Bangka Belitung University, is accredited by the Ministry of Higher Education, Science, and Technology of the Republic of Indonesia—covering the period from Volume 12, Number 1 (April 2025) through Volume 16, Number 2 (April 2029)—based on Decree No. 295/C/C3/KPT/2026, attaining a Rank of 2 (SINTA 2). Hopefully, in the future, Jurnal Ecotipe can improve the quality and quantity of publishing quality scientific articles and improve its accreditation ranking

Currently, Jurnal Ecotipe volume 13, issue 1, April 2026, has been published. In this edition, the journal articles are entirely in English and consist of 15 articles by authors from outside the institution, numbered from pages 1-160. Hopefully, in the future, articles included in the journal's next edition will come from outside academia, both domestically and internationally.

Our highest appreciation goes to the Reviewers, Editorial Board, Authors, and all parties involved in the preparation and publication of the Jurnal Ecotipe volume 13 issue 1 April 2026. Hopefully, this journal can provide benefits and add scientific insight into the field of Electrical Engineering in particular and engineering in general. Therefore, we still hope for suggestions and constructive criticism for improvements and improvements for the progress of this journal.

Editor-in-Chief

Indexed journal on:

Publisher Address:
Electrical Engineering Department
Faculty of Science and Engineering - Bangka Belitung University
Balunijuk, Bangka Regency, Bangka Belitung Islands Province, Indonesia
Phone (0717) 4260033 ext. 2125, 2128
Website : https://journal.ubb.ac.id/index.php/ecotipe
E-mail : jurnal.ecotipe@yahoo.com / jurnalecotipe@ubb.ac.id

JURNAL ECOTIPE
Electronic, Control, Telecommunication, Information, and Power Engineering
ISSN 2355-5068
e-ISSN 2622-4852
Volume 13, Issue 1, April 2026
DOI : 10.33019/jurnalecotipe.v13i1

Table of Content

JURNAL ECOTIPE
Electronic, Control, Telecommunication, Information, and Power Engineering

Volume 13, Issue 1, April 2026, pp. 1-9
ISSN 2355-5068 ; e-ISSN 2622-4852
DOI: 10.33019/jurnalecotipe.v13i1.4565

Design of Sepic Converter as Battery Charger with Artificial Neural Network - PID Method for Load Variation

R. Nur Alfian Pribadi[1], Endro Wahjono[2], Suryono[3]
[1,2,3] Politeknik Elektronika Negeri Surabaya, Jl. Raya ITS, Surabaya, 60111

ARTICLE INFO

Article historys:

Received : 16/07/2025
Revised : 21/09/2025
Accepted : 30/04/2026

Keywords:

Artificial Neural Network; Battery Adaptive Charge; PID; Sepic Converter

ABSTRACT

More adaptable charging methods are required as a result of the growing variety of electronic gadgets that use rechargeable batteries brought about by technological advancements. When trying to charge different battery types with a same charger, differences in battery parameters, like voltage and capacity, present difficulties. This study suggests an adaptive charging system that can charge several battery types using a single port connection in order to solve this problem. To transform a 24 V DC input into an output voltage appropriate for the particular battery requirements, the system uses a SEPIC converter whose duty cycle is controlled by a microprocessor. The duty cycle rises until a specific current level is measured when a battery is attached and the limit switch is activated. The measured voltage and current data are then processed by an Artificial Neural Network (ANN) algorithm to determine the battery type and set the appropriate charging voltage setpoint. After that, a PID controller is used to keep the charging conditions steady. LiFePO4 (12.8 V, setpoint 14.6 V), Li-ion (14.8 V, setpoint 16.8 V), and Lead Acid (12 V, setpoint 14.4 V) batteries were used to test the system. The system successfully charged all three battery types with an average error of 0.174%, according to experimental findings, demonstrating precise and reliable control performance.

Corresponding Author:

R. Nur Alfian Pribadi
Politeknik Elektronika Negeri Surabaya, 60111, Surabaya
Email: alfianprbd02@pe.student.pens.ac.id

1. INTRODUCTION

Battery Battery charging is the process of charging a battery until it reaches the voltage specified in the battery's datasheet. Generally, the battery charging process requires an external power source, but in this study, a 24 VDC power supply was used [1].

The increasingly diverse technology of rechargeable electronic devices requires flexible charging systems. Batteries used in electronic devices have limited storage capacity; therefore, if their capacity decreases, they must be recharged immediately for the device to operate properly. Typically, each battery has a dedicated charger tailored to its characteristics and specifications. However, a problem arises when a single charger must be used for multiple devices with different battery specifications. This can pose a risk of overcharging, potentially affecting battery lifespan [5].

Given these issues, a flexible battery charging system that can operate at various battery voltages is needed [6]. Because conventional battery charging systems are designed for a single type of battery, they usually do not detect the type of battery being charged. Therefore, this adaptive battery charging

Volume 13, Issue 1, April 2026, pp. 1-9
ISSN 2355-5068 ; e-ISSN 2622-4852
DOI: 10.33019/jurnalecotipe.v13i1.4565

system uses an Artificial Neural Network (ANN) technique to determine the battery type and PID (Proportional-Integral-Derivative) control to perform the charging process [4].

The first steps in this adaptive charging system are battery type identification, charging setpoint voltage determination, and charging process stabilization. In this study, the input voltage from a 24 V DC power source was converted to an output voltage that satisfies the requirements of the battery using a SEPIC Converter (Single-Ended Primary Inductor Converter) acting as a DC-DC converter. Because it can adjust the voltage as needed, the SEPIC Converter has an advantage over buck or boost converters [7].

Constant Voltage (CV) is the charging technique that is employed because of its straightforward circuitry and controllability [8]. The charging voltage can be stabilized in accordance with the setpoint voltage established by the ANN through the use of PID control with a feedback mechanism [9] to maintain a consistent output voltage.

2. RESEARCH METHOD

A sepic converter with an artificial neural network and proportional, integral, and derivative control makes up this research system, which can charge a variety of battery types with a single converter output. In this study, three distinct battery types with differing capacities and voltages were used: LifePO4, Li-ion, and lead acid batteries. Below is a block schematic of the system as it appears in **Figure 1**. Several charging voltage levels are available in this adaptive charging system, depending on the load requirements as determined by sensor inputs.

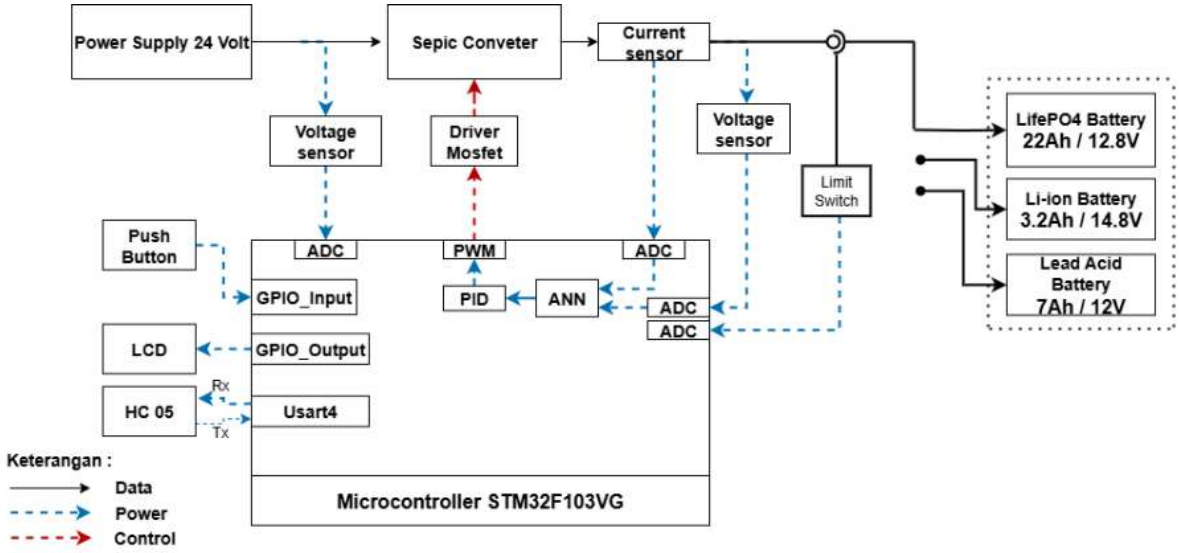

Figure 1. Block diagram system

According to **Figure 1**, the system operates using a 24 V DC source, which delivers power to the SEPIC converter before being directed to the battery load. During the charging process of a LiFePO4 battery, the voltage and current values are monitored through sensor measurements. The Artificial Neural Network (ANN) then identifies the battery type and provides the appropriate setpoint. Subsequently, the PID controller adjusts the duty cycle through the switching driver to regulate the converter operation, ensuring the output voltage matches the required charging setpoint.

2.1. Design of Sepic Converter

The evolution of the buck-boost topology led to the creation of the SEPIC (Single-Ended Primary Inductor Converter) kind of DC-DC converter. The output voltage can be greater or lower than the input voltage by using this converter to step up or step down the voltage. Because SEPIC keeps the output voltage polarity positive, unlike traditional buck-boost, it is safer and more adaptable for usage in a variety of applications, including power supplies with variable voltage sources and battery charging

JURNAL ECOTIPE
Electronic, Control, Telecommunication, Information, and Power Engineering
Volume 13, Issue 1, April 2026, pp. 1-9
ISSN 2355-5068 ; e-ISSN 2622-4852
DOI: 10.33019/jurnalecotipe.v13i1.4565

systems [12]. A 24 V DC source input voltage was used in this investigation. Figure 2 shows the sepic converter's basic circuit.

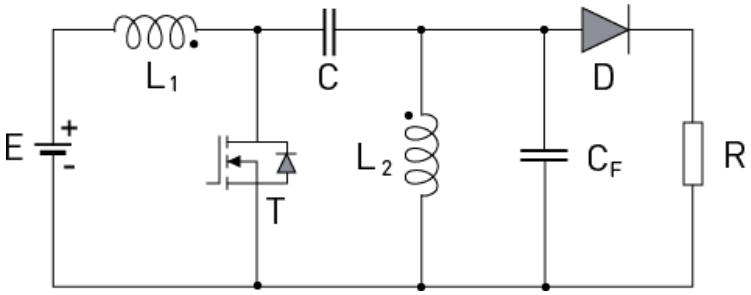

Figure 2. Sepic Converter Circuit

$$V_o = \frac{V_o}{V_{in} + V_o} \quad (1)$$

$$\Delta IL = 20\% \; x \; Iin \quad (2)$$

$$L = \frac{Vin \; x \; D}{\Delta IL \; x \; F} \quad (3)$$

$$\Delta Vo = 1\% \; x \; Vo \quad (4)$$

$$R = \frac{Vo}{Io} \quad (5)$$

$$C = \left(\frac{Vo \; x \; D}{R \; x \; \Delta Vo \; x \; F}\right) \quad (6)$$

Note :

Vin	: Input Voltage	(V)
Vo	: Output Voltage	(V)
Iin	: Input Current	(A)
R	: Resistance Output	(Ω)
L	: Inductance Value	(uH)
C	: Capasitance Value	(uF)
D	: Duty Cycle	
F	: Frequency	(Hz)
ΔVo	: Forward Reverse	(V)
ΔiL	: Ripple Current	(A)

Table 1. Parameters design of Sepic Converter

Parameters	Symbol	Value	Units
Input Voltage	Vin	24	V
Output Voltage	Vo	16.8	V
Frequency	F	40	kHz
Inductor	L	256	uH
Capasitor	C	2200	uF
Ripple Current	ΔiL	0.88	A

The Sepic converter's parameter design is shown in **Table 1**, after which a PowerSIM simulation circuit is created. After that, use equation 1 to make calculations. Because the battery voltage requirements of 14.6 V, 14.4 V, and 16.8 V have been adjusted, there are three duty cycle calculations. The duty cycle of each load is 30.7%, 40.4%, and 47.19% if Vin is taken to be stable at 24 V based on the open loop simulation.

JURNAL ECOTIPE
Electronic, Control, Telecommunication, Information, and Power Engineering
Volume 13, Issue 1, April 2026, pp. 1-9
ISSN 2355-5068 ; e-ISSN 2622-4852
DOI: 10.33019/jurnalecotipe.v13i1.4565

The open-loop response of the Sepic converter is tested using this simulation. It is evident from **Figure 3**'s open-loop Sepic converter simulation results that there is steady-state inaccuracy and voltage overshoot. A straight line indicates the output voltage, whereas a dotted line indicates the setpoint value. **Table 2** displays more specific information.

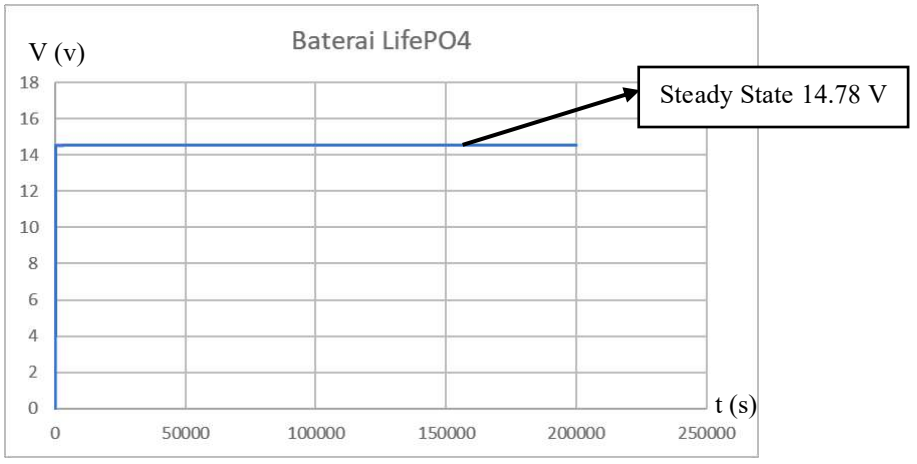

(a)

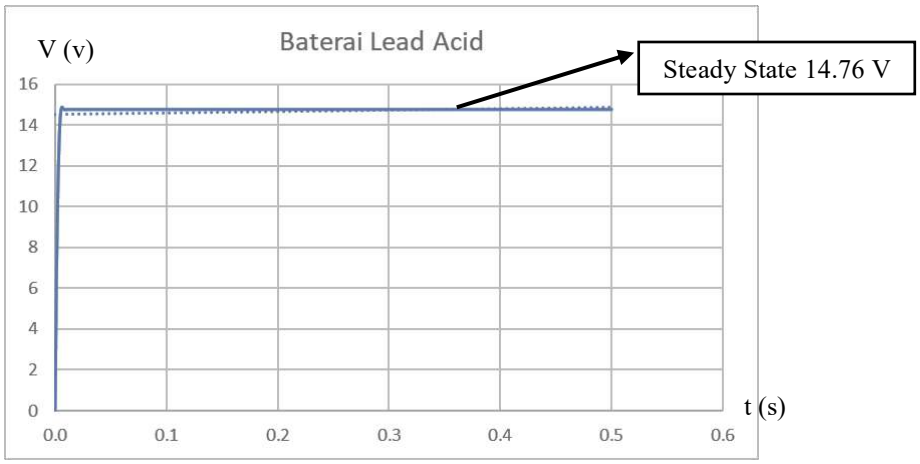

(b)

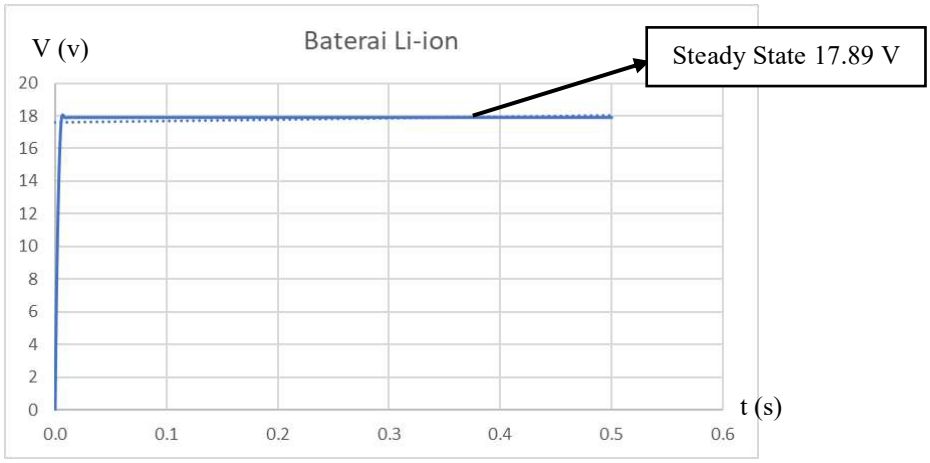

(c)

Figure 3. Simulation curve of sepic converter with load variation : (a) LifePO4 with duty cycle 30.7%, (b) Lead Acid with duty cycle 40.4% and (c) Li – ion with duty cycle 47.19%

JURNAL ECOTIPE
Electronic, Control, Telecommunication, Information, and Power Engineering
Volume 13, Issue 1, April 2026, pp. 1-9
ISSN 2355-5068 ; e-ISSN 2622-4852
DOI: 10.33019/jurnalecotipe.v13i1.4565

The comprehensive simulation results for battery improvements based on the open-loop sepic converter simulation's findings are shown in **Table 2**. displays the thorough simulation results for battery modifications based on the findings of the open-loop sepic converter simulation. The three duty cycle variations have been adjusted to the setpoints of the three battery types: Li-ion, Lead Acid, and LifePO4.

Table 2. Sepic Converter simulation open loop result

No	Type of Battery	Duty Cycle (%)	Vo theory (Volt)	Vo simulation (Volt)	Error Vo (%)
1	LifePO4	30.7	14.6	14.78	1.21
2	Lead Acid	40.4	14.4	14.76	2.43
3	Li - ion	47.19	16.8	17.89	6.09
Averages Error (%)					3.92

Based on the statistics in **Table 2**, the average open-loop voltage output error for the three batteries is 3.92%. The Li-ion battery type has the highest error value, measuring 16.8 volts with an error value of 6.09%. Control is therefore necessary for the sepic converter to reach the battery's setpoint in order to keep the output voltage of the converter at the setpoint value.

2.2. Design of ANN-PID Controller

The control strategy in this adaptive charging study combines ANN and PID controllers. The PID controller uses an artificial neural network (ANN) to compute the charging setpoint voltage value. It is noteworthy that artificial neural networks can tackle problems of different types and interpretations [10].

LifePO4 had a charging voltage of 14.6 V, Lead Acid had a charging voltage of 14.4 V, and Li-ion had a charging voltage of 16.8 V. These three types of battery loads provided the training data for the charging voltage and charging current characteristics. In order to modify the output voltage to match the detected battery voltage, which is 14.6 V, 14.4 V, and 16.8 V, an ANN target—that is, the setpoint for each battery—is necessary because these values change.

This study uses a particular kind of ANN algorithm known as feed forward backpropagation. An ANN with two inputs (voltage and current), a first hidden layer (four neurons), and an output layer (one neuron) with a 208-iteration epoch is depicted in block diagram form in **Figure 4**. Logsig-tansig is the activation function that is employed. In this study, the back-propagation ANN model was trained using the Levenberg-Marquardt learning strategy. **Figure 5's** learning objectives produced a regression value of 0.99998.

Figure 4. NNTool training

JURNAL ECTIPE
Electronic, Control, Telecommunication, Information, and Power Engineering
Volume 13, Issue 1, April 2026, pp. 1-9
ISSN 2355-5068 ; e-ISSN 2622-4852
DOI: 10.33019/jurnalecotipe.v13i1.4565

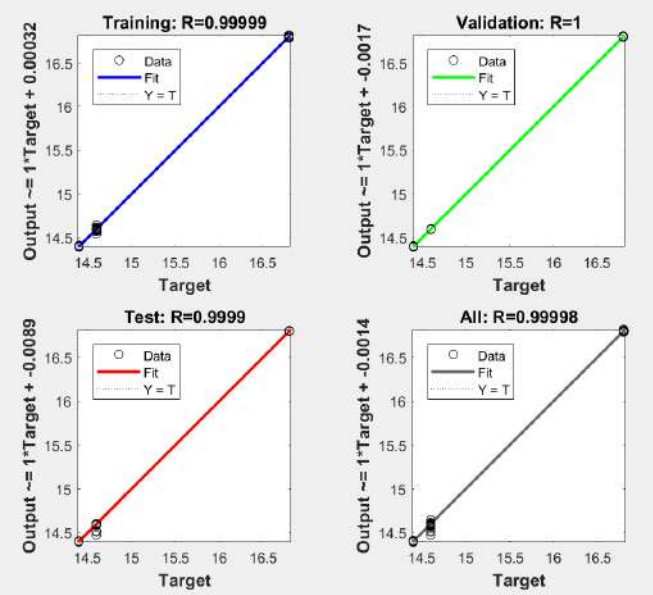

Figure 5. Regresi value NNTool

The input layer, the hidden layer, and the output layer are the three primary parts of the backpropagation algorithm's architecture. Without doing any calculations, the input layer's sole function is to receive the input signal and forward it to the hidden layer. Weight and bias calculations take place in the output and hidden layers. A particular activation function is used to determine the output of both layers [4]. Tansig is the activation function utilized in the layer 1 output of this ANN architecture.

$$Tansig\ (n) = \frac{2}{(1-exp^{=2n})} - 1 \quad (4)$$

After obtaining the setpoint values from different types of batteries, the PID controller will next execute the ANN output for the constant voltage charging process. By calculating the setpoint error value in relation to the feedback value, the PID controller unifies three control systems: proportional control (P), integral control (I), and derivative control (D). **Figure 6** shows the block diagram for the PID controller.

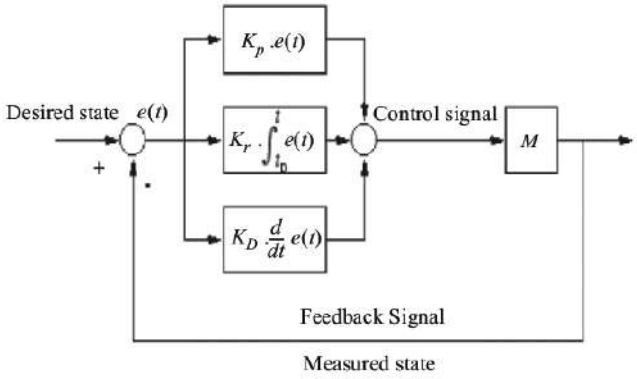

Figure 6. Block diagram of a system with PID controller [11]

Kp, ki, and kd design values for PID control.

$Kp = 0.48102$ (5)
$Ki = 21.2621$ (6)
$Kd = 0.0113$ (7)

Note :

Kp : proportional gain
Ki : integral gain

JURNAL ECOTIPE
Electronic, Control, Telecommunication, Information, and Power Engineering
Volume 13, Issue 1, April 2026, pp. 1-9
ISSN 2355-5068 ; e-ISSN 2622-4852
DOI: 10.33019/jurnalecotipe.v13i1.4565

Kd : derivative gain

3. RESULTS AND DISCUSSION

PowerSimulation software was used to design the simulation circuit for variable battery charging that is shown in **Figure 7**. The three battery types utilized in this circuit are Li-ion batteries with a charging voltage of 14.4 V, LifePO4 batteries with a setpoint voltage of 14.6 V, and Li-ion batteries with a setpoint voltage of 16.8 V. It consists of a circuit for a Sepic converter that is ANN-PID driven.

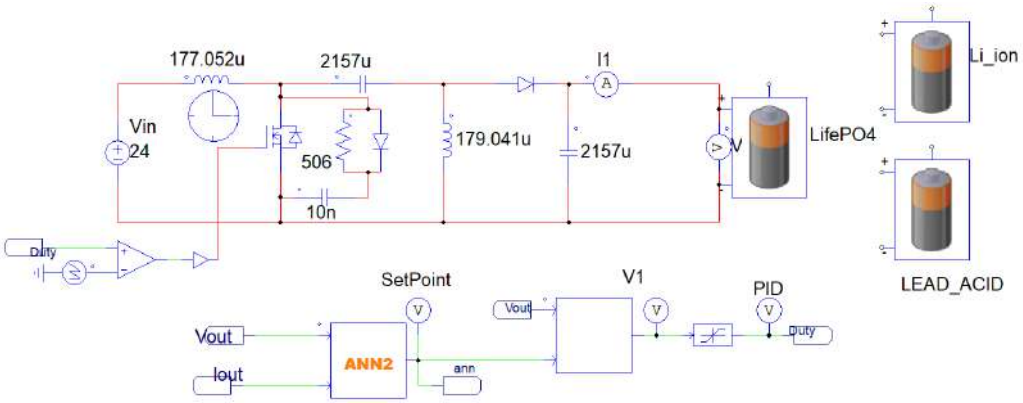

Figure 7. Closed-loop adaptive charging system simulation circuit

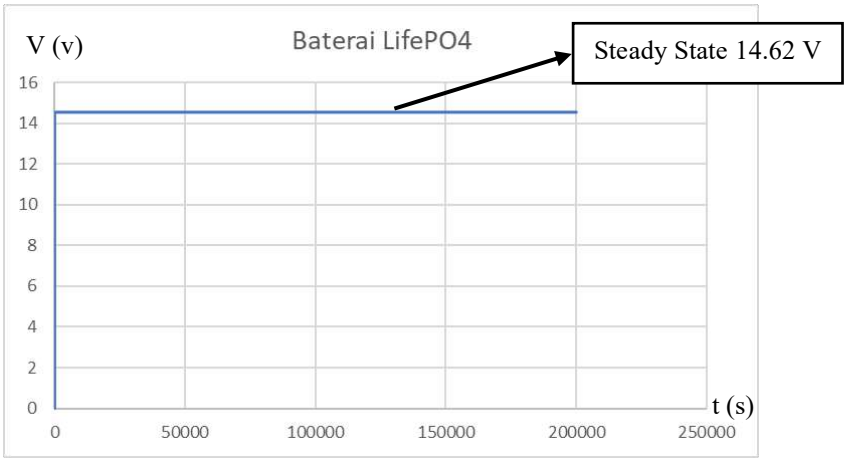

(a)

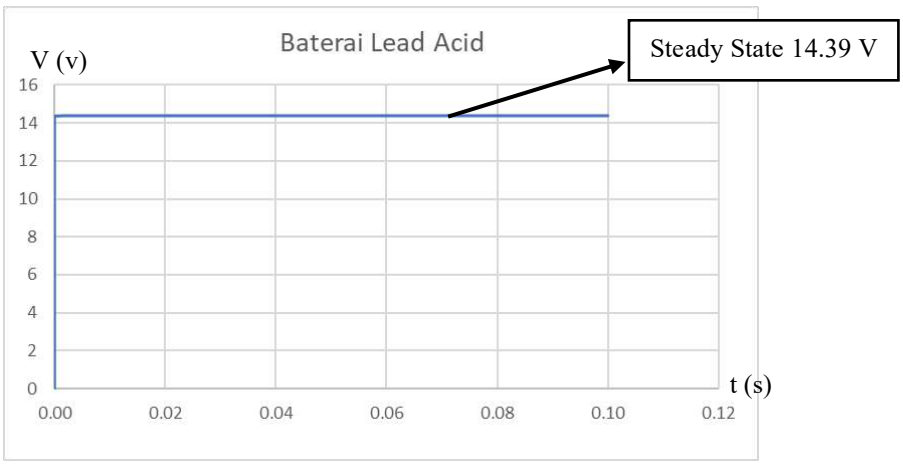

(b)

JURNAL ECOTIPE
Electronic, Control, Telecommunication, Information, and Power Engineering
Volume 13, Issue 1, April 2026, pp. 1-9
ISSN 2355-5068 ; e-ISSN 2622-4852
DOI: 10.33019/jurnalecotipe.v13i1.4565

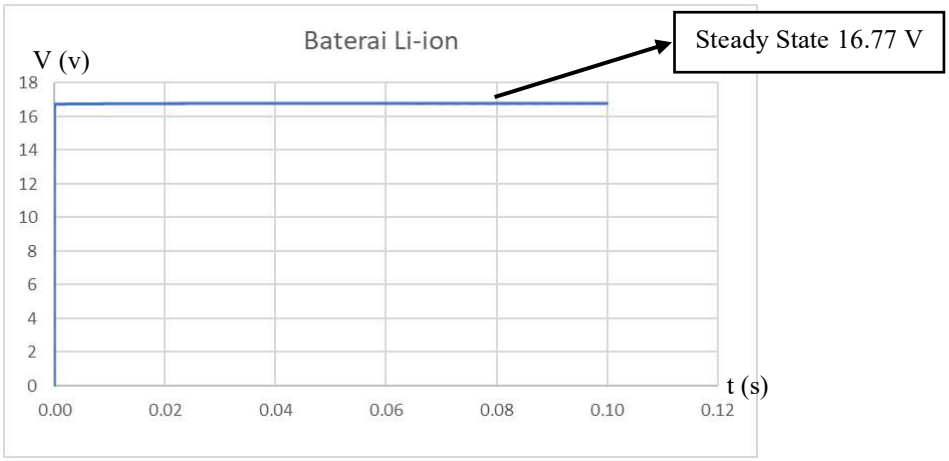

(c)

Figure 8. Adaptive charging with variable load using the ANN-PID method (a) LifePO4 Battery, (b) Lead Acid Battery and (c) Li-ion Battery

Figure 8 (a) shows the charging curve for a Lifepo4 battery with a setpoint of 14.6 volts, while **Figure 8 (b)** shows the charging curve for a Lead Acid battery with a setpoint of 14.4 volts, and **Figure 8 (c)** shows the charging curve for a Li-ion battery with a setpoint of 16.8 volts.

Table 3. ANN-PID output result

No	Type of battery	Setpoint Voltage (Volt)	Output Voltage	Error (%)
1	LifePO4	14.6	14.62	0.27
2	Lead Acid	14.4	14.39	0.069
3	Li-ion	16.8	16.77	0.178
Averages error				0.174

One of three battery types is linked to the SEPIC converter output, as shown in **Figure 9**. The ANN-PID control method regulates the converter's output voltage when a LiFePO4 battery is connected. In order to establish the battery status and the proper charging setpoint, which in this case is 14.6 V, the ANN analyzes the measured voltage and current data. After comparing the feedback signal and the ANN-generated setpoint, the PID controller determines the error and modifies the duty cycle until the feedback reaches the target value. The other battery kinds, each of which has a different charging voltage setpoint, go through the same process.

According to the performance evaluation, which is shown in **Table 4**, there is very little difference between the ANN output and the desired reference data. The observed inaccuracy for the LiFePO4 battery with a setpoint of 14.6 V is 0.27%. The error for the Li-ion battery at 16.8 V is 0.178%, whereas the error for the Lead Acid battery at 14.4 V is 0.069%. The calculated average system error is 0.174% overall. These findings show that the suggested ANN-PID control approach provides great precision and stability in supporting the adaptive charging process.

.

4. CONCLUSION

The results of a number of experimental tests verify that the suggested approach's application is in good agreement with earlier research. The findings show that by examining the voltage and current profiles of three distinct battery types, They can be effectively identified by the Artificial Neural Network (ANN) in combination with Proportional-Integral-Derivative (PID) control. The ANN-PID control technique created in this work is quite appropriate for adaptive battery charging applications, as seen by the charging system's average variance of just 0.174% between its output and the desired setpoint.

Volume 13, Issue 1, April 2026, pp. 1-9
ISSN 2355-5068 ; e-ISSN 2622-4852
DOI: 10.33019/jurnalecotipe.v13i1.4565

REFERENCES

[1] I. Yustikasari, E. Sunarno, and P. A. Mahadi Putra, "Desain dan Simulasi Buck Konverter Dengan Kontrol Logika Fuzzy untuk Pengisian Baterai," *Jurnal Ecotipe (Electronic, Control, Telecommunication, Information, and Power Engineering)*, vol. 8, no. 2, pp. 59–64, Jul. 2021, doi: 10.33019/jurnalecotipe.v8i2.2389.

[2] K. Hidayat, M. C. Hasani, N. A. Mardiyah, and M. Effendy, "Strategi Pengisian Baterai pada Sistem Panel Surya Standalone Berbasis Kontrol PI Multi-Loop," *Jurnal Teşknik Elektro*, vol. 13, no. 1, pp. 25–33, Jun. 2021, doi: 10.15294/jte.v13i1.29765.

[3] S. Chakraborty, M. M. Hasan, I. Worighi, O. Hegazy, and M. A. Razzak, "Performance Evaluation of a PID-Controlled Synchronous Buck Converter Based Battery Charging Controller for Solar-Powered Lighting System in a Fishing Trawler," *Energies (Basel)*, vol. 11, no. 10, 2018, doi: 10.3390/en11102722.

[4] I. Sudiharto, F. D. Murdianto, and A. Wulandari, "Adaptive charging control using ANN-PID controllers on multiple DC loads with varying battery voltages," *International Journal of Power Electronics and Drive Systems*, vol. 13, no. 1, pp. 620–630, Mar. 2022, doi: 10.11591/ijpeds.v13.i1.pp620-630.

[5] R. Nur and A. Barry, "Optimalisasi Waktu Pengisian Dengan Smart Dual Charger Plug and Play pada Kendaraan Listrik Bertenagakan Baterai SLA/VRLA," *Jtam Rotary*, vol. 6, no. 2, p. 193, Sep. 2024, doi: 10.20527/jtam_rotary.v6i2.13070.

[6] A. N. Maulidyna, I. Sudiharto, and F. D. Murdianto, "Multi DC Load Single Port Output Adaptive Power Charge Using Fuzzy Logic Controller," *IOP Conf Ser Mater Sci Eng*, vol. 1096, no. 1, p. 012063, Mar. 2021, doi: 10.1088/1757-899x/1096/1/012063.

[7] N. Fuada and I. Husnaini, "Rancang Bangun Buck Converter dengan Kontrol PID Berbasis Mikrokontroller Arduino," *JTEIN: Jurnal Teknik Elektro Indonesia*, vol. 4, no. 2, pp. 781–791, Oct. 2023, doi: 10.24036/jtein.v4i2.513.

[8] F. D. Murdianto, I. Sudiharto, I. Irianto, and A. Wulandari, "Adaptive Power Charge Using PID Controller on DC Load Application," *INTEK: Jurnal Penelitian*, vol. 7, no. 2, pp. 138–144, Feb. 2021, doi: 10.31963/intek.v7i2.2652.

[9] M. Irwanto *et al.*, "Photovoltaic powered DC-DC boost converter based on PID controller for battery charging system," in *Journal of Physics: Conference Series*, Institute of Physics Publishing, Jan. 2020. doi: 10.1088/1742-6596/1432/1/012055.

[10] *IREC2015 Inteşrnational Renewable Energy Congress : the Sixth Inteşrnational Renewable Energy Congress : 2015 6th International Renewable Energy Congress (IREC), March 24-26, 2015, Sousse, Tunisia*. IEEE, 2015.

[11] H. Om Bansal and H. O. Bansal, "Tuning of PID Controllers using Simulink." [Online]. Available: https://www.researchgate.net/publication/268802558

[12] Sudiharto, I., Okky Anggriawan, D., Jufriyadi, M., Elektronika Negeri Surabaya, P., Anggriawan, D. O., & Jufriyadi, M. (2024). Design of SEPIC Converter for Battery Charging System using ANFIS. *KINETIK*, *9*(2), 203–212.

JURNAL ECOTIPE
Electronic, Control, Telecommunication, Information, and Power Engineering

Volume 13, Issue 1, April 2026, pp. 10-19
ISSN 2355-5068 ; e-ISSN 2622-4852
DOI: 10.33019/jurnalecotipe.v13i1.4588

Harmonic Distortion Assessment of Nonlinear Medical Loads in a Hospital Distribution Network Using ETAP Simulation

Dultudes Mangopo[1], Rimbawati[2], Partaonan Harahap[3], Nurdiansyah[4]
[1]Departement of Electrical Engineering Faculty of Engineering, Universitas Cenderawasih, Jayapura, Papua, Indonesia
[2,3,4]Department of Electrical Engineering, Faculty of Engineering, Universitas Muhammadiyah Sumatera Utara, Indonesia

ARTICLE INFO

Article historys:

Received : 04/02/2026
Revised : 18/02/2026
Accepted : 30/04/2026

Keywords:

ETAP Simulation; Harmonic Distortion; Hospital Power System; Nonlinear Loads; Power Quality

ABSTRACT

The growing use of power-electronics-based medical equipment has significantly altered the load characteristics of hospital electrical distribution systems. As nonlinear devices increase, harmonic distortion becomes a critical power quality concern that may affect equipment reliability and operational safety. This study investigates harmonic behavior in a 20 kV/0.4 kV hospital distribution network through harmonic load flow simulation using ETAP software. Total Harmonic Distortion of Voltage (THDv) and Total Harmonic Distortion of Current (THDi) are evaluated at selected buses and at the Point of Common Coupling (PCC), with reference to IEEE Std. 519-2014. Simulation results indicate that two low-voltage buses supplying high-capacity medical equipment exhibit THDv values of 8.21% and 6.74%, exceeding the recommended 5% limit. The THDi at the PCC reaches 14.37%, surpassing the allowable limit for the calculated short-circuit ratio (Isc/IL = 8.43). Dominant harmonic components are identified at the 5th and 7th orders, confirming the influence of rectifier-based medical systems and UPS units. The findings demonstrate that nonlinear medical loads significantly contribute to harmonic propagation, increased branch losses, and voltage distortion. Appropriate mitigation strategies, including harmonic filtering and load configuration adjustments, are therefore essential to ensure compliance with power quality standards and to maintain reliable hospital operation.

Corresponding Author:

Dultudes Mangopo
Departement of Electrical Engineering Faculty of Engineering, Universitas Cenderawasih, Jayapura, Papua, Indonesia
Email: dultudes_mangopo@ft.uncen.ac.id

1. INTRODUCTION

The rapid advancement of electrical and electronic technologies has significantly transformed modern power systems, increasing the complexity of generation, transmission, and distribution networks. This transformation is particularly evident in facilities that rely heavily on sensitive and high-precision electrical equipment, such as hospitals and healthcare centers. In such environments, electrical energy is not merely a supporting utility but a critical infrastructure element that directly influences operational continuity, diagnostic accuracy, and patient safety. Hospitals require electrical power systems that are highly reliable, continuously available, and capable of maintaining superior power quality under varying load conditions. Any deviation from acceptable power quality parameters may lead to equipment malfunction, inaccurate medical diagnostics, operational interruptions, or even life-threatening situations[1],[2].

Volume 13, Issue 1, April 2026, pp. 10-19
ISSN 2355-5068 ; e-ISSN 2622-4852
DOI: 10.33019/jurnalecotipe.v13i1.4588

The importance of power quality in hospitals is amplified by the continuous operation of critical medical equipment and life-support systems. Equipment such as Magnetic Resonance Imaging (MRI), Computed Tomography (CT) scanners, X-ray systems, ventilators, infusion pumps, laboratory analyzers, and digital monitoring devices are highly sensitive to electrical disturbances. Power quality problems, including voltage distortion, harmonic distortion, and transient disturbances, can degrade equipment performance, reduce imaging accuracy, and cause unexpected shutdowns[3]. Therefore, maintaining a stable and distortion-free power supply is a fundamental requirement in hospital electrical distribution systems.

Among various power quality issues, harmonic distortion has emerged as one of the most significant challenges in contemporary electrical distribution networks. Harmonics are defined as voltage or current components whose frequencies are integer multiples of the fundamental frequency (50 Hz). Harmonic distortion primarily originates from nonlinear loads, which draw non-sinusoidal currents even when supplied with sinusoidal voltage. Unlike linear loads, nonlinear loads do not maintain proportionality between voltage and current, resulting in waveform distortion that propagates throughout the electrical system[4],[5].

The proliferation of nonlinear loads has increased substantially due to the widespread adoption of power-electronics-based equipment. In hospital electrical systems, nonlinear loads are predominantly associated with medical imaging devices, laboratory instruments, uninterruptible power supplies (UPS), switch-mode power supplies (SMPS), and variable speed drives (VSD) used in HVAC systems[5],[6]. While these devices are essential for modern healthcare operations, they inject harmonic currents into the network, leading to distorted voltage and current waveforms across the distribution system. As the penetration level of such equipment continues to grow, harmonic distortion becomes increasingly difficult to control, particularly in complex hospital distribution networks.

Excessive harmonic distortion can cause a wide range of adverse effects on power system components and overall system performance. Harmonic currents increase copper and core losses in transformers and conductors, resulting in excessive heating and reduced efficiency. Transformers operating under high harmonic content may experience core saturation, increased eddy current losses, and accelerated insulation aging, which ultimately shortens their service life[7]. In addition, harmonic distortion may lead to malfunction or misoperation of protective devices, nuisance tripping of circuit breakers, inaccurate metering readings, and electromagnetic interference affecting communication systems. In hospital environments, such disturbances pose significant operational risks due to the continuous and sensitive nature of medical equipment.

Even moderate levels of voltage harmonic distortion can negatively affect imaging quality, sensor accuracy, and control system stability. Prolonged exposure to harmonic-rich environments may increase maintenance requirements, elevate operational costs, and compromise overall system reliability. Therefore, monitoring, analyzing, and managing harmonic distortion levels in hospital electrical distribution systems are essential to ensure compliance with power quality standards and to maintain safe and reliable healthcare services[8],[2].

To address harmonic-related power quality issues, international standards have been established, among which IEEE Std. 519-2014 is widely recognized. This standard provides recommended practices and limits for harmonic control in electrical power systems [5]. It specifies acceptable levels of voltage and current harmonic distortion at the Point of Common Coupling (PCC) to protect both utility systems and end-user equipment. For systems below 69 kV, the recommended maximum Total Harmonic Distortion of Voltage (THDv) at the PCC is 5%, while current distortion limits depend on the short-circuit ratio (Isc/IL). Compliance with these limits is crucial to maintaining system integrity and preventing adverse effects associated with harmonic propagation.

Despite the availability of such standards, practical implementation remains challenging, particularly in hospital electrical systems with high concentrations of nonlinear medical loads. Several studies have reported that harmonic distortion levels in healthcare facilities often approach or exceed recommended thresholds due to the cumulative operation of multiple nonlinear devices[9],[6]. This condition highlights the necessity for comprehensive harmonic assessment to identify distortion sources, evaluate system vulnerability, and determine appropriate mitigation strategies.

Volume 13, Issue 1, April 2026, pp. 10-19
ISSN 2355-5068 ; e-ISSN 2622-4852
DOI: 10.33019/jurnalecotipe.v13i1.4588

Analytical and simulation-based approaches have become indispensable tools for harmonic analysis in complex power systems. Simulation techniques enable engineers to model electrical networks, analyze load behavior, and predict harmonic propagation without interrupting actual system operation. Such approaches are especially valuable in hospital environments where system downtime is unacceptable [10]. By simulating different loading scenarios, potential power quality issues can be identified proactively and mitigation measures can be evaluated prior to implementation.

ETAP (Electrical Transient and Analysis Program) is one of the most widely used software platforms for power system studies, including load flow, short-circuit analysis, transient stability, and harmonic analysis. ETAP provides comprehensive modeling capabilities that allow accurate representation of electrical distribution systems and nonlinear load characteristics[11]. Through harmonic load flow analysis, ETAP can calculate Total Harmonic Distortion of Voltage (THDv) and Total Harmonic Distortion of Current (THDi), evaluate harmonic propagation across buses and feeders, and assess compliance with IEEE Std. 519-2014 under various operating conditions[12],[13].

Although previous research has demonstrated the effectiveness of ETAP-based harmonic analysis in industrial and commercial facilities [8],[2]. studies specifically focusing on hospital electrical distribution systems remain limited, particularly in the context of increasing nonlinear medical load penetration. Considering the critical nature of healthcare facilities, detailed harmonic assessment tailored to hospital environments is essential to support informed decision-making in system design, operation, and maintenance.

Therefore, this study presents a comprehensive harmonic distortion analysis of nonlinear medical loads in a hospital electrical distribution system using ETAP simulation. The analysis evaluates voltage and current harmonic distortion at various buses and at the PCC, and compares the results with the limits specified in IEEE Std. 519-2014 [14],[5]. By identifying buses with excessive harmonic levels and examining the contribution of nonlinear medical equipment to overall system performance, this research aims to provide technical insights into power quality conditions in hospital environments. The findings are expected to serve as a practical reference for engineers, facility managers, and policymakers in enhancing reliability, efficiency, and safety of electrical distribution systems in healthcare facilities[15],[16].

2. RESEARCH METHOD

This research employs a simulation-based analytical approach to evaluate harmonic distortion caused by nonlinear medical loads in a hospital electrical distribution system. The methodology is designed to identify harmonic characteristics, assess power quality conditions, and compare the simulation results with established international standards[17],[18].The overall research procedure consists of system modeling, load characterization, harmonic simulation, and result evaluation.

2.1. Research Design

The research uses a quantitative descriptive method based on power system simulation. Harmonic analysis is conducted using ETAP software, which allows accurate modeling of electrical distribution networks and nonlinear load behavior. The study focuses on steady-state harmonic conditions under normal operating scenarios of hospital electrical loads[19].

2.2. Electrical Distribution System Modeling

The hospital electrical distribution system is modeled in ETAP based on the actual configuration of the low-voltage distribution network. The modeled system includes power sources, transformers, main distribution panels, feeders, cables, and load buses[20],[21].Transformer ratings, cable parameters, and system voltage levels are defined according to nameplate data and design specifications. The single-line diagram is developed to represent the real operating conditions of the hospital power system[12],[22],[23].

2.3. Nonlinear Load Characterization

Nonlinear loads in the hospital are identified and categorized based on their operational characteristics. These loads include medical imaging equipment, laboratory instruments, uninterruptible power supplies (UPS), and other power-electronics-based devices. Each nonlinear load

Volume 13, Issue 1, April 2026, pp. 10-19
ISSN 2355-5068 ; e-ISSN 2622-4852
DOI: 10.33019/jurnalecotipe.v13i1.4588

is modeled in ETAP using harmonic current spectra that represent typical operating behavior. The harmonic order and magnitude are defined based on standard harmonic profiles available in ETAP and relevant technical references[24],[25]. Linear loads are also included in the model to reflect realistic load composition within the hospital electrical system.

2.4. Harmonic Analysis Using ETAP

Harmonic analysis is performed using the harmonic load flow module in ETAP. The simulation calculates voltage and current harmonic components at various buses within the distribution network. Key parameters evaluated in this study include total harmonic distortion of voltage (THDv) and total harmonic distortion of current (THDi). The analysis is conducted under normal operating conditions to observe harmonic propagation from nonlinear load buses to upstream distribution points.

2.5. Evaluation Based on IEEE Standards

The simulation results are evaluated by comparing the calculated THDv and THDi values with the recommended limits specified in IEEE Std. 519-2014. Voltage harmonic distortion limits are assessed at the point of common coupling (PCC), while current harmonic distortion is evaluated based on system short-circuit capacity. This comparison is used to determine whether the harmonic levels in the hospital electrical distribution system comply with acceptable power quality standards[26].

2.6. Data Analysis and Interpretation

The obtained simulation data are analyzed to identify buses with the highest harmonic distortion levels and to determine the contribution of nonlinear medical loads to overall system harmonics. The results are presented in graphical and tabular forms to facilitate interpretation. The analysis emphasizes the relationship between nonlinear load penetration and harmonic distortion severity, providing insights into potential risks to system reliability and equipment performance.

3. RESULTS AND DISCUSSION

3.1. Harmonic Distortion Results

ETAP harmonic load flow simulation reveals that harmonic distortion is unevenly distributed throughout the hospital electrical distribution system. Several buses exhibit elevated THDv values, particularly those supplying nonlinear medical loads. The highest THDv value of 17.57% is observed at Bus7 (150 kV), followed by Bus9 (25 kV) with 12.30% and Bus8 (125 kV) with 8.57%.

The harmonic load flow simulation results obtained from ETAP are summarized in Table 1, which presents the total harmonic distortion of voltage (THDv) at various buses in the hospital electrical distribution system.

Table 1. THDv at low voltage buses

Bus ID	Voltage Level	THDv (%)	IEEE Limit (5%)	Status
LV-1	0.4 kV	8.21	5%	Exceeds
LV-2	0.4 kV	6.74	5%	Exceeds
LV-3	0.4 kV	4.32	5%	Within
LV-4	0.4 kV	3.15	5%	Within
PCC	0.4 kV	5.48	5%	Slightly Exceeds

The highest THDv (8.21%) occurs at LV-1, which supplies MRI and UPS loads. Distortion decreases toward upstream buses due to impedance attenuation. Although some buses comply with IEEE limits, the PCC slightly exceeds the 5% threshold, indicating system-level harmonic propagation.

JURNAL ECTIPE
Electronic, Control, Telecommunication, Information, and Power Engineering
Volume 13, Issue 1, April 2026, pp. 10-19
ISSN 2355-5068 ; e-ISSN 2622-4852
DOI: 10.33019/jurnalecotipe.v13i1.4588

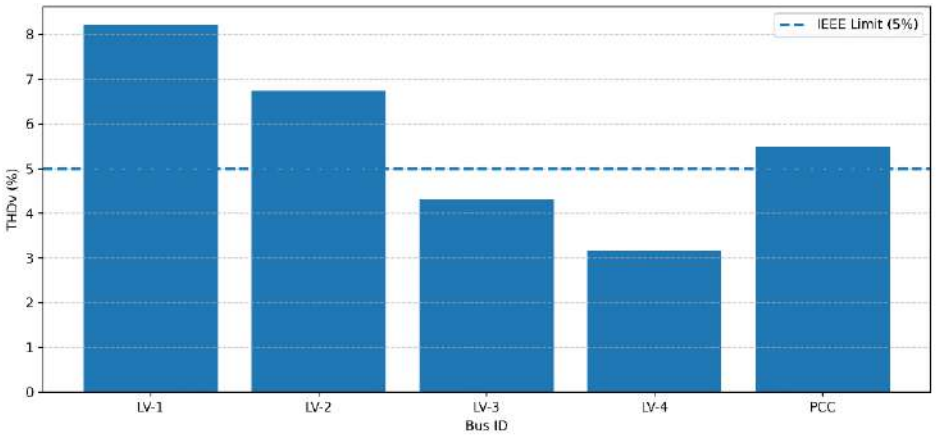

Figure 1. THDv (%) comparison per bus (0.4 kV)

The figure illustrates the distribution of Total Harmonic Distortion of Voltage (THDv) values at several low-voltage buses (0.4 kV) within the hospital electrical distribution system. The horizontal line in the graph represents the maximum allowable THDv limit of 5%, as recommended by IEEE Std. 519-2014 for systems operating below 69 kV. Based on the graph, Bus LV-1 records the highest THDv value at 8.21%, followed by LV-2 at 6.74%. Both buses significantly exceed the 5% standard limit and are therefore classified as non-compliant with power quality requirements. The elevated THDv levels at LV-1 and LV-2 indicate a high concentration of nonlinear loads, such as power-electronics-based medical equipment (e.g., MRI systems and UPS units), which typically generate dominant 5th- and 7th-order harmonic currents.

The PCC bus exhibits a THDv value of 5.48%, which slightly exceeds the recommended limit. This condition indicates that harmonic distortion is not confined locally to load buses but has propagated to the Point of Common Coupling (PCC). Such propagation may affect overall system power quality and potentially impact other equipment connected to the same electrical network. In contrast, LV-3 and LV-4 show THDv values of 4.32% and 3.15%, respectively, both of which remain below the 5% threshold. This suggests that harmonic distortion decreases with increasing electrical distance from the dominant nonlinear load sources and is influenced by the impedance characteristics of the distribution system.

Overall, the graph indicates that voltage harmonic distortion in the hospital electrical distribution system does not fully comply with IEEE 519-2014 standards, particularly at feeders supplying nonlinear medical loads. Therefore, further technical evaluation and the implementation of mitigation strategies—such as harmonic filter installation or feeder configuration optimization—are necessary to improve power quality and ensure the reliable operation of critical medical equipment.

3.2. Voltage Harmonic Distortion Evaluation

According to IEEE Std. 519-2014, the allowable THDv limit for systems below 69 kV is 5%. Simulation results show that multiple buses exceed this limit, including Bus7, Bus8, Bus9, Bus14, and Bus15. Buses closer to nonlinear load concentrations experience higher distortion levels due to increased harmonic current injection and system impedance interaction. Although several buses maintain THDv values within acceptable limits, the presence of localized harmonic hotspots indicates potential risks to sensitive medical equipment and long-term system reliability.

To visualize the distribution of voltage harmonic distortion across the system, the ETAP harmonic bus information diagram is shown in figure 2.

JURNAL ECOTIPE
Electronic, Control, Telecommunication, Information, and Power Engineering
Volume 13, Issue 1, April 2026, pp. 10-19
ISSN 2355-5068 ; e-ISSN 2622-4852
DOI: 10.33019/jurnalecotipe.v13i1.4588

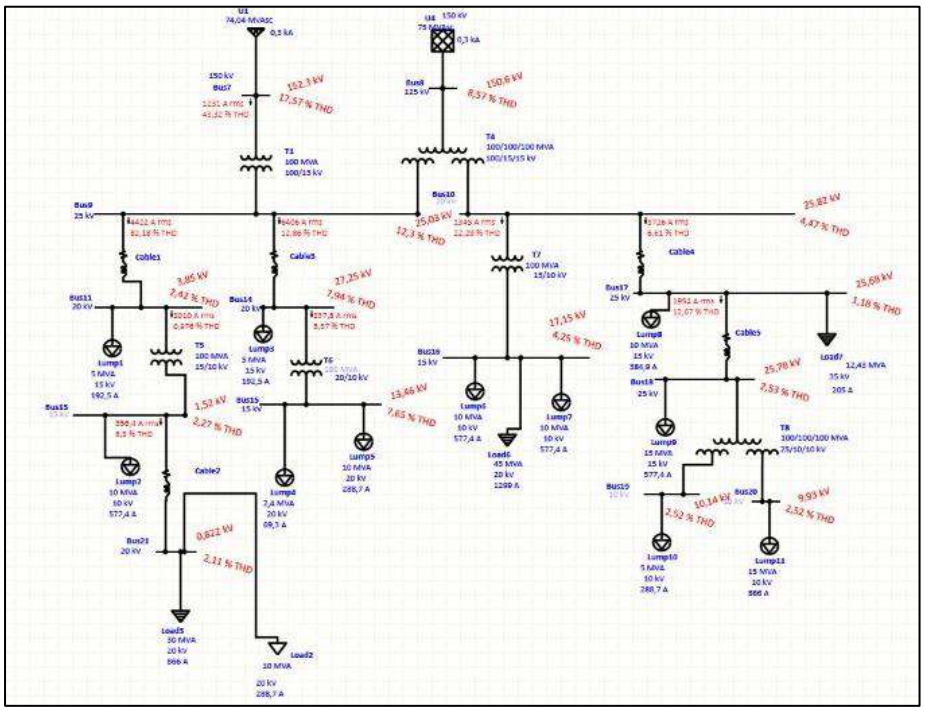

Figure 2. System harmonics bus information

The figure presents the single-line diagram of the hospital electrical distribution system modeled and analyzed using ETAP harmonic load flow simulation. The system is supplied from a 150 kV utility source, stepped down through main transformers to 20 kV and subsequently distributed to various medium- and low-voltage buses supplying medical and supporting loads. The diagram illustrates the distribution of harmonic distortion across multiple buses, feeders, transformers, and loads. Red annotations indicate real power losses (kW) and Total Harmonic Distortion (THD %) values at different points in the network, while blue annotations represent voltage levels and current magnitudes.

From the upstream side, the utility source (150 kV) shows relatively low harmonic distortion, indicating that the primary contribution of harmonics originates from internal nonlinear loads rather than the grid supply. As power flows downstream through transformers and feeders, harmonic distortion becomes more pronounced, particularly at buses supplying nonlinear medical equipment.Several buses at the 20 kV and 25 kV levels exhibit elevated THD values, especially those connected to large-capacity loads such as imaging systems, UPS units, and motor-driven equipment. These buses show harmonic distortion levels exceeding 5%, indicating non-compliance with IEEE Std. 519-2014 voltage distortion limits. The presence of multiple transformers (e.g., T1, T6, T7, and T8) contributes to harmonic propagation due to impedance interaction and nonlinear load aggregation.

The diagram also shows variations in harmonic distortion across different branches. Feeders supplying concentrated nonlinear loads demonstrate higher THD values compared to branches serving predominantly linear loads. This confirms that harmonic distortion is strongly influenced by load composition and network impedance characteristics.In addition to harmonic distortion, the figure highlights power losses along several cables and transformers. Branches with higher harmonic currents experience increased losses, which may lead to additional thermal stress on conductors and equipment. This condition can accelerate insulation aging and reduce equipment lifespan if not properly mitigated.

Overall, the harmonic distribution pattern shown in the diagram indicates that distortion is not uniformly distributed but concentrated near nonlinear load centers. The propagation of harmonics from downstream buses toward upstream sections emphasizes the importance of harmonic mitigation strategies at dominant load locations. Installing tuned passive filters, redistributing nonlinear loads, or upgrading transformer configurations may significantly reduce harmonic levels and improve overall

JURNAL ECOTIPE
Electronic, Control, Telecommunication, Information, and Power Engineering
Volume 13, Issue 1, April 2026, pp. 10-19
ISSN 2355-5068 ; e-ISSN 2622-4852
DOI: 10.33019/jurnalecotipe.v13i1.4588

power quality. The simulation results demonstrated in the figure confirm that harmonic distortion in the hospital electrical system is primarily driven by nonlinear medical loads and requires systematic monitoring and mitigation to ensure compliance with IEEE 519-2014 and to maintain reliable operation of critical healthcare equipment.

3.3. Discussion and Practical Implications

The results confirm that nonlinear medical loads significantly contribute to harmonic propagation in hospital electrical systems. Elevated THDv levels may increase thermal stress on transformers and cables, accelerate insulation aging, and reduce equipment lifespan. Therefore, harmonic mitigation measures such as passive or active filters, load redistribution, or transformer derating should be considered to improve power quality. The ETAP-based approach proves effective in identifying harmonic distortion characteristics and supporting proactive power quality management in healthcare facilities.

In addition to harmonic distortion, power losses and voltage drops were evaluated to assess their impact on system performance. The branch losses summary obtained from ETAP simulation is presented in Table 2.

Table 2. Total Harmonic Distortion of Current (THDi) at PCC

Parameter	Value	IEEE 519-2014 Limit	Status
THDi	14.37%	12% (8 < Isc/IL < 20)	Exceeds
Isc/IL Ratio	8.43	-	-
5th Harmonic	9.8%	-	Dominant
7th Harmonic	6.1%	-	Dominant

Table 2 shows that the measured THDi at the PCC reached 14.37%, exceeding the permissible limit of 12% for a system with an Isc/IL ratio of 8.43. The dominant harmonic components—the 5th harmonic (9.8%) and 7th harmonic (6.1%)—are characteristic of 6-pulse rectifier-based equipment, which is commonly used in medical imaging systems and UPS installations. The presence of these dominant harmonic orders is consistent with the distortion distribution observed in the single-line diagram, particularly at buses directly connected to high-capacity nonlinear loads.

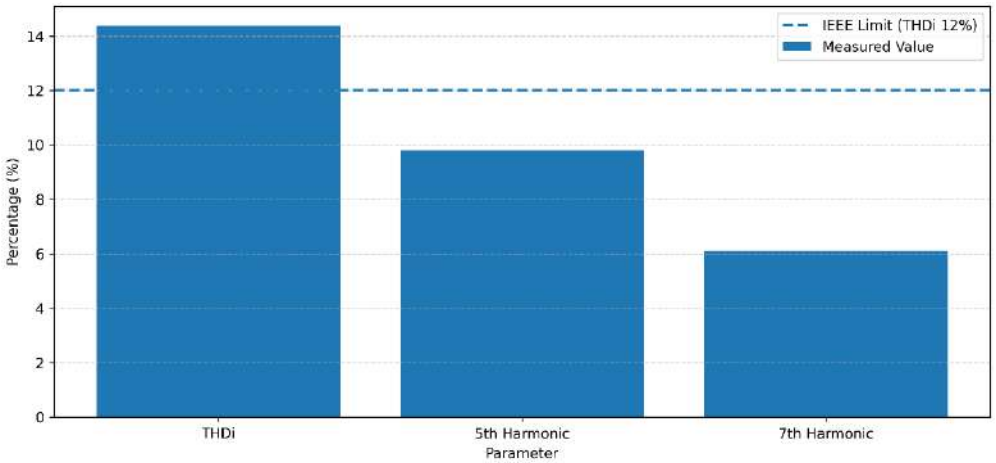

Figure 3. Current harmonic distortion and dominant harmonics

Table 2 presents the measured Total Harmonic Distortion of Current (THDi) at the Point of Common Coupling (PCC) and its comparison with the limits specified in IEEE Std. 519-2014. The simulation results indicate that the THDi at the PCC reaches 14.37%, exceeding the allowable limit of 12% for systems with a short-circuit ratio (Isc/IL) between 8 and 20. The calculated Isc/IL ratio of 8.43 places the system within this category, confirming that the applicable current distortion limit is 12%. The exceedance of the THDi limit indicates that nonlinear load penetration in the hospital electrical distribution system significantly affects current waveform quality. High THDi levels at the PCC suggest that harmonic currents generated by downstream medical and supporting equipment propagate upstream and accumulate at the system interface with the utility network.

Volume 13, Issue 1, April 2026, pp. 10-19
ISSN 2355-5068 ; e-ISSN 2622-4852
DOI: 10.33019/jurnalecotipe.v13i1.4588

Further harmonic spectrum analysis reveals that the dominant harmonic components are the 5th harmonic (9.8%) and the 7th harmonic (6.1%). These harmonic orders are characteristic of six-pulse rectifier-based equipment, which is widely used in medical imaging systems, uninterruptible power supplies (UPS), and other power-electronics-based devices. The prominence of these harmonic orders confirms that such nonlinear equipment constitutes the primary source of harmonic current injection within the system.

Elevated current harmonic distortion can lead to several technical consequences, including increased thermal stress in conductors and transformers, additional I^2R losses, and potential misoperation of protective devices. Moreover, excessive harmonic currents at the PCC may negatively affect the utility grid and could result in penalties or compliance issues if not properly mitigated.

Overall, the results presented in Table 2 demonstrate that the hospital electrical distribution system does not fully comply with IEEE 519-2014 current distortion limits at the PCC. Therefore, appropriate harmonic mitigation strategies—such as passive or active filtering, load redistribution, or transformer upgrading—are necessary to reduce THDi levels and ensure stable and reliable system operation.

3.4. Discussion and Practical Implications

The combined results from harmonic distortion and branch losses analysis clearly indicate that nonlinear medical loads have a substantial impact on both power quality and overall system efficiency in hospital electrical distribution systems. Elevated total harmonic distortion of voltage (THDv) and current (THDi), as observed at several buses supplying critical medical equipment, demonstrate that harmonic propagation is not localized but spreads throughout the distribution network. This condition increases electrical stress on system components and reduces the stability margin of the hospital power system.

High THDv levels, particularly those approaching or exceeding the limits recommended by IEEE Std. 519-2014, can adversely affect the performance and reliability of sensitive medical equipment. Voltage waveform distortion may lead to inaccurate readings, malfunction of electronic control circuits, and unexpected shutdowns of life-support and diagnostic devices. In parallel, elevated THDi contributes to additional thermal stress in transformers, cables, and switchgear, accelerating insulation degradation and shortening equipment lifespan. These effects are especially critical in hospital environments where continuity of service and operational reliability are mandatory.

The branch losses and voltage drop results further confirm the negative impact of harmonic-rich nonlinear loads on system efficiency. Significant voltage drops observed in feeder branches supplying high concentrations of nonlinear medical equipment indicate increased power losses and inefficient energy utilization. Excessive losses not only raise operational costs but also increase heat dissipation within cables and distribution panels, potentially leading to overheating and higher maintenance demands. In long-term operation, such conditions may compromise system safety and necessitate premature equipment replacement.

From a practical perspective, the findings of this study highlight the urgent need for harmonic mitigation strategies in hospital electrical systems. The installation of passive or active harmonic filters, proper sizing and configuration of transformers, and the segregation of nonlinear loads from sensitive equipment feeders can significantly reduce harmonic distortion levels. Additionally, incorporating power quality monitoring systems enables continuous assessment of THDv and THDi, allowing early detection of abnormal conditions and preventive maintenance planning.

Furthermore, the use of simulation tools such as ETAP proves valuable for hospital power system design and evaluation. ETAP-based harmonic studies allow engineers to predict the impact of future load expansion, assess compliance with power quality standards, and evaluate the effectiveness of mitigation solutions before implementation. This approach minimizes operational risks and supports evidence-based decision-making in healthcare facility management.

Overall, the discussion reinforces that harmonic distortion in hospital electrical distribution systems is not merely a technical issue but a critical operational concern with direct implications for patient safety, equipment reliability, and energy efficiency. Therefore, integrating harmonic analysis

Volume 13, Issue 1, April 2026, pp. 10-19
ISSN 2355-5068 ; e-ISSN 2622-4852
DOI: 10.33019/jurnalecotipe.v13i1.4588

and mitigation planning into hospital electrical system design and maintenance practices is essential to ensure sustainable, safe, and reliable healthcare services.

.

4. CONCLUSION

This study evaluated harmonic distortion in a hospital electrical distribution system using ETAP harmonic load flow simulation. The analysis shows that two low-voltage buses supplying major nonlinear medical equipment exceed the 5% THDv limit, with values of 8.21% and 6.74%. The THDv at the PCC slightly surpasses the recommended threshold, indicating system-wide harmonic propagation.

The THDi at the PCC reaches 14.37%, exceeding the 12% allowable limit for the calculated short-circuit ratio (Isc/IL = 8.43). Dominant 5th and 7th harmonic components confirm the influence of rectifier-based medical equipment and UPS systems.

These findings demonstrate that nonlinear medical loads significantly affect power quality in hospital distribution systems. Implementing appropriate harmonic mitigation strategies is necessary to enhance reliability, reduce losses, and ensure compliance with IEEE 519-2014 standards.

REFERENCES

[1] Ł. Michalec and M. Jasi, "Impact of Harmonic Currents of Nonlinear Loads on Power Quality of a Low Voltage Network – Review and Case Study," 2021, doi: 10.3390/en14123665.

[2] P. Harahap, dkk. "Performance of Grid-Connected Rooftop Solar PV System for Households during Covid-19 Pandemic," *J. Electr. Technol. UMY*, vol. 5, no. 1, pp. 26–31, 2021, doi: 10.18196/jet.v5i1.12089.

[3] "Core Medical Equipment Core medical equipment - Information", [Online]. Available: https://www.who.int/publications/i/item/WHO-HSS-EHT-DIM-11.03

[4] A. Information, "Power Quality," pp. 1–8, 2007, [Online]. Available: https://link.springer.com/book/10.1007/978-1-84628-772-5

[5] E. Sumarno and E. Sumarno, "Analisis Distorsi Harmonisa Kualitas Daya Listrik Tiga Fasa Panel Distribusi Menggunakan Power Quality Analyzer di Rumah Sakit X," vol. 3, no. 2, pp. 147–155, 2025, doi: https://doi.org/10.32493/yepei.v3i2.53736.

[6] IEEE, "Book IEEE Std 519-2014 (Revision of IEEE Std 519-1992), IEEE Recommended Practice and Requirements for Harmonic Control in Electric Power Systems," *IEEE Std 519-2014 (Revision IEEE Std 519-1992)*, vol. 2014, pp. 1–29, 2014, [Online]. Available: http://ieeexplore.ieee.org/servlet/opac?punumber=6826457

[7] U. Wiharja, S. P. Santosa, and L. Aditya, "Harmonic Distortion As A Reference For The Quality Of The Electrical Distribution System In The PT . Gojek Tokopedia Logistics," vol. 13, no. 3, 2023, doi: JITET (Jurnal Informatikadan Teknik Elektro Terapan)Vol. 13No. 3S1, pISSN: 2303-0577 eISSN: 2830-7062.

[8] I. N. Agus *et al.*, "Simulasi Peredaman Distorsi Harmonisa Menggunakan Filter Aktif Dan Analisis Rugi- Rugi Daya Pada Sistem Kelistrikan Di Hotel The Bene Kuta," vol. 4, no. 2, pp. 113–121, 2017, doi: https://doi.org/10.24843/SPEKTRUM.2017.v04.i02.p15.

[9] P. Harahap, M. I. Hamid, and A. Hazmi, "A New 12-Phase Toroidal Transformer Design to Improve Efficiency and Power Quality in Electric Vehicle Fast Charging Systems," vol. 12, no. 2, pp. 245–253, 2025, doi: 10.33019/jurnalecotipe.v12i2.4568.

[10] A. H. Azis, Cholish, Rimbawati, and N. Evalina, "Comparative analysis between the switch mode power supply (SMPS) using IC Tl494cn transformer based on power supply linear," *IOP Conf. Ser. Mater. Sci. Eng.*, vol. 674, no. 1, 2019, doi: 10.1088/1757-899X/674/1/012035.

[11] U. Network and H. Analysis, "Unbalanced Network Harmonic Analysis," pp. 1–8, 2022, [Online]. Available: https://etap.com/product/unbalanced-network-harmonic-

Volume 13, Issue 1, April 2026, pp. 10-19
ISSN 2355-5068 ; e-ISSN 2622-4852
DOI: 10.33019/jurnalecotipe.v13i1.4588

analysis?utm_source=chatgpt.com

[12] K. M. Alawasa and A. H. Al-badi, "Institution ' s Electrical Distribution System," 2024, doi: https://doi.org/10.3390/en17163998.

[13] J. Arrillaga and N. R. Watson, "Power System Harmonics About this book," no. September, pp. 3–5, 2003, doi: 10.1002/0470871229.

[14] P. Harahap, M. I. Hamid, and A. Hazmi, "Comprehensive Review of Advanced Multi-Pulse Rectifier Technology and Its Application in Electric Vehicle Fast Charging Systems," vol. 05, no. 01, 2025.

[15] M. H. J. Bollen and I. Y. Gu, "Signal Processing of Power Quality Disturbances About this book," no. October 2005, pp. 2–5, 2006, doi: 10.1002/0471931314.

[16] C. This, "Power disturbance classifier using a rule-based method and wavelet packet-based hidden Markov model," pp. 1–2, doi: 10.1109/61.974212.

[17] C. This, "519-2014 - IEEE Recommended Practice and Requirements for Harmonic Control in Electric Power Systems," pp. 1–2, 2014, doi: 10.1109/IEEESTD.2014.6826459.

[18] D. Alame, M. Azzouz, and N. Kar, "Assessing and mitigating impacts of electric vehicle harmonic currents on distribution systems," *Energies*, vol. 13, no. 12, 2021, doi: 10.3390/en13123257.

[19] F. G. Merconchini, L. V. Seidedos, J. C. Oliva, J. Ricardo, N. Alvarez, and D. Checa-cervantes, "Study of electric power quality indicators by simulating a hybrid generation system," vol. 14, no. 2, pp. 1044–1054, 2023, doi: 10.11591/ijpeds.v14.i2.pp1044-1054.

[20] A. F. Abidin, N. I. K. Hakimi, and N. I. K. Ali, "Turkish Journal of Electrical Engineering and Computer Sciences Harmonic classification of different lighting technologies using empirical mode decomposition and support vector machines," vol. 33, no. 3, 2025, doi: 10.55730/1300-0632.4130.

[21] Y. M. Al-sharif, G. M. Sowilam, and T. A. Kawady, "Harmonic Analysis of Large Grid-Connected PV Systems in Distribution Networks : A Saudi Case Study," vol. 2022, 2022.

[22] Harmonic propagation on an electric distribution system : Field measurements compared with computer simulation," 1993.

[23] A. Jamal, S. G. Putri, A. Nur, N. Chamim, and R. Syahputra, "Power Quality Evaluation for Electrical Installation of Hospital Building," vol. 10, no. 12, pp. 380–388, 2019.

[24] J. Arteaga, Y. U. López, and J. A. López, "Decoding Harmonics : Total Harmonic Distortion in Solar Photovoltaic Systems with Integrated Battery Storage," 2025.

[25] S. F. Mekhamer, "Design Practices in Harmonic Analysis Studies Applied to Industrial Electrical Power Systems," vol. 3, no. 4, pp. 467–472, 2013.

[26] P. Quality and E. Machines, *Power Quality in Power Systems and Electrical Machines*.

JURNAL ECOTIPE
Electronic, Control, Telecommunication, Information, and Power Engineering
Volume 13, Issue 1, April 2026, pp. 20-30
ISSN 2355-5068 ; e-ISSN 2622-4852
DOI: 10.33019/jurnalecotipe.v13i1.4573

Design and Operational Evaluation of Off-Grid Solar Power Plants with Integrated Automatic Cleaning Systems for Enhanced Performance

Akbar Abadi[1], Nazris Nazaruddin[2], Yani Kamisa Putri[3], Dedi Erawadi[4], Herisajani[5], Hanalde Andre[6], Ahmad Ilyas Putra Riancefi[7]
[1,2,3,4,5,7,] Electrical Engineering, Padang State Polytechnics, Jl.Kampus, Limau Manis, Padang 25164, Indonesia.
[6] Department of Electrical Engineering, Universitas Andalas, Padang, Indonesia

ARTICLE INFO

Article historys:

Received : 08/08/2025
Revised : 05/02/2026
Accepted : 30/04/2026

Keywords:

Automatic Solar Panel; Low-Voltage Disconnect; Off-grid Photovoltaic System; PV Performance; Solar Charge Controller

ABSTRACT

This study details the design and experimental evaluation of an off-grid photovoltaic (PV) system equipped with an automatic solar panel cleaning mechanism to address performance degradation due to dust accumulation. The system integrates a mechanical wiper-based cleaning unit, solar charge controller (SCC), inverter, and low-voltage disconnect (LVD) to maintain reliable and stable operation in stand-alone settings. Experimental tests were performed on a 50 Wp PV module under actual outdoor conditions in Padang, Indonesia. System performance was assessed before and after panel cleaning using key electrical parameters, such as output voltage, current, output power, and relative efficiency improvement. Results show that the automatic cleaning mechanism increased the average PV output power from 0.88 W to 1.71 W, representing an efficiency improvement of approximately 11.89% compared to the uncleaned state. In contrast to previous studies that focus on grid-connected systems or manual cleaning methods, this research introduces a low-cost, self-operating cleaning solution tailored for small-scale off-grid PV applications in tropical environments. The proposed system offers practical benefits for enhancing energy yield, system reliability, and maintenance efficiency in remote solar installations.

Corresponding Author:

Akbar Abadi
Electrical Engineering, Padang State Polytechnics, Jl.Kampus, Limau Manis, Padang 25164, Indonesia.
Email: akbarabadi@ono.ac.id

1. INTRODUCTION

Renewable energy is a sustainable and eco-friendly source of power that can decrease reliance on fossil fuels, thereby contributing to a reduction in greenhouse gas emission. Additionally, renewable energy power plants can provide electricity to remote regions that lack accsess to teh electical grid. A potential renewable energy source in Indonesia is solar energy which has an average solar radiation intensity of around 4.8 kWh/m2 per day throughout Indonesia[1][2]. Solar photovoltaic (PV) technology converts solar radiation into electrical energy through the photovoltaic effect, in which photons excite charge carriers in semiconductor materials, generating direct current electricity[3][4][5]. The more energy absorbed by the solar panel, the more electrical energy is generated. However, this does not apply if the surface of the solar panel is not clean because it is caused by several factors that can reduce the efficiency of the solar panel [6].

JURNAL ECOTIPE
Electronic, Control, Telecommunication, Information, and Power Engineering
Volume 13, Issue 1, April 2026, pp. 20-30
ISSN 2355-5068 ; e-ISSN 2622-4852
DOI: 10.33019/jurnalecotipe.v13i1.4573

Off-grid solar PV systems face critical challenges related to system reliability, energy availability, and strong dependence on battery storage[7]. Variations in solar irradiance can cause unstable power supply, while limited battery capacity and charging efficiency directly affect load continuity and system reliability[8]. Any reduction in PV generation efficiency shortens battery autonomy and increases the risk of load disconnection, thereby degrading overall system performance.

One of the major factors that degrades PV performance is surface soiling caused by dust, dirt, water stains, leaves, and other particles [9], [10], [11], [12], . In addition, there are other factors, namely the implementation of unscheduled cleaning causing the accumulation of dust or dirt or objects on the surface of the solar panel and human error when cleaning the surface of the solar panel which has the potential to damage one of the cells on the solar panel [13] .

Previous studies report that dust accumulation can reduce PV output by approximately 10% in mild conditions and over 40% in arid environments [14]. In off-grid systems, such losses directly degrade battery charging performance and supply reliability, making panel cleanliness critical for stable energy availability and system operation. Automatic cleaning systems provide an effective solution by enabling regular maintenance, reducing human error, and minimizing the risk of surface damage compared to manual cleaning [15], [16]. This approach is particularly beneficial for remote off-grid installations, as it helps sustain energy production, extend battery lifetime, and improve overall system reliability.

Although many studies have examined the effects of dust accumulation and cleaning methods on PV performance, most focus on grid-connected or laboratory-scale systems. Comprehensive investigations that integrate the design and operational performance evaluation of automatic cleaning systems in real off-grid PV applications, including their interaction with energy management components, remain limited. This gap restricts practical understanding of the long-term reliability and energy sustainability of off-grid PV systems.

This study aims to design and evaluate an off-grid PV system integrated with an automatic cleaning mechanism. The objectives are to assess system performance before and after cleaning and to analyze the impact of panel cleanliness on energy generation, battery charging, and system reliability. The main contributions of this study include the development of an integrated off-grid PV system with automatic cleaning and an experimental evaluation of its operational performance under real environmental conditions, providing practical insights for off-grid PV deployment.

2. RESEARCH METHOD

2.1. Design

The proposed off-grid PV system consists of a 50 Wp solar panel, a solar charge controller (SCC), a 12 V 8 Ah battery, a low voltage disconnect (LVD), an inverter, and an AC load in the form of a 5 W LED lamp. The SCC regulates the battery charging process to prevent overcharging and deep discharge, while the LVD protects the battery by disconnecting the load when the voltage drops below a predefined threshold. The design of the tool can be seen in Figure 1 and Figure 2.

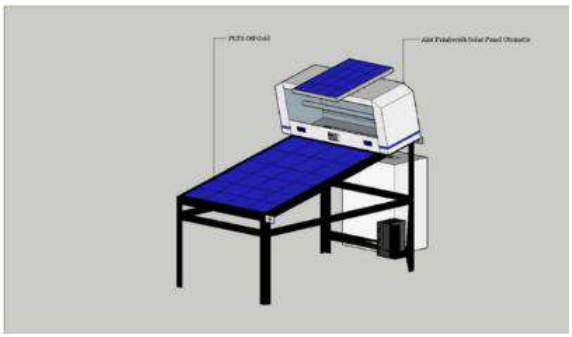

Figure 1. Design tools

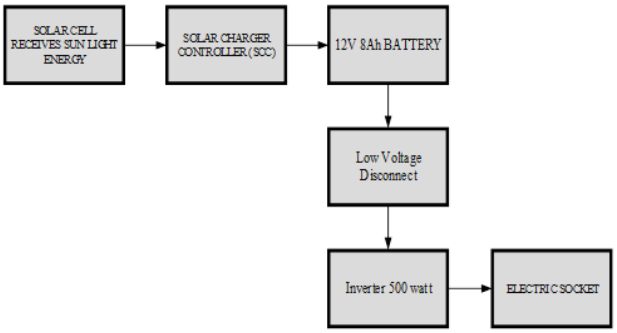

Figure 2. Schematic for off-grid solar power plant planning

JURNAL ECOTIPE
Electronic, Control, Telecommunication, Information, and Power Engineering
Volume 13, Issue 1, April 2026, pp. 20-30
ISSN 2355-5068 ; e-ISSN 2622-4852
DOI: 10.33019/jurnalecotipe.v13i1.4573

Based on the Figure 2 illustrates the operational configuration of the proposed system. The system utilizes a 50 Wp solar panel as the primary power source. The solar panel converts solar irradiance into electrical energy, which is subsequently stored in a 12 V, 8 Ah battery. The battery charging process is regulated by a solar charge controller (SCC) to control the charging voltage, prevent overcharging, and provide protection during the charging process. The battery output is connected to a low voltage disconnect (LVD), which manages load connection and disconnection based on the battery voltage level. The output of the LVD is then connected to a 12 V DC relay coil, which activates the inverter through the relay contacts. The inverter converts direct current (DC) into alternating current (AC), and the AC output is finally supplied to the electrical socket to power the load, that can see in Figure 3.

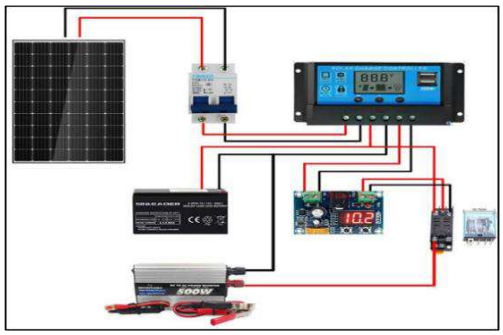

Figure 3. PLTS wiring diagram

The wiring diagram in Figure 3 presents the wiring configuration of the off-grid PV system. The battery is connected first to the solar charge controller (SCC) to enable automatic voltage detection and prevent controller damage. The PV module is then connected to the low voltage disconnect (LVD), which regulates the battery–load connection based on battery voltage. Finally, the battery output is supplied to the inverter to provide AC power to the load.

2.2. Flowchart

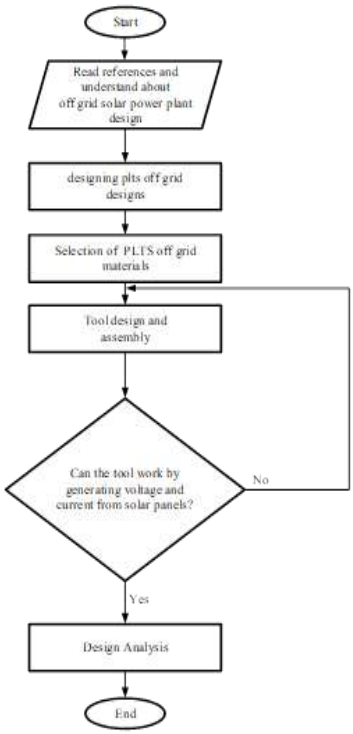

Figure 4. Flowchart

Volume 13, Issue 1, April 2026, pp. 20-30
ISSN 2355-5068 ; e-ISSN 2622-4852
DOI: 10.33019/jurnalecotipe.v13i1.4573

The automatic cleaning mechanism employs a mechanical wiper driven by a DC motor powered by the system battery. The wiper moves linearly across the surface of the solar panel to remove dust and dirt without using water, thereby minimizing energy consumption and maintenance requirements. Cleaning is activated at predetermined intervals to ensure consistent panel cleanliness while avoiding excessive mechanical wear. This design prioritizes simplicity, reliability, and suitability for off-grid applicationsThe flowchart in Figure 4 explains how the automatic solar panel cleaning tool works concisely and efficiently.

3. RESULTS AND DISCUSSION

3.1. Solar Panel Device Analysis

The tool's overall form, which includes the off-grid PLTS design, is shown in Figure 5. After putting this instrument through its paces, testing revealed that it functions as intended and that each of its parts is functional and appropriate for use.

Figure 1. Overall Structure of the Tool

3.2. Solar Panel Device Analysis

Solar panels convert solar radiation into electrical energy through the photovoltaic effect. The electrical output depends on solar irradiance, where higher irradiance results in higher voltage and current. The generated energy is used to charge the battery, and the charging process is influenced by weather conditions and solar intensity.The solar charge controller (SCC) regulates the battery charging process by preventing overcharging and deep discharge, thereby extending battery lifetime. In addition, the SCC provides protection and ensures safe and stable battery operation during charging.

3.3. Testing on Solar Panels (Solar Cells)

Experimental testing was conducted under outdoor conditions with varying solar irradiance and weather conditions. Measurements were taken at 30-minute intervals over a 4.5-hour period. The evaluated parameters included output voltage (V), output current (A), and output power (W), calculated as the product of voltage and current. Relative efficiency improvement was determined by comparing the electrical output before and after panel cleaning. Environmental conditions such as solar irradiance (lux) and weather conditions were recorded to support result interpretation. The testing and measurement of the solar panel before and after cleaned up can be seen in Figure 6 and Figure 7.

Figure 6. Testing and measuring solar panels before cleaned up

Figure 7. Testing and measuring solar panels after cleaned up

JURNAL ECOTIPE
Electronic, Control, Telecommunication, Information, and Power Engineering
Volume 13, Issue 1, April 2026, pp. 20-30
ISSN 2355-5068 ; e-ISSN 2622-4852
DOI: 10.33019/jurnalecotipe.v13i1.4573

3.4. Solar Panel Test Data

1) Solar panel test data before cleaning Tuesday/July 23, 2024

Based on the test data results obtained from testing before the panel was cleaned on Tuesday, July 23, 2024, which can be seen in Table 1. The results of the voltage and current produced can also be seen in Figure 8.

Table 1. Solar panel testing before cleaned up Tuesday / July 23 , 2024

NO	Time	LUX (x100)	Weather Condition	Digital VoltmeterAmmeter			Volt SCC	PV Module Voltage (V)
				V	I	W		
1	11:00	314	Sunny and Cloudy	12,4	0,06	0,74	12,5	18,50
2	11.30	216	Sunny and Cloudy	12,2	0,05	0,61	12,5	17,80
3	12.00	901	Sunny	12,6	0,10	2,15	12,6	19,67
4	12.30	118	Cloudy	12	0	0	12,4	17,4

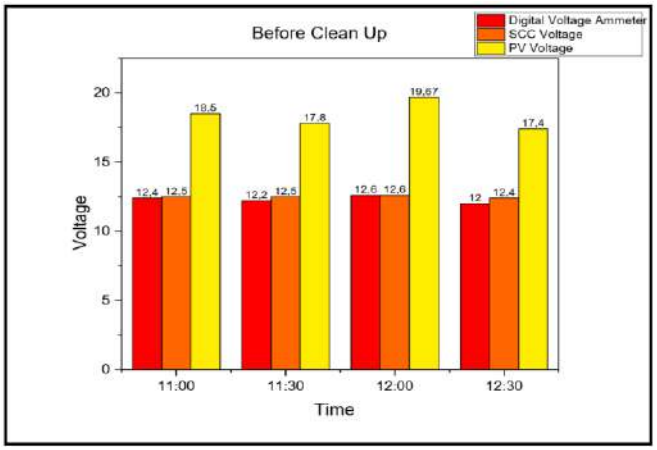

Figure 2. Voltage and current on Solar Charger Controller and digital voltamper meter

Find the average voltage using the following equation:

$$\text{Average} = \frac{Vtotal}{h} \quad (1)$$

Where :

$V_{average}$ = Average charging voltage (V)

V_{total} = Total charging voltage from 11.00 – 12.30 (V)

h = Test duration (per- 30 minutes)

Average Voltage of Solar Panels

$$\text{Average} = \frac{Vtotal}{h}$$

$$= \frac{18{,}50+17{,}80+19{,}67+17{,}4}{4} = 18.34 \text{ V}$$

Finding the average current on a digital ammeter can be done using the following equation:

$$\text{I average} = \frac{\text{Itotal}}{h} \quad (2)$$

Where :

I average = Average charging current (A)

I tot = Total charging current from 11.00- 12.30(A)

h = Test duration (Per 30 minutes)

Based on the equation above, the average battery charging current can be calculated using data from the test table. The following is the calculation for finding the average current:

Volume 13, Issue 1, April 2026, pp. 20-30
ISSN 2355-5068 ; e-ISSN 2622-4852
DOI: 10.33019/jurnalecotipe.v13i1.4573

$$\text{Average} = \frac{\text{Itotal}}{h}$$
$$= \frac{0{,}06+0{,}05+0{,}10+0}{4} = 0.052 \text{ A}$$

2) Solar panel test data during charging after cleaning on Tuesday/23 July 2024

Based on the test data results obtained from testing after the panel was cleaned on Tuesday, July 23, 2024, which can be seen in Table 2. The results of the voltage and current produced can also be seen in Figure 9.

Table 2. Solar panel testing after cleaned up Tuesday / July 23 , 2024

NO	Time	LUX (x100)	Weather Condition	Digital Voltmeter Ammeter			Volt SCC	PV Module Voltage (V)
				V	I	W		
1	13:00	700	Sunny	12,6	0,16	2,01	12,6	20,52
2	13.30	684	Cloudy	12,5	0,12	1,5	12,5	20,3
3	14.00	912	Sunny	12,7	0,19	2,41	12,5	21,6
4	14.30	211	Cloudy	12,4	0,08	0,9	12,5	18,58

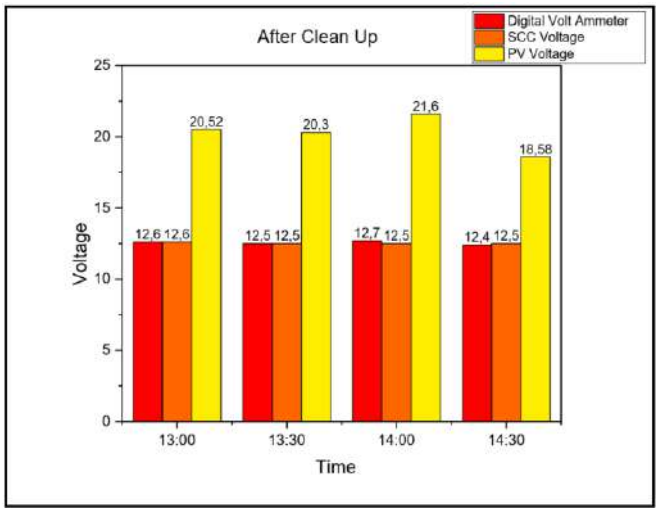

Figure 3. Voltage and current on *the* Solar Charger Controller and digital voltampere meter

Find the average voltage using the following equation (1):

Average Voltage of Solar Panels

$$\text{Average} = \frac{\text{Vtotal}}{h}$$
$$= \frac{20{,}52+20{,}3+21{,}6+18{,}58}{4} = 20.52 \text{ V}$$

Based on the equation (2) above, the average battery charging current can be calculated using data from the test table. The following is the calculation for finding the average current:

$$\text{Average} = \frac{\text{Itotal}}{h}$$
$$= \frac{0{,}16+0{,}12+0{,}19+0{,}08}{4} = 0.13 \text{ A}$$

3) Effect of Panel Cleaning on PV Output Power

Volume 13, Issue 1, April 2026, pp. 20-30
ISSN 2355-5068 ; e-ISSN 2622-4852
DOI: 10.33019/jurnalecotipe.v13i1.4573

As a representative indicator of photovoltaic system performance, the output power was used to assess the effectiveness of the proposed cleaning mechanism. Accordingly, the output power of the photovoltaic module was calculated using the basic electrical relationship:

$$P = V\ X\ \mathrm{I} \tag{3}$$

where:
P is the output power of the photovoltaic module (W), V is the measured output voltage of the PV module (V), and I is the measured output current of the PV module (A).

Therefore, the average output power before cleaning was calculated as:

$$P_{\text{before}} = V_{\text{before}} \times I_{\text{before}}$$
$$P_{\text{before}} = 18.34 \times 0.052 \approx 0.88\ \text{W}$$

After the panel cleaning process, the average output voltage and current were measured as:

$$V_{\text{after}} = 20.52\ \text{V}$$
$$I_{\text{after}} = 0.13\ \text{A}$$

Thus, the average output power after cleaning was calculated as:

$$P_{\text{after}} = V_{\text{after}} \times I_{\text{after}}$$
$$P_{\text{after}} = 20.52 \times 0.13 \approx 1.71\ \text{W}$$

The relative performance improvement of the photovoltaic module due to the panel cleaning process was quantified based on the output power using the following expression:

$$\eta_{\text{improvement}}(\%) = \frac{P_{\text{after}} - P_{\text{before}}}{P_{\text{before}}} \times 100\% \tag{4}$$

where:
$\eta_{\text{improvement}}$ is the relative performance improvement (%), P_{before} is the average output power before cleaning (W), P_{after} is the average output power after cleaning (W)

Therefore, the relative performance improvement is calculated as follows:

$$\eta_{\text{improvement}} = \frac{1.71 - 0.88}{0.88} \times 100\%$$
$$\eta_{\text{improvement}} = \frac{0.83}{0.88} \times 100\% \approx 94.32\%$$

This result indicates that the output power of the photovoltaic module increased by approximately 94.32% after the application of the automatic cleaning mechanism. The relatively high percentage improvement is attributed to the low initial output power under soiled panel conditions and moderate solar irradiance during the experimental period, which makes the relative increase more pronounced after cleaning.

4) Solar Panel Cleaning Efficiency

To calculate the efficiency of solar panel cleaning, we can compare the voltage (V) produced by the solar panel before and after cleaning using the following equation:

$$Efisiensi = \frac{\bar{V}_{After} - \bar{V}_{Before}}{\bar{V}_{before}}\ x\ 100\% \tag{5}$$
$$Efisiensi = \frac{20{,}52 - 18{,}34}{18{,}34}\ x\ 100\% = 11.89\%$$

Based on the calculation above, the result of the increase in solar panel efficiency is 11.89%. This means that after cleaning, the solar panel produces a voltage of about 11.89% compared to before cleaning.

JURNAL ECOTIPE
Electronic, Control, Telecommunication, Information, and Power Engineering
Volume 13, Issue 1, April 2026, pp. 20-30
ISSN 2355-5068 ; e-ISSN 2622-4852
DOI: 10.33019/jurnalecotipe.v13i1.4573

3.5. The Effect of Light Intensity on Current, Voltage, and Power Output

Graph of the effect of solar irradiance on the output current and power of the PV module before cleaning. Under the pre-cleaning condition, solar irradiance increased from 11,800 lux to 90,100 lux, resulting in an increase in output voltage from 17.4 V to 19.67 V, output current from 0 A to 0.10 A, and output power from 0 W to 1.97 W., can also be seen in Figure 10.

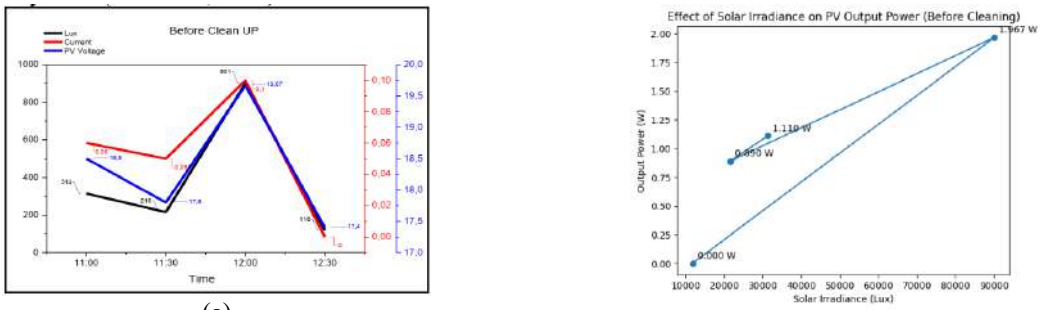

(a) (b)

Figure 10. Graph influence intense i bag sunlight to (a) current and voltage, (b) power output before cleaned up

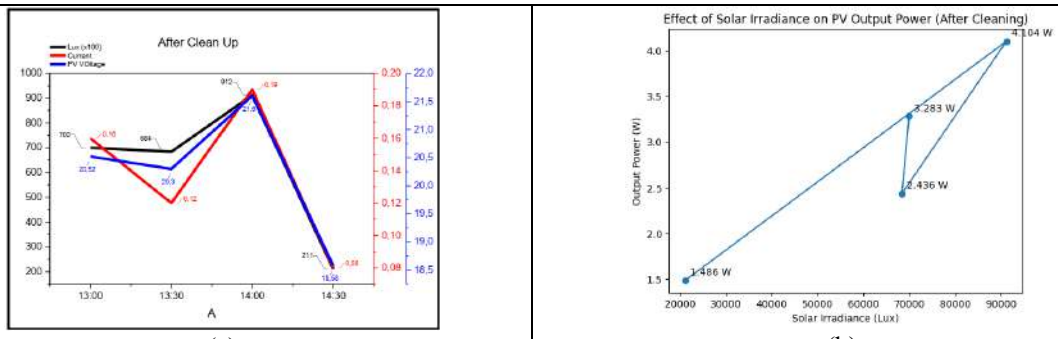

(a) (b)

Figure 11. Graph influence intense i bag sunlight to (a) current and voltage, (b) power output after cleaned up

Figure 11 illustrates the effect of solar irradiance on the PV module output power after the panel cleaning process. Following cleaning, an increase in solar irradiance from 21,100 lux to 91,200 lux resulted in a corresponding rise in output power from 1.49 W to 4.10 W. The results indicate that higher solar irradiance leads to greater power generation; however, for similar irradiance levels, the post-cleaning condition yields significantly higher output power compared to the pre-cleaning condition. This improvement demonstrates that the removal of surface soiling effectively enhances light absorption by the PV module, thereby improving energy conversion efficiency and overall system performance.

3.6. Battery Calculation

1. Calculating battery charging time

To calculate the charging time and battery usage time, we use an efficiency of 80%. Since the battery capacity used is 8Ah, the battery capacity used is:
Used capacity = 80% x 8 Ah = 6.4 Ah.
Based on the equation above, the battery charging time can be calculated as follows:

$$Charging\ Time\ (h) = \frac{Battery\ Capacity \times \eta battery}{Charging\ Current \times \eta charger} \quad (6)$$

where:

Charging Time (h) is the required time to fully charge the battery (hours), *Battery Capacity* is the rated battery capacity (Ah), Charging Current is the average charging current (A), $\eta_{battery}$ is the battery efficiency, and $\eta_{charger}$ is the efficiency of the charging system (e.g., solar charge controller).

JURNAL ECOTIPE
Electronic, Control, Telecommunication, Information, and Power Engineering
Volume 13, Issue 1, April 2026, pp. 20-30
ISSN 2355-5068 ; e-ISSN 2622-4852
DOI: 10.33019/jurnalecotipe.v13i1.4573

Based on the equation presented above, the charging current generated by the photovoltaic module can be calculated as follows:

$$I_{\text{charge}} = \frac{P_{\text{in}} \times \eta}{V_{\text{battery}}} \tag{7}$$

where:

I_{charge} is the charging current (A), P_{in} is the input power from the solar panel (W), η is the charging system efficiency, and V_{battery} is the nominal battery voltage (V).

By substituting the measured values into Eq. (7), the charging current is obtained as:

$$I_{\text{charge}} = \frac{50 \times 0.80}{12} = 3.33 \text{ A}$$

Once the charging current is determined, the required charging time can be estimated using:

$$t_{\text{charge}} = \frac{C_{\text{battery}}}{I_{\text{charge}} \times \eta} \tag{8}$$

where:

t_{charge} is the charging time (h), and C_{battery} is the battery capacity (Ah).

Thus, for a 12 V battery with a capacity of 6.4 Ah, the estimated charging time is:

$$t_{\text{charge}} = \frac{6.4}{3.33 \times 0.80} \approx 2.40 \text{ h}$$

Based on the calculation results, a 12 V battery with a nominal capacity of 6.4 Ah charged at an average current of 3.33 A requires approximately 2.40 h to reach full charge, assuming a charging system efficiency of 80%.

2. Calculating battery discharge time

Battery capacity utilization can be evaluated through analytical calculation. The duration for which the battery can supply the load (discharge time) can be estimated using the following equation:

$$t_{\text{discharge}} = \frac{C_{\text{battery}} \times \eta_{\text{battery}}}{I_{\text{DC}}} \tag{9}$$

where:

$t_{\text{discharge}}$ is the battery discharge time (h), C_{battery} is the battery capacity (Ah), η_{battery} is the battery efficiency, and I_{DC} is the DC current drawn from the battery (A).

To determine the DC current drawn from the battery when supplying an AC load through an inverter, the DC input power to the inverter is first calculated as:

$$P_{\text{DC}} = \frac{P_{\text{AC}}}{\eta_{\text{inv}}} \tag{10}$$

where:

P_{DC} is the DC input power to the inverter (W), P_{AC} is the AC load power (W), and η_{inv} is the inverter efficiency.

For a 5 W LED lamp supplied through an inverter with an efficiency of 85%, the required DC input power is:

$$P_{\text{DC}} = \frac{5}{0.85} = 5.88 \text{ W}$$

The corresponding DC current drawn from a 12 V battery is then calculated as:

$$I_{\text{DC}} = \frac{P_{\text{DC}}}{V_{\text{battery}}} \tag{11}$$

$$I_{\text{DC}} = \frac{5.88}{12} = 0.49 \text{ A}$$

Volume 13, Issue 1, April 2026, pp. 20-30
ISSN 2355-5068 ; e-ISSN 2622-4852
DOI: 10.33019/jurnalecotipe.v13i1.4573

Once the DC current is obtained, the battery discharge time can be estimated as:

$$t_{\text{discharge}} = \frac{6.4}{0.49} \approx 13.06\,\text{h}$$

Based on the calculation results, a 12 V battery with a nominal capacity of 6.4 Ah can supply a 5 W AC load through an inverter with 85% efficiency for approximately 13 h under the assumed operating conditions.

4. CONCLUSION

This study demonstrates that integrating an automatic solar panel cleaning mechanism into a small-scale off-grid photovoltaic system can significantly enhance electrical performance and operational reliability. Experimental results show that panel cleaning increased the average output power from 0.88 W to 1.71 W, corresponding to a relative performance improvement of approximately 94.32% under the tested operating conditions. This substantial increase confirms that surface soiling imposes significant optical losses on photovoltaic modules and that the proposed cleaning mechanism effectively restores light transmittance, thereby improving power generation. The integration of a solar charge controller, inverter, and low voltage disconnect further enhances battery protection and overall system stability.

The primary contribution of this work lies in the development of a practical, low-cost, and easily implementable automatic cleaning solution to enhance off-grid PV system performance in tropical environments. Although the results are promising, this study is limited by the relatively short testing duration and the specific environmental conditions considered. Therefore, future research should focus on long-term performance evaluation across different seasons, optimization of cleaning frequency, assessment of the energy consumption of the cleaning mechanism, and comparative analysis with alternative automatic cleaning technologies to further strengthen the scientific contribution and practical applicability of the proposed system.

REFERENCES

[1] H. Sikumbang, A. Haris, and M. J. Elly, “Sistem Kendali Dan Monitoring Dengan Syaraf Tiruan Pada Pembangkit Listrik Tenaga Surya,” *Petir*, vol. 13, no. 2, pp. 119–127, 2020, doi: 10.33322/petir.v13i2.1066.

[2] L.-H. Fatima, L. N. Mamadou, K. U. Anna, and C. A. Mohamed, “Performance analysis of the 23 MWp grid connected photovoltaic plant in Diass Senegal,” *Int. J. Phys. Sci.*, vol. 16, no. 4, pp. 115–122, 2021, doi: 10.5897/ijps2021.4953.

[3] C. Egbon, A. Oyekola, and T. T. Lie, “Design of stand alone photovoltaic system in developing countries: A case study of Kano, Nigeria,” *Australas. Univ. Power Eng. Conf. AUPEC 2018*, pp. 1–6, 2018, doi: 10.1109/AUPEC.2018.8757895.

[4] A. Syafiq, A. K. Pandey, N. N. Adzman, and N. A. Rahim, “Advances in approaches and methods for self-cleaning of solar photovoltaic panels,” *Sol. Energy*, vol. 162, no. May 2017, pp. 597–619, 2018, doi: 10.1016/j.solener.2017.12.023.

[5] A. K. Pandey, V. V. Tyagi, J. A. Selvaraj, N. A. Rahim, and S. K. Tyagi, “Recent advances in solar photovoltaic systems for emerging trends and advanced applications,” *Renew. Sustain. Energy Rev.*, vol. 53, pp. 859–884, 2016, doi: 10.1016/j.rser.2015.09.043.

[6] S. S. Panagoda *et al.*, “Advancements In Photovoltaic (Pv) Technology for Solar Energy Generation,” *J. Res. Technol. Eng*, vol. 4, no. 3, pp. 30–72, 2023, [Online]. Available: https://www.researchgate.net/publication/372364724

[7] J. E. Madu, K. E. ; Nosegbe, U. ; Orhorhoro, E. K. ; and Igbagbon, “Performance Evaluation of a Photovoltaic System for Household in Asaba, Nigeria,” *Afropolitan Journals*, vol. 19, no. 1, pp. 42–60, 2025, doi: https://doi.org/10.62154/ajesre.2025.019.01012.

Volume 13, Issue 1, April 2026, pp. 20-30
ISSN 2355-5068 ; e-ISSN 2622-4852
DOI: 10.33019/jurnalecotipe.v13i1.4573

[8] L. M. Adesina, O. Ogunbiyi, and K. Makinde, "Design, implementation and performance analysis of an off- grid solar powered system for a Nigerian household," *MethodsX*, vol. 10, no. December 2022, 2023, doi: 10.1016/j.mex.2023.102247.

[9] I. Al Siyabi, A. Al Mayasi, A. Al Shukaili, and S. Khanna, "Effect of soiling on solar photovoltaic performance under desert climatic conditions," *Energies*, vol. 14, no. 3, 2021, doi: 10.3390/en14030659.

[10] A. A. Hachicha, I. Al-Sawafta, and Z. Said, "Impact of dust on the performance of solar photovoltaic (PV) systems under United Arab Emirates weather conditions," *Renew. Energy*, vol. 141, pp. 287–297, 2019, doi: 10.1016/j.renene.2019.04.004.

[11] H. Abuzaid, M. Awad, and A. Shamayleh, "Impact of dust accumulation on photovoltaic panels: a review paper," *Int. J. Sustain. Eng.*, vol. 15, no. 1, pp. 266–287, 2022, doi: 10.1080/19397038.2022.2140222.

[12] A. Shariah and E. A. Al-Ibrahim, "Impact of Dust and Shade on Solar Panel Efficiency and Development of a Simple Method for Measuring the Impact of Dust," *J. Sustain. Dev. Energy, Water Environ. Syst.*, vol. 11, no. 2, pp. 1–14, 2023, doi: 10.13044/j.sdewes.d11.0448.

[13] M. Rashid, M. Yousif, Z. Rashid, A. Muhammad, M. Altaf, and A. Mustafa, "Effect of dust accumulation on the performance of photovoltaic modules for different climate regions," *Heliyon*, vol. 9, no. 12, pp. 957–964, 2023, doi: 10.1016/j.heliyon.2023.e23069.

[14] R. Nahar Myyas, M. Al-Dabbasa, M. Tostado-Véliz, and F. Jurado, "A novel solar panel cleaning mechanism to improve performance and harvesting rainwater," *Sol. Energy*, vol. 237, no. May, pp. 19–28, 2022, doi: 10.1016/j.solener.2022.03.068.

[15] H. A. Kazem, M. T. Chaichan, A. H. A. Al-Waeli, and K. Sopian, "A review of dust accumulation and cleaning methods for solar photovoltaic systems," *J. Clean. Prod.*, vol. 276, p. 123187, 2020, doi: 10.1016/j.jclepro.2020.123187.

[16] M. R. W. Kusuma, E. Apriaskar, and D. Djunaidi, "Rancang Bangun Sistem Pembersih Otomatis Pada Solar Panel Menggunakan Wiper Berbasis Mikrokontroler," *Techné J. Ilm. Elektrotek.*, vol. 19, no. 01, pp. 23–32, 2020, doi: 10.31358/techne.v19i01.220.

JURNAL ECOTIPE
Electronic, Control, Telecommunication, Information, and Power Engineering

Volume 13, Issue 1, April 2026, pp. 31-42
ISSN 2355-5068 ; e-ISSN 2622-4852
DOI: 10.33019/jurnalecotipe.v13i1.4580

Intelligent Fault Detection In a 25 MVA Transformer Using ANFIS

Azriyenni Azhari Zakri[1], Hari Firdaus[2], Wahri Sunanda[3], Boy Ihsan[4], Jafaru Usman[5]
[1,2,4] Department of Electrical Engineering, Faculty of Engineering, Universitas Riau, Riau, Indonesia
[3] Department of Electrical Engineering, Universitas Bangka Belitung, Bangka, Indonesia
[5]Department of Electrical and Electronic Engineering, Faculty of Engineering, University of Maiduguri, Nigeria

ARTICLE INFO

Article historys:

Received : 10/09/2025
Revised : 16/02/2026
Accepted : 30/04/2026

Keywords:

Adaptive Neuro-Fuzzy Inference System (ANFIS); Digital Relay Protection; Fault Classification; Power Transformer

ABSTRACT

This study aims to develop an intelligent fault prediction model for a 25 MVA power transformer using the Adaptive Neuro-Fuzzy Inference System (ANFIS), to improve classification accuracy and ensure selective, reliable protection decisions in power systems. The research is grounded in the limitations of traditional differential relay protection, which struggles to distinguish between internal and external faults during transient conditions. ANFIS combines fuzzy logic's ability to handle uncertainty with the adaptive learning of neural networks, making it a suitable tool for non-linear fault data analysis. A simulation was carried out in MATLAB/Simulink. Current signals from CTs on both primary and secondary sides served as input features. The model was trained using 270 data samples and tested with 30 samples. Two membership functions generalized bell-shaped (Gbell) and triangular (Tri) were evaluated. RMSE was used as the performance metric. The ANFIS model with Gbell MF yielded a lower RMSE (0.0116) compared to Tri MF (0.0445), indicating better prediction accuracy and stability. The system consistently identified internal faults (output 1), and external faults (output 0) based on a 0.5 decision threshold. The findings validate the potential of ANFIS for integration into digital relay systems, enhancing real-time transformer protection through adaptive learning.

Corresponding Author:

Azriyenni Azhari Zakri
Department of Electrical Engineering, Faculty of Engineering, Universitas Riau, Indonesia
Email: azriyenni@eng.unri.ac.id

1. INTRODUCTION

Power transformers play a fundamental role in electrical power systems by enabling energy transfer across different voltage levels [1]. Because they operate as strategic nodes within transmission and generation networks, transformer failures may trigger extensive system disturbances and lead to substantial economic losses [2]. For this reason, protection schemes must ensure high reliability, selectivity, and fast operation. Differential protection (87T) remains one of the most widely implemented methods, operating on the principle of comparing primary and secondary currents within a defined protection zone [3], [4]. Despite its practical effectiveness, conventional differential relays encounter limitations under transient conditions, particularly in discriminating internal faults from external disturbances during magnetizing inrush or other dynamic events [5-7].

Internal faults occur within the transformer protection zone, such as inter-winding faults or ground faults, and may result in severe and irreversible damage. In contrast, external faults originate outside

Volume 13, Issue 1, April 2026, pp. 31-42
ISSN 2355-5068 ; e-ISSN 2622-4852
DOI: 10.33019/jurnalecotipe.v13i1.4580

the protected zone and generally do not necessitate transformer isolation [8]. Incorrect classification of these conditions can either cause unnecessary tripping or delay protective action, both of which compromise system stability and asset integrity.

In response to increasing system complexity, Artificial Intelligence (AI) has emerged as a promising tool for enhancing power system operation, planning, and control [9-11]. Within the protection domain, AI-based methods have been explored to overcome the rigidity of deterministic threshold-based logic. Techniques such as Artificial Neural Networks (ANN), Fuzzy Logic, Support Vector Machines (SVM), and hybrid models have demonstrated improved adaptability and classification capability in power system fault analysis [12-15].

Among these approaches, the Adaptive Neuro-Fuzzy Inference System (ANFIS) integrates the learning capacity of neural networks with the uncertainty-handling capability of fuzzy inference. The standard ANFIS framework consists of five layers encompassing fuzzification, rule evaluation, normalization, and defuzzification processes [16]. Its structure enables nonlinear mapping between input features and classification outputs, making it suitable for modeling complex fault current patterns. The selection of membership functions (MF), such as generalized bell-shaped and triangular types, directly influences training convergence and prediction performance [17], [18].

ANFIS has been extensively investigated for fault detection and classification in power networks [19-21]. In transformer protection applications, it has shown the ability to distinguish internal faults, external faults, and transient inrush conditions with high accuracy. Azriyenni et al. [22], for example, demonstrated the effectiveness of ANFIS in differential relay protection by achieving accurate classification across multiple fault scenarios, including single-phase-to-ground and three-phase faults. Furthermore, hybrid approaches integrating ANFIS with signal processing techniques have been reported. Suliman and Al-Khayyat [23] combined Discrete Wavelet Transform (DWT) with ANFIS to extract transient features from differential currents, enabling accurate discrimination between inrush and internal faults using MATLAB/Simulink and laboratory validation. Similarly, Salama et al. [24] implemented a DWT-ANFIS protection algorithm for a 40 MVA transformer, confirming reliable and fast fault identification through ATP/EMTP and MATLAB/Simulink simulations.

Despite these advancements, studies integrating a physically validated equivalent circuit model with ANFIS-based protection for medium-capacity transformers remain limited. This study addresses that gap by developing and validating an ANFIS-based fault discrimination model for a 25 MVA transformer using a realistic equivalent circuit representation. The proposed framework evaluates the impact of two membership function types generalized bell and triangular on classification performance and is implemented within a MATLAB/Simulink environment. By coupling detailed transformer modeling with adaptive fault classification, this work aims to enhance selectivity and robustness in transformer differential protection.

The main contribution of this study lies in the structured integration of a physically parameterized 25 MVA transformer equivalent circuit with an ANFIS-based adaptive fault classification framework within a unified MATLAB/Simulink environment. Unlike conventional differential protection approaches that rely on fixed harmonic restraint thresholds, the proposed method employs multi-feature learning incorporating differential current, restraint current, RMS magnitude, and second harmonic ratio to construct adaptive decision boundaries under transient operating conditions. In addition, the comparative evaluation of generalized bell-shaped and triangular membership functions provides quantitative insight into the influence of membership design on convergence behavior and prediction accuracy. By combining realistic transformer modeling with intelligent classification, this work contributes a scalable and simulation-validated methodology for enhancing selectivity and stability in digital transformer protection systems.

2. RESEARCH METHOD

This study adopts the quantitative approach founded on simulation methods using the MATLAB/Simulink software to model the system of the power transformer and examine the system response to faults. Simulation is directed at the three-phase, 25 MVA transformer with a voltage level of 150/20 kV which is the case study of the gas turbine power plant. The modeled system includes the delta–wye grounded winding configuration, the transformer impedance, and the location of two

Volume 13, Issue 1, April 2026, pp. 31-42
ISSN 2355-5068 ; e-ISSN 2622-4852
DOI: 10.33019/jurnalecotipe.v13i1.4580

current transformers (CT1 at the primary side and CT2 at the secondary side) as input current sensors. The simulation setup proceeds by including several three-phase fault sources inside and outside the internal and external areas of the transformer. Included fault types are the single line-to-ground (AG), line-to-line (BC), three-phase (ABC), and double line-to-ground (BCG) faults. Faults are applied at the time t = 0.15 seconds to initiate the system transient response. The object of study is a 25 MVA, 150/20 kV, three-phase power transformer operating at 50 Hz. The transformer is modelled using a per-phase equivalent circuit referred to the high-voltage side.

The base impedance is calculated as:

$$Z_{base} = \frac{V^2}{S} = \frac{(150\times10^3)^2}{25\times10^6}$$

Given a short-circuit impedance of 12%, the equivalent leakage impedance is:

$$Z_{eq} = 0.12 \times Z_{base} = 108\ \Omega$$

The equivalent circuit consists of: Series winding resistance and leakage reactance and Magnetizing branch. This model provides realistic electrical behaviour under normal and fault conditions. To generate representative datasets, multiple operating conditions are simulated:

1. Normal operating condition
2. Magnetizing inrush current
3. Internal winding faults
4. External short-circuit faults

Faults are introduced using the Three-Phase Fault block in Simulink at predetermined time intervals. Current signals from both primary and secondary sides are measured using current transformers (CTs).

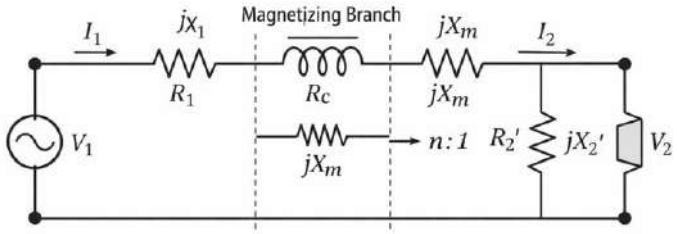

Figure 1. Equivalent circuit of 25 MVA transformer

The equivalent circuit of the 25 MVA in Figure 1, 150/20 kV transformer is modeled on a per-phase basis and referred to the high-voltage side to enable accurate fault analysis. The series impedance, composed of winding resistance and leakage reactance, represents copper losses and short-circuit characteristics, while the shunt magnetizing branch models core excitation and iron losses. Using the rated capacity and 12% short-circuit impedance, the equivalent parameters are derived to reflect practical operating conditions. This model provides a reliable basis for calculating differential and restraint currents under normal operation, magnetizing inrush, and internal or external fault scenarios, thereby supporting the implementation of the proposed ANFIS-based protection algorithm.

2.1. ANFIS System Input and Output

In intelligent protection systems, the selection of representative input and output variables plays a decisive role in ensuring accurate fault pattern recognition. In this study, current measurements obtained from the primary and secondary Current Transformers (CT1 and CT2) of a 25 MVA transformer serve as the fundamental data source for the Adaptive Neuro-Fuzzy Inference System (ANFIS). These measurements capture the electrical response of the transformer under normal operation, internal fault, and external fault conditions.

To align with the operating principle of differential protection (87T), the extracted features are derived from the relationship between primary and secondary currents. Instead of relying solely on

Volume 13, Issue 1, April 2026, pp. 31-42
ISSN 2355-5068 ; e-ISSN 2622-4852
DOI: 10.33019/jurnalecotipe.v13i1.4580

raw peak values, the model employs processed electrical parameters that better represent system dynamics. The selected input features for ANFIS training are:

1. Differential current (I_{diff})
2. Restraint current (I_{rest})
3. RMS current magnitude
4. Second harmonic ratio (H_2)

The differential current reflects the imbalance between CT1 and CT2 within the protection zone, while the restraint current provides stabilization against external disturbances. The inclusion of RMS magnitude and harmonic content enhances discrimination capability during transient conditions, particularly magnetizing inrush events.

Unlike conventional deterministic relay logic, which operates using fixed thresholds, ANFIS applies data-driven learning to model nonlinear relationships between input features and fault categories [16]. The classifier produces a binary output, where a value of 0 corresponds to an external fault and a value of 1 indicates an internal fault within the protected zone. This output functions as the decision signal for issuing a trip command or maintaining normal operation.

By integrating adaptive learning with fuzzy inference, ANFIS provides enhanced robustness in handling measurement uncertainty and complex transient patterns [25]. Previous studies have demonstrated its effectiveness in analyzing CT-based current signals for short-circuit detection and imbalance identification [26]. The adaptive structure and efficient training process enable improved classification stability compared with conventional rule-based methods.

2.2. Membership Function Variations

Within the ANFIS structure, membership functions (MFs) govern the fuzzification stage, where numerical input features namely differential current (I_{diff}), restraint current (I_{rest}), RMS magnitude, and second harmonic ratio (H_2) are transformed into fuzzy membership degrees. The selection of MF shape directly influences the representation of nonlinear relationships among these electrical parameters and consequently affects convergence behavior and classification performance.

This study evaluates two commonly applied MF types in ANFIS models: the generalized bell-shaped (Gbell) function and the triangular (Tri) function. The Gbell MF is characterized by a smooth and continuous curve with adjustable parameters that control width and slope, enabling flexible adaptation to complex input distributions [16]. In contrast, the triangular MF is defined by three characteristic points (lower bound, center, and upper bound) and offers computational simplicity, making it suitable for systems with limited processing requirements.

As reported by Janková and Rakovská [18], the predictive capability of fuzzy-based models is highly sensitive to MF selection. An overly narrow MF may cause excessive sensitivity to minor variations, whereas an overly broad MF can reduce classification resolution. Therefore, systematic evaluation of MF configurations is necessary to ensure stable convergence and reliable fault discrimination within the proposed ANFIS-based protection framework.

2.3. ANFIS Training and Validation Procedure

The ANFIS model was implemented using the MATLAB ANFIS Editor toolbox and trained through a hybrid learning algorithm that combines Least Squares Estimation (LSE) in the forward pass with gradient descent optimization in the backward pass. The training dataset consisted of 270 samples derived from simulated transformer operating conditions, while 30 independent samples were reserved for testing. The dataset encompassed multiple internal and external fault scenarios, including AG, BC, ABC, and BCG faults, ensuring variability in fault characteristics and operating conditions. The input feature set comprising differential current (I_{diff}), restraint current (I_{rest}), RMS magnitude, and second harmonic ratio (H_2) was consistently used during both training and testing phases. To examine the influence of membership function (MF) design on classification performance, generalized bell-shaped (Gbell) and triangular (Tri) MFs were evaluated separately under identical training configurations. Model outputs were compared with target labels generated from the simulated protection zone status to assess predictive consistency.

The adopted hybrid training framework aligns with recent developments in ANFIS-based transformer protection, where signal processing and optimization techniques have been integrated to

Volume 13, Issue 1, April 2026, pp. 31-42
ISSN 2355-5068 ; e-ISSN 2622-4852
DOI: 10.33019/jurnalecotipe.v13i1.4580

enhance classification robustness in practical applications [23]. Model validation was conducted by analyzing the agreement between predicted outputs and actual fault categories, using both classification accuracy and statistical error metrics. This combined evaluation approach provides a balanced assessment of convergence behavior and discrimination reliability under varying fault conditions.

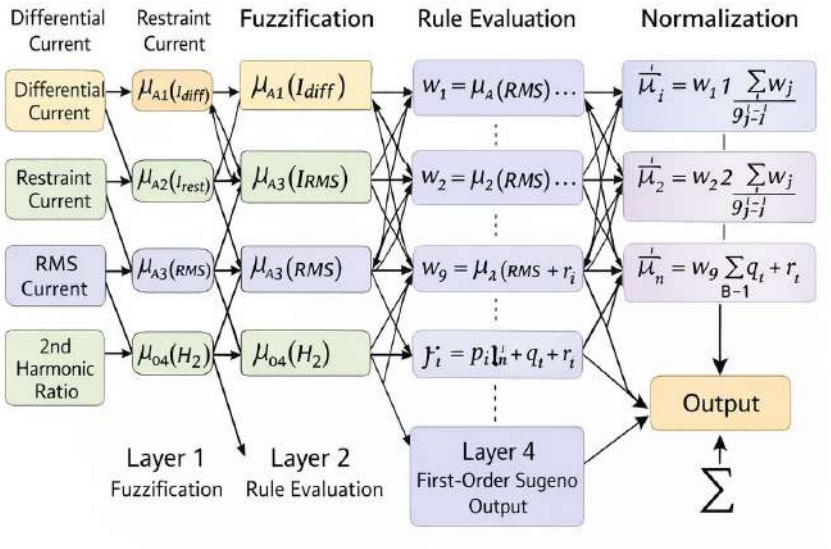

Figure 2. ANFIS Architecture

The designed ANFIS architecture in Figure 2 comprises five sequential layers that map extracted transformer fault features into a classification output. The inputs differential current, restraint current, RMS current, and second harmonic ratio are first fuzzified using Gaussian membership functions. The rule layer computes and normalizes the firing strengths, followed by first-order Sugeno consequent evaluation. The final layer aggregates the weighted outputs to generate a decision signal, enabling accurate discrimination between internal faults and non-fault conditions such as magnetizing inrush.

2.4. Membership Function Variations

To objectively evaluate the performance of the ANFIS system, the Root Mean Square Error (RMSE) is used as the primary metric. RMSE measures the average squared differences between the model's predicted outputs (y_i) and the actual target values ($\hat{y}_i$). In essence, it shows how far off the predictions are from the true results, where a lower RMSE indicates better accuracy. The standard formula for calculating RMSE is as follows:

$$RMSE = \sqrt{\frac{1}{n}\sum_{i=1}^{n}(y_i - \hat{y_i})^2}$$

The evaluation results showed that the lowest RMSE was achieved when the generalized bell-shaped membership function (GbellMF) was used. This low error suggests that the ANFIS model with Gbell MF delivers higher accuracy and better stability in identifying fault patterns compared to the model using the triangular MF. These findings are consistent with those of Nezami et al. [27], who highlighted that smooth, curve-based membership functions like Gbell can greatly enhance a system's ability to respond to variations in fault current patterns within electrical power systems.

3. RESULTS AND DISCUSSION

The equivalent circuit of the 25 MVA, 150/20 kV transformer was first validated under steady-state conditions to ensure parameter consistency prior to fault analysis. Using a 12% short-circuit impedance, the calculated leakage impedance of 108 Ω produced nominal current magnitudes

JURNAL ECTIPE
Electronic, Control, Telecommunication, Information, and Power Engineering
Volume 13, Issue 1, April 2026, pp. 31-42
ISSN 2355-5068 ; e-ISSN 2622-4852
DOI: 10.33019/jurnalecotipe.v13i1.4580

consistent with theoretical expectations. The simulated no-load current and voltage profiles confirmed that the magnetizing branch parameters adequately represent excitation behavior. This validation step ensures that subsequent fault simulations are physically meaningful and not merely algorithm-driven. Under fault conditions, the equivalent circuit demonstrated expected behavior: internal winding faults generated significant current asymmetry between primary and secondary sides, while external faults produced high current magnitudes but minimal differential imbalance. This confirms that accurate electrical parameterization directly influences the reliability of feature extraction.

The ANFIS model training and testing in this research were aimed at assessing its capability in classifying types of faults in power transformers, specifically in distinguishing between internal and external faults. In the testing, 30 data samples were created from fault simulations conducted on a 25 MVA transformer system in MATLAB/Simulink. To determine the influence of the membership function type on the model performance, two were experimented with; the generalized bell-shaped (Gbell) and the triangular (Tri) function. The classification accuracy of the model was quantified by the Root Mean Square Error (RMSE), which is the average of the squared difference between predicted outputs and actual target values. From the simulation, the RMSE values for both membership functions are as follows:

1. RMSE for GbellMF: 0.0116
2. RMSE for Triangular MF: 0.0445

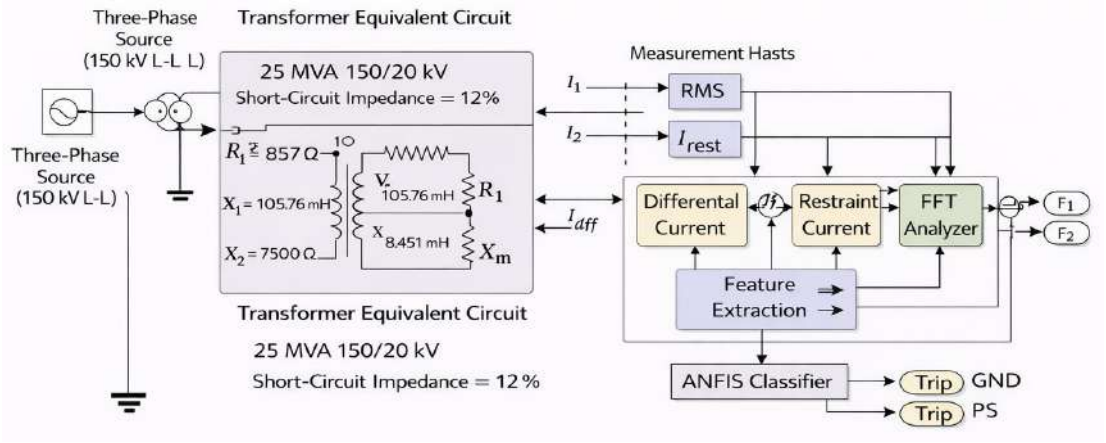

Figure 3. Model of the 25 MVA transformer

The model of the 25 MVA transformer (Figure 3) is developed to represent both the electrical behavior of the equivalent circuit and the implementation of the proposed differential protection scheme within a unified simulation environment. The model begins with a three-phase 150 kV source supplying the transformer equivalent circuit, which incorporates the series winding impedance and the magnetizing branch derived from the rated short-circuit impedance of 12%. Primary and secondary currents are measured through current transformers and processed to obtain RMS values, differential current, and restraint current. An FFT analyzer is employed to extract the second harmonic component required to distinguish magnetizing inrush from internal fault conditions. These extracted features are then fed into the ANFIS classifier, which generates the trip decision signal. This integrated structure allows realistic time-domain fault simulation while simultaneously evaluating the performance of the intelligent protection algorithm under various operating conditions.

The ANFIS configuration employing the generalized bell-shaped membership function (GbellMF) yielded a substantially lower RMSE compared to the triangular MF, indicating improved convergence stability and predictive consistency. The smoother and parameter-adjustable structure of the GbellMF enables more flexible representation of nonlinear relationships among the input features namely differential current (I_{diff}), restraint current (I_{rest}), RMS magnitude, and second harmonic ratio (H_2). In contrast, the piecewise-linear nature of the triangular MF limits its ability to model subtle variations in transient fault patterns. The lower error magnitude observed with the GbellMF confirms

Volume 13, Issue 1, April 2026, pp. 31-42
ISSN 2355-5068 ; e-ISSN 2622-4852
DOI: 10.33019/jurnalecotipe.v13i1.4580

its enhanced capability in capturing complex electrical behavior associated with internal and external fault conditions.

To provide a comprehensive assessment beyond RMSE, additional performance metrics were considered, including Mean Absolute Error (MAE), classification accuracy, and confusion matrix analysis. These indicators offer complementary perspectives on both regression convergence and classification reliability. Furthermore, to reduce the influence of dataset partitioning and to evaluate model generalization capability, a 5-fold cross-validation procedure was implemented. The dataset was iteratively divided into five subsets, ensuring that each subset served as validation data while the remaining subsets were used for training. This strategy minimizes overfitting risk and strengthens confidence in the model's predictive performance when exposed to previously unseen fault scenarios.

3.1. ANFIS Training and Testing Results

These findings are consistent with the observations reported by Janková and Rakovská [18], who highlighted that the selection of an appropriate membership function significantly influences the generalization capability of fuzzy-based systems. In this study, the generalized bell-shaped MF demonstrated improved representation of nonlinear fault characteristics compared to the triangular MF, contributing to enhanced convergence stability and classification performance. The predicted outputs closely correspond to the target labels for both internal faults (1) and external faults (0), indicating that the model effectively captured the underlying fault discrimination patterns embedded in the training data. The consistency between predicted and actual classifications further supports the suitability of the selected MF configuration within the proposed ANFIS-based protection framework.

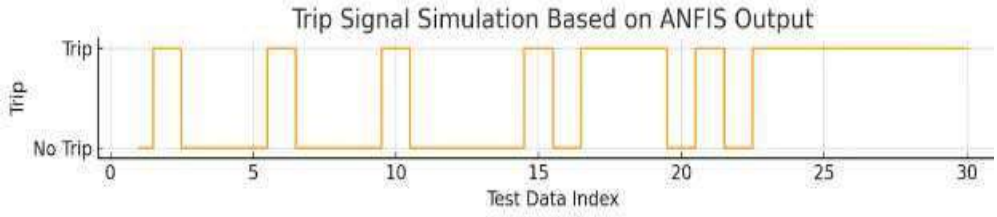

Figure 4. Simulation of trip signals based on ANFIS output

Figure 4 presents the trip signal generated by the ANFIS model configured with the generalized bell-shaped membership function. The horizontal axis represents the index of the testing samples, while the vertical axis shows the corresponding decision output. A value of 1 denotes an internal fault condition requiring a trip command, whereas 0 indicates an external fault or normal operating state. A decision threshold of 0.5 was applied, whereby predicted outputs exceeding this value were classified as internal faults, and values below it were categorized as non-trip conditions. The transition points in the trip signal correspond closely with the expected fault labels, indicating consistent discrimination between internal and external disturbances. The model demonstrates stable switching behaviour without spurious oscillations around the decision threshold, suggesting reliable classification under the tested scenarios. The binary structure of the output facilitates straightforward interfacing with digital relay logic, supporting selective transformer protection based on adaptive feature mapping rather than fixed threshold rules.

JURNAL ECTIPE
Electronic, Control, Telecommunication, Information, and Power Engineering
Volume 13, Issue 1, April 2026, pp. 31-42
ISSN 2355-5068 ; e-ISSN 2622-4852
DOI: 10.33019/jurnalecotipe.v13i1.4580

3.2. Comparison of Membership Functions

The generalized bell-shaped membership function (GbellMF) produced prediction outputs that closely followed the target labels, exhibiting smaller error deviations compared to the triangular membership function (Tri MF), which showed more pronounced fluctuations. This behavior indicates that the smoother and parameter-adjustable structure of the GbellMF provides improved representation of nonlinear relationships among the selected fault features. As illustrated in Figure 2, the prediction curve demonstrates strong agreement with the expected classification outcomes, consistent with the lower RMSE value of 0.0116 obtained for the Gbell configuration. The continuity and flexibility of the Gbell function enable more stable mapping between input parameters differential current (I_{diff}), restraint current (I_{rest}), RMS magnitude, and second harmonic ratio (H_2) and the corresponding fault categories. The reduced error dispersion and stable convergence behavior support the model's capacity to generalize across varying fault scenarios, thereby improving discrimination between internal and external transformer faults within the proposed protection framework.

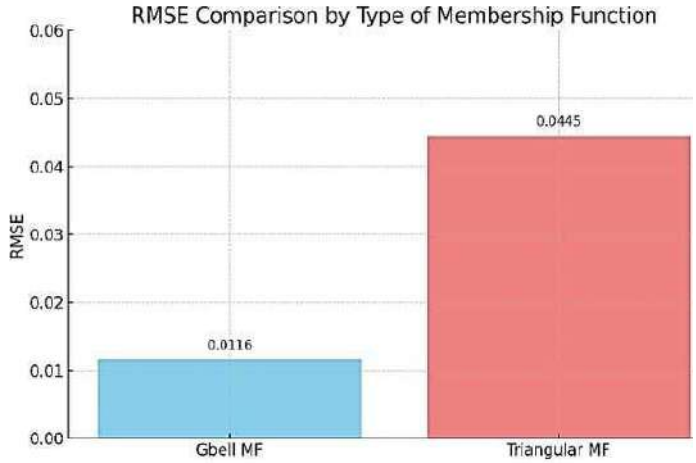

Figure 5. Comparison of RMSE based on membership function type

Figure 5 presents the comparison between the target fault labels and the predicted outputs generated by the ANFIS model configured with the generalized bell-shaped membership function (Gbell MF) for the 30 testing samples. The vertical axis represents the classification outcome, where 0 denotes external faults and 1 indicates internal faults, while the horizontal axis corresponds to the sequence of test samples. The predicted outputs closely align with the target classifications, indicating consistent fault discrimination across the testing dataset. This agreement is consistent with the low RMSE value of 0.0116 obtained during evaluation, reflecting stable convergence and limited prediction deviation. The results suggest that the Gbell MF effectively captures the nonlinear characteristics embedded in the selected electrical features. Moreover, the uniform classification behavior across different fault types supports the model's generalization capability within the simulated transformer protection framework.

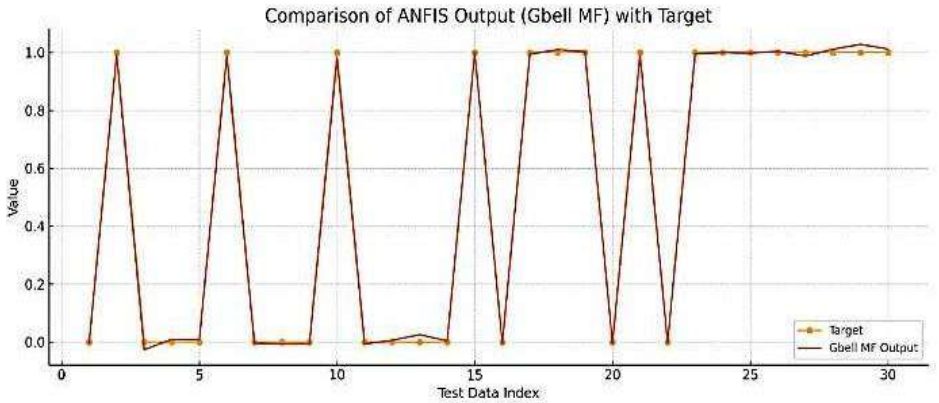

Figure 6. Comparison between ANFIS output (Gbell MF) and target values

JURNAL ECOTIPE
Electronic, Control, Telecommunication, Information, and Power Engineering
Volume 13, Issue 1, April 2026, pp. 31-42
ISSN 2355-5068 ; e-ISSN 2622-4852
DOI: 10.33019/jurnalecotipe.v13i1.4580

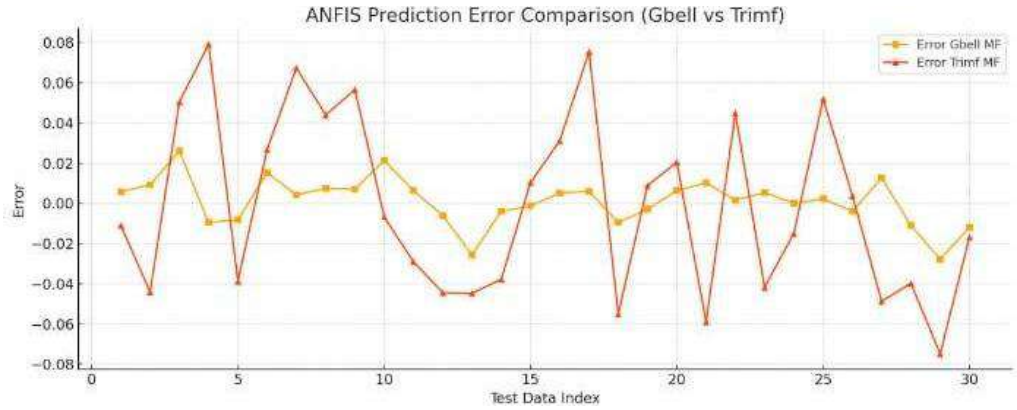

Figure 7. ANFIS prediction error analysis: GbellMF vs. TriMF

Figure 7 presents a comparison of prediction errors obtained using two membership function configurations in the ANFIS model: the generalized bell-shaped (GbellMF) and the triangular (TriMF) functions. The error values, defined as the difference between predicted outputs and corresponding target labels across the 30 testing samples, highlight the performance contrast between the two configurations. The GbellMF exhibits smaller and more uniformly distributed errors concentrated near zero, indicating improved prediction stability. In contrast, the TriMF demonstrates larger deviations and greater variability, suggesting reduced consistency in capturing the underlying fault patterns. These observations are consistent with the RMSE results, where the GbellMF achieved a lower error value (0.0116) compared to the TriMF (0.0445). The smoother and parameter-adjustable structure of the generalized bell function enables more flexible modeling of nonlinear relationships among the selected electrical features. The reduced error dispersion observed in the Gbell configuration reflects improved convergence behavior and enhanced generalization capability within the simulated transformer protection framework. Overall, the comparative analysis confirms that membership function selection significantly influences ANFIS classification performance.

3.3. Interpretaation of Fault Prediction

The ANFIS system separates internal faults well by giving output values that are roughly 1 while output values for external faults are about 0. Based on the decision threshold of 0.5, the system always issues the trip command for internal faults and does not unnecessarily trip for external faults.

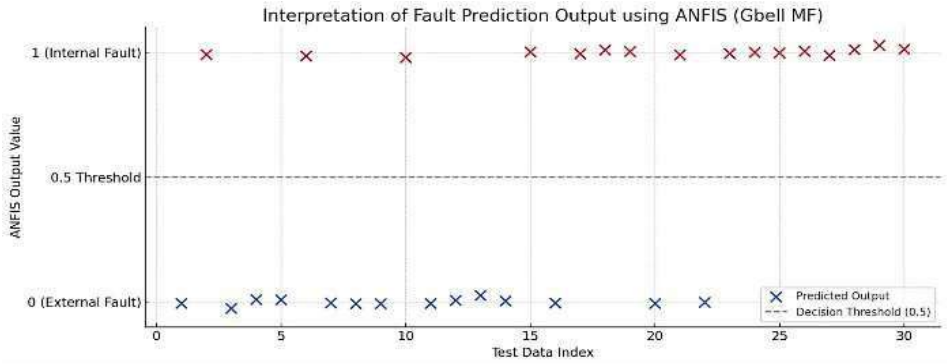

Figure 8. Fault prediction analysis based on ANFIS output

Figure 8 depicts the output of the ANFIS model using the generalized bell function membership function determining the transformer faults as internal or external. Each point on the graph is the output predicted by the model for one test sample and varies between 0 and 1. There is also a horizontal dashed line at 0.5 that is the decision boundary: the predictions above or on this line are internal faults that would trigger the trip signal, while the ones below are external faults that would not require any action.The visualization illustrates the clear and consistent segregation between the two fault types. Forecasts for internal faults are closely grouped around 1, while forecasts for external faults are around 0. The clear segregation reflects the ability of the model to efficiently interpret

Volume 13, Issue 1, April 2026, pp. 31-42
ISSN 2355-5068 ; e-ISSN 2622-4852
DOI: 10.33019/jurnalecotipe.v13i1.4580

sophisticated current pattern signatures and translate them into reliable fault classifications. These results illustrate the high selectivity and reliability of two critical requirements for transformer protection systems. Its ability to reduce spurious trips while efficiently detecting actual internal faults illustrates the potential for the ANFIS model in real-time intelligent relay applications.

4. CONCLUSION

This study demonstrates that the proposed ANFIS-based protection model provides accurate and adaptive discrimination between internal and external faults in a 25 MVA power transformer under simulated operating conditions. By integrating a physically validated transformer equivalent circuit with multi-feature input signals including differential current, restraint current, RMS magnitude, and second harmonic ratio the model achieves reliable classification performance. The generalized bell-shaped membership function outperformed the triangular function, yielding a lower RMSE of 0.0116 compared to 0.0445, indicating superior convergence and nonlinear pattern recognition capability. The results confirm that ANFIS enhances fault selectivity by reducing false trips during magnetizing inrush while maintaining high sensitivity to internal faults. Compared with conventional differential relay logic based on fixed harmonic thresholds, the proposed approach introduces adaptive decision boundaries that improve protection stability under transient conditions. The main contribution of this work lies in the structured integration of realistic transformer modelling and intelligent fault classification within a unified MATLAB/Simulink framework. This provides a scalable foundation for implementing adaptive protection strategies in digital relay systems. Future work will focus on experimental validation using real transformer data and performance evaluation under varying fault resistance and system operating scenarios to further assess field applicability.

Acknowledgments

The authors would like to express sincere gratitude towards PT PLN (Persero) for the valuable information regarding transformer protection systems and LPPM Universitas Riau for the research facilities and assistance. Their contribution significantly helped in the successful completion of this research.

REFERENCES

[1] F. Gui, H. Chen, X. Zhao, P. Pan, C. Xin, and X. Jiang, “Enhancing Economic Efficiency: Analyzing Transformer Life-Cycle Costs in Power Grids,” Energies (Basel), vol. 17, no. 3, Jan. 2024, doi: 10.3390/en17030606.

[2] Md. A. H. S. Kamal and Md. S. Anower, “Design and Implementation of Differential Relay for Power Transformer Protection,” in 2024 3rd International Conference on Advancement in Electrical and Electronic Engineering (ICAEEE), Gazipur, Bangladesh: IEEE, Jun. 2024, pp. 1–6. doi: 10.1109/ICAEEE62219.2024.10561871.

[3] D. A. Purba and U. A. Gani, “Study of Siemens 7UT86 Percentage Differential Relay as Protection of 60 MVA Power Transformer at 150 GIS kV Dayauh Kolot,” Telecommunications, Computers, and Electricals Engineering Journal (TELECTRICAL), vol. 2, no. 2, pp. 208–223, Oct. 2024, doi: 10.26418/telectrical.v2i2.84598.

[4] M. C. Nițu, I. D. Nicolae, L. A. Dina, and P. M. Mircea, “Power Transformer Inrush Current Analysis: Simulation, Measurement and Effects,” Applied Sciences (Switzerland), vol. 14, no. 23, pp. 1–16, Dec. 2024, doi: 10.3390/app142310926.

[5] L. Wang, R. Liu, Y. Huang, Y. Li, and Y. Wang, “Simulation study on transformer inrush current and its suppression,” J Phys Conf Ser, vol. 2029, pp. 1–6, 2021, doi: 10.1088/1742-6596/2029/1/012010.

[6] M. A. M. Qasem and N. M. Nasr, “Effect of the Impulse Phenomenon on the Differential Protection of the Power Transformer,” SSRG International Journal of Electrical and Electronics

Volume 13, Issue 1, April 2026, pp. 31-42
ISSN 2355-5068 ; e-ISSN 2622-4852
DOI: 10.33019/jurnalecotipe.v13i1.4580

Engineering (SSRG-IJEEE), vol. 5, no. 11, pp. 12–18, 2018, [Online]. Available: http://www.internationaljournalssrg.org

[7] "IEEE Guide for Protective Relay Applications to Power Transformers," IEEE Std C37.91-2000 (Revision of IEEE Std C37.91-1985), pp. 1–85, 2000, doi: 10.1109/IEEESTD.2000.91943.

[8] I. Alhamrouni et al., "A Comprehensive Review on the Role of Artificial Intelligence in Power System Stability, Control, and Protection: Insights and Future Directions," Applied Sciences (Switzerland), vol. 14, no. 14, Jul. 2024, doi: 10.3390/app14146214.

[9] Y. Huang et al., "Artificial Intelligence for Resilient Power System: Motivations, Advances, and Challenges," Smart Power & Energy Security, Jun. 2025, doi: 10.1016/j.spes.2025.06.001.

[10] H. Cao, C. Zhou, Y. Meng, J. Shen, and X. Xie, "Advancement in transformer fault diagnosis technology," Front Energy Res, vol. 12, Jul. 2024, doi: 10.3389/fenrg.2024.1437614.

[11] A. N. Hamoodi, M. A. Ibrahim, and B. M. Salih, "An intelligent differential protection of power transformer based on artificial neural network," Bulletin of Electrical Engineering and Informatics, vol. 11, no. 1, pp. 93–102, Feb. 2022, doi: 10.11591/eei.v11i1.3547.

[12] R. I. H. Hussein et al., "Enhanced Transformer Protection Using Fuzzy-Logic-Integrated Differential Relays: A Comparative Study with Rule-based Methods," Journal of Robotics and Control (JRC), vol. 5, no. 5, pp. 1299–1310, 2024, doi: 10.18196/jrc.v5i5.21937.

[13] L. D. Simões, H. J. D. Costa, M. N. O. Aires, R. P. Medeiros, F. B. Costa, and A. S. Bretas, "A power transformer differential protection based onsupport vector machine and wavelet transform," Electric Power Systems Research, vol. 197, 2021, doi: 10.1016/j.epsr.2021.107297.

[14] P. Kumar Choudhary and D. Kumar Das, "Optimal Coordination of Over-current Relay Using Particle Swarm Optimization (PSO) Algorithm," in Proceedings of 2020 IEEE Applied Signal Processing Conference, ASPCON 2020, Kolkata, India: Institute of Electrical and Electronics Engineers Inc., Oct. 2020, pp. 308–312. doi: 10.1109/ASPCON49795.2020.9276703.

[15] J.-S. R. Jang, "ANFIS : Adaptive-Network-Based Fuzzy Inference System," IEEE Trans Syst Man Cybern, vol. 23, no. 3, pp. 665–685, Jun. 1993, doi: 10.1109/21.256541.

[16] P. R. B. Dharmarajan, "Performance Analysis of Various Membership Functions using ANFIS for the Detection of Type-II Diabetes," in 2021 IEEE 4th International Conference on Computing, Power and Communication Technologies (GUCON), Kuala Lumpur, Malaysia: IEEE, Sep. 2021. doi: 10.1109/GUCON50781.2021.9573682.

[17] Z. Janková and E. Rakovská, "Comparison Uncertainty of Different Types of Membership Functions in T2FLS: Case of International Financial Market," Applied Sciences (Switzerland), vol. 12, no. 2, Jan. 2022, doi: 10.3390/app12020918.

[18] S. Kanwal and S. Jiriwibhakorn, "Advanced Fault Detection, Classification, and Localization in Transmission Lines: A Comparative Study of ANFIS, Neural Networks, and Hybrid Methods," IEEE Access, vol. 12, pp. 49017–49033, 2024, doi: 10.1109/ACCESS.2024.3384761.

[19] S. Ahmad, A. A. Zakri, M. Oktaviandri, W. Sunanda, and A. Suryadi, "Penetration of DWT & ANFIS to Power Transmission Disturbances," International Journal of Electrical, Energy and Power System Engineering, vol. 6, no. 1, pp. 105–112, Feb. 2023, doi: https://doi.org/10.31258/ijeepse.6.1.105-110.

[20] C. F. Mbey, V. J. Foba Kakeu, A. T. Boum, and F. G. Y. Souhe, "Fault detection and classification using deep learning method and neuro-fuzzy algorithm in a smart distribution grid," The Journal of Engineering, vol. 2023, no. 11, 2023, doi: 10.1049/tje2.12324.

[21] A. Azhari Zakri, M. W. Mustafa, H. Firdaus, and I. Sofimieari, "Assess The Risk Level of Power Transformer Due Short-Circuit Faults Based on ANFIS," SINERGI, vol. 23, no. 2, pp.

Volume 13, Issue 1, April 2026, pp. 31-42
ISSN 2355-5068 ; e-ISSN 2622-4852
DOI: 10.33019/jurnalecotipe.v13i1.4580

99–106, Jun. 2019, doi: 10.22441/sinergi.2019.2.002.

[22] M. Y. Suliman and M. T. Al-Khayyat, "Discrimination between inrush and internal fault currents in protection based power transformer using DWT," International Journal on Electrical Engineering and Informatics, vol. 13, no. 1, pp. 1–20, Mar. 2021, doi: 10.15676/ijeei.2021.13.1.1.

[23] A. M. Salama, K. M. Abdel-Latif, M. M. Ismail, and S. M. Mousa, "A New Hybrid Protection Algorithm for Protection of Power Transformer Based on Discrete Wavelet Transform and ANFIS Inference Systems," International Journal of Emerging Electric Power Systems, vol. 19, no. 3, 2018, doi: 10.1515/ijeeps-2017-0248.

[24] S. N. Sivanandam, S. N. Deepa, and S. Sumathi, Introduction to Fuzzy Logic Using MATLAB. Berlin: Springer, 2007.

[25] E. Andikan, "Detection And Classification of High Impedance Fault (HIF) In The 330kv High Voltage Power System Network in Nigerian with ANFIS Adaptive Neuro-Fuzzy Inference System (ANFIS)," Proceedings of International Conference on Scientific, Cultural Innovations and Sustainable Development, vol. 12, no. 3, pp. 33–42, 2020.

[26] M. M. Nezami, M. D. Equbal, S. A. Khan, and S. Sohail, "An ANFIS Based Comprehensive Correlation Between Diagnostic and Destructive Parameters of Transformer's Paper Insulation," Arab J Sci Eng, vol. 46, pp. 1541–1547, Jan. 2021, doi: 10.1007/s13369-020-05180-4.

JURNAL ECOTIPE
Electronic, Control, Telecommunication, Information, and Power Engineering

Volume 13, Issue 1, April 2026, pp. 43-55
ISSN 2355-5068 ; e-ISSN 2622-4852
DOI: 10.33019/jurnalecotipe.v13i1.4590

Development of E-Tourism System for the Bangka Islands Using the Extreme Programming Method Towards Digital Tourism

Iski Zaliman[1], Fardhan Arkan[2], Wenni Anggita[3], Nurhaeka Tou[4], Nanda Aulia Ilmatus Sakdiyah[5], Risnina Wafiqoh[6], Putri Mentari Endraswari[7]
[1,4,7]Information Technology Study Program, Universitas Bangka Belitung, Indonesia
[2,5]Electrical engineering Study Program, Universitas Bangka Belitung, Indonesia
[3]Accounting Study Program, Universita Bangka Belitung, Indonesia
[6]Mathematics education Study Program, Universitas Muhammadiyah Bangka Belitung, Indonesia

ARTICLE INFO

Article historys:

Received : 20/02/2026
Revised : 01/04/2026
Accepted : 30/04/2026

Keywords:

E-Tourism; Extreme Programming; System Usability Scale; Tourism Information System

ABSTRACT

Regional tourism often faces obstacles in providing fast, accurate, and easily accessible destination information to tourists. Many regions lack a digital platform capable of presenting information in an integrated manner, making it difficult for tourists to obtain an overview of tourist attractions, supporting facilities, and travel routes. This information accessibility problem affects the efficiency of tourism promotion and results in suboptimal implementation of digital transformation concepts. This study aims to develop and evaluate a E- Tourism application to improve the accessibility of tourism destination information and support digital transformation in the regional tourism sector. The system development was carried out using the Extreme Programming (XP) approach to ensure a fast iterative process, flexibility to respond to changing user needs, and software quality improvement in each testing cycle. Usability evaluation was conducted using the System Usability Scale (SUS) method involving 70 general user respondents. The test results show that the application obtained a SUS score of 75.74 in the acceptable category, indicating that the application is easy to use, clear, and aligned with tourism information needs.

Corresponding Author:
Iski Zaliman
[1]Information Technology Study Program, University of Bangka Belitung, Indonesia
Email: iski.zaliman@ubb.ac.id

1. INTRODUCTION

Tourism is one of the development sectors that is currently the focus of the goverment because it plays an important role in supporting the national economy [1]. This sector not only contributes to increasing regional and national income, but also serves as a means of introducing Indonesia's natural wealth, culture, and local wisdom to the world [2,3]. Tourism provides opportunities for visitors to explore destinations and engage in various activities during their leisure time and vacations [4], offering them enjoyable and interesting experiences. Such tourism activities enhance visitor satisfaction and well-being [5]. As awareness of the enormous potential of tourism grows, the government continues to strive to deliver innovations to improve the quality of services and tourist experiences, one of which is through the use of digital technology. The rapid development of information and communication technology (ICT) in the last decade has brought about major changes in various fields, including tourism. This digital transformation not only makes it easier for tourists to find and access information, but also

JURNAL ECTIPE
Electronic, Control, Telecommunication, Information, and Power Engineering
Volume 13, Issue 1, April 2026, pp. 43-55
ISSN 2355-5068 ; e-ISSN 2622-4852
DOI: 10.33019/jurnalecotipe.v13i1.4590

changes the way they interact with destination managers and local governments in enjoying a smarter and more connected travel experience.

Alongside digital transformation development, the concept of smart tourism plays an important role in the development of smart cities. Both share the same vision: to utilize advances in information and communication technology to improve the efficiency of public services, including tourism services. Information and communication technology are an important factor in establishing a smart city. As for tourism, information and communication technology currently plays a fundamental role in many services such as transportation, cultural activities, and entertainment.

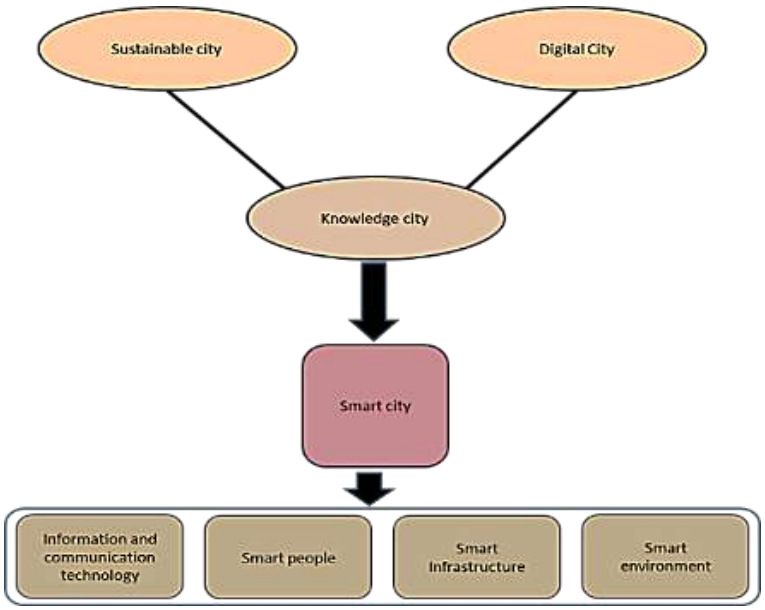

Figure 1. The relationship between smart cities and smart tourism [6]

Figure 1 illustrates the relationship between smart cities and smart tourism. Within the context of Smart Cities, Smart Tourism can be seen as a sectoral implementation of the Smart City concept. Smart Tourism uses the means of ICT, digital platform, and data analytics and combines them with smart/integrated infrastructure to enhance tourism services, improve visitor experience, and facilitate the management of tourism destinations. According to "2050—TOMORROW'S TOURISM" by Yeoman and Yu, technological advancements allow tourists to obtain information about tourism more quickly, precisely, and conveniently. This information can be acquired through a variety of user-friendly digital tools, exemplifying the key feature of the smart tourism concept: technology helps make the visitor experience more comfortable and practical [7]. The implementation of smart tourism also plays a role in increasing the competitiveness of destinations, strengthening regional tourism promotion, and encouraging the realization of sustainable tourism development. Therefore, the development of smart tourism-based applications is a strategic step toward realizing a smart tourism ecosystem that aligns with the vision of smart city development in Indonesia.

Bangka Island is part of Bangka Belitung Province, with the provincial capital, Pangkal Pinang, located on the island. The island is divided into four districts: West Bangka Regency, Central Bangka Regency, South Bangka Regency, and Bangka Regency [8]. Geographically, the Bangka Belitung Islands are bounded by the Bangka Strait to the west and the Karimata Strait to the east [8]. The Bangka Belitung Islands possess enormous potential and could become a promising destination for tourism development [9]. The region features beaches, natural attractions and religious tourism sites, making the Bangka Islands a promising destination for tourists. The strategic location of the Bangka Islands is already widely recognized by domestic and international tourists, providing numerous opportunities in the tourism sector. Beyond tourism, the economic and cultural development of local communities will also benefit positively [10] from the geographical location of the Bangka Belitung Islands, which offer interesting natural tourism potential, exotic beaches, and meaningful religious sites.

Volume 13, Issue 1, April 2026, pp. 43-55
ISSN 2355-5068 ; e-ISSN 2622-4852
DOI: 10.33019/jurnalecotipe.v13i1.4590

While the use of information technology and the internet for tourism information dissemination is well-established in Indonesia, its adoption in Bangka Belitung remains limited among tourists. The use of internet technology for tourism promotion which facilitates tourist access to information anytime and anywhere. This concept, also known as E-Tourism can be utilized in developing information technology for the tourism industry, proving useful for promoting destinations, existing facilities, available accommodations, and transportation to tourist attractions [11]. Additionally, as digital services and data flows produced by online interactions allow for more intelligent, data-driven administration of visitor activities and destination operations, e-tourism is essential to the growth of smart tourism [12].

Currently, tourism promotion in Bangka Belitung has not fully embraced E-Tourism concepts. Tourists still frequently search for information on the internet from sources that may not be reliable, or they seek information through relatives or family members in Bangka Belitung to learn about natural tourist destinations, beach tourism, and religious tourism. At present, tourism promotion primarily relies on word-of-mouth recommendations and existing social media platforms. However, comprehensive tourist information covering all attractions in the Bangka Islands is not yet available. The analysis of the website owned by the Bangka Belitung Tourism Office reveals several obstacles in promoting tourist attractions, including incomplete information displays about destinations and facilities [13]. Route information to tourist attractions remains unclear, with the official website primarily featuring only photographs and basic descriptions. These limitations contribute to a relatively low level of tourist visits.

E-tourism platforms could be the primary tool for tourists in determining their destination choices [14]. With access to more specific information, tourists can search for attractions with greater confidence and satisfaction, while also viewing reviews from other tourists who have used e-tourism services. The presence of E-Tourism is expected to transform the Bangka Islands into a Digital Tourism Island. There are many software development methodologies for completing projects [15], one of which is the agile methodology. Agile methods are iterative and incremental, so user requirements are met by continuously providing partial and incomplete software. Any changes in client requirements can also be easily handled at each stage of development. These models have proven effective in dealing with constantly changing business environments. Agile methodologies have been gaining recognition in recent years due to their simplicity, flexibility, and suitability for today's software development needs [16]. The most widely used agile frameworks are Scrum and Extreme Programming.

Extreme Programming (XP) is one of the most influential Agile-based software development approaches, as it emphasizes an adaptive development process that focuses on quality and is responsive to changing requirements [17]. In [18], Extreme Programming emphasizes simplifying the development process by encouraging intensive communication between all team members and customers involved [19]. This direct collaboration enables the identification of solutions that are more accurate, efficient, and within budget. In addition, XP ensures rapid feedback through regular unit testing and integration testing, so that software quality can be monitored and continuously improved throughout the development process.

Researchers will develop Digital Tourism using the Extreme Programming development method. For tourists, this platform will provide essential information to help them determine which attractions to visit. This development is integral to information technology advancement and can serve as a primary application of IT in the tourism sector. The development of E-Tourism information technology using the Extreme Programming method is essential and necessary to serve as an effective tool for promoting natural attractions, beach tourism, and religious tourism in the Bangka Islands, thereby improving the availability and quality of tourism information. One form of E-tourism information technology utilization can be seen through website-based tourist platforms. Additionally, it can serve as an alternative medium to promote tourism widely through E-Tourism channels. The implementation of E-Tourism aims to enhance tourism sector development in the Bangka Islands. Fundamentally, the e-tourism concept represents one approach to applying information technology in the tourism industry. By utilizing E-tourism information technology, tourists can obtain comprehensive information on tourist destinations and receive personalized recommendations for their visits.

JURNAL ECOTIPE
Electronic, Control, Telecommunication, Information, and Power Engineering
Volume 13, Issue 1, April 2026, pp. 43-55
ISSN 2355-5068 ; e-ISSN 2622-4852
DOI: 10.33019/jurnalecotipe.v13i1.4590

2. RESEARCH METHOD

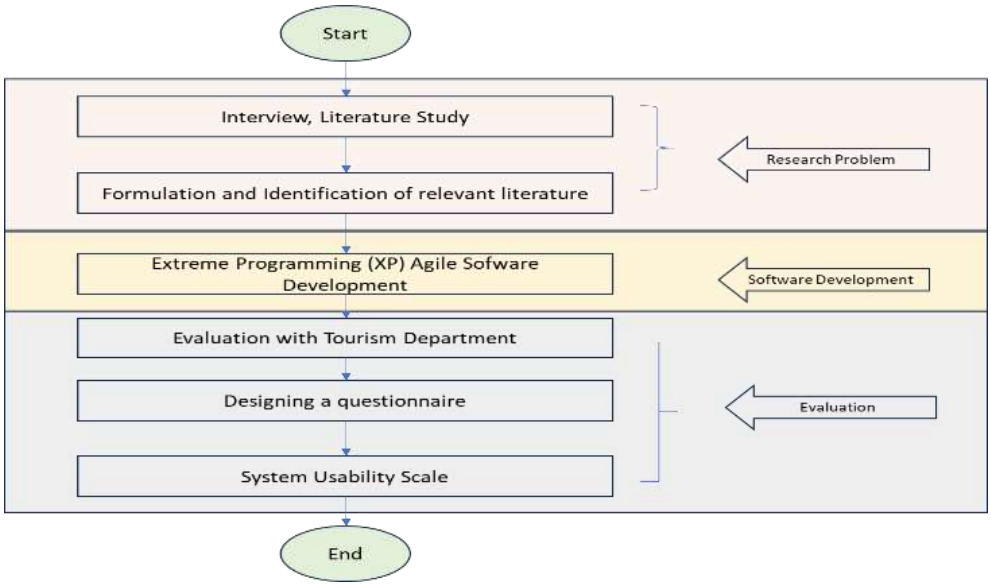

Figure 2. The research step

This research process was divided into several stages, as shown in Figure 2. The first stage was the collection of initial data and information, which was carried out through interviews and literature reviews. Interviews were conducted with the Pangkalpinang City Tourism Office to obtain data and information related to regional tourism activities and conditions. Interviews took the form of discussions and question-and-answer sessions during socialization activities at the Tourism Office. In addition, a literature study was conducted to collect references, secondary data, and supporting theories relevant to the research needs.

The second stage was software development, which was carried out based on the results of needs analysis and input from the Tourism Office as the main user. At this stage, the system was designed and implemented in accordance with the specified requirements.

The third stage was system evaluation and testing. The evaluation was conducted by the Tourism Office to assess the functionality and usefulness of the developed system. Next, a survey was conducted among the public using the System Usability Scale (SUS) method to measure the ease of use (usability) and user satisfaction with the resulting system.

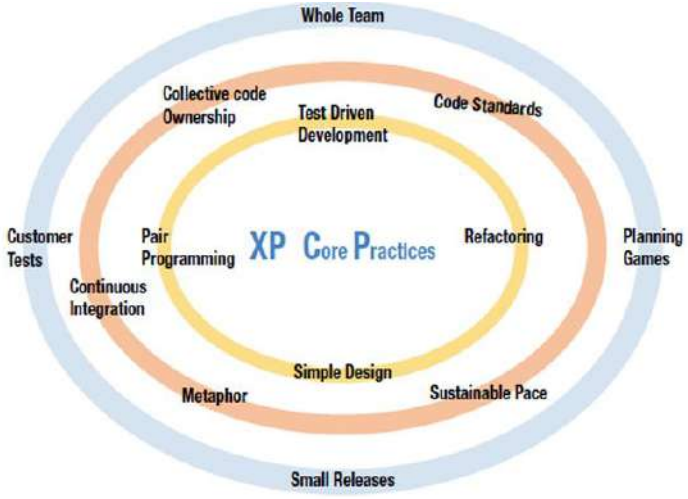

Figure 3. Extreme programming

The selected system development process was Extreme Programming (XP) Agile Software Development. Extreme Programming is an agile software development methodology [20]. This

Volume 13, Issue 1, April 2026, pp. 43-55
ISSN 2355-5068 ; e-ISSN 2622-4852
DOI: 10.33019/jurnalecotipe.v13i1.4590

approach was chosen because it is suitable for addressing the identified problems. The software being developed is not highly complex and falls into the category of small-scale software that requires relatively short and iterative development cycles. Extreme Programming also helps improve software quality incrementally, encouraging collaborative project development in which programmers and customers are actively involved. During the software development process, customers can propose changes and updates as needed, as their understanding of the problem improves over time [21], making the work process more efficient. The diagram figure 3 illustrates the Core Practices of Extreme Programming (XP), an Agile software development methodology that emphasizes flexibility, collaboration, rapid feedback, and continuous improvement. At the center of the diagram are the XP Core Practices, which represent the fundamental technical and collaborative principles that guide the development process. Surrounding these core practices are additional supporting practices that ensure the method works effectively as an integrated system. This approach is divided into several activities. That is Planning, Design, Coding, and Testing.

The planning stage, as the first step in the Extreme Programming (XP) method, determines the direction and scope of system development. At this stage, data collection and analysis activities explore user requirements. The main objective is to provide the development team with a comprehensive understanding of the processes involved in selecting tourism categories. Through this stage, the team can measurably identify the functional and non-functional requirements of the system so that the developed software design can effectively support the organization's objectives. The results of this planning process include an overview of the system, a list of key features, and the core functionality of the application to be implemented. Thus, the planning stage not only forms the basis for system development but also ensures that each software component aligns with user needs and is capable of producing relevant and measurable outputs.

The second stage in the Extreme Programming (XP) method is the design phase. At this stage, the development team designs the system structure to serve as a guideline for realizing the user requirements identified in the previous stage. Although the design phase is often considered flexible or even postponable in practice, it plays an important role in this study as the conceptual foundation for system implementation. The design phase includes the architecture of the software, system workflow, user interface, and relationships between the main components of the application. With systematic documentation, subsequent development proceeds more efficiently and with greater focus. In addition, the results of this phase serve as a communication guide between the development team and users, ensuring that each party has a shared understanding of the structure and function of the system to be developed. Thus, the design phase ensures that the resulting application not only meets functional requirements but is also intuitive and accessible to end users.

The third phase in the Extreme Programming (XP) method is the coding phase. This phase is the core of software development, where developers translate the system design into executable program code. In this phase, developers focus on implementing key features in accordance with the specified requirements. The coding process in XP is carried out iteratively and collaboratively, allowing the team to make changes or improvements without restarting the entire development process. In addition, this phase includes the creation of test cases designed to verify the accuracy and reliability of the written code. After each piece of code successfully passes the testing stage, the results are gradually integrated into the system. This approach allows the development team to identify and fix errors early in the process. Thus, the coding stage not only focuses on writing code but also becomes a continuous process that supports software quality. This stage prepares the foundation for the next step, the testing phase to ensure that the system functions as expected.

The fourth stage is the testing phase, which is an essential component of the Extreme Programming (XP) approach. At this stage, verification and validation processes are carried out on the software components that have been developed to ensure that all system functions operate in accordance with the established requirements and specifications. The testing phase in XP is continuous, where each module or feature that has been developed is immediately tested using specialized tests designed based on user requirements. This approach allows the development team to quickly evaluate each change and ensure no regression disrupts existing system functions. In addition, the testing phase focuses on usability testing, which involves users directly to assess the ease, reliability, and effectiveness of the system in

JURNAL ECTIPE
Electronic, Control, Telecommunication, Information, and Power Engineering
Volume 13, Issue 1, April 2026, pp. 43-55
ISSN 2355-5068 ; e-ISSN 2622-4852
DOI: 10.33019/jurnalecotipe.v13i1.4590

supporting their activities. The results of this testing process form the basis for further refinement of the system, both from technical and user experience perspectives. Thus, the testing phase not only serves as final validation but also as an iterative mechanism to ensure software quality and user satisfaction.

2.1. Functional Requirement Analysis

Figure 4. Use case diagram

Figure 4 shows the use case diagram for this study. It illustrates the interaction between actors and the system in developing digital tourism services, including the roles, activities, and relationships between users and features. The developed system has three main actors: User, Service Provider, and Admin. Each actor has different responsibilities, access rights, and interaction objectives, yet they are all interrelated in supporting the continuity of the digital tourism service process.

The User actor represents the end user of the application and interacts directly with its services. This actor can perform activities such as authentication (login, registration, and logout), browsing the list of services, and booking the desired service. Users also have access to service provider contact information for direct communication and can provide feedback on services to improve the quality of tourism offerings. These activities enable two-way interaction between users and service providers within the digital ecosystem.

The Service Provider actor provides services within the system. The main roles of this actor include verifying booking availability to ensure schedules align with available service capacity, as well as managing service content to update relevant information. In addition, service providers can view booking requests and review user feedback as evaluation material to improve the quality and relevance of the services offered. Service providers maintain control over the content and performance of their services within the system.

Meanwhile, the Admin is responsible for ensuring the continuity, validity, and consistency of the application's operations as the main system administrator. The Admin's main functions include adding new service provider accounts, managing menu content, and creating informative content such as tips and usage guides to educate and guide the users. Thus, the admin manages data and controls system operations between users and service providers.

JURNAL ECOTIPE
Electronic, Control, Telecommunication, Information, and Power Engineering
Volume 13, Issue 1, April 2026, pp. 43-55
ISSN 2355-5068 ; e-ISSN 2622-4852
DOI: 10.33019/jurnalecotipe.v13i1.4590

2.2. Activity Diagram

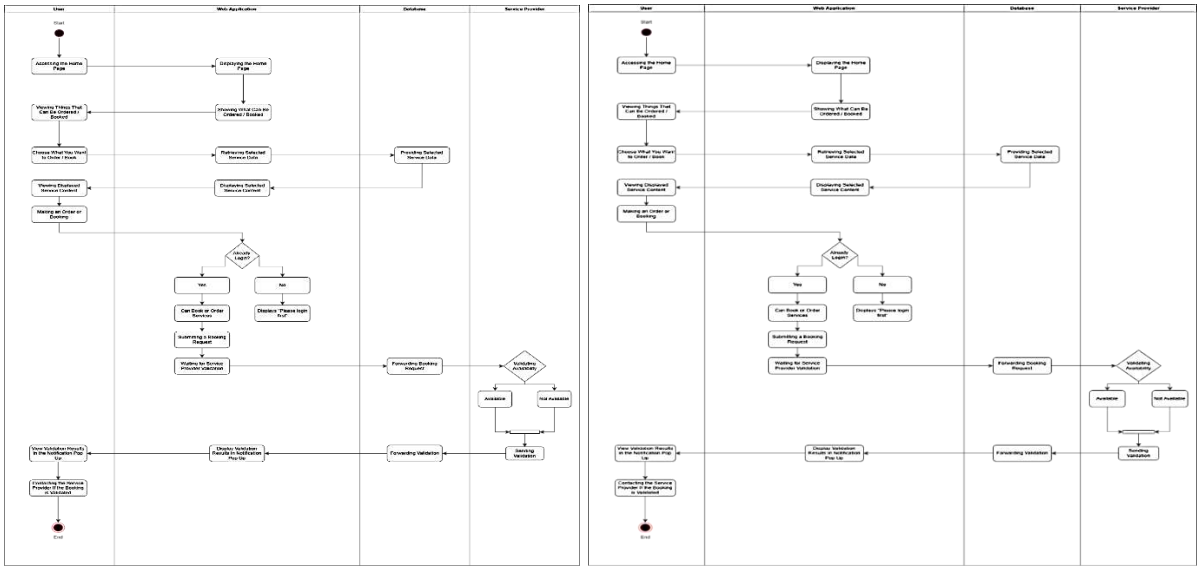

Figure 5. Activity Diagram

The Activity Diagram in Figure 5 describes the flow of activities and interactions between components in the Bangka Island Smart E-Tourism application system, reflecting the main business processes in booking tourism services. This diagram is designed to show the logical sequence of steps taken by the main actor (User) and how the system responds to each action systematically through the Web Application, Database, and Service Provider components.

The process begins when the user accesses the application's home page, after which the system displays the main homepage. Users can view the various travel services available for booking, and the system will display a list of available services. When the user selects one of the services they want to book, the system retrieves the selected service data from the database, which is provided by the service provider. Detailed information about the service is displayed to the user through the application interface.

Next, users can place a booking. At this stage, the system verifies the user's authentication status. If the user is already logged in, the system allows the booking process to continue. However, if the user has not logged in, the system displays a warning to log in first.

After the authentication process is successful, the user submits a booking request, which is then forwarded by the system to the service provider for validation. At this stage, the service provider validates the availability of the service. If the service is available, the service provider sends the validation results to the system, while if the service is unavailable, the system displays information that the service cannot be booked at the specified time.

After the validation results are received, the system displays the results in the form of a notification to the user. Users can view the booking validation results and contact the service provider directly if the booking has been validated. This process is the final stage of the service booking activity, which marks successful communication and transaction between the user and the service provider.

This Activity Diagram illustrates how the Smart Tourism system integrates user activities, system mechanisms, and service provider validation processes in a synchronized and structured manner. The model reflects workflow automation principles applied to tourism information systems. The model aims to improve process efficiency, reduce manual errors, and provide a more interactive and transparent user experience. The diagram helps developers and researchers understand the system's overall functional flow, providing a reference for ongoing implementation and evaluation.

JURNAL ECOTIPE
Electronic, Control, Telecommunication, Information, and Power Engineering
Volume 13, Issue 1, April 2026, pp. 43-55
ISSN 2355-5068 ; e-ISSN 2622-4852
DOI: 10.33019/jurnalecotipe.v13i1.4590

2.3. Class Diagram

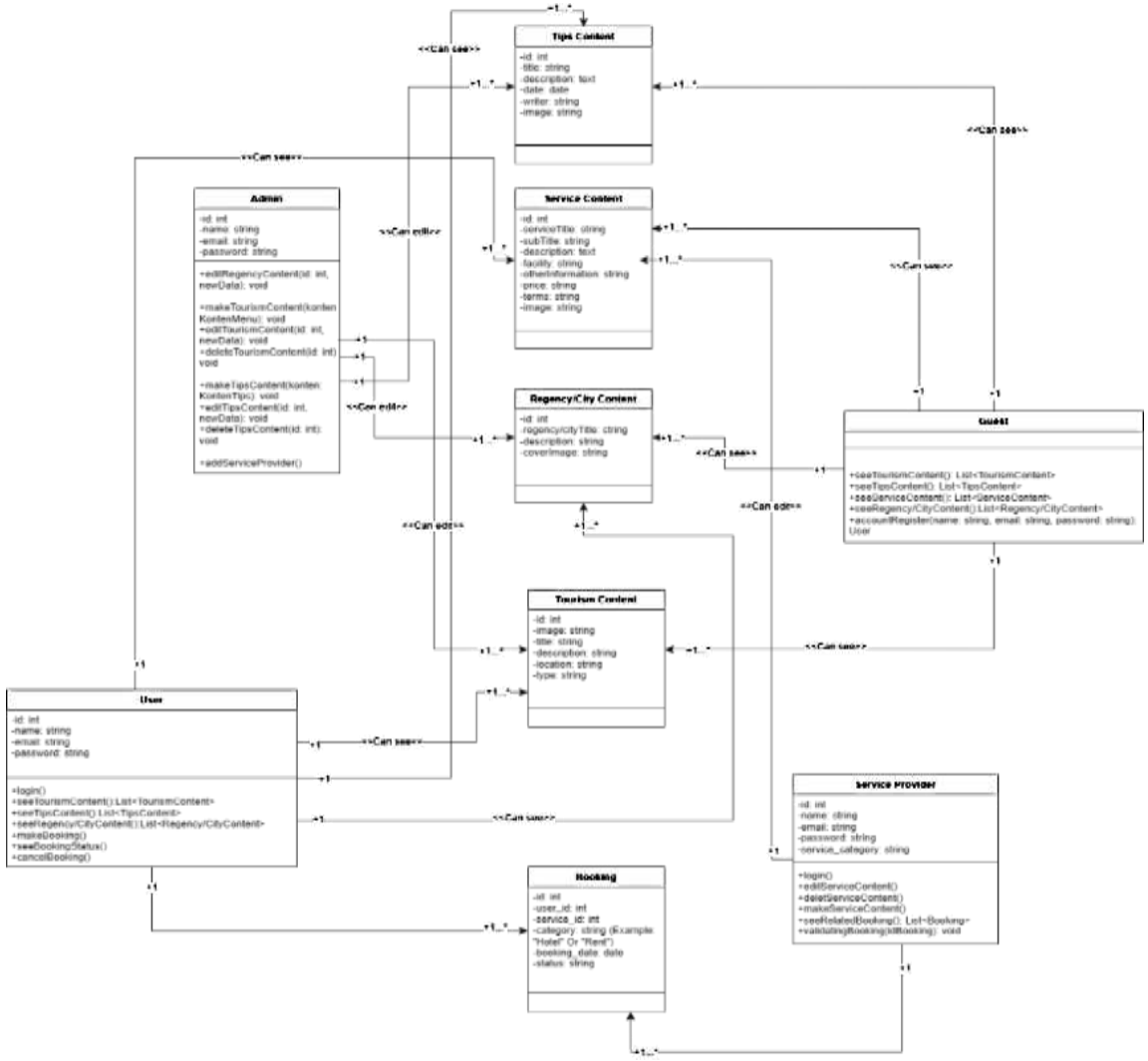

Figure 6. Class Diagram

The class diagram shown in Figure 6 describes the structure of the Bangka Island Smart Tourism system, showing the relationships between classes, attributes, and operations that support the overall functionality of the system. This diagram is a conceptual representation of the database design and application logic that supports the digital tourism information management process. The system consists of several main classes: Admin, User, Guest, Service Provider, Tourism Content, Service Content, Regency/City Content, Tips Content, and Booking. A more detailed explanation of Figure 6 can be seen in Table 1 below.

Table 1. Class diagram information

No	Class	Information
1	Admin	Admins can edit content related to services, tourist destinations, cities/districts, and travel tips.
2	User	Registered system users who have the ability to view various available content and place service orders through the booking class.
3	Guest	Guests can only view basic information about destinations and travel services without the right to make reservations.
4	Service Provider	Tourism service providers who interact directly with the system to manage service availability and receive orders submitted by users.
5	Booking	The link between users and service providers, responsible for recording and validating booking activities carried out through the system.

JURNAL ECOTIPE
Electronic, Control, Telecommunication, Information, and Power Engineering
Volume 13, Issue 1, April 2026, pp. 43-55
ISSN 2355-5068 ; e-ISSN 2622-4852
DOI: 10.33019/jurnalecotipe.v13i1.4590

3. RESULTS AND DISCUSSION

A web-based smart tourism application has been developed for Bangka Island. This smart tourism application facilitates tourist access to destination information, support services, and interactive features that enhance the tourist experience on Bangka Island.

Figure 7. Smart tourism web-based application interface

The web-based smart tourism interface is shown in Figure 7. The main page displays a hero banner featuring a typical Bangka Island beach scene, which serves as the main visual element to attract attention and establish an initial impression of the region's identity. Horizontal navigation is placed in the header section, allowing users to systematically access several categories including Home, Tourism, Tour Packages, Hotels, Rentals, and Contact.

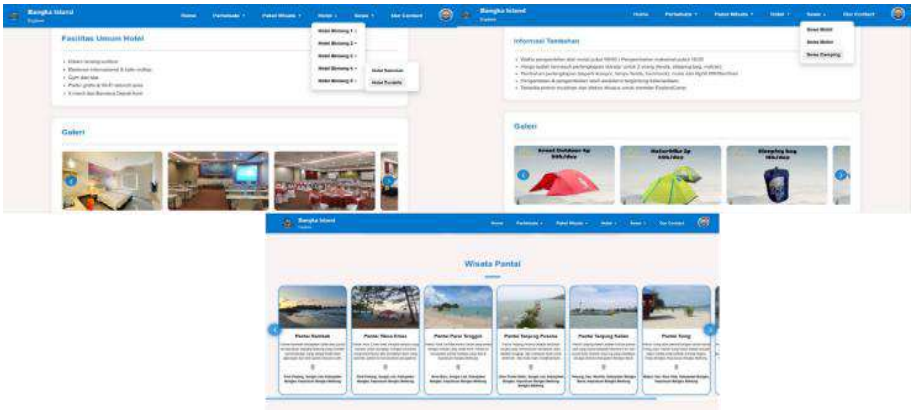

Figure 8. Smart Tourism web-based application information display

The information needed by users is shown in Figure 8. The hotel information page includes a list of general facilities such as swimming pool, international restaurant, fitness center, parking, and Wi-Fi. The information is presented in bullet list format, enabling users to quickly review available services. Additionally, a carousel-based gallery feature allows users to interactively view images of rooms, meeting facilities, and supporting facilities, thereby enhancing information delivery quality and supporting the decision-making process of potential travelers.

The rental services page displays additional information related to rental terms, including pickup times, equipment capacity, and price variations. This section features a gallery of equipment available for rent, such as tents, camping gear, and other outdoor equipment. Each gallery item is accompanied by an image and price description, enabling users to evaluate their options efficiently.

In the tourist destination information section, the system uses a card-based layout to display a list of beach attractions. Each card contains a destination photo, brief description, and administrative location, facilitating tourist browsing according to their preferences. The carousel feature in this section also supports a more dynamic exploration experience without overloading the main page display.

JURNAL ECOTIPE
Electronic, Control, Telecommunication, Information, and Power Engineering
Volume 13, Issue 1, April 2026, pp. 43-55
ISSN 2355-5068 ; e-ISSN 2622-4852
DOI: 10.33019/jurnalecotipe.v13i1.4590

Figure 9. User authentication page

Users can create accounts with the display shown in Figure 9. The user authentication page provides several access options: logging in with internal credentials, authentication using a Google account, and guest access mode. The purpose of this service is to increase user flexibility and comfort, as well as to implement the principle of inclusivity in a web-based public information system.

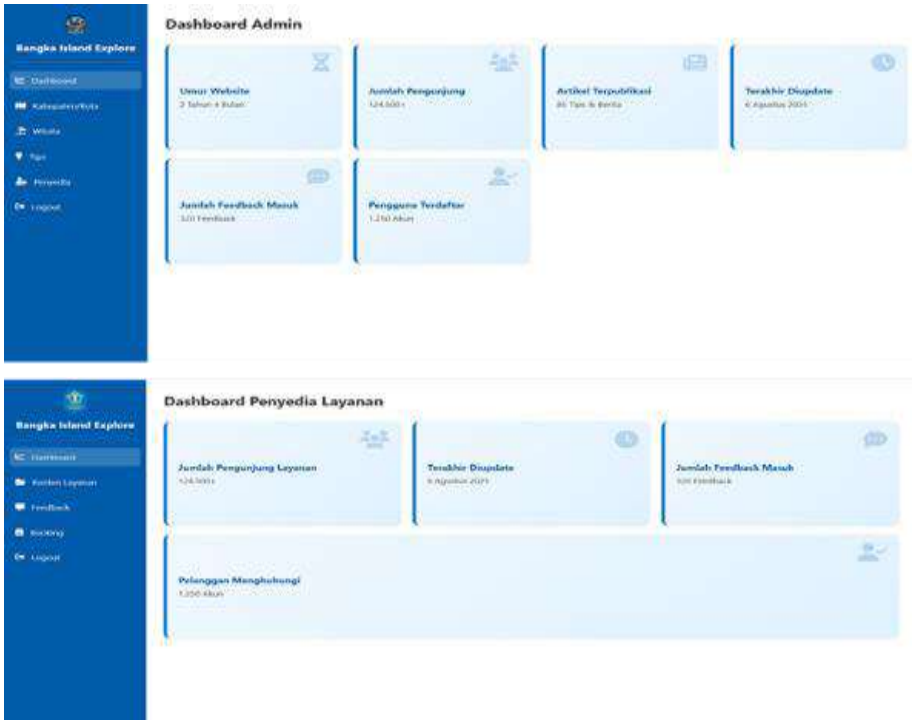

Figure 10. Smart Tourism web-based application information display

The next section shows the Admin Dashboard as shown Figure 10, which serves as a center for monitoring and managing the system's operational data. This dashboard presents key performance indicators including the website's operational age, number of visitors, number of articles published, amount of feedback received, and number of registered users. The presentation of data in information card format with concise layout and consistent visuals allows administrators to quickly evaluate system conditions and make more effective data-driven decisions.

Furthermore, the Service Provider Dashboard (e.g., hotels, rental providers, or tourism businesses) is also displayed as part of the application ecosystem. This dashboard provides relevant operational information for service providers, including the number of service visitors, the date of the last data update, the amount of customer feedback, and a list of customers who have contacted them. The provision of a dedicated dashboard for these stakeholders strengthens the system's function as a collaborative platform that supports data integration, service transparency, and the management of interactions between service providers and tourists.

Volume 13, Issue 1, April 2026, pp. 43-55
ISSN 2355-5068 ; e-ISSN 2622-4852
DOI: 10.33019/jurnalecotipe.v13i1.4590

Based on the results of system development and testing, modeling in the Extreme Programming (XP) approach contributes significantly to the speed of system development iterations, flexibility in responding to user requirement changes, and improved software quality.

The XP method was implemented to actively engage relevant parties including the Pangkalpinang City Tourism Office, micro and macro MSME players, and visitors in every development stage. This resulted in a system that is more responsive to tourist needs, such as searching for tourist destinations, booking tourism services, and integrating maps with location-based local information (geo-tagging). The advantages of this approach can also be seen in the system's ability to provide smart recommendations for tourists using a search feature based on tourist interests and preferences.

3.1. Evaluating the Smart Tourism Application

The evaluation process in this study used the System Usability Scale (SUS) as a usability evaluation method. SUS was chosen because of its simplicity and high reliability, as proven by various previous studies. SUS produces quantitative scores that enable objective and comparative interpretation based on international acceptance categories. In line with the findings of Brooke [22], who introduced the SUS as a practical evaluation scale, as well as empirical reinforcement from Lewis and Sauro [23], this method has been proven to provide consistent, valid, and relevant usability indicators for assessing the comfort and ease of use of the developed smart tourism system.

The research participants in this study were general respondents who were potential users of the E-Tourism application. Respondents were asked to complete an online survey via Google Forms. All data collected focused on user perceptions and experiences regarding the use and implementation of the smart tourism system. A total of 70 respondents participated in this survey, and the data obtained was used as the basis for evaluating usability and analyzing user acceptance of the developed application.

SUS is presented in the form of a questionnaire containing 10 statements. Respondents provide scores using a Likert scale of 1–5, where Scale 1 = Strongly disagree, Scale 2 = Disagree, Scale 3 = Undecided, Scale 4 = Agree, and Scale 5 = Strongly agree, as shown in Table 2 below.

Table 2. Standard SUS

No	Question	1	2	3	4	5
1	I plan to use this system again					
2	I find this system complicated to use					
3	I find this system easy to use					
4	I need help from others in using this system					
5	I feel that the features of this system are working properly					
6	I feel that there are many inconsistencies in this system					
7	I feel that others will quickly understand how to use this system					
8	I find this system confusing					
9	I feel that there are no obstacles in using this system					
10	I need to familiarize myself with this system first					

Table 2 presents the questionnaire given to respondents. The questionnaire consists of 5 positive questions and 5 negative questions in accordance with the SUS standard. For questions 1, 3, 5, 7, and 9, the contribution score equals the scale position minus 1. Conversely, for questions 2, 4, 6, 8, and 10, the contribution score is calculated as 5 minus the scale position. The scores are then summed and multiplied by 2.5 to obtain the overall SUS score.

The SUS score is used as an important parameter for assessing the level of user acceptance of a system. A score below 68 indicates usability barriers, requiring in-depth analysis to identify and resolve problems. Conversely, a score above 68 indicates that the system meets basic usability standards, although minor improvements may still be considered to optimize user experience.

Volume 13, Issue 1, April 2026, pp. 43-55
ISSN 2355-5068 ; e-ISSN 2622-4852
DOI: 10.33019/jurnalecotipe.v13i1.4590

The calculation results obtained a SUS score of 75.74, indicating that users consider the Smart Tourism application interface design to be acceptable, and that the system provides a user interface (UI) and user experience (UX) that adequately supports their needs in accessing tourism information and services.

3.2. Discussion

Equations The performance of this web-based smart tourism system is considered satisfactory, based on testing its responsiveness across various platforms, data security measures, and user experience. With interactive displays of tourist destination information, complete with reviews by previous tourists, multimedia galleries for each tourism category, and integration with social media and digital maps, this system can increase tourist engagement both before and during their trip to Bangka Island.

In terms of system sustainability, this system can generate significant opportunities for broader local tourism promotion, especially for lesser-known destinations that have great potential to be discovered. The digitization of tourism information will enable local stakeholders to expand the market reach of each tourist attraction while simultaneously promoting more effective destination management based on visitor data and tourist feedback.

However, several challenges still need to be addressed, including the limited digital infrastructure in remote areas of Bangka Island, the need for digital literacy among tourism stakeholders, and the requirement for ongoing training and assistance. Therefore, collaboration between academics, the Pangkalpinang Tourism Office, and tourism industry stakeholders is essential to ensure the sustainability and development of this system in the future.

Overall, the smart tourism system developed demonstrates that the application of the Extreme Programming (XP) software development method can accelerate the digital transformation of tourism on Bangka Island while simultaneously addressing the challenges of adapting to developments in information technology within the tourism economy sector.

4. CONCLUSION

The development of web-based Smart Tourism has been effective and able to meet the fundamental needs of users in obtaining digital tourism information. Based on usability evaluation using the System Usability Scale (SUS) method, the developed application scored 75.74, which is classified as acceptable, indicating that the quality of the user interface and user experience (UI/UX) was deemed adequate by the respondents. These findings confirm that the Smart Tourism application has succeeded in providing ease of use, clear navigation structure, and functionality relevant to user needs. Overall, this study confirms that the integration of the smart tourism concept through a web-based platform has significant potential in improving the accessibility of destination information and supporting digital transformation efforts in the regional tourism sector.

Acknowledgments

The authors would like to express their sincere gratitude to Universitas Bangka Belitung for providing financial support for this research through the university-level research scheme in 2025.

REFERENCES

[1] I. W. R. Junaedi, D. Waruwu, I. M. Sumartana, B. Hida-, P. Nguyen, and C. Ngin, “Investment Opportunities and Tourism Business Development in The Village of Siallagan Village , Batak Adat Village,” vol. 7, no. 2, pp. 253–268, 2023.

[2] D. A. Lestari, E. Huda, J. Subarkah, and A. Restaman, “Cultural Preservation Strategy Through Tourism : A Case Study of the Surakarta Palace,” pp. 0–4, 2025.

[3] F. Nurul, W. Farahani, I. D. Pramudiana, and D. Ferriswara, “Tourism Sector Development Policy in Increasing Local Income in Gresik Regency,” vol. 2, no. 3, pp. 74–89, 2025.

[4] H. L. Vogel, “Tourism BT - Travel Industry Economics: A Guide for Financial Analysis,” H.

Volume 13, Issue 1, April 2026, pp. 43-55
ISSN 2355-5068 ; e-ISSN 2622-4852
DOI: 10.33019/jurnalecotipe.v13i1.4590

Vogel, Ed., Cham: Springer International Publishing, 2016, pp. 233–255. doi: 10.1007/978-3-319-27475-1_7.

[5] L. Liu, Y. Zhou, and X. Sun, "The Impact of the Wellness Tourism Experience on Tourist Well-Being : The Mediating Role of Tourist Satisfaction," pp. 1–24, 2023.

[6] N. Jasim and S. Talib, "HighTech and Innovation Relationship of Smart Cities and Smart Tourism : An Overview," vol. 1, no. 4, pp. 194–202, 2020.

[7] B. I. Yeoman, T. Li, M. Mars, M. Wouters, C. View, and P. Kay, "2050 — TOMORROW ' S TOURISM," vol. 41, pp. 257–258, 2013.

[8] B. K. B. dan P. P. K. B. Belitung, "Kondisi Geografis." [Online]. Available: https://kesbangpol.babelprov.go.id/content/kondisi-geografis

[9] Z. B. Rasuan, "The Role of Guide and Local Government ….. The Role Of Guide And Local Government In Improving Tourism Acceleration In Bangka Belitung Zulfikri B. Rasuan 1," vol. 1, no. 1, pp. 92–112, 2016.

[10] J. Ilmu, "Accelerating the Development of Bangka Island through Sustainable Tourism by Strengthening the Roles of Multi-stakeholder," vol. 22, no. 3, 2015.

[11] N. Shahirah, M. Shariffuddin, M. Azinuddin, and N. Ezzah, "Heliyon Navigating the tourism digital landscape : The interrelationship of online travel sites ' affordances , technology readiness , online purchase intentions , trust , and E-loyalty," *Heliyon*, vol. 9, no. 8, p. e19135, 2023, doi: 10.1016/j.heliyon.2023.e19135.

[12] E. Widarti and M. Erkamim, "Big Data in Tourism Destinations : A Systematic Literature Review," vol. 4, no. July, pp. 719–724, 2024.

[13] R. Wicaksono, "INTEGRATED TOURISM PLANNING FOR URBAN AND COASTAL AREA , DISCOURSE : BANGKA BELITUNG," vol. 5, no. 1, pp. 1–19, 2025.

[14] X. Guo, J. Pesonen, and R. Komppula, "Comparing online travel review platforms as destination image information agents," *Inf. Technol. Tour.*, vol. 23, no. 2, pp. 159–187, 2021, doi: 10.1007/s40558-021-00201-w.

[15] M. K. Kodmelwar, P. R. Futane, and P. S. D. Pawar, "A Comparative Study of Software Development Waterfall , Spiral and Agile Methodology," vol. 6, no. 3, pp. 7013–7017, 2022.

[16] G. S. Matharu, "Empirical Study of Agile Software Development Methodologies : A Comparative Analysis".

[17] S. Gbli, "Empirical Study of Agile Software Development Methodologies : A Comparative Analysis," vol. 17, no. 5, pp. 30–42, 2024, doi: 10.9734/AJRCOS/2024/v17i5436.

[18] I. Journal and C. Science, "Extreme Programming Vs Scrum: A Comparison of Agile Models Asma Akhtar, Birra Bakhtawar, Samia Akhtar," vol. 2, no. 2, pp. 80–96, 2022.

[19] S. Parikh, "A Review on Extreme Programming in Software Development," no. September, pp. 1354–1358, 2023.

[20] A. Aljehani, "Agile Method : Challenges and Adaptations for Complex Project Environments," vol. 17, no. 3, pp. 84–98, 2025, doi: 10.5815/ijieeb.2025.03.06.

[21] A. Shrivastava, I. Jaggi, N. Katoch, and D. Gupta, "A Systematic Review on Extreme Programming," 2021, doi: 10.1088/1742-6596/1969/1/012046.

[22] J. Brooke, "SUS : A Retrospective," vol. 8, no. 2, pp. 29–40, 2013.

[23] J. J. R. Lewis, "Revisiting the Factor Structure of the System Usability Scale," vol. 12, no. 4, pp. 183–192, 2017.

JURNAL ECOTIPE
Electronic, Control, Telecommunication, Information, and Power Engineering
Volume 13, Issue 1, April 2026, pp. 56-68
ISSN 2355-5068 ; e-ISSN 2622-4852
DOI: 10.33019/jurnalecotipe.v13i1.4583

Microwave Sensing of Sugar Solution Concentration Using a 2.4 GHz Microstrip Antenna

Hanalde Andre[1], Jimmy Nelson[2], Rizki Wahyu Pratama[3], Toha Zaky[4]
[1,2,3] Universitas Andalas, Limau Manis, Padang 25163, Indonesia
[4] National Research and Innovation Agency Republic of Indonesia (BRIN), South Tangerang 15314 Indonesia

ARTICLE INFO

Article historys:

Received : 26/11/2025
Revised : 22/01/2026
Accepted : 30/04/2026

Keywords:

Dielectric Constant; Microstrip Antenna; Sugar Solution; Split Ring Resonator (SRR)

ABSTRACT

Microstrip antennas are widely used in sensing applications according to compact, low-cost, and easy to fabricate. This study presents the design and evaluation of a 2.4 GHz circular patch microstrip antenna integrated with a split-ring resonator (SRR) for sensing sugar-solution concentration through dielectric property induced perturbations. The antenna employs an inset feed configuration and is implemented on an FR4 substrate. The design and parametric analysis are carried out in simulation by placing sugar solutions with mole fractions from 0 to 0.04 in the sensing region. In result, we observe changes in resonant frequency, minimum return loss, and quality factor (Q). The simulations indicate monotonic trends with concentration, with the minimum return loss becoming less negative as concentration increases, accompanied by reductions in resonant frequency and Q. Experimental measurements of the fabricated prototype, however, show weaker and less consistent correlations across the same parameters, highlighting the sensitivity of the response to practical factors such as sample positioning, fabrication tolerances, and measurement repeatability.

Corresponding Author:

Hanalde Andre
Universitas Andalas, Limau Manis, Padang 25163, Indonesia
Email: hanalde.andre@eng.unand.ac.id

1. INTRODUCTION

Sugar is a vital component in human life, serving as a primary energy source that is easily absorbed by the body. Its demand continues to increase to meet the needs of the food and pharmaceutical industries, as well as its use as a raw material in bioconversion processes [1-3]. Sugar is widely present in various sweet foods and beverages. In Indonesia, the consumption of high-sugar foods and drinks has grown increasingly popular among the public. However, excessive sugar intake can adversely affect health, with one of the most notable consequences being a higher risk of obesity [4-5]. Therefore, to avoid excessive sugar consumption, it is essential to monitor and quantify the amount of sugar being consumed.

Like most substances, sugar exhibits specific electrical properties influenced by internal factors such as moisture content, chemical composition, acidity level, and other intrinsic characteristics. One important electrical property is the dielectric constant, which indicates a material's ability to store electric charge. The dielectric constant varies according to the concentration of the substance within a solution [6-7].

Volume 13, Issue 1, April 2026, pp. 56-68
ISSN 2355-5068 ; e-ISSN 2622-4852
DOI: 10.33019/jurnalecotipe.v13i1.4583

The relationship between solution concentration and dielectric constant has long been an important topic of interest across disciplines, including physical chemistry and sensing technology. This relationship is significant because the dielectric constant of a solution not only reflects its electrical properties but can also provide valuable information regarding changes in its internal structure and composition. In practical applications, understanding dielectric behavior is useful for accurately measuring solution concentration, monitoring crystallization processes in industrial settings, and developing electrochemical sensors that detect chemical environment changes [8-10].

With rapid technological advancements, particularly in wireless communication, various devices have been developed to address challenges in sugar concentration detection. One of the most widely used wireless technologies is the microstrip antenna. Its selection is motivated by advantages such as ease of fabrication, low production cost, mechanical robustness, fast response, and high sensitivity [11-13]. A microstrip antenna can function as a microwave sensor by detecting changes in the dielectric properties of materials located within its near-field region [6]. Although simple, this method holds great potential for development as a non-contact, real-time sugar concentration sensor, particularly beneficial for the beverage industry in maintaining product quality efficiently.

Several previous studies have explored microstrip antennas as sensors for detecting salt and sugar concentrations in water. One such study [14-16], utilized a crescent-shaped radiating element operating from 2.50 GHz to 18 GHz. The antenna served as a sensor to detect salt and sugar content based on the dielectric constants of the solutions. The results indicated that solution concentration is inversely proportional to dielectric constant, where increases in salt or sugar content led to decreases in dielectric constant. Another relevant study [18-20], used salt and sugar samples tested by immersing the antenna directly into solution containers. The findings revealed that higher salt or sugar concentrations increased reflection coefficients, while the dielectric constant decreased.

This work proposes the design of a circular-patch microstrip antenna integrated with a Split Ring Resonator (SRR) operating at the 2.4-GHz WiFi band for sensing variations in sugar-solution concentration. The proposed antenna leverages the sensitivity of resonant structures to dielectric changes, enabling detection based on shifts in resonant characteristics. The detailed design, simulation, and performance evaluation of the antenna as a microwave-based sugar concentration sensor are presented in this paper.

2. RESEARCH METHOD

The first stage of the design process involves determining the operating frequency of the antenna, which is set at 2.4 GHz, along with the desired antenna characteristics, namely VSWR and return loss. The antenna dimensions—including the patch, ground plane, feed line, and substrate—are then calculated using standard design equations, followed by the integration of an SRR structure on the patch. After obtaining the antenna dimensions, a tube is added as the container for sugar-solution testing. The tube is cylindrical with a diameter of 15 mm and a height of 40 mm. The complete design is subsequently simulated using CST Studio Suite. If the simulation results do not meet the expected antenna parameters and target performance, an optimization process is carried out.

Once the antenna optimization is completed, simulations are performed to obtain the return loss and VSWR values prior to the introduction of the sugar solution. Sugar solutions with mole fractions ranging from 0 to 0.040 are then tested using the tube, based on their dielectric constants. The results of these evaluations are analyzed to draw conclusions. The flowchart of the research procedure is illustrated in Figure 1.

JURNAL ECTIPE
Electronic, Control, Telecommunication, Information, and Power Engineering
Volume 13, Issue 1, April 2026, pp. 56-68
ISSN 2355-5068 ; e-ISSN 2622-4852
DOI: 10.33019/jurnalecotipe.v13i1.4583

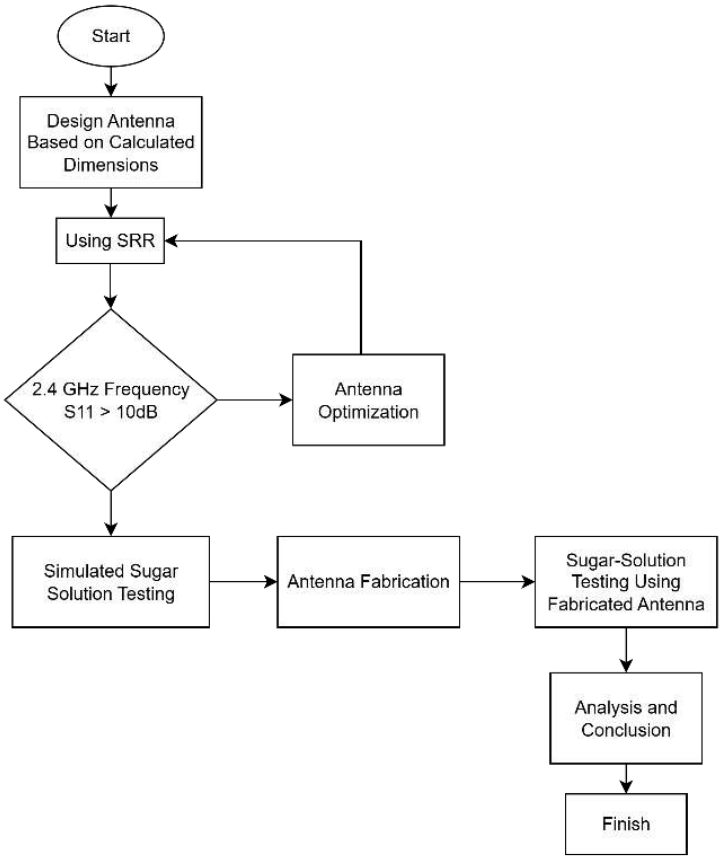

Figure 1. Flowchart of the antenna design and testing process

2.1. Antenna Calculation

The antenna substrate is composed of a dielectric material whose properties have a significant impact on the antenna performance. Different substrate types exhibit varying dielectric constant (ε_r) and dielectric loss tangent (tan δ). In this work, an FR4 (Epoxy) substrate is employed, and its material characteristics are summarized in Table 1.

Table 1. FR4 (Epoxy) substrate characteristics

Spesification	Value
Dielectric Constant (ε_r)	4.4
Substrate thickness	1.6 mm
Dielectric loss tangent ($tan\ \delta$)	0.02

The patch used in this design has a circular shape; therefore, the first step is to determine the patch radius. Prior to calculating the radius, the logarithmic function of the patch (F) must be obtained. The logarithmic function for the circular patch represents the resonant frequency equation and the dielectric constant of the antenna substrate. To obtain the radius of the antenna patch (a), the calculation is performed using the logarithmic function, the substrate thickness, and the substrate dielectric constant, as shown in the equation below.

$$F = \frac{8{,}791 \times 10^9}{2.4 \times 10^9 \sqrt{4.4}} = 1.746$$

$$a = \frac{1.746}{\left\{1 + \frac{2 \times 0.16\ cm}{3.14 \times 4.4 \times 1.746}\left[\ln\left(\frac{3.14 \times 1.746}{2 \times 0.16}\right) + 1.7726\right]\right\}^{1/2}}$$

$$a = 1.69\ cm = 16.9\ mm \approx 17\ mm$$

JURNAL ECOTIPE
Electronic, Control, Telecommunication, Information, and Power Engineering
Volume 13, Issue 1, April 2026, pp. 56-68
ISSN 2355-5068 ; e-ISSN 2622-4852
DOI: 10.33019/jurnalecotipe.v13i1.4583

2.2. Split Ring Resonator (SRR)

A Split Ring Resonator (SRR) is an artificial structure used to implement planar technology and is commonly applied in compact microwave components. An SRR is typically made of a metallic material and consists of two closed conductive rings with splits positioned on opposite sides. The spacing between the two rings introduces a high capacitance value, which leads to a reduction in the resonant frequency. SRRs are widely used to enhance the performance of information and communication technology devices—particularly filters and antennas—without altering their primary features or increasing their physical dimensions. The type, pattern, arrangement, and gap spacing of the SRR significantly influence the resulting electromagnetic behavior [15]. SRR structure can shown in Figure 1.

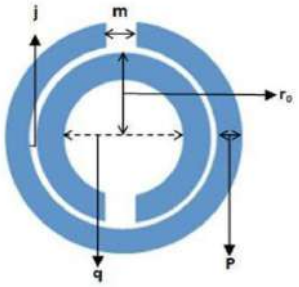

Figure 2. SRR structure

The proposed sensing antenna incorporates a Split Ring Resonator (SRR) structure that is embedded within the radiating patch to enhance the electric-field concentration in the designated sensing region. The SRR functions as a subwavelength resonant inclusion capable of supporting strong localized electric fields due to its capacitive gap and circulating surface currents. This local field enhancement mechanism is critical for improving the interaction between the electromagnetic wave and the analyte under test, thereby increasing the overall sensitivity of the sensor to small variations in the dielectric properties of sugar–water solutions.

The design process began with a conventional rectangular microstrip patch operating at the target resonant frequency. Subsequently, a single-stage and later a multi-stage SRR topology were evaluated to determine the configuration providing the highest perturbation response. Key geometrical parameters—including the outer ring radius, ring width, inter-ring spacing, and the gap size—were systematically optimized using full-wave electromagnetic simulations. A parametric sweep was performed to study the impact of each parameter on the resonance shift, electric-field distribution, and quality factor (Q-factor). The SRR was strategically positioned at the location of maximum electric-field density on the patch to maximize its coupling to the sensing medium.

To account for the presence of the liquid sample, a fluidic channel (or dielectric layer) was modeled above the SRR region, enabling accurate prediction of the field–matter interaction. Boundary conditions, substrate material properties, and meshing strategies were carefully selected to ensure numerical stability and convergence. The final antenna layout, including the SRR configuration, feedline geometry, and sensing chamber placement, is illustrated in Figure 3.

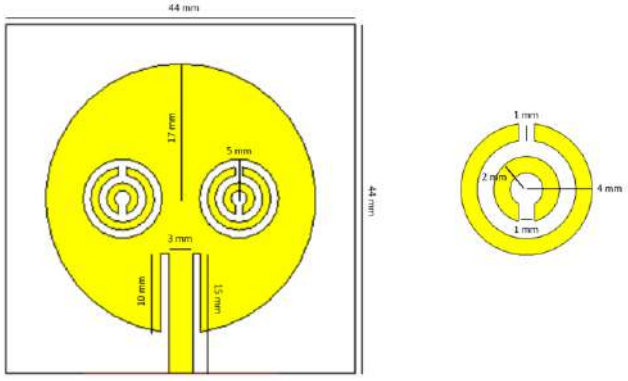

JURNAL ECTIPE
Electronic, Control, Telecommunication, Information, and Power Engineering
Volume 13, Issue 1, April 2026, pp. 56-68
ISSN 2355-5068 ; e-ISSN 2622-4852
DOI: 10.33019/jurnalecotipe.v13i1.4583

Figure 3. Antenna design

2.3. Sugar Solution Sensing

A solution is a homogeneous mixture consisting of two or more substances with variable composition. The substance present in a smaller amount is referred to as the solute, while the substance present in a larger amount is known as the solvent. The properties of a solution are strongly influenced by its composition, which is expressed through its concentration. This concentration represents the ratio of the amount of solute to the amount of solvent [18].

The concentration of a solution represents the ratio between the amount of solute and the amount of solvent. The solubility of a substance can vary widely, ranging from very low to very high. If the amount of solute exceeds its saturation point, the excess solute will precipitate at the bottom of the solution. Under certain conditions, a solution may contain more solute than the amount normally present at saturation. The concentration of a substance can be expressed in various ways, one of which is the mole fraction, denoted by X. The formula for the mole fraction is shown in the following equation [19].

$$Mole\ Fraction = X_A = \frac{Number\ of\ moles\ of\ A}{Total\ number\ of\ moles\ of\ all\ components}$$

Sugar is a form of carbohydrate that serves as a primary energy source for the body and provides sweetness to food and beverages. One type of sugar is sugar, a simple carbohydrate commonly referred to as a simple sugar. Sugar is widely used as an additional sweetener [20]. Sugar can be found in several forms, including anhydrous sugar and monohydrate sugar. The primary difference between these forms lies in the presence of water molecules within their structures.

Anhydrous sugar is the pure form of sugar without any crystalline water molecules, meaning each sugar molecule ($C_6H_{12}O_6$) stands alone. This form is often used in the pharmaceutical and food industries due to its high purity and greater stability against moisture [21]. In contrast, monohydrate sugar contains one water molecule bound within its crystalline structure for each sugar molecule. Its chemical formula is $C_6H_{12}O_6 \cdot H_2O$. This form is more commonly available and frequently used in products requiring rapid solubility or as a sweetener in beverages and processed foods. The presence of the water molecule results in slight differences in molecular weight and certain physical properties compared to anhydrous sugar [22]. When sugar is dissolved in water, it forms a sugar solution. This solution is classified as a non-electrolyte, meaning it does not conduct electricity because it does not produce free-moving ions in the solution [5].

The performance of the proposed antenna as a dielectric sensor was experimentally evaluated using a cylindrical sample holder positioned precisely above the sensing region of the antenna, as illustrated in Figure 4. The cylindrical container, fabricated from a low-loss dielectric material to minimize additional parasitic loading, was employed to confine and stabilize the liquid under test during measurement. Its geometry ensures uniform sample thickness above the SRR-enhanced sensing area, thereby improving measurement repeatability and reducing uncertainty caused by sample displacement or surface perturbations.

During testing, the cylindrical vessel was aligned with the antenna's electric-field hotspot to maximize electromagnetic coupling between the resonant structure and the sugar–water solutions. The container dimensions—specifically, its inner diameter, wall thickness, and height—were selected to avoid unintended resonances or mode coupling that could distort the antenna's response. All samples were introduced into the holder in controlled volumes to maintain a constant sensing depth across measurements.

JURNAL ECTIPE
Electronic, Control, Telecommunication, Information, and Power Engineering
Volume 13, Issue 1, April 2026, pp. 56-68
ISSN 2355-5068 ; e-ISSN 2622-4852
DOI: 10.33019/jurnalecotipe.v13i1.4583

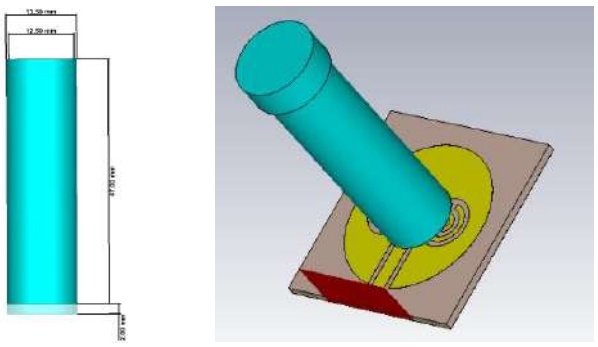

(a) (b)

Figure 4. (a) Tube dimension, (b) Tube position

3. RESULTS AND DISCUSSION

The experimental evaluation was conducted to investigate the influence of sugar-solution concentration on the antenna's sensing characteristics, including return loss, VSWR, resonant frequency, and quality factor (Q-factor). A fixed sample volume of 4 mL was used for all measurements to maintain consistent sensing depth and minimize geometric variations within the sensing region.

Sugar–water solutions were prepared with molar fractions ranging from 0 to 0.04, with an incremental step of 0.005 between successive concentrations. Each solution was introduced into the cylindrical sample holder and positioned above the antenna as described previously. For every concentration level, the antenna response was recorded using a calibrated Vector Network Analyzer (VNA), ensuring that any observed variations in the measured parameters were solely attributable to changes in the dielectric properties of the solution

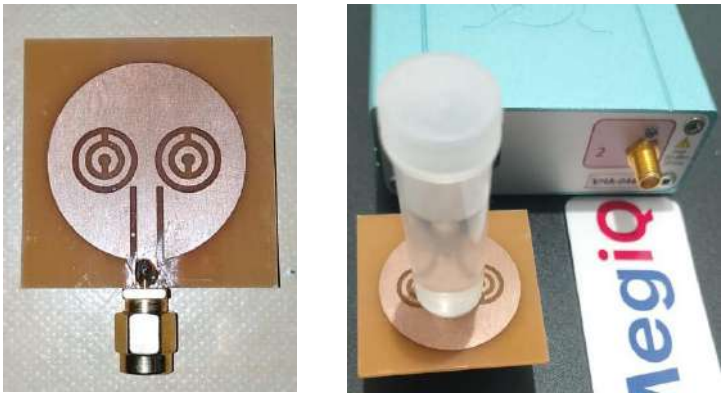

(a) (b)

Figure 5. (a) Antenna fabrication, (b) Measurement procedure using a Vector Network Analyzer

3.1. Simulation Result

The frequency variation after measurement is presented in Figure 6. As shown, the antenna's resonant frequency exhibits a slight decrease with increasing sugar molar fraction before stabilizing. This behavior does not align with the general theoretical expectation, in which a reduction in dielectric constant should cause the resonant frequency to increase. One possible explanation for this phenomenon is the use of the SRR structure in the antenna design, which results in a more complex electric-field response. A decrease in dielectric constant may alter the electric-field distribution around the sensing region, leading to a nonlinear or even counterintuitive resonant behavior compared to conventional theory.

Therefore, the frequency response is influenced not only by the dielectric constant itself but also by how the solution affects the electromagnetic field distribution around the patch and the SRR elements. Furthermore, Figure 6 shows that beyond a molar fraction of 0.025, the resonant frequency tends to

JURNAL ECTIPE
Electronic, Control, Telecommunication, Information, and Power Engineering
Volume 13, Issue 1, April 2026, pp. 56-68
ISSN 2355-5068 ; e-ISSN 2622-4852
DOI: 10.33019/jurnalecotipe.v13i1.4583

remain constant, indicating a saturation point in the solution's influence on the antenna resonance. This also suggests a reduction in system sensitivity to further changes in the dielectric constant.

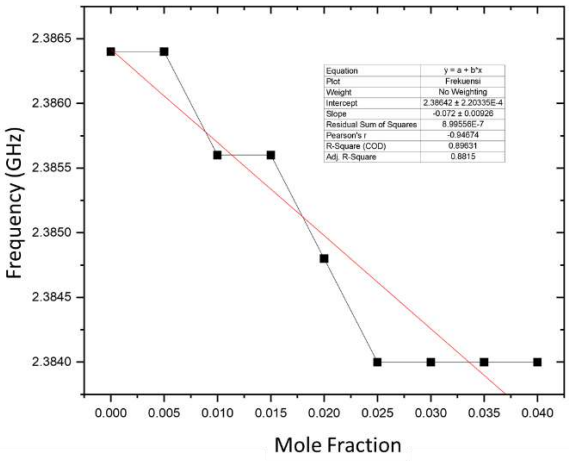

Figure 6. Simulated frequency resonant response

In the simulation-based evaluation, the antenna exhibited noticeable variations in the return loss characteristics after the introduction of sugar solutions. At a mole fraction of 0 (pure water), the simulated return loss was measured at –14.711 dB. As the mole fraction of sugar increased, the return loss showed a consistent upward trend, indicating a progressive degradation in impedance matching due to changes in the dielectric properties of the sensing medium.

Figure 7 presents the simulated return loss obtained after varying the sugar-solution concentration. A clear linear relationship is observed between the mole fraction of sugar and the return loss magnitude. As the mole fraction increases, the return loss performance degrades, with its value shifting closer to 0 dB, indicating higher power reflection and reduced impedance-matching efficiency. This degradation is accompanied by a resonance-frequency shift toward lower frequencies, which is attributed to the decrease in the effective dielectric constant of the solution. The resulting change in dielectric characteristics drives the system away from its optimal matching condition, thereby reducing the overall return-loss performance.

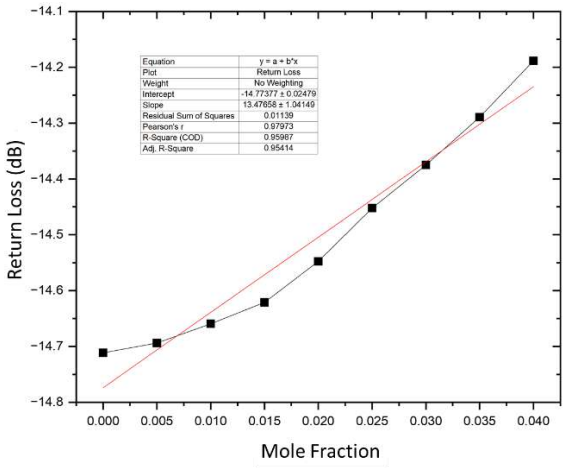

Figure 7. Simulated return loss response

The relationship between the mole fraction of the sugar solution and the return loss can be analyzed using a simple linear regression model. The linear regression equation describes the effect of the sugar-solution mole fraction (x) on the return loss (y). The model also includes the coefficient of determination (R^2), which indicates how much of the variation in the return loss (y) can be explained by changes in the mole fraction (x). In other words, R^2 represents the percentage of variability in y that is attributable to x, while the remaining portion is influenced by other factors. Because the predicted y values are not

JURNAL ECOTIPE
Electronic, Control, Telecommunication, Information, and Power Engineering
Volume 13, Issue 1, April 2026, pp. 56-68
ISSN 2355-5068 ; e-ISSN 2622-4852
DOI: 10.33019/jurnalecotipe.v13i1.4583

perfectly accurate, the Root Mean Square Error (RMSE) of the regression model is also computed to evaluate the model's prediction error. In addition, the strength of the linear relationship between x and y is quantified using the correlation coefficient (R). From the return-loss graph, the correlation coefficient is calculated to be 0.97973, and the coefficient of determination is 0.95987. This indicates that 95.99% of the variation in return loss is explained by the mole fraction of the sugar solution, with the remaining portion caused by other factors. The RMSE obtained from the regression equation is 0.03557491.

The simulated antenna test shows a change in the Q factor compared to the value obtained prior to the addition of the sugar solution. The Q factor at a mole fraction of 0 is 50.77447, whereas after increasing the mole fraction to 0.010, the Q factor decreases slightly to 50.75745. The frequency response after testing is presented in Figure 8. It can be observed that the Q-factor decreases as the sugar solution concentration increases. This trend indicates that higher molar fraction or dielectric constant values lead to a lower antenna Q-factor. Consequently, the antenna exhibits reduced frequency selectivity and a broader bandwidth. The reduction in Q-factor ultimately degrades the sensor's frequency-shift resolution.

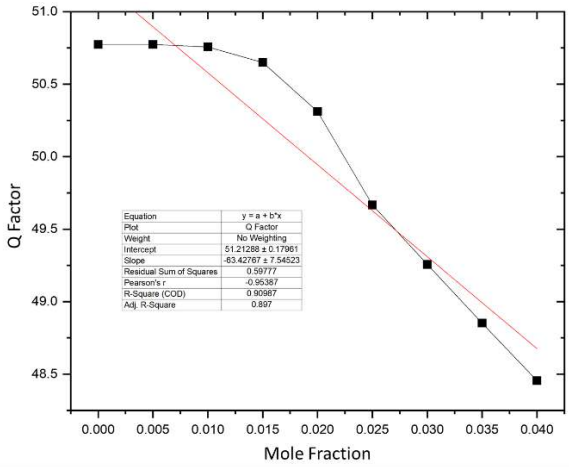

Figure 8. Simulated Q-factor response

The relationship between the molar fraction of the sugar solution and the Q-factor can be analyzed using a simple linear regression model. In this model, the coefficient of determination (R^2) quantifies how much of the variation in (y) is explained by changes in (x). In other words, the variation in the Q-factor is explained by the molar fraction of the sugar solution, while the remaining percentage is attributed to other uncontrolled factors. This indicates that the predicted values are not entirely accurate, and therefore the Root Mean Square Error (RMSE) must also be evaluated to assess the model's reliability. Additionally, the strength of the linear relationship is measured using the correlation coefficient. From the Q-factor regression plot, the correlation coefficient is obtained as −0.95387 and the coefficient of determination as 0.90987. These results indicate that the molar fraction of the sugar solution contributes 90.99% to the variation in the Q-factor, while the remaining variation is influenced by other factors.

3.2. Measurement of the Fabricated Antenna Using the Solution

The frequency variation after measurement is presented in Figure 9. It can be observed that changes in the sugar molar fraction do not exhibit a linear relationship with the resonant frequency. The measured frequency values fluctuate irregularly, indicating that the addition of sugar does not consistently affect the antenna's resonant behavior. However, despite these fluctuations, a general downward trend in frequency can still be identified at certain molar fraction intervals.

Theoretically, increasing sugar concentration should lower the dielectric constant of the solution and consequently increase the resonant frequency. One possible cause of the deviation from this expected behavior is the non-uniformity of the sugar solution, resulting in micro-scale concentration

JURNAL ECTIPE
Electronic, Control, Telecommunication, Information, and Power Engineering
Volume 13, Issue 1, April 2026, pp. 56-68
ISSN 2355-5068 ; e-ISSN 2622-4852
DOI: 10.33019/jurnalecotipe.v13i1.4583

variations that affect the local dielectric properties around the patch and SRR. Additional factors, such as interference from the connectors, non-ideal substrate characteristics, and fabrication imperfections on the patch and SRR gaps, may also introduce unexpected perturbations in the resonant pattern. Since microstrip antennas are highly sensitive to their surrounding environment, particularly in regions of strong electric fields such as the patch and SRR gaps, even small variations can significantly disrupt the resonance characteristics.

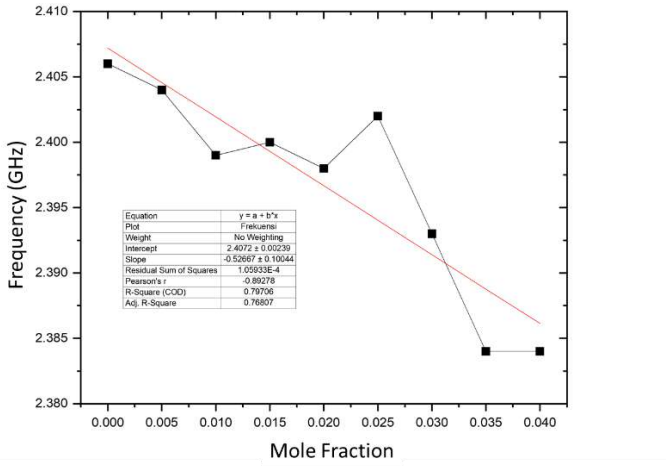

Figure 9. Measured frequency resonant of the fabricated antenna

The fabricated antenna was printed and soldered at the feed line, where an SMA connector was attached to interface the antenna with the measurement equipment. Sugar solutions with molar fractions ranging from 0 to 0.040, at an interval of 0.005, were used for the measurements. During testing, each sugar solution was placed in a tube with a volume of 4 mL. A vector network analyzer (VNA) was employed to characterize the antenna, and all measurements were conducted in the Telecommunication Laboratory. The measurement results of the fabricated antenna were then compared with the simulation results to identify and analyze the sources of discrepancy between the two.

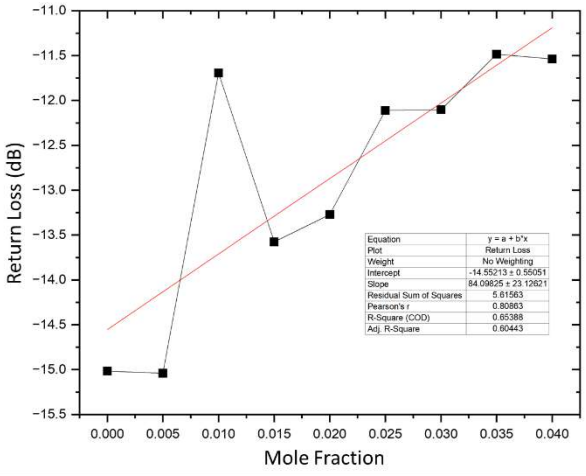

Figure 10. Measured return loss of the fabricated antenna

From the return loss plot in Figure 10, the correlation coefficient is obtained as 0.80863, while the coefficient of determination (R^2) is 0.65388. This indicates that the molar fraction of the sugar solution accounts for 65.39% of the variation in the return loss, with the remaining variation influenced by other factors. The RMSE calculated from the corresponding linear regression model is 0.7899104.

The Q-factor variation after measurement is presented in Figure 11. The relationship between the sugar molar fraction and the Q-factor is non-linear and does not exhibit a consistent trend. The Q-factor values fluctuate as the molar fraction increases, with an average value of 49.5. From the Q-factor plot,

Volume 13, Issue 1, April 2026, pp. 56-68
ISSN 2355-5068 ; e-ISSN 2622-4852
DOI: 10.33019/jurnalecotipe.v13i1.4583

the correlation coefficient is obtained as –0.78017, while the coefficient of determination (R^2) is 0.60867. This indicates that the molar fraction of the sugar solution accounts for 60.87% of the variation in the Q-factor, with the remaining variation influenced by other factors. The RMSE computed from the corresponding linear regression model is 3.47035054.

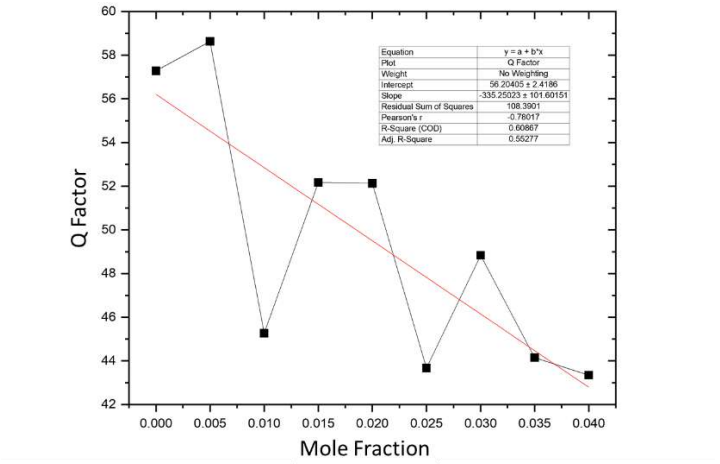

Figure 11. Measured Q-factor of the fabricated antenna

3.3. Comparison of Simulated and Measured Antenna Performance

Based on Figure 12, a clear difference in the overall trend is observed between the simulated and measured results. The simulated return loss demonstrates a consistent increase with higher molar fractions of the sugar solution, whereas the measured return loss exhibits a fluctuating and irregular pattern. These discrepancies can be attributed to several factors, including suboptimal soldering at the feed line, dimensional tolerances between the simulated and fabricated prototypes, variations in substrate material properties, and the inherent measurement uncertainty of the instrumentation used.

In addition, environmental factors—such as temperature, humidity, and the presence of surrounding objects may influence the measured response, as fabricated antennas are significantly more sensitive to external perturbations compared to their simulated counterparts. The simulation environment benefits from idealized conditions with perfect material models and boundary settings, thereby minimizing noise and parasitic effects. Conversely, the fabricated antenna is influenced by manufacturing imperfections, slight misalignments, and non-ideal feeding conditions, all of which contribute to the observed deviations.

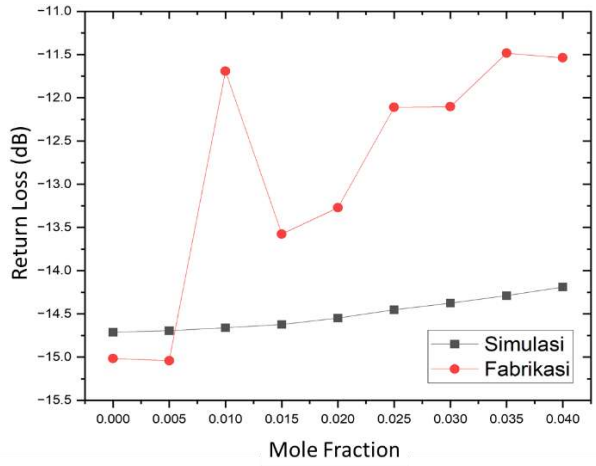

Figure 12. Comparison of the simulated and measured return loss

JURNAL ECTIPE
Electronic, Control, Telecommunication, Information, and Power Engineering
Volume 13, Issue 1, April 2026, pp. 56-68
ISSN 2355-5068 ; e-ISSN 2622-4852
DOI: 10.33019/jurnalecotipe.v13i1.4583

Based on the plot in Figure 13, a clear difference in trend can be observed between the simulated and measured results. The simulated Q-factor exhibits a decreasing trend as the molar fraction of the sugar solution increases, whereas the measured Q-factor shows a fluctuating and irregular pattern. These discrepancies can be attributed to several factors, including suboptimal soldering, dimensional deviations between the simulated and fabricated antennas, and variations in connector quality. Simulation-based testing benefits from ideal and highly controlled conditions, resulting in minimal errors caused by external influences. In contrast, measurements on the fabricated antenna are affected by numerous external factors, such as environmental noise, imperfect feeding conditions, and material inconsistencies, which contribute to the non-uniform response.

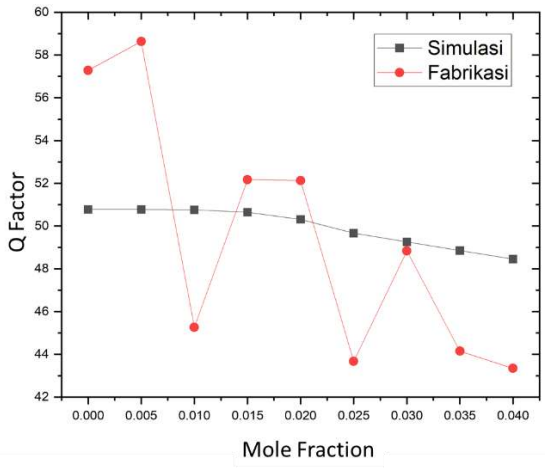

Figure 13. Comparison of the simulated and measured Q-factor

Based on the graph in Figure 14, a clear difference in trend is observed between the simulated and fabricated antenna results. The simulated antenna exhibits a decreasing frequency trend as the molar fraction increases. In contrast, the fabricated antenna shows fluctuating and inconsistent frequency values across the molar fraction variations. These discrepancies can be attributed to several factors, including suboptimal soldering, dimensional deviations between the simulated and fabricated antennas, and variations in the quality of the measurement connectors. Simulation-based testing provides a controlled environment with minimal external interference, thereby reducing the likelihood of measurement errors. Conversely, measurements on the fabricated antenna are influenced by numerous external factors, such as environmental noise, imperfect feeding conditions, and material inconsistencies, all of which contribute to the observed fluctuations in frequency response.

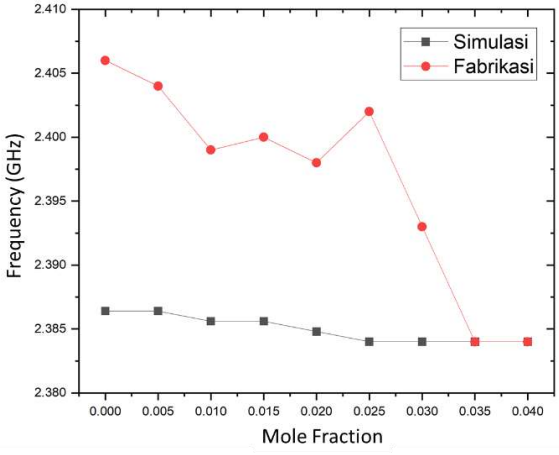

Figure 11. Comparison of the simulated and measured frequency resonant

Volume 13, Issue 1, April 2026, pp. 56-68
ISSN 2355-5068 ; e-ISSN 2622-4852
DOI: 10.33019/jurnalecotipe.v13i1.4583

4. CONCLUSION

This work designed and evaluated a circular-patch microstrip antenna integrated with a split-ring resonator (SRR) for sensing sugar-solution concentration through dielectric perturbation. The simulation results show consistent monotonic changes in resonant frequency, minimum return loss, and quality factor as the sugar concentration increases, indicating that the proposed antenna–SRR structure is sensitive to concentration-dependent dielectric variations under controlled modeling conditions. Measurements on the fabricated prototype exhibit weaker and less consistent trends compared with the simulations. Although the experimental responses generally follow the expected direction of change, the increased scatter suggests that practical non-idealities—such as sample positioning, container influence, fabrication tolerances, connector/solder losses, and measurement repeatability—significantly affect the observed sensing performance. Among the evaluated metrics, the resonant-frequency shift appears to be the most robust experimental indicator, while return loss and quality factor are more susceptible to measurement conditions. Overall, the results support the feasibility of the antenna–SRR approach for dielectric-based sugar-solution sensing and highlight the need for improved experimental control and material characterization to better align simulations with measurements.

Acknowledgments

This research was supported by the Penelitian Dosen Teknik Elektro scheme contract number B/ 66 /UN.16.09/SPK/PT.01.03/RKA T-UNAND/2025, Universitas Andalas, under the 2025 Research Program. The authors would like to express their gratitude to the Department of Electrical Engineering for providing laboratory facilities and technical support throughout the completion of this work.

REFERENCES

[1] Parnasari, M. Nurhanisa, and B. S. Nugroho, “Studi Kapasitansi dan Konstanta Dielektrik Pada Karbon Aktif Tandan Kosong Kelapa Sawit,” vol. 10, no. 1, pp. 98–104, 2022.

[2] C. Daniel, “Faktor Dominan yang Berhubungan dengan Konsumsi Gula pada Mahasiswa Nonkesehatan,” vol. 12, no. 2, pp. 93–106.

[3] J. N. Arini, “Perancangan Antena Mikrostrip Circular *Patch* 2,4 GHz Sebagai Sensor Untuk Mendeteksi Larutan Gula Dengan Metode Transmisi Langsung,” Universitas Andalas, 2023.

[4] S. Alam and K. A. Santoso, “Antena Mikrostrip Segitiga Dengan Parasitic Untuk Aplikasi Wireless Fidelity,” vol. 2, no. 1, pp. 25–37, 1945.

[5] Ismail and K. Budayawan, “VoteTEKNIKA,” *J. Vocat. Tek. Elektron. dan Inform.*, vol. 10, no. 1, pp. 20–27, 2022.

[6] A. E. Omer *et al.*, “Multiple-Cell Microfluidic Dielectric Resonator for Liquid Sensing Applications,” *IEEE Sens. J.*, vol. 21, no. 5, pp. 6094–6104, 2021.

[7] M. T. Islam, N. Rahman, M. S. J. Singh, and Samsuzzaman, “Detection of Salt and Sugar Contents in Water on the basis of Dielectric Properties using Microstrip Antenna-based Sensor,” vol. 3536, pp. 1–9, 2017, doi: 10.1109/ACCESS.2017.2787689.

[8] S. Jain, “Early Detection of Salt and Sugar by Microstrip Moisture Sensor Based on Direct Transmission Method,” *Wirel. Pers. Commun.*, no. 0123456789, pp. 1–9, 2021, doi: 10.1007/s11277-021-08914-1.

[9] C. A. Balanis, *Antenna Theory Analysis And Design Fourth Edition*, 4th ed. New Jerseys: John Wiley & Sons. Inc, 2016.

[10] Z. Liu and K. Chen, “Crack Monitoring Method for an FRP-Strengthened Steel Structure Based on an Antenna Sensor,” *Sensors (Switzerland)*, vol. 17, no. 10, 2017, doi: 10.3390/s17102394.

[11] N. Julardi and A. H. Rambe, “Rancang Bangun Antena Mikrostrip *Patch* Circular (2,45 GHz)

Volume 13, Issue 1, April 2026, pp. 56-68
ISSN 2355-5068 ; e-ISSN 2622-4852
DOI: 10.33019/jurnalecotipe.v13i1.4583

Dengan Teknik Planar Array Sebagai Penguat Sinyal Wi-Fi," vol. 1, no. 2, pp. 59–64, 2013.

[12] Y. Christyono, I. Santoso, and R. D. Cahyo, "Perancangan Antena Mikrostrip Array Pada Frekuensi 850 MHz," *Transmisi*, vol. 18, no. 2, pp. 88–95, 2016.

[13] M. I. Setiawan and J. Endri, "Rancang Bangun Antena Mikrostrip Path Rectangular pada Frekuensi 900 MHz untuk Aplikasi GSM," *Teknol. Inf.*, vol. 14, no. 2, pp. 53–60, 2019.

[14] Z. Faisal, "Rancang Bangun Antena Mikrostrip *Patch* Sirkular Dengan Metode Insert Feeding Untuk Aplikasi LTE di Frekuensi 2.600 MHz," Akademi Telkom Jakarta, 2016.

[15] Kusmadi and T. Mulyana, "Metoda Split Ring Resonator Untuk Performansi Bandpass Filter Pada Aplikasi Pemanen Energi," *J. Infotronik*, vol. 7, no. 1, pp. 50–63, 2022, doi: 10.32897/infotronik.2022.7.1.1433.

[16] B. E. Cahyono, Misto, and H. N. Arivah, "Analisa Kualitas Semen Melalui Pengukuran," *R.E.M. (Rekayasa Energi Manufaktur) J.*, vol. 2, no. 2, pp. 57–61, 2017, doi: 10.21070/r.e.m.v2i2.1199.

[17] L. Mei, A. Putri, T. Prihandono, and B. Supriadi, "Air adalah suatu zat kimia yang penting bagi semua bentuk kehidupan yang diketahui sampai saat ini di bumi ," *J. Pembelajaran Fis.*, vol. 6, no. 2, pp. 147–153, 2017.

[18] M. A. Ridhani, I. P. Vidyaningrum, N. N. Akmala, S. Azzahro, and N. Aini, "Potensi Penambahan Berbagai Jenis Gula Terhadap Sifat Sensori Dan Fisikokimia Roti Manis : Review," *Pas. Food Technol. J.*, vol. 8, no. 3, pp. 61–68, 2021.

[19] "Dextrose anhydrous," ChemBK. Accessed: Jul. 14, 2025. [Online]. Available: https://www.chembk.com/en/chem/Dextrose anhydrous

[20] Y. Liang, M. Ma, F. Zhang, F. Liu, and Z. Liu, "An LC Wireless Microfluidic Sensor Based on Low Temperature Co-Fired Ceramic (LTCC) Technology," *Sensors (Switzerland)*, vol. 19, no. 5, 2019, doi: 10.3390/s19051189.

JURNAL ECOTIPE
Electronic, Control, Telecommunication, Information, and Power Engineering

Volume 13, Issue 1, April 2026, pp. 82-92
ISSN 2355-5068 ; e-ISSN 2622-4852
DOI: 10.33019/jurnalecotipe.v13i1.4586

Analysis of Energy Management System and Feasibility of 25 kWp Rooftop Solar Power Plant using Techno-Economic Method in DKI Jakarta Regional Government Building

Angga Septian[1], Chairul G. Irianto[2], Lydia Sari[3]
[1]Graduate Program of Electrical Engineering Trisakti University, Kyai Tapa No. 1, Jakarta 114400, Indonesia
[2,3]Department of Electrical Engineering Trisakti University, Kyai Tapa No. 1, Jakarta 114400, Indonesia

ARTICLE INFO

Article historys:

Received : 26/01/2026
Revised : 28/02/2026
Accepted : 30/04/2026

Keywords:

Energy Efficiency Retrofit; Energy Management; Public Building; Rooftop Solar PV; Techno-economic Analysis

ABSTRACT

The building sector is a major contributor to energy consumption and greenhouse gas emissions in Indonesia, accounting for approximately 50% of national energy use and nearly 30% of total emissions. This study evaluates the implementation of an ISO 50001–based Energy Management Systems (EnMS) in a government building in Jakarta, combining energy efficiency retrofits with rooftop photovoltaic (PV) integration. The research contributes a comprehensive technical and economic assessment that quantifies energy savings, emission reductions, and financial feasibility within a replicable public-sector framework. The methodology included an ISO 50001–aligned energy audit, building energy simulation using DesignBuilder, PV system design with PVsyst, and economic feasibility analysis. LED lighting retrofits reduced lighting energy consumption by 38.14%, while air-conditioning optimization improved thermal comfort. A 24.75 kWp rooftop PV system generated 33,428 kWh annually, supplying 17.97% of the building's electricity demand. In total, the integrated measures achieved annual energy savings of 37,587 kWh and reduced emissions by 31.57 tons of CO_2. Economic analysis indicated that the project was financially feasible, with a positive NPV, a 6% IRR, an 8.18% ROI, and a payback period of approximately 14 years. The integrated approach proved effective and showed strong potential for replication in similar public buildings.

Corresponding Author:

Lydia Sari
Electrical Engineering Department, Kyai Tapa No. 1, Jakarta 114400, Indonesia
Email: lydia_sari@trisakti.ac.id.

1. INTRODUCTION

Climate change is a global challenge that has significant impacts on the environmental, health, and economic sectors, including in Indonesia. To reduce the rate of global temperature increase, a transition to a sustainable energy system is imperative [1]. The building sector plays a crucial role in this effort, given its significant contribution to energy consumption and greenhouse gas emissions. In Indonesia, the building sector contributes approximately 30% of national emissions, making increasing energy efficiency and utilizing renewable energy, particularly in government buildings, a key strategy in climate change mitigation [2-4].

Indonesia has enormous solar energy potential, but its utilization—especially through rooftop solar power plants (PLTS)—is still relatively limited. Several studies have shown that the implementation of

JURNAL ECOTIPE
Electronic, Control, Telecommunication, Information, and Power Engineering
Volume 13, Issue 1, April 2026, pp. 82-92
ISSN 2355-5068 ; e-ISSN 2622-4852
DOI: 10.33019/jurnalecotipe.v13i1.4586

energy efficiency and rooftop PV in government buildings can significantly reduce energy consumption, carbon emissions, and operational costs [5-8]. These efforts need to be supported by the implementation of an ISO 50001-based Energy Management System (SME) and national and regional policies, such as Government Regulation No. 70 of 2009, the Minister of Energy and Mineral Resources Regulation on Energy Management, and the National Energy General Plan (RUEN) and Regional Energy General Plan (RUED) [9-12]. In DKI Jakarta, this policy is strengthened through Regional Regulation No. 5 of 2023, which emphasizes the importance of energy audits and the adoption of renewable energy in government buildings [13].

Despite the availability of a policy framework, integrated studies combining building energy performance analysis, energy efficiency retrofit scenarios, SME implementation, and the technical and economic feasibility of rooftop solar power plants (PV) in government buildings are still limited. Therefore, this study aims to analyze the techno-economic feasibility of implementing an energy management system, energy efficiency retrofit, and rooftop solar power plants in the Palmerah District Office Building, West Jakarta. The analysis includes an evaluation of existing energy consumption, potential energy savings and emission reductions, and the economic feasibility of the investment. The results of this study are expected to serve as a model for replication for other government buildings in supporting the energy transition, increasing energy efficiency, and achieving renewable energy mix targets at the regional and national levels.

2. RESEARCH METHOD

This study uses a quantitative approach with techno-economic analysis, which aims to evaluate building energy performance, energy efficiency potential, and the feasibility of implementing an Energy Management System (SME) and rooftop solar power plants in government buildings. This method was chosen because it can comprehensively integrate technical, economic, and environmental aspects in making sustainable energy investment decisions. In general, the research flow follows a systematic process as shown in Figure 1.

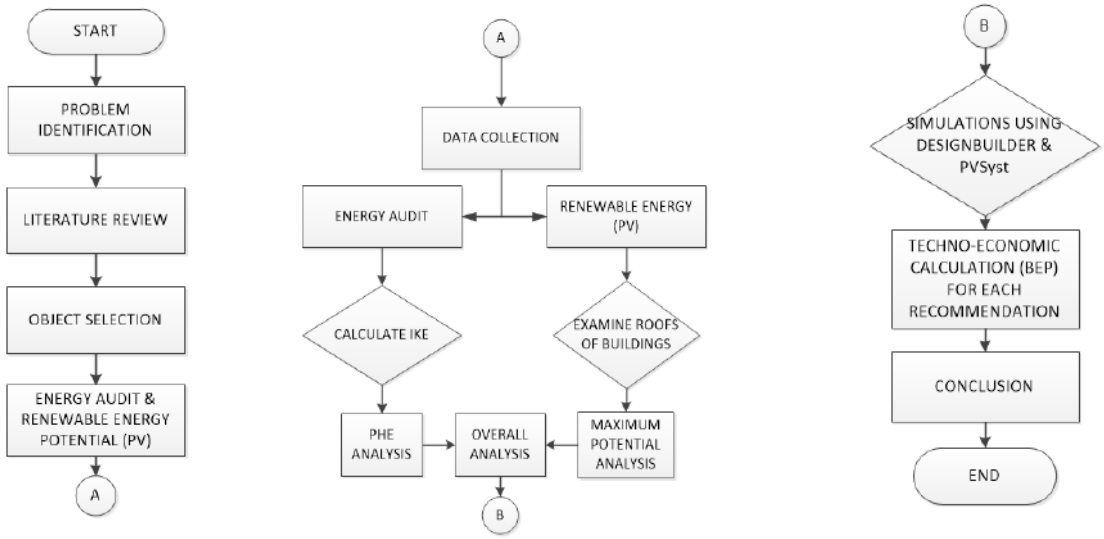

Figure 1. Research Flowchart

2.1. Energy Simulation with DesignBuilder

The performance simulations of the building energy were conducted using DesignBuilder software, as shown in Figure 2. The simulation phase began with the collection of baseline building data, including floor plans, construction specifications, electrical equipment data, and the creation of a three-dimensional (3D) model of the building. At this stage, parameters related to building envelope materials, openings, and the division of thermal zones into air-conditioned ("conditioned") and non-air-conditioned ("unconditioned") areas were defined and input.

JURNAL ECOTIPE
Electronic, Control, Telecommunication, Information, and Power Engineering
Volume 13, Issue 1, April 2026, pp. 82-92
ISSN 2355-5068 ; e-ISSN 2622-4852
DOI: 10.33019/jurnalecotipe.v13i1.4586

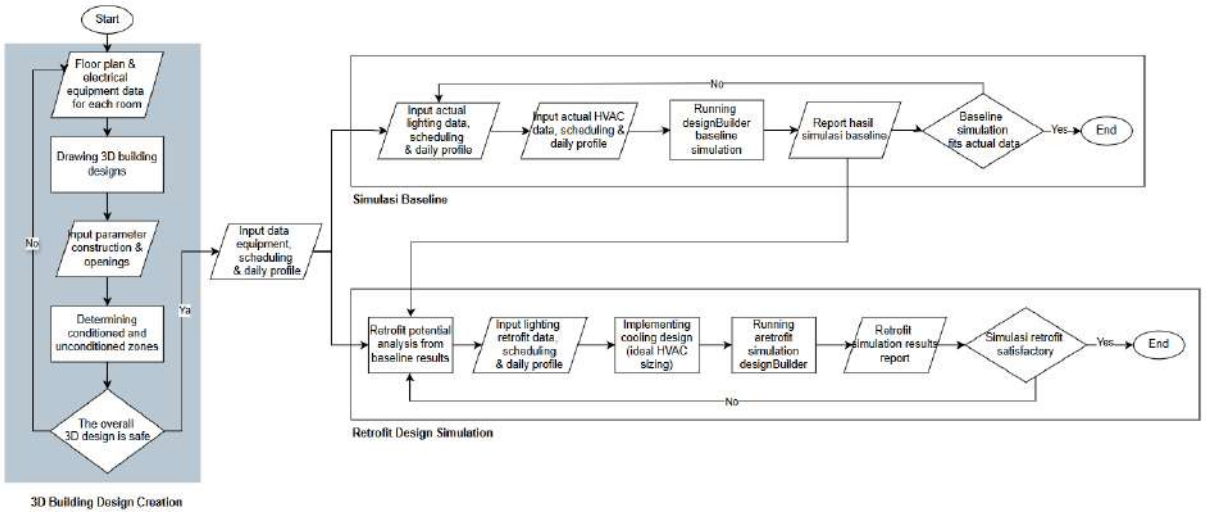

Figure 2. DesignBuilder simulation flowchart

The next stage was the baseline simulation, which represented the existing building conditions. Lighting and HVAC system parameters, including installed power, equipment efficiency, operating schedules, and energy usage profiles, were input into the model. The baseline simulation results were then validated against the building's actual electricity consumption data through an iterative process until an adequate level of agreement was achieved.

After the baseline model was validated, an energy efficiency retrofit simulation was conducted, which included improvements to the lighting and HVAC systems to meet energy efficiency standards. The retrofit simulation results were used to calculate potential energy savings, IKE reductions, and their impact on the building's overall energy performance.

2.2. Rooftop Solar Power System Simulation with PVsyst

The performance analysis of the rooftop photovoltaic (PV) system was conducted using PVsyst software, following the simulation workflow illustrated in Figure 3. The initial simulation stage involved inputting site location parameters and meteorological data derived from the Meteonorm database to estimate the available solar irradiance. Subsequently, the PV array orientation—specifically the tilt angle and azimuth—was defined and adjusted according to the geometric characteristics of the building roof.

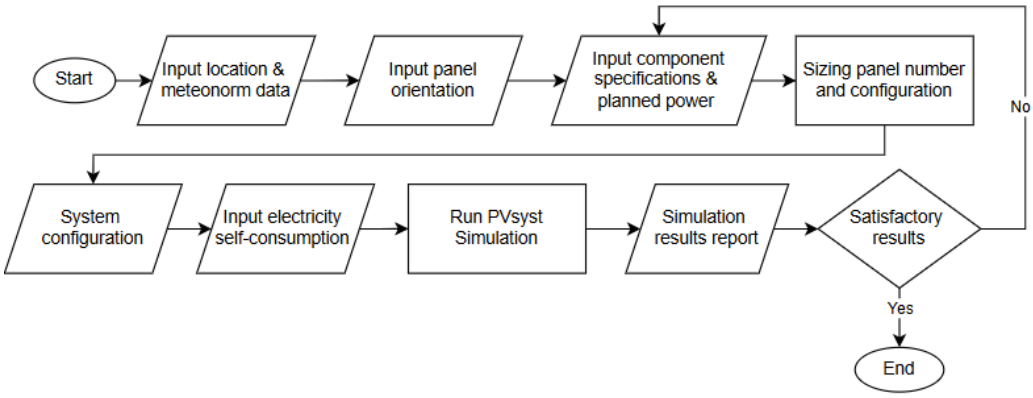

Figure 3. PVsyst simulation flowchart

The planning of solar panel capacity, the selection of solar modules and inverters, as well as the string and connection system configurations were done based on the available roof area and energy requirements. The building's electricity consumption profile was also included to analyze the self-consumption rate and the compatibility between PV energy production and the building load.

Pvsyst simulations provided key system performance parameters, such as annual energy production, performance ratio, and system loss components. If the simulation results do not meet

Volume 13, Issue 1, April 2026, pp. 82-92
ISSN 2355-5068 ; e-ISSN 2622-4852
DOI: 10.33019/jurnalecotipe.v13i1.4586

technical criteria or physical limitations of the roof, parameter adjustments and re-simulations are performed until an optimal and feasible system configuration is achieved.

2.3. Techno-Economics Feasibility Analysis

The next stage of the research is a techno-economic analysis, which aims to assess the feasibility of implementing a combination of SME, energy efficiency retrofits, and rooftop solar power plants. The technical analysis is based on the results of DesignBuilder and PVsyst simulations, while the economic analysis is carried out by calculating investment and operational costs, as well as evaluating financial feasibility indicators, including NPV (net present value), IRR (internal rate of return), payback period, and ROI (Return of Investment) [14,15].

Additionally, an environmental impact analysis was conducted by calculating the reduction in greenhouse gas (GHG) emissions from energy savings obtained based on the GHG emission factor in the Java, Madura, and Bali grid, or Jamali [16].

The results of this analysis were used to evaluate the best recommended options that could simultaneously provide technical, economic, and environmental benefits. All stages of this methodology are designed to produce efficient, sustainable, and applicable energy solutions for government buildings.

3. RESULTS AND DISCUSSION

3.1. Research Object and Building Profile Description

The object of this research is the Palmerah District Office Building in West Jakarta, which functions as a government office building. It is located in a densely populated urban area with high levels of administrative activity. The four-story building has a north-south orientation, which is technically ideal for installing a rooftop solar power plant (PLTS) because it minimizes variations in the solar radiation incidence angle throughout the year [17].

Figure 4. Palmerah District Office Building

Originally constructed in 1990 and renovated in 2014, this building was chosen as a case study because it represents a typical government building in Jakarta, making the study's findings potentially replicable in similar buildings. Furthermore, this research is also relevant in supporting the implementation of the Jakarta Regional Energy General Plan (RUED) as stipulated in Regional Regulation No. 5 of 2023.

3.2. Building Energy Audit Results

1. Lighting System

   The audit results showed that most workspaces still use non-LED lamps, such as non-LED fluorescent lamps and CFLs, as their primary lighting source. Furthermore, several spaces still use incandescent lamps, including the Civil Service Police Unit (Satpol PP), Population and Civil Registration Unit (Dukcapil), and restrooms. Furthermore, the main problem lies not only in the type of lamp, but also in the mismatch of lighting levels to the function of the space.

JURNAL ECTIPE
Electronic, Control, Telecommunication, Information, and Power Engineering
Volume 13, Issue 1, April 2026, pp. 82-92
ISSN 2355-5068 ; e-ISSN 2622-4852
DOI: 10.33019/jurnalecotipe.v13i1.4586

Measurements showed that the average lighting level in the workspace was only around 100 lux, far below the recommended minimum of 300 lux for office spaces. This low lighting condition has the potential to reduce visual comfort, increase eye fatigue, and negatively impact work productivity. These findings emphasize that lighting system evaluations must consider light quantity, not just light source efficiency.

2. Air Conditioning System (HVAC)

An HVAC system audit revealed that most rooms had air temperatures above 26°C, even though the split AC system was operating at a lower temperature setpoint. This indicates that the cooling system was not performing optimally in achieving thermal comfort.

Key factors identified included a lack of routine maintenance (dirty filters and condensers), suboptimal room insulation, the influence of outside air temperature, and inadequate AC capacity relative to the actual cooling load. Consequently, despite energy consumption, building occupants' thermal comfort remained suboptimal. These findings demonstrate that improving HVAC efficiency depends not only on unit efficiency but also on the appropriate capacity and building conditions.

3.3. Lighting and Air Conditioning System Retrofit Design Strategy

Lighting system retrofit design is based on lumen requirements calculations to achieve standard illumination levels without significantly increasing energy costs. In some spaces, the number of existing light sources is limited, making the use of high-power lamps inefficient and difficult to obtain commercially. Therefore, additional light sources are added using outbow downlights, which can be installed without major modifications to the electrical system. Tables 1 and 2 depict the existing and the retrofit light recapitulations, consecutively.

Table 1. Existing lighting recapitulation

Specification	Number of Existing Units
Light Bulb 25W	2
Light Bulb 36W	4
CFL Downlight 24W	66
CFL Downlight 36W	34
LED 16W	10
LED 18W	1
LED Downlight 18W	6
Incandescent light bulb 18W	3
Incandescent light bulb 24W	22
Incandescent light bulb 36W	3
TL 16W	2
TL 36W	64
TL LED 48W	2
TL-D 10W	3
Total number	**222**

JURNAL ECTIPE
Electronic, Control, Telecommunication, Information, and Power Engineering
Volume 13, Issue 1, April 2026, pp. 82-92
ISSN 2355-5068 ; e-ISSN 2622-4852
DOI: 10.33019/jurnalecotipe.v13i1.4586

Table 2. Retrofit Light Recapitulation

Specification	Number of Retrofit Units
Downlight Inbow 24 W	9
Downlight LED Inbow 12 W	3
Downlight LED Inbow 18 W	3
Downlight LED Inbow 24 W	18
Downlight LED Inbow 3 W	14
Downlight LED Inbow 5 W	35
Downlight LED Inbow 7 W	16
Downlight LED Inbow 9 W	8
Downlight LED Outbow 18 W	5
Downlight LED Outbow 24 W	2
Downlight Outbow 24 W	5
LED 12 W	23
LED 18 W	3
LED 20 W	9
LED 25 W	2
LED 30 W	2
LED 40 W	6
LED 5 W	2
TL LED 12 W	1
TL LED 12W	10
TL LED 18 W	2
TL LED 20 W	9
TL LED 30 W	16
TL LED 40 W	22
TL LED 4W	1
TL LED 9 W	10
Total number	**236**

A similar approach is applied to HVAC systems. Instead of replacing large-capacity AC units, smaller units are added to improve operational efficiency and flexibility. For spaces with irregular use, such as meeting rooms, portable standing AC units are used to adjust energy consumption to actual needs. Tables 3 and 4 shows the existing and retrofitted split AC recapitulations, respectively.

Table 3. Existing Split AC Recapitulation

Specification	Number of Existing Units
0.5 PK	5
1 PK	33
1.5 PK	12
2 PK	1
5 PK	2
Total number	**53**

Volume 13, Issue 1, April 2026, pp. 82-92
ISSN 2355-5068 ; e-ISSN 2622-4852
DOI: 10.33019/jurnalecotipe.v13i1.4586

Table 4. Retrofit Split AC Recapitulation

Specification	Number of Existing Units
0.5 PK	6
1 PK	9
1,5 PK	4
1.5 PK	22
2 PK	9
2.5 PK	3
5 PK	2
Total number	**55**

3.4. Building Energy Performance Analysis (Baseline and Retrofit)

1. Baseline Condition

The results of the existing (baseline) condition simulation using DesignBuilder, as presented in Figure 5, shows that the building's annual electrical energy consumption reaches 156,138.91 kWh/year, with an Energy Consumption Intensity (IKE) value of 90.6 kWh/m²/year. Based on ESDM Regulation No. 3 of 2025, this value is still considered efficient for the office building category.

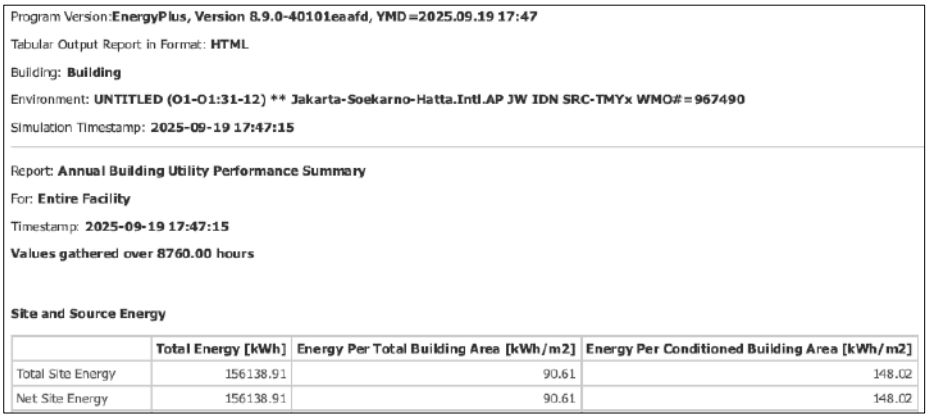
Program Version:**EnergyPlus, Version 8.9.0-40101eaafd, YMD=2025.09.19 17:47**
Tabular Output Report in Format: **HTML**
Building: **Building**
Environment: **UNTITLED (O1-O1:31-12) ** Jakarta-Soekarno-Hatta.Intl.AP JW IDN SRC-TMYx WMO#=967490**
Simulation Timestamp: **2025-09-19 17:47:15**

Report: **Annual Building Utility Performance Summary**
For: **Entire Facility**
Timestamp: **2025-09-19 17:47:15**
Values gathered over 8760.00 hours

Site and Source Energy

	Total Energy [kWh]	Energy Per Total Building Area [kWh/m2]	Energy Per Conditioned Building Area [kWh/m2]
Total Site Energy	156138.91	90.61	148.02
Net Site Energy	156138.91	90.61	148.02

Figure 5. Baseline simulation results with DesignBuilder

However, field audit results revealed a discrepancy between quantitative energy efficiency categories and actual comfort quality, particularly in lighting and air conditioning. This indicates that low energy efficiency does not necessarily equate to good indoor environmental quality.

2. Retrofit Design Conditions

In the retrofit design scenario, as presented in Figure 6, building energy consumption increased to 186,026.75 kWh/year with an IKE value of 107.96 kWh/m²/year, which is in the fairly efficient category. This increase in energy consumption was primarily due to adjustments to the HVAC system capacity to meet thermal comfort standards.

JURNAL ECOTIPE
Electronic, Control, Telecommunication, Information, and Power Engineering
Volume 13, Issue 1, April 2026, pp. 82-92
ISSN 2355-5068 ; e-ISSN 2622-4852
DOI: 10.33019/jurnalecotipe.v13i1.4586

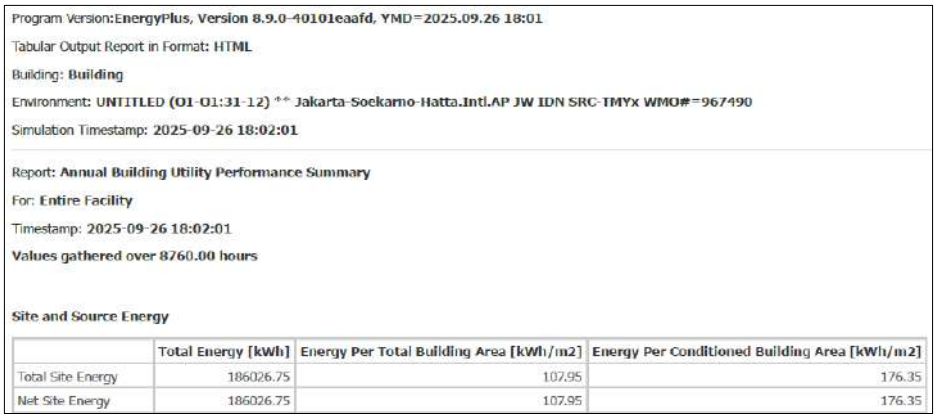

Program Version:EnergyPlus, Version 8.9.0-40101eaafd, YMD=2025.09.26 18:01
Tabular Output Report in Format: HTML
Building: Building
Environment: UNTITLED (01-01:31-12) ** Jakarta-Soekarno-Hatta.Intl.AP JW IDN SRC-TMYx WMO#=967490
Simulation Timestamp: 2025-09-26 18:02:01

Report: Annual Building Utility Performance Summary
For: Entire Facility
Timestamp: 2025-09-26 18:02:01
Values gathered over 8760.00 hours

Site and Source Energy

	Total Energy [kWh]	Energy Per Total Building Area [kWh/m2]	Energy Per Conditioned Building Area [kWh/m2]
Total Site Energy	186026.75	107.95	176.35
Net Site Energy	186026.75	107.95	176.35

Figure 6. Design simulation results with DesignBuilder

Despite the increase in energy consumption, lighting quality and thermal comfort have significantly improved. Lighting Power Density (LPD) has been reduced from 3.4 W/m² to 2.1 W/m², while illuminance levels have met SNI 6197:2020 standards. In the HVAC system, the cooling load has increased from 49.13 kW to 81.68 kW as a consequence of meeting thermal comfort requirements according to standards.

3.5. Rooftop Solar Power Simulation Results

Based on the analysis of the roof area and conditions, the rooftop solar PV system was designed with an installed capacity of 24.75 kWp using a total of 45 solar modules. PVsyst simulation results show that this system is capable of producing 33,428 kWh/year of electrical energy, with a specific yield of 1,351 kWh/kWp/year and a performance ratio (PR) of 80.13%, indicating good system performance for tropical climates.

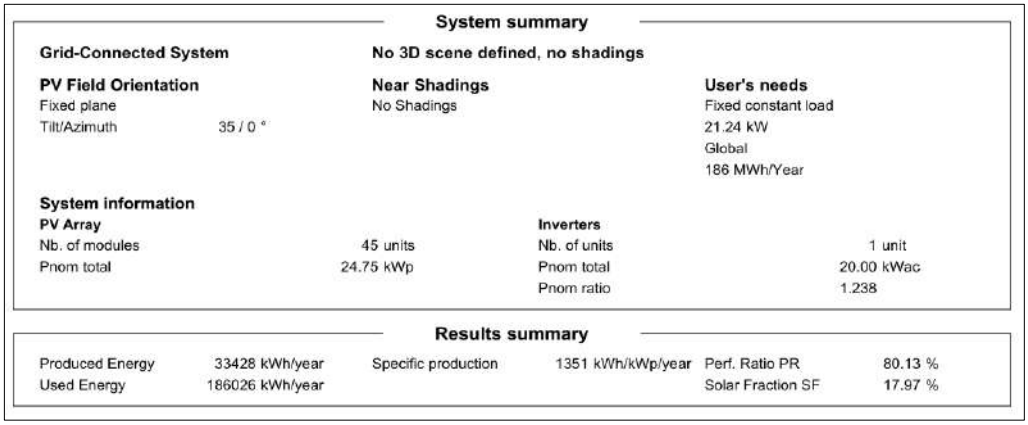

System summary

Grid-Connected System — No 3D scene defined, no shadings

PV Field Orientation
Fixed plane
Tilt/Azimuth 35 / 0 °

Near Shadings
No Shadings

User's needs
Fixed constant load
21.24 kW
Global
186 MWh/Year

System information

PV Array
Nb. of modules 45 units
Pnom total 24.75 kWp

Inverters
Nb. of units 1 unit
Pnom total 20.00 kWac
Pnom ratio 1.238

Results summary

Produced Energy	33428 kWh/year	Specific production	1351 kWh/kWp/year	Perf. Ratio PR	80.13 %
Used Energy	186026 kWh/year			Solar Fraction SF	17.97 %

Figure 7. Rooftop solar power simulation results with PVsyst

The solar fraction value of 17.97% indicates that nearly 18% of the building's annual electricity needs can be met by rooftop solar power plants. This demonstrates that rooftop solar power integration plays a significant role in reducing dependence on fossil-based electricity.

3.6. Economic Analysis of Retrofit

Figure 8 presents the economic feasibility results of the integrated retrofit project, including lighting upgrades, HVAC improvements, and rooftop PV installation. Based on total annual electricity savings of 37,587 kWh and a PLN tariff of Rp1,699/kWh with a 3% escalation rate, the project requires a total CAPEX of Rp878,830,572 and annual OPEX of Rp8,788,306 over a 25-year lifespan with a 5% discount rate.

JURNAL ECTIPE
Electronic, Control, Telecommunication, Information, and Power Engineering
Volume 13, Issue 1, April 2026, pp. 82-92
ISSN 2355-5068 ; e-ISSN 2622-4852
DOI: 10.33019/jurnalecotipe.v13i1.4586

Parameter	Value
Total Retrofit Saving (kWh)	37.587,03
PLN Electricity Tariff (Rp/kWh)	1.699,00
Electricity Tariff Escalation (%)	3,00
CAPEX total retrofit (Rp)	878.830.572,00
Annual OPEX for roof PV, lightings, AC (Rp)	8.788.306,00
Project Lifespan (years)	25
Discount rate (%)	5,00

NPV (Rp)	Rp85.535.196
IRR	6%
Payback Period (years)	14
Annual ROI	8,18%

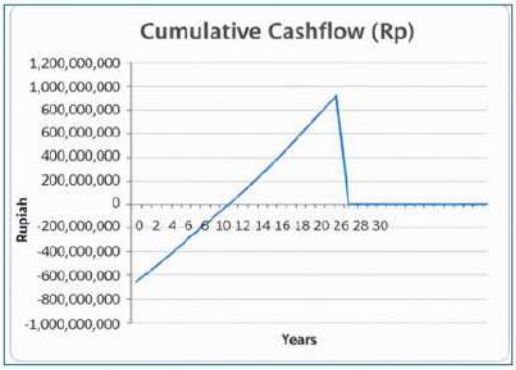

Figure 8. Economic analysis results for the overall retrofit

Overall, the combination of retrofitting the lighting system, air conditioning, and installing rooftop solar panels yields financial feasibility with a positive NPV of Rp85,535,196, an IRR of 6%, an annual ROI of 8.18%, and a payback period of 14 years, which is still considered reasonable for a long-term project where the lifespan of a rooftop solar panel can reach 25 years.

3.7. Environmental Impact

The energy savings and contribution of rooftop solar power plants resulted in a reduction in electricity consumption from the grid by 37,587 kWh per year. Referring to the Jamali grid emission factor of 0.84 tons CO_2/MWh, this effort contributed to a reduction in emissions of approximately 31.57 tons CO_2 per year. These findings confirm that energy efficiency and renewable energy strategies in government buildings have a significant impact on climate change mitigation.

4. CONCLUSION

This study demonstrates that HVAC and lighting systems are the dominant energy consumers in the Palmerah District Office Building, accounting for 69.4% and 23.6% of total electricity use, respectively, under a baseline consumption of 156,138.91 kWh/year (IKE 90.6 kWh/m²/year). Targeted retrofit measures, LED lighting replacement and HVAC optimization, reduced lighting energy consumption by 38.14% and significantly improved thermal comfort.

The integration of a 24.75 kWp rooftop PV system further strengthened building performance, generating 33,428 kWh/year, covering 17.97% of annual demand, and contributing to total grid electricity savings of 37,587 kWh/year and emission reductions of 31.57 tons CO_2 annually. From a techno-economic perspective, the integrated retrofit scenario is financially feasible, with a positive NPV of Rp85,535,196, an IRR of 6%, an ROI of 8.18%, and a 14-year payback period over a 25-year project lifespan.

The novelty of this research lies in its integrated ISO 50001–based EnMS framework that combines validated building energy simulation (DesignBuilder), PV performance modeling (PVsyst), and comprehensive financial analysis within a single case study of a public building. Unlike studies that assess efficiency or PV deployment separately, this research provides a holistic decision-making model linking energy performance, occupant comfort, carbon mitigation, and financial feasibility. The findings offer a replicable and practical roadmap for scaling sustainable energy interventions in government buildings across urban Indonesia.

Volume 13, Issue 1, April 2026, pp. 82-92
ISSN 2355-5068 ; e-ISSN 2622-4852
DOI: 10.33019/jurnalecotipe.v13i1.4586

REFERENCES

[1] N. Rahmandani and E. P. Dewi, "Pengaruh energi terbarukan, emisi karbon, dan foreign direct investment terhadap pertumbuhan ekonomi negara anggota OKI," *J. Ilm. Ekon. Islam*, vol. 9, no. 1, pp. 405–417, 2023.

[2] J. Windarta and C. Cahyadi, "Kajian Tekno-Ekonomi Potensi Penghematan Energi Pencahayaan pada Gedung Pemerintah Menggunakan Retscreen," *G-Tech J. Teknol. Terap.*, vol. 8, no. 3, pp. 1584–1594, 2024.

[3] Shah, Sheikh Khaleduzzaman, Peter Graham, Craig Burton, and Philip Harrington. "An Assessment of Long-Term Climate Change on Building Energy in Indonesia. " *Energies* 16, no. 21: 7231, 2023.

[4] W. S. P. Harris, Purwito, and A. Ashar, "Analisis Sistem Manajemen Audit Penggunaan Energi Listrik Pada Kantor Bupati Sinjai Provinsi Sulawesi Selatan Berbasis Appsheet," in *Prosiding Seminar Nasional Teknik Elektro dan Informatika (SNTEI) 2023-Teknik Listrik*, 2023.

[5] A. Ardiansyah, "Perancangan Teknis dan Analisis Ekonomi Pembangkit Listrik Tenaga Surya Dengan Sistem On Grid Di Kantor Bupati Sambas." Universitas Tanjungpura, 2023.

[6] I. K. A. Partayasa, I. M. A. Mahendra, and I. M. Juniastra, "Analisis Penghematan Energi Listrik Dalam Mewujudkan Konsep Green Solar Panel Pada Industri Perhotelan di Bali. Studi Kasus Di Bvlgari Hotel And Resort Bali," *J. Ilm. Vastuwidya*, vol. 6, no. 2, pp. 79–87, 2023.

[7] A. N. Widyanto, M. Gaviarsha, F. Husnayain, A. R. Utomo, and I. M. Ardita, "Studi Tekno-Ekonomi Sistem Fotovoltaik On-Grid Pada Bangunan Industri Kontrol Satelit," *Electrices*, vol. 5, no. 1, pp. 37–47, 2023.

[8] D. P. Irwangsa, J. Windarta, and S. Handoko, "Rancangan dan Implementasi Sistem Manajemen Energi dan Audit Energi Berbasis ISO: 50001 di Kampus Universitas Islam Kalimantan," *Sci. J. Mech. Eng. Kinemat.*, vol. 8, no. 2, pp. 94–108, 2023.

[9] A. A. Rahmawati and S. Abduh, "Audit Energi Gedung Kampus A Universitas Muhammadiyah Tangerang untuk Penerapan Sistem Manajemen Energi Berbasis ISO 50001: 2018," *Energi & Kelistrikan*, vol. 14, no. 2, pp. 187–195, 2022.

[10] S. Sunarto, K. Khotimah, and S. Santosa, "Pelaksanaan Konservasi Energi di Batan melalui Penerapan Sistem Manajemen Energi Berbasis ISO 50001," *Pertemuan Dan Presentasi Ilmiah Standardisasi*, vol. 2021, pp. 37–44, Mar. 2022, doi: 10.31153/ppis.2021.109.

[11] Pemerintah Republik Indonesia, "Perpres No 79 Tahun 2023 tentang Tata Cara Penyusunan Rencana Umum Energi Nasional dan Rencana Umum Energi Daerah," 2023.

[12] Kementerian ESDM RI, "33 Provinsi Telah Masukkan RUED dalam Peraturan Daerah," 2024. [Online]. Available: https://www.esdm.go.id/id/media-center/arsip-berita/33-provinsi-telah-masukkan-rued-dalam-peraturan-daerah. [Accessed: Mar. 3, 2026]

[13] Pemerintah Provinsi Daerah Khusus Ibukota Jakarta, "Peraturan Daerah Provinsi Daerah Khusus Ibukota Jakarta Nomor 5 Tahun 2023 tentang Rencana Umum Energi Daerah Tahun 2023-2050, " 2023.

[14] Policy Factsheet, "Valuation of Energy Efficiency Measures for On-Bill Schemes," *POLICY*, 2022.

[15] Youssefi, I., Celik, T. and Azimli, A., "Financial feasibility analysis for different retrofit strategies on an institutional building. " *Sustainable Energy Technologies and Assessments*, *52*, p.102342, 2022.

[16] Dirjen Kelistrikan Kementerian ESDM, "Faktor Emisi Gas Rumah Kaca Sistem Kelistrikan Indonesia," 2019. [Online]. Available: https://gatrik.esdm.go.id/assets/uploads/download_index/files/96d7c-nilai-fe-grk-sistem-

Volume 13, Issue 1, April 2026, pp. 82-92
ISSN 2355-5068 ; e-ISSN 2622-4852
DOI: 10.33019/jurnalecotipe.v13i1.4586

ketenagalistrikan-tahun-2019.pdf. [Accessed: Mar. 3, 2026].

[17] Paramita, B., R. A. Mangkuto, A. G. Djafar, and N. Jamala. "Energy yield of solar PV in 34 Indonesian cities with respect to various roof pitches and orientations. " *International Journal of Environmental Science and Technology* 22, no. 12: 11253-11266, 2025.

JURNAL ECOTIPE
Electronic, Control, Telecommunication, Information, and Power Engineering
Volume 13, Issue 1, April 2026, pp. 69-81
ISSN 2355-5068 ; e-ISSN 2622-4852
DOI: 10.33019/jurnalecotipe.v13i1.4589

Optimization of Smart Building Electrical Load Prediction Using Long Short-Term Memory

Ali Aqil[1], Yoga Tri Nugraha[2], Sumita Wardani[3], Mawardi[4], Muhammad Irwanto[5]
[1,2,3]Department of Electrical Engineering, Universitas Al-Azhar, Medan 20142, Indonesia
[4]Department of Mechanical Engineering, Universitas Al-Azhar, Medan 20142, Indonesia
[5]Department of Electrical Engineering, Universitas Prima Indonesia, Medan 20118, Indonesia

ARTICLE INFO

Article historys:

Received : 13/02/2026
Revised : 08/03/2026
Accepted : 30/04/2026

Keywords:

Electrical Load Prediction; Energy Management; Long Short-Term Memory; Smart Building; Time Series

ABSTRACT

The advancement of smart building technologies requires energy management systems that are both efficient and capable of adapting to dynamic operational conditions. A key component of such systems is reliable electrical load forecasting, as building energy demand is affected by environmental conditions, occupancy behavior, and operational activities that exhibit nonlinear and time-dependent characteristics. This study explores the use of the Long Short-Term Memory (LSTM) approach for forecasting smart building electricity consumption based on multivariate time-series data. The input dataset incorporates temporal features, ambient temperature, humidity levels, occupancy-related patterns, and major electrical load components within the building. The research workflow consists of data preprocessing, normalization, time-series construction using a sliding window strategy, LSTM model training, and evaluation of forecasting performance. The findings indicate that the building's electricity demand varies approximately between 6 kW and 17 kW, with an average load ranging from 11 to 12 kW. Performance assessment yields an RMSE of about 3 kW and a MAPE of roughly 25%. The largely symmetric error distribution around zero suggests minimal systematic bias in the predictions, although the model's accuracy during peak demand periods remains limited.

Corresponding Author:

Yoga Tri Nugraha
Department of Electrical Engineering, Universitas Al-Azhar, Medan 20142, Indonesia
Email: yogatrinugraha16@gmail.com

1. INTRODUCTION

The rapid adoption of smart building technologies has significantly transformed the way electrical energy is monitored, managed, and optimized in modern infrastructures. Smart buildings integrate advanced sensing, communication, and automation systems to improve energy efficiency, operational reliability, and sustainability. However, the increasing penetration of intelligent devices and dynamic user behavior has resulted in highly volatile and non-linear electrical load patterns. These characteristics make accurate electrical load prediction a critical yet challenging task, as reliable forecasts are essential for effective energy management[1], [2], demand response strategies, and optimal operation of smart building energy systems.

Traditional electrical load forecasting approaches, including statistical and regression-based models, have been widely applied in building energy prediction[3], [4], [5], [6]. Although these approaches are relatively simple and easy to interpret, they often lack the capacity to model the complex

Volume 13, Issue 1, April 2026, pp. 69-81
ISSN 2355-5068 ; e-ISSN 2622-4852
DOI: 10.33019/jurnalecotipe.v13i1.4589

temporal dynamics and nonlinear interactions present in electricity load time-series data. In smart building contexts, power consumption is shaped by numerous time-dependent factors, including occupancy dynamics, environmental variations, and operational scheduling, which give rise to both short-term fluctuations and long-term dependencies. Traditional prediction models typically struggle to capture these patterns effectively, resulting in reduced forecasting accuracy, especially during peak demand periods or sudden shifts in consumption behavior.

Recent advances in artificial intelligence, particularly deep learning techniques, have provided promising alternatives for modeling complex time-series data. The LSTM [6], [7], [8], [9], [10], a specialized form of RNN, has demonstrated superior capability in learning long-term temporal dependencies through its gated memory structure. This architecture effectively addresses the vanishing gradient problem commonly encountered in standard RNNs, enabling more stable and accurate learning processes. Consequently, LSTM has been increasingly adopted for electrical load forecasting applications[11], [12], including those in smart grids and building energy systems.

Although LSTM models offer strong capabilities for time-series forecasting, their prediction accuracy is highly sensitive to proper model design, including network structure, hyperparameter tuning, and the selection of input features. Inadequate parameter configurations can result in overfitting, inefficient training convergence, or limited generalization to unseen data. In addition, the lack of a structured optimization framework may restrict the model's effectiveness in capturing the temporal dynamics inherent in smart building electricity demand. Consequently, enhancing and optimizing LSTM-based load forecasting models remains an important research problem for achieving reliable and robust predictive performance.

Within this framework, the present study introduces an optimized LSTM-based methodology for electricity load forecasting in smart building systems. The proposed approach emphasizes systematic optimization procedures and thorough performance evaluation using established quantitative error indicators. The anticipated contributions include improved forecasting precision and greater adaptability to fluctuating load patterns, thereby supporting intelligent energy management strategies and advancing data-driven solutions for smart building applications.

2. RESEARCH METHOD

Electrical load prediction in smart buildings is a complex time series forecasting problem due to its nonlinear behavior, temporal dependencies, and sensitivity to various external factors such as occupant activity, environmental conditions, and operational schedules. Conventional statistical methods, including linear regression and autoregressive models, generally rely on linearity and stationarity assumptions, thus limiting their application in the dynamic environment of smart buildings. As data on building energy systems becomes increasingly abundant, data-driven approaches are increasingly being used due to their ability to learn complex patterns directly from historical consumption data. However, CNN [13], [14], [15], [16], [17] lacking temporal memory, are unable to optimally capture long-term dependencies in sequential electrical load data, resulting in inadequate prediction performance. To clarify the research context and characteristics of the data used in developing the prediction model, a summary of the dataset specifications is presented in Table 1.

To overcome these limitations, this study adopted a Long Short-Term Memory (LSTM) neural network as the primary prediction model [6], [7], [8], [18]. Long Short-Term Memory (LSTM) represents an advanced form of Recurrent Neural Networks that addresses the vanishing gradient limitation by employing internal memory units regulated by gating components, specifically the input, forget, and output gates. These mechanisms govern the information flow within the network, allowing relevant historical features to be retained while insignificant data are selectively discarded. Consequently, LSTM is well suited for modeling electrical load time-series data, as it can effectively learn both short-term fluctuations and long-range temporal dependencies. This characteristic makes LSTM particularly well suited for smart building applications, where electricity consumption follows complex daily, weekly, and seasonal behavior that needs to be learned concurrently.

Volume 13, Issue 1, April 2026, pp. 69-81
ISSN 2355-5068 ; e-ISSN 2622-4852
DOI: 10.33019/jurnalecotipe.v13i1.4589

Table 1. Characteristics of research data

No	Data Parameters	Description
1	Research object	The smart building is a multi-storey academic building consisting of teacher rooms, administration rooms and public areas, with an approximate floor area of ± 2,500–3,000 m²
2	Data source	Smart building energy monitoring system
3	Data types	Multivariate time series data
4	Target variable	Total building electrical load (kW)
5	Input variables	Ambient temperature (°C), humidity (%), number of occupants (occupancy), time indicator (hours), type of day (weekday/weekend)
6	Sampling interval	15 minutes
7	Observation period	3 months
8	Number of data samples	± 8.640 data
9	Electrical load range	6 kW – 17 kW
10	Average electrical load	11 – 12 kW
11	Dominant load system	HVAC, lighting, and office equipment
12	Load characteristics	Nonlinear, fluctuating, influenced by occupancy and environmental conditions

The research methodology used in this study follows a quantitative and data-driven framework aimed at optimizing the performance of LSTM models in electrical load prediction[2], [4], [19], [20]. Historical electrical load data is obtained from a smart building energy monitoring system and recorded at uniform time intervals. In addition to load data, additional variables such as ambient temperature, time of day indicators, and weekday and holiday classifications are included as input features to enrich the information and improve prediction accuracy. These variables represent operational and environmental characteristics that influence energy consumption behavior in smart buildings. Prior to model development, the dataset underwent a comprehensive preprocessing stage. Missing values caused by temporary sensor communication failures were handled using linear interpolation, while abnormal readings resulting from sensor noise or unexpected operating conditions were identified using statistical thresholding and subsequently smoothed. All numerical variables were normalized using min–max scaling to transform data into a comparable range, thereby improving numerical stability and accelerating convergence during LSTM training[21], [22]. A sliding window technique was employed to convert the time-series data into supervised learning sequences, enabling the model to learn temporal dependencies across consecutive observations. To ensure reproducibility and systematic model optimization, this study adopted a grid search-based hyperparameter tuning strategy. Several critical hyperparameters were evaluated, including the number of LSTM units, learning rate, batch size, input window length, and dropout rate. Each configuration was trained and validated using the same data partitioning scheme, and model performance was compared based on validation RMSE. The optimal configuration was selected by balancing prediction accuracy and training stability, ensuring that the final model does not suffer from overfitting or underfitting. The configuration of the optimized LSTM hyperparameters is summarized in Table 2.

Considering that prediction accuracy typically degrades during peak demand periods, specific strategies were incorporated at the methodological level. Peak load instances were explicitly included in the training dataset to prevent data imbalance. The multivariate input design allows the model to associate sudden load increases with changes in occupancy and environmental conditions. In addition, an early stopping mechanism based on validation loss was implemented to prevent excessive model fitting to extreme values.

Volume 13, Issue 1, April 2026, pp. 69-81
ISSN 2355-5068 ; e-ISSN 2622-4852
DOI: 10.33019/jurnalecotipe.v13i1.4589

Table 2. LSTM hyperparameter configuration

No	Hyperparameter	Tested Values / Range	Selected Value
1	Model Architecture	Multivariate LSTM	Multivariate LSTM
2	Number of LSTM Layers	1 – 3 layers	2 layers
3	Number of LSTM Units	32, 64, 128	64 units
4	Time Window Length (Window Size)	12, 24, 48	24-time steps
5	Activation Function	Tanh	Tanh
6	Dropout Rate	0.1 – 0.5	0.2
7	Optimizer	Adam	Adam
8	Learning Rate	0.001, 0.0005, 0.0001	0.001
9	Mini-Batch Size	16, 32, 64	32
10	Maximum Number of Epochs	50 – 200	100
11	Early Stopping	Enabled / Disabled	Enabled
12	Optimization Method	Grid Search	Grid Search
13	Loss Function	Mean Squared Error (MSE)	MSE

An electricity load forecasting model based on Long Short-Term Memory (LSTM) is developed by employing a multivariate framework combined with a sliding window technique to effectively learn temporal relationships within the input data. Time-ordered data sequences are provided to one or multiple stacked LSTM layers, allowing internal memory cells to capture and learn long-term patterns from historical electricity consumption. The feature representations generated by the LSTM layers are subsequently forwarded to a dense output layer to produce the predicted load values. To enhance the model's generalization capability and mitigate overfitting, dropout regularization is incorporated during training. Critical architectural settings, including the depth of the LSTM network, the number of hidden units, and the size of the input time window, are selected through empirical performance analysis. Model optimization is conducted by systematically tuning hyperparameters such as learning rate, mini-batch size, training iterations, and the choice of optimization strategy. An adaptive optimizer is utilized to update network parameters efficiently while maintaining training stability. In addition, an early stopping strategy based on validation loss is implemented to prevent excessive training and ensure optimal predictive performance. Multiple experimental configurations are evaluated to determine the most suitable model structure for smart building electricity load forecasting.

The training process involves iterative weight updates using backpropagation through time, with the objective of minimizing the mean squared error between predicted and actual load values. Model performance is continuously monitored using validation data to guide optimization decisions. After training is complete, the optimized LSTM model is evaluated on the testing dataset using standard performance metrics, including RMSE [11], [13], [23], [24], [25], and MAPE. These evaluation metrics offer a thorough measure of forecasting precision and model robustness. The findings confirm the capability of the optimized LSTM framework to effectively learn complex temporal dependencies and to enhance the accuracy of electrical load predictions in smart building contexts. Model accuracy is evaluated using RMSE [23], [26] and MAPE [27], [28], [29], with RMSE measuring the average magnitude of prediction errors in the original data units as follow:

$$\text{RMSE} = \sqrt{\frac{1}{n}\sum_{i=1}^{n}(yi - \hat{y}i)^2} \quad (1)$$

Meanwhile, MAPE is used to express the level of prediction error in percentage form and is formulated as:

$$\text{MAPE} = \frac{100}{n}\sum_{i=1}^{n}\left|\frac{yi-\hat{y}i}{yi}\right| \quad (2)$$

Beyond numerical performance metrics, the model outcomes are also examined through visual analysis, including comparisons between observed and predicted electricity load profiles, error distribution plots, and cumulative error trends over time. These visual evaluations are intended to offer deeper insight into the model's capability to accurately track smart building load behavior, particularly during peak demand intervals and variations caused by changes in occupancy patterns. By adopting this

Volume 13, Issue 1, April 2026, pp. 69-81
ISSN 2355-5068 ; e-ISSN 2622-4852
DOI: 10.33019/jurnalecotipe.v13i1.4589

comprehensive evaluation framework, the proposed LSTM model is expected to deliver highly accurate and consistent electricity load forecasts for smart building applications. Such predictions can serve as a reliable foundation for energy management decision-making, including HVAC control optimization, demand response strategies, and overall improvements in energy efficiency. The overall research workflow follows a sequential process consisting of data acquisition, preprocessing, feature normalization, time-series segmentation, LSTM model construction, hyperparameter optimization, model training, and performance evaluation[30], [31]. This structured flow ensures that each stage builds upon the previous one in a systematic manner, allowing the forecasting framework to be clearly understood even without direct reference to the flowchart illustration shown in Figure 1.

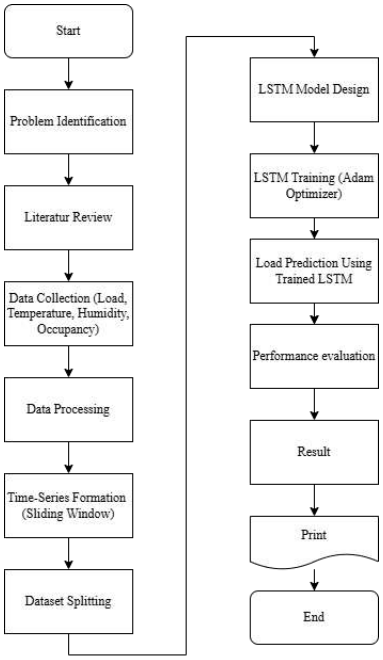

Figure 1. Research flowchart

3. RESULTS AND DISCUSSION

Experimental results of smart building electrical load prediction using the Long Short-Term Memory (LSTM) method based on multivariate time series data. The results are visualized in several graphs representing the characteristics of the initial data, the normalization process, the model's prediction performance, and the prediction error analysis. These graphs aim to provide a comprehensive overview of building energy consumption patterns, the relationship between environmental variables and occupancy, and the LSTM model's ability to learn the temporal dynamics of electrical load. The total electrical load profile of the smart building during the observation period, which shows significant fluctuations due to occupant activity and building operational conditions, is shown in Figure 2. Next, graphs of the normalized environmental and occupancy data are displayed to demonstrate the relative variation between the input variables used in model training. Normalization ensures all variables are on a comparable scale, allowing the neural network to learn stably and efficiently, as shown in Figure 3.

The main results of the study are demonstrated through a comparison graph between the actual electrical load and the LSTM prediction results. This graph provides an initial indication of the model's accuracy in following the actual electrical load pattern shown in Figure 4. In addition, a scatterplot between the actual and predicted values is presented, which is used to evaluate the closeness of the predicted results to the ideal values shown in Figure 5. To complete the analysis, a graph of the prediction error and error distribution is presented to assess the stability of the model and detect any bias or systematic deviations shown in Figure 6. By presenting this series of graphs, this section provides a

JURNAL ECTIPE
Electronic, Control, Telecommunication, Information, and Power Engineering
Volume 13, Issue 1, April 2026, pp. 69-81
ISSN 2355-5068 ; e-ISSN 2622-4852
DOI: 10.33019/jurnalecotipe.v13i1.4589

visual basis for further discussion of the performance of the LSTM model, the advantages achieved, and the limitations that still exist in the context of smart building electrical load prediction.

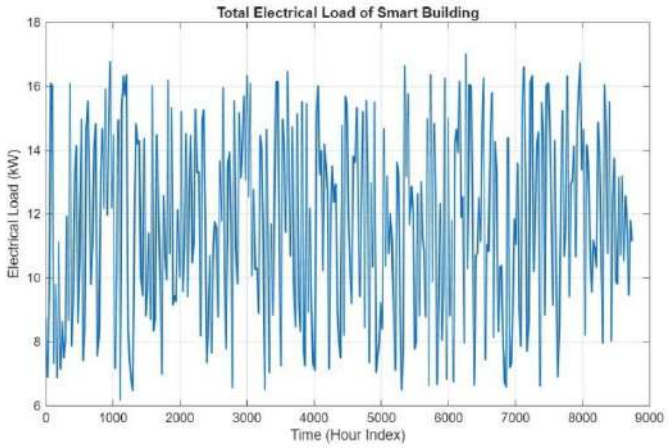

Figure 2. Total electrical load of smart building

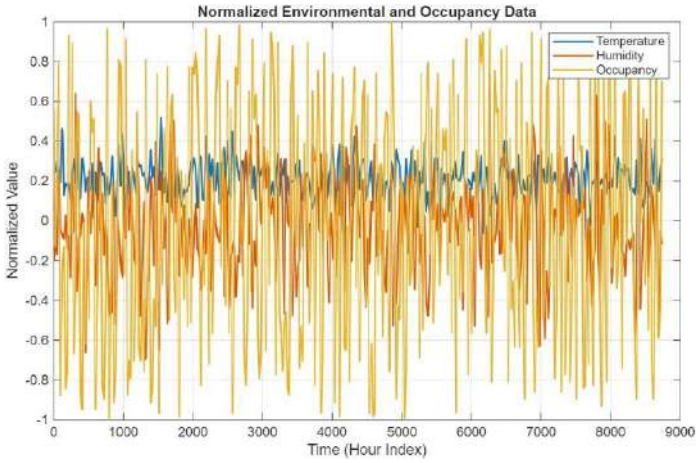

Figure 3. Normalized environmental and occupancy data

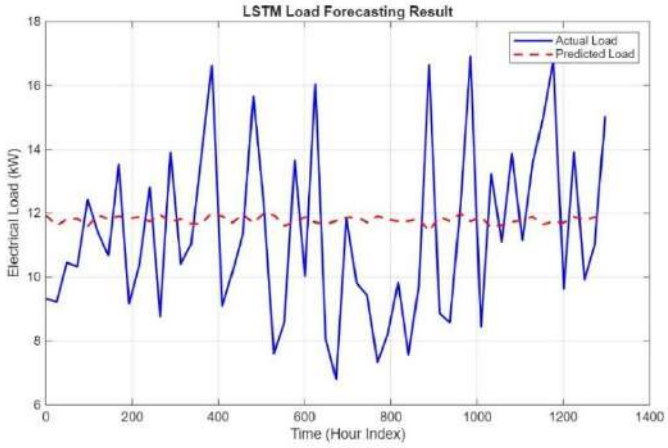

Figure 4. LSTM load forecasting result

JURNAL ECTIPE
Electronic, Control, Telecommunication, Information, and Power Engineering
Volume 13, Issue 1, April 2026, pp. 69-81
ISSN 2355-5068 ; e-ISSN 2622-4852
DOI: 10.33019/jurnalecotipe.v13i1.4589

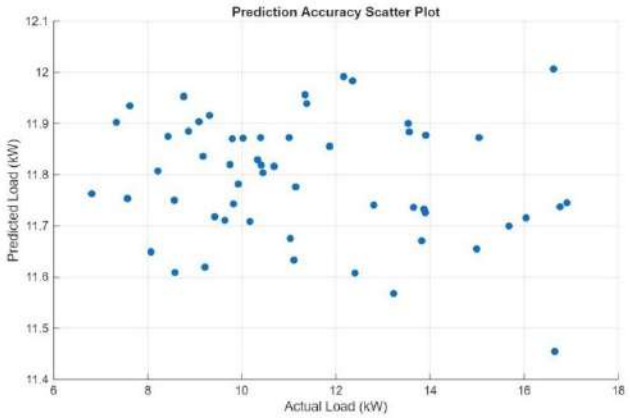

Figure 5. Prediction accuracy scatter plot

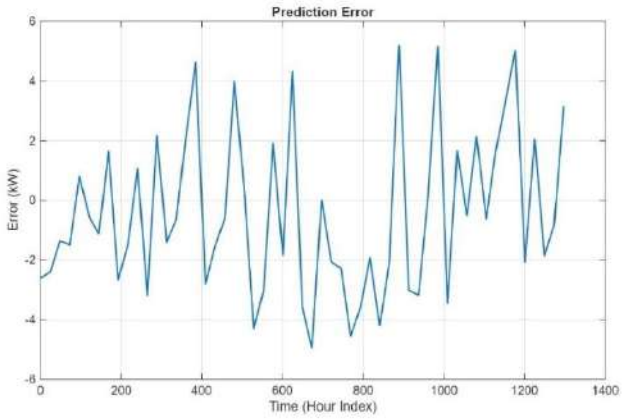

Figure 6. Prediction error

Based on Figure 2 above, energy consumption exhibits a fairly complex fluctuation pattern with significant daily variations. The electrical load ranges from approximately 6 kW to 17 kW, with an average value of 11–12 kW. This fluctuation pattern reflects the typical characteristics of smart buildings, where the electrical load is strongly influenced by occupancy levels, HVAC system usage, and other operational activities. The wide variation in load between the minimum and maximum values indicates high energy consumption dynamics over time. This situation emphasizes that a simple linear model-based prediction approach will struggle to accurately capture load dynamics, thus utilizing a Long Short-Term Memory (LSTM) model becomes relevant for modeling nonlinear relationships and long-term temporal dependencies.

Figure 3 shows that each input variable varies over time, with a normalized value ranging from –1 to 1. The occupancy variable exhibits the largest fluctuation compared to temperature and humidity, indicating that human activity plays a dominant role in changes in the building's electrical load. This variation provides a crucial source of information for the LSTM model to study the nonlinear relationship between environmental conditions and energy consumption. The LSTM prediction results shown in Figure 4 demonstrate that the model is able to follow the general trend of the actual electricity load quite well, with the average predicted value being around 11.7–11.9 kW. However, there are still quite clear differences at peak load points, especially when the actual load increases above 15 kW. This indicates that extreme load spikes due to sudden changes in occupancy or certain intensive activities still pose a challenge for the model. Figure 5 shows a distribution of points that is relatively close to the diagonal line, indicating a positive correlation between the predicted results and the actual values. Most points are concentrated in the load range of 8–14 kW, although there are some deviations at high loads. The still quite wide distribution of points indicates that the prediction accuracy is not yet fully optimal.

Volume 13, Issue 1, April 2026, pp. 69-81
ISSN 2355-5068 ; e-ISSN 2622-4852
DOI: 10.33019/jurnalecotipe.v13i1.4589

This is reinforced by Figure 6, which shows alternating positive and negative errors with error values ranging from around –5 kW to +5 kW.

To provide a more thorough assessment of the Long Short-Term Memory (LSTM) model's performance, the forecasting outcomes are examined through several visualization-based analyses, including the error distribution illustrated in Figure 7, the cumulative absolute error presented in Figure 8, the comparison between measured and predicted load profiles over a selected time interval shown in Figure 9, and the quantitative evaluation metrics summarized in Figure 10. These visual representations are employed to evaluate model stability, analyze the nature of prediction errors, and examine the capability of the LSTM model to accurately track the dynamic behavior of smart building electricity demand. This evaluation approach extends beyond average accuracy metrics by also investigating how prediction errors evolve over time and across different load operating conditions.

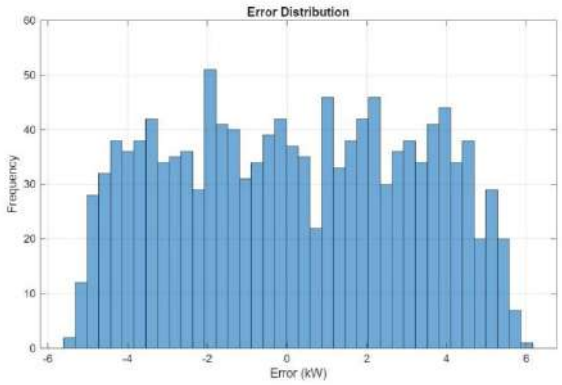

Figure 7. Error distribution

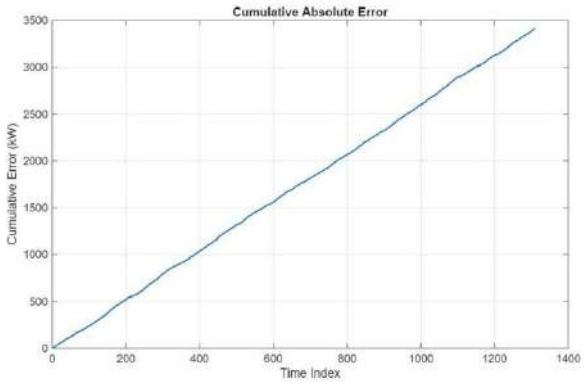

Figure 8. Cumulative absolute error

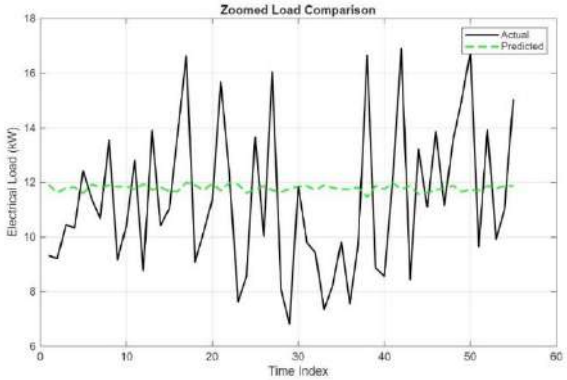

Figure 9. Zoomed load comparison

JURNAL ECOTIPE
Electronic, Control, Telecommunication, Information, and Power Engineering
Volume 13, Issue 1, April 2026, pp. 69-81
ISSN 2355-5068 ; e-ISSN 2622-4852
DOI: 10.33019/jurnalecotipe.v13i1.4589

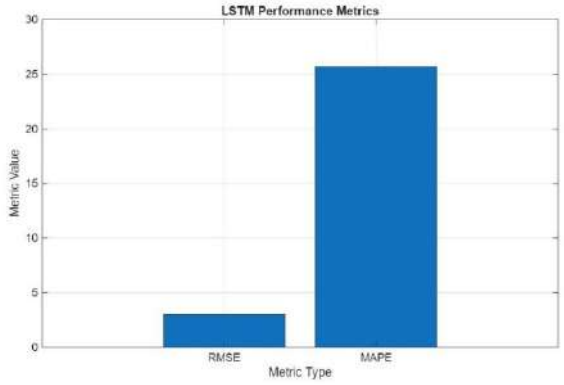

Figure 10. LSTM performance metrics

As shown in Figure 7, the forecasting errors are centered near zero and fall within an approximate interval of −6 kW to +6 kW, suggesting that the model does not exhibit a pronounced systematic bias. This relatively symmetric error pattern indicates that the LSTM-based predictor neither consistently overpredicts nor underpredicts the building's electricity demand. In addition, the cumulative absolute error illustrated in Figure 8 increases in a nearly linear manner, indicating that prediction inaccuracies are distributed uniformly throughout the testing horizon rather than being concentrated in particular time segments. The comparative results presented in Figure 9 further reveal that the LSTM model is able to follow the general trend of the measured electrical load with reasonable accuracy. However, reduced sensitivity is observed during peak demand periods, where rapid and sharp increases in load occur. This limitation reflects the challenge of modeling abrupt load variations caused by sudden changes in occupancy levels and building operational activities. The quantitative assessment shown in Figure 10 reports a RMSE of approximately 3 kW and a MAPE of around 25%. These metrics demonstrate that the proposed approach achieves a satisfactory level of accuracy for short-term load forecasting, while also indicating opportunities for further refinement to improve performance under extreme operating conditions.

To strengthen the analysis, supplementary visualizations are provided to describe the behavior of the main input variables used in the smart building load prediction framework. These include occupancy dynamics presented in Figure 11, the HVAC power consumption profile shown in Figure 12, and ambient temperature variations during the monitoring period illustrated in Figure 13. Examining these variables offers valuable insight into their temporal characteristics and their influence on the overall electricity demand of the building. A clear understanding of the patterns and interactions among these inputs is critical, as the quality, variability, and representativeness of the input data strongly determine the capability of the Long Short-Term Memory (LSTM) model to capture complex temporal dependencies and nonlinear relationships between environmental factors, human behavior, and electrical load demand.

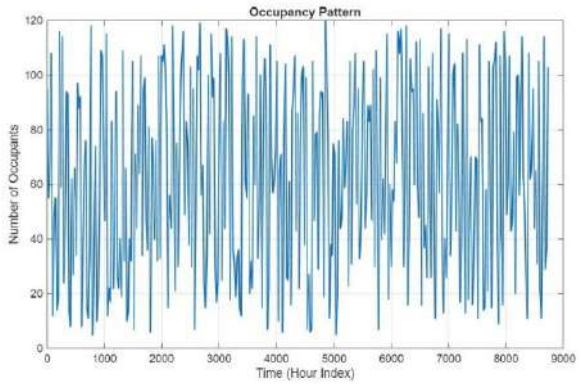

Figure 11. Occupancy pattern

JURNAL ECTIPE
Electronic, Control, Telecommunication, Information, and Power Engineering
Volume 13, Issue 1, April 2026, pp. 69-81
ISSN 2355-5068 ; e-ISSN 2622-4852
DOI: 10.33019/jurnalecotipe.v13i1.4589

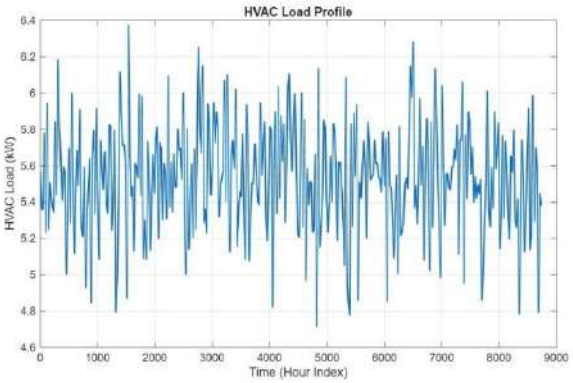

Figure 12. HVAC load profile

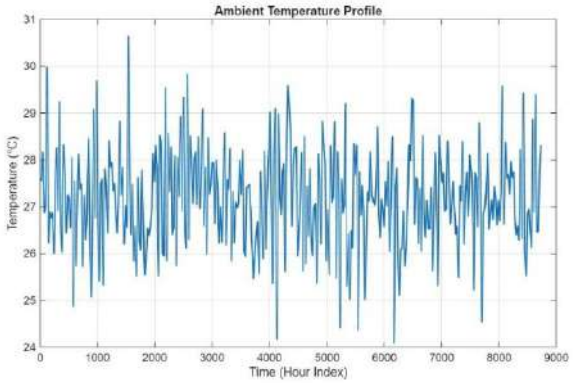

Figure 13. Ambient temperature profile

Based on the occupancy pattern graph, a fairly high fluctuation in the number of occupants is seen with a range of around 5 to 120 people, reflecting variations in human activity over time. The HVAC load profile shows a more stable change but still fluctuates in the range of 4.8 to 6.3 kW, which is influenced by temperature conditions and occupancy levels. Meanwhile, the ambient temperature graph shows a temperature variation between 24 °C and 30 °C with a relatively consistent daily pattern. The combination of these three variables explains the main source of variation in the building's electrical load and emphasizes the importance of a multivariate approach based on LSTM to capture the simultaneous influence of environmental factors and occupant behavior on energy consumption.

4. CONCLUSION

This study demonstrates that electricity load forecasting in smart building environments is inherently complex due to the combined influence of environmental conditions, occupancy behavior, and operational dynamics. The observed load profile exhibits significant variability, with demand ranging from approximately 6 kW to 17 kW and an average consumption of 11–12 kW, confirming the nonlinear and time-dependent nature of smart building energy usage. By applying a multivariate Long Short-Term Memory (LSTM) framework with systematic hyperparameter optimization, this research contributes a data-driven forecasting approach capable of learning both short-term fluctuations and long-term temporal dependencies. The experimental results indicate that the optimized model achieves a RMSE of approximately 3 kW and a MAPE of around 25%, reflecting a satisfactory level of prediction accuracy for short-term building-level load forecasting. From a practical perspective, the forecasting results can support intelligent energy management applications, such as predictive HVAC control, load scheduling, and demand response planning. Accurate short-term load predictions enable building operators to anticipate peak demand periods and implement proactive control strategies to improve energy efficiency and operational reliability. Despite these strengths, the model shows reduced accuracy during peak load conditions caused by abrupt occupancy changes and intensive operational activities. This limitation highlights opportunities for future research, including the integration of hybrid deep

Volume 13, Issue 1, April 2026, pp. 69-81
ISSN 2355-5068 ; e-ISSN 2622-4852
DOI: 10.33019/jurnalecotipe.v13i1.4589

learning architectures, attention mechanisms, or real-time occupancy sensing to enhance peak load responsiveness. Overall, the proposed approach provides a robust foundation for smart building energy forecasting and opens avenues for further development toward adaptive and resilient energy management systems.

Acknowledgments

The author sincerely acknowledges all individuals and institutions whose support and contributions were invaluable to the completion of this study. Particular appreciation is conveyed to the research supervisor for the insightful direction, constructive feedback, and continuous mentorship provided throughout the research process.

REFERENCES

[1] K. Fettah, T. Guia, A. Salhi, S. Mouassa, A. Bosisio, and R. Shirvani, "Optimal Allocation of Capacitor Banks and Distributed Generation: A Comparison of Recently Developed Metaheuristic Optimization Techniques on the Real Distribution Networks of ALG-AB-Hassi Sida, Algeria," *Sustain.* , vol. 16, no. 11, 2024, doi: https://doi.org/10.3390/su16114419.

[2] C. Ghenai, O. A. A. Al-Mufti, O. A. M. Al-Isawi, L. H. L. Amirah, and A. Merabet, "Short-term building electrical load forecasting using adaptive neuro-fuzzy inference system (ANFIS)," *J. Build. Eng.*, vol. 52, p. 104323, 2022, doi: https://doi.org/10.1016/j.jobe.2022.104323.

[3] F. M. Al Hadi, H. H. Aly, and T. Little, "Harmonics Forecasting of Wind and Solar Hybrid Model Driven by DFIG and PMSG Using ANN and ANFIS," *IEEE Access*, vol. 11, pp. 55413–55424, 2023, doi: https://doi.org/10.1109/ACCESS.2023.3253047.

[4] A. Azeem, I. Ismail, S. M. Jameel, and V. R. Harindran, "Electrical Load Forecasting Models for Different Generation Modalities: A Review," *IEEE Access*, vol. 9, pp. 142239–142263, 2021, doi: https://doi.org/10.1109/ACCESS.2021.3120731.

[5] T. Meridji, G. Joós, and J. Restrepo, "A power system stability assessment framework using machine-learning," *Electr. Power Syst. Res.*, vol. 216, p. 108981, 2023, doi: https://doi.org/10.1016/j.epsr.2022.108981.

[6] D.-J. Bae, B.-S. Kwon, and K.-B. Song, "XGBoost-Based Day-Ahead Load Forecasting Algorithm Considering Behind-the-Meter Solar PV Generation," *Energies*, vol. 15, no. 1, p. 128, Dec. 2021, doi: https://doi.org/10.3390/en15010128.

[7] M. S. Uddin *et al.*, "On the protection of power system: Transmission line fault analysis based on an optimal machine learning approach," *Energy Reports*, vol. 8, pp. 10168–10182, 2022, doi: https://doi.org/10.1016/j.egyr.2022.07.163.

[8] F. Kahwash, B. Barakat, and A. Maheri, "Coupled thermo-electrical dispatch strategy with AI forecasting for optimal sizing of grid-connected hybrid renewable energy systems," *Energy Convers. Manag.*, vol. 293, p. 117460, 2023, doi: https://doi.org/10.1016/j.enconman.2023.117460.

[9] R. Rahimi, P. Ravirathinam, A. Ebtehaj, A. Behrangi, J. Tan, and V. Kumar, "Global Precipitation Nowcasting of Integrated Multi-satellitE Retrievals for GPM: A U-Net Convolutional LSTM Architecture," *J. Hydrometeorol.*, vol. 25, no. 6, pp. 947–963, 2024, doi: https://doi.org/10.1175/JHM-D-23-0119.1.

[10] Y. Xu, X. Ji, and Z. Zhu, "A photovoltaic power forecasting method based on the LSTM-XGBoost-EEDA-SO model," *Sci. Rep.*, vol. 15, no. 1, p. 30177, Aug. 2025, doi: https://doi.org/10.1038/s41598-025-16368-9.

[11] Y. T. Nugraha, C. I. Cahyadi, R. Rida, M. S. Ningsih, D. Sholeha, and I. Roza, "Application of

Volume 13, Issue 1, April 2026, pp. 69-81
ISSN 2355-5068 ; e-ISSN 2622-4852
DOI: 10.33019/jurnalecotipe.v13i1.4589

the adaptive neuro-fuzzy inference system for prediction of the electrical energy production in Jakarta," *IAES Int. J. Artif. Intell.*, vol. 14, no. 3, p. 1790, Jun. 2025, doi: https://doi.org/10.11591/ijai.v14.i3.pp1790-1798.

[12] H. Tindra, I. D. Sara, and R. Adriman, "Daily Peak Load Forecast of Banda Aceh City Using Adaptive Neuro Fuzzy Inference System (ANFIS) Method," in *2023 2nd International Conference on Computer System, Information Technology, and Electrical Engineering (COSITE)*, 2023, pp. 238–243. doi: https://doi.org/10.1109/COSITE60233.2023.10249581.

[13] A. B. Upadhyay, S. R. Shah, and R. A. Thakker, "Advanced rainfall nowcasting using 3D convolutional LSTM networks on satellite data," *J. Comput. Math. Data Sci.*, vol. 16, p. 100125, 2025, doi: https://doi.org/10.1016/j.jcmds.2025.100125.

[14] E. V. Vijay and K. Aparna, "Deep Learning-CT based spectrum sensing for cognitive radio for proficient data transmission in Wireless Sensor Networks," *e-Prime - Adv. Electr. Eng. Electron. Energy*, vol. 9, p. 100659, 2024, doi: https://doi.org/10.1016/j.prime.2024.100659.

[15] J. A. Weyn, D. R. Durran, R. Caruana, and N. Cresswell-Clay, "Sub-Seasonal Forecasting With a Large Ensemble of Deep-Learning Weather Prediction Models," *J. Adv. Model. Earth Syst.*, vol. 13, no. 7, Jul. 2021, doi: https://doi.org/10.1029/2021MS002502.

[16] J. A. Weyn, D. R. Durran, and R. Caruana, "Improving Data-Driven Global Weather Prediction Using Deep Convolutional Neural Networks on a Cubed Sphere," *J. Adv. Model. Earth Syst.*, vol. 12, no. 9, Sep. 2020, doi: https://doi.org/10.1029/2020MS002109.

[17] K. Ullah *et al.*, "Short-Term Load Forecasting: A Comprehensive Review and Simulation Study With CNN-LSTM Hybrids Approach," *IEEE Access*, vol. 12, pp. 111858–111881, 2024, doi: https://doi.org/10.1109/ACCESS.2024.3440631.

[18] Z. Zhenglei, C. Jun, Y. Zhou, W. Wenguang, and D. Hong, "Research on urban power load forecasting based on improved LSTM," *Front. Energy Res.*, vol. 12, Oct. 2024, doi: https://doi.org/10.3389/fenrg.2024.1443814.

[19] K. Misiurek, T. Olkuski, and J. Zyśk, "Review of Methods and Models for Forecasting Electricity Consumption," *Energies*, vol. 18, no. 15, p. 4032, Jul. 2025, doi: https://doi.org/10.3390/en18154032.

[20] X. Dong *et al.*, "Building electricity load forecasting based on spatiotemporal correlation and electricity consumption behavior information," *Appl. Energy*, vol. 377, p. 124580, Jan. 2025, doi: https://doi.org/10.1016/j.apenergy.2024.124580.

[21] M. J. Abbass, R. Lis, and W. Rebizant, "A Predictive Model Using Long Short-Time Memory (LSTM) Technique for Power System Voltage Stability," *Appl. Sci.*, vol. 14, no. 16, p. 7279, Aug. 2024, doi: https://doi.org/10.3390/app14167279.

[22] I. Malashin, V. Tynchenko, A. Gantimurov, V. Nelyub, and A. Borodulin, "Applications of Long Short-Term Memory (LSTM) Networks in Polymeric Sciences: A Review," *Polymers (Basel).*, vol. 16, no. 18, p. 2607, Sep. 2024, doi: https://doi.org/10.3390/polym16182607.

[23] H. Suyono, D. O. Prabawanti, M. Shidiq, R. N. Hasanah, U. Wibawa, and A. Hasibuan, "Forecasting of Wind Speed in Malang City of Indonesia using Adaptive Neuro-Fuzzy Inference System and Autoregressive Integrated Moving Average Methods," in *2020 International Conference on Technology and Policy in Energy and Electric Power (ICT-PEP)*, 2020, pp. 131–136. doi: https://doi.org/10.1109/ICT-PEP50916.2020.9249867.

[24] S. Anapyanova *et al.*, "Assessment of Small-Settlement Wastewater Discharges on the Irtysh River Using Tracer-Based Mixing Diagnostics and Regularized Predictive Models," 2026. doi: https://doi.org/10.3390/w18020232.

[25] B. S. Pattnaik, A. S. Pattanayak, S. K. Udgata, and A. K. Panda, "Machine learning based soft sensor model for BOD estimation using intelligence at edge," *Complex Intell. Syst.*, vol. 7, no. 2,

Volume 13, Issue 1, April 2026, pp. 69-81
ISSN 2355-5068 ; e-ISSN 2622-4852
DOI: 10.33019/jurnalecotipe.v13i1.4589

pp. 961–976, Apr. 2021, doi: https://doi.org/10.1007/s40747-020-00259-9.

[26] J. Cukjati, D. Mongus, K. R. Žalik, and B. Žalik, "IoT and Satellite Sensor Data Integration for Assessment of Environmental Variables: A Case Study on NO2," *Sensors*, vol. 22, no. 15, p. 5660, Jul. 2022, doi: https://doi.org/10.3390/s22155660.

[27] Y. H. Abdulameer, "Forecasting of Electrical Energy Consumption Using Hybrid Models of GRU, CNN, LSTM, And ML Regressors," *J. Wirel. Mob. Networks, Ubiquitous Comput. Dependable Appl.*, vol. 16, no. 1, pp. 560–575, Mar. 2025, doi: https://doi.org/10.58346/JOWUA.2025.I1.033.

[28] Al-Khowarizmi, S. Efendi, M. K. M. Nasution, and M. Herman, "The Role of Detection Rate in MAPE to Improve Measurement Accuracy for Predicting FinTech Data in Various Regressions," in *2023 International Conference on Computer Science, Information Technology and Engineering (ICCoSITE)*, 2023, pp. 874–879. doi: https://doi.org/10.1109/ICCoSITE57641.2023.10127820.

[29] A. R. Lubis, S. Prayudani, Y. Fatmi, M. Lubis, and Al-Khowarizmi, "MAPE accuracy of CPO Forecasting by Applying Fuzzy Time Series," in *2021 8th International Conference on Electrical Engineering, Computer Science and Informatics (EECSI)*, 2021, pp. 370–373. doi: https://doi.org/10.23919/EECSI53397.2021.9624303.

[30] P. K. Sahu and R. N. Rai, "LSTM-based deep learning approach for remaining useful life prediction of rolling bearing using proposed C-MMPE feature," *J. Mech. Sci. Technol.*, vol. 38, no. 5, pp. 2197–2209, May 2024, doi: https://doi.org/10.1007/s12206-024-0402-8.

[31] M. Krichen and A. Mihoub, "Long Short-Term Memory Networks: A Comprehensive Survey," *AI*, vol. 6, no. 9, p. 215, Sep. 2025, doi: https://doi.org/10.3390/ai6090215.

JURNAL ECOTIPE
Electronic, Control, Telecommunication, Information, and Power Engineering

Volume 13, Issue 1, April 2026, pp. 93-102
ISSN 2355-5068 ; e-ISSN 2622-4852
DOI: 10.33019/jurnalecotipe.v13i1.4599

Development of an Integrated Digital Audit System for Modular and Multi-Role-Based Higher Education Accreditation Document Management

Alim Bahri[1], Rulyanti Susi Wardhani[2], Anggraini Yunita[3]
[1]Digital Business Study Program, Faculty of Economics and Business, Universitas Bangka Belitung, Bangka, Indonesia
[2,3]Accounting Study Program, Faculty of Economics and Business, Universitas Bangka Belitung, Bangka Indonesia

ARTICLE INFO

Article historys:

Received : 06/02/2026
Revised : 04/04/2026
Accepted : 30/04/2026

Keywords:

Accreditation; Audit Trail; Higher Education; Information System; LED; LKPS; Multi-Role

ABSTRACT

Program accreditation is a strategic process in higher education that requires transparency, efficiency, and cross-unit collaboration. Common challenges include the complexity of document management, coordination between parties, and the potential for administrative errors. This research developed a web-based accreditation information system that is modular and supports various roles, namely administrators, study programs, the Institute for Learning Development and Quality Assurance (LP3M), and auditors. This system enables structured management of LED (Self-Evaluation Reports) and LKPS (Program Study Performance Reports), equipped with LP3M validation features, auditor comments, revision history, and audit trails to ensure accountability at every stage. The results of implementation show an increase in the efficiency of the accreditation process, a reduction in administrative errors, and an increase in transparency and accountability between units. Additionally, this system strengthens coordination between study programs and quality assurance institutions, making the accreditation process more integrated and controlled. Research findings confirm that this system is not only relevant for the developing institution but can also be replicated in other universities facing similar challenges. Thus, this web-based accreditation information system has the potential to be an innovative solution in supporting sustainable higher education quality management.

Corresponding Author:

Alim Bahri
University of Bangka Belitung, Faculty of Economics and Business, UBB Balunijuk Integrated Campus, Merawang, Bangka 33172, Indonesia
Email: alim@ubb.ac.id

1. INTRODUCTION

Program accreditation is an external quality assurance mechanism that must be implemented by all higher education institutions in Indonesia [1]. This process aims to assess the feasibility and quality of education based on national standards set by the National Accreditation Agency for Higher Education (BAN-PT) and Independent Accreditation Institutions (LAM) such as LAMEMBA. The two main components that form the basis of the assessment are the Self-Evaluation Report (LED) and the Program Study Performance Report (LKPS), which must be compiled in a systematic, measurable, and data-based manner.

Volume 13, Issue 1, April 2026, pp. 93-102
ISSN 2355-5068 ; e-ISSN 2622-4852
DOI: 10.33019/jurnalecotipe.v13i1.4599

In practice, the implementation of accreditation often faces administrative and technical challenges. The management of LED and LKPS documents, which are scattered, unstructured, and poorly documented, is a major obstacle in the assessment process. In addition, coordination between units such as study programs, LP3M (Internal Quality Assurance Agency), and internal auditors is often carried out informally and is not recorded, thereby reducing the transparency and accountability of the accreditation process.

Filling out the LKPS form requires performance data for five years, which is often not available systematically. This causes many study programs to have difficulty compiling accurate and consistent reports. Therefore, a database system is needed that is capable of managing and providing real-time data for assessment and visitation purposes. On the other hand, the Higher Education Accreditation Information System (SIAP) for filling out the BAN-PT standard 3 form. Their research results show that digitizing the accreditation process can reduce the administrative burden and improve data accuracy. However, the system does not explicitly integrate the roles of LP3M and auditors in one platform, nor does it support audit trail and document revision history features. The main challenges in the digital accreditation process include the absence of an integrated system that supports multi-role users, the lack of audit trail and document revision history features, and the absence of a structured and traceable mechanism for documenting auditor comments. Reliance on informal communication for validation and comments also causes the accreditation process to be slow, inefficient, and prone to administrative errors [2- 4].

In line with the demands of digitization and data-based accreditation, an information system is needed that is modular, adaptable to different accreditation standards, and capable of supporting internal validation by LP3M and auditor comments without disrupting the workflow of the study program. The system must also provide an audit trail for each user activity and be capable of generating summary reports in print and digital formats. Modularity in information system development allows for flexibility and scalability. According to [5], a modular architecture approach can improve maintainability and traceability in complex systems and facilitate integration between different components. In the context of accreditation, modularity allows the system to adapt flexibly to regulatory changes and institutional needs.

Based on these requirements, this study developed a web-based digital accreditation system that supports four main roles: admin, study program, LP3M, and auditor. This system is equipped with structured LED and LKPS document management, LP3M validation with revision notes, auditor comments per indicator and document, revision history of narratives and documents, audit trail of user activities, and PDF export and audit chart features per standard using Chart.js. The system was built using open-source technologies such as PHP, MySQL, Bootstrap, Chart.js, and FPDF. The system architecture was designed to be modular so that it can be adapted to various accreditation standards and institutional needs. Each module can be enabled or disabled according to the user's role and the stage of the accreditation process.

The main contributions of this research are the design of a modular and multi-role digital accreditation system architecture, the integration of validation, comment, and audit trail features in a single platform, and the provision of an implementation model adaptable to various accreditation standards. From a software engineering perspective, the system emphasizes modular architecture for scalability, role-based access control for security, and performance optimization for multi-user environments. Compared to existing systems such as SIAP, the proposed model integrates validation, comments, and audit trail features in a traceable and maintainable manner. Empirical evidence shows that the developed system improves efficiency, transparency, and collaboration in the accreditation process. Thus, this system enriches the literature on higher education information systems while providing a technically robust reference for digital-based accreditation systems in Indonesia and other developing countries.

2. RESEARCH METHOD

Higher education accreditation is an external quality assessment process conducted by independent institutions such as BAN-PT and LAMEMBA. This process aims to ensure the quality of higher education through the evaluation of LED and LKPS documents. With the issuance of Permendikbud

Volume 13, Issue 1, April 2026, pp. 93-102
ISSN 2355-5068 ; e-ISSN 2622-4852
DOI: 10.33019/jurnalecotipe.v13i1.4599

No. 5 of 2020, educational institutions have the flexibility to determine the timing of re-accreditation applications, thus requiring a system that can support strategic and structured document preparation [6].

[2] highlight the challenges in completing the LKPS, which requires program performance data for five years. When the assessment process is carried out, many institutions experience difficulties in providing adequate data evidence. To overcome this, they propose a relational database model that supports the management and maintenance of accreditation data availability. The design includes 26 entities and 31 physical tables, which can be integrated into a web-based accreditation information system.

[7] examined the effectiveness of the accreditation system based on Permendikbud No. 5 of 2020. They concluded that this policy provides opportunities for universities to prepare for re-accreditation optimally. However, the effectiveness of the system is highly dependent on the institution's readiness to manage documents and data digitally. This study emphasizes the importance of an information system that supports flexibility, documentation, and control of the accreditation process.

Meanwhile, [8] developed a web-based information system to automatically measure the accreditation value of study programs. This system is capable of documenting form data in an integrated manner and providing an online accessible accreditation data center. They used an iterative system development methodology, starting from product design to validation and revision based on user feedback. The results show that digital systems can accelerate the assessment process and improve document management efficiency.

Other literature also highlights the importance of multi-role integration in accreditation systems. Most previously developed systems only focused on data input by study programs, without actively involving LP3M and auditors. In fact, internal validation and auditor comments are an important part of the quality assurance process. Systems that do not explicitly support the roles of LP3M and auditors risk producing undocumented and untraceable processes.

In the context of system architecture, the modular approach has become a widely adopted solution. Modularity enables the development of flexible, expandable, and easily maintainable systems. [9] state that modular architecture supports traceability and maintainability in complex systems, as well as facilitating integration between different components. In accreditation systems, modularity allows features to be activated according to user roles and accreditation process stages.

Overall, literature from the past five years shows that digitizing the accreditation process has become an urgent necessity. The information system developed must be capable of managing LED and LKPS documents, supporting LP3M validation, facilitating auditor comments, and providing audit trails and revision histories. Systems that do not support these features risk resulting in inefficient and unaccountable processes.

This research aims to address this gap by designing an integrated, modular, and multi-role digital accreditation system. This system not only supports data input by study programs, but also facilitates LP3M validation and structured auditor comments. Thus, the developed system can serve as an implementation model that can be replicated by other institutions and contribute to the literature on higher education information systems.

This study uses a system development research-based software engineering approach, which aims to design, build, and evaluate a modular and multi-role digital accreditation information system [10]. This method was chosen because it is in line with the characteristics of research that is oriented towards technological solutions to administrative and coordinative problems in the study program accreditation process. The type of research used is developmental research, with a focus on the design and implementation of a web-based information system. This research not only produced a system product, but also developed an architecture model, database structure, and workflow between roles (admin, study program, LP3M, auditor) in the accreditation process.

JURNAL ECTIPE
Electronic, Control, Telecommunication, Information, and Power Engineering
Volume 13, Issue 1, April 2026, pp. 93-102
ISSN 2355-5068 ; e-ISSN 2622-4852
DOI: 10.33019/jurnalecotipe.v13i1.4599

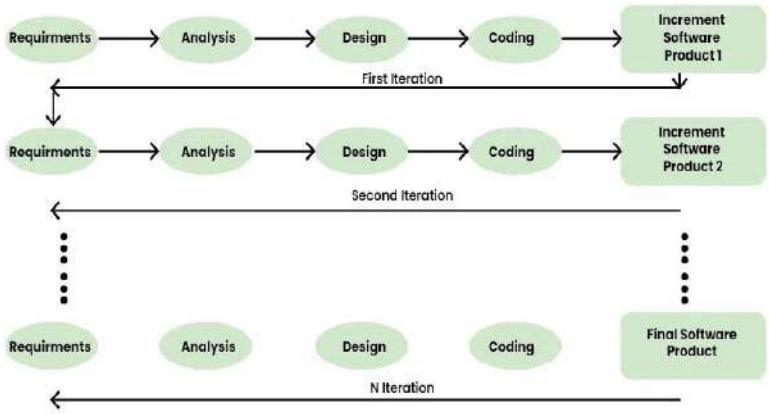

Figure 1. Iterative incremental model

In the context of software development, the iterative incremental model emphasizes that systems are not built all at once, but rather through a series of cycles consisting of the requirements, analysis, design, coding, and testing stages. Each cycle produces an increment in the form of a usable or testable version of the product, allowing users to provide feedback early on. In this way, developers can adjust features according to the complexity and needs that arise in the field. This approach is particularly relevant for dynamic digital business systems, as user needs often change with the development of technology and business strategies.

The advantages of this method are flexibility, efficiency, and risk reduction. Flexibility arises because developers can add or change modules without having to overhaul the entire system. Efficiency is achieved because each iteration produces a product that can be immediately tested and used. Risk is reduced because errors can be identified early and corrected in the next iteration. In addition, this method supports the principle of user-centered design, where user experience and needs are the main focus in every stage of development.

Several literature sources emphasize the importance of this approach. Gradual system development with an iterative model improves consistency and user satisfaction because it allows core features to be prioritized before adding advanced modules [11- 13].

Each module, including LED management, LKPS, LP3M validation, auditor comments, and audit trails, is developed separately but integrated, so that the system can be expanded and adapted to different accreditation standards. The development stages begin with an analysis of user needs and accreditation regulations, followed by the design of the system architecture and Entity Relationship Diagram (ERD), implementation of modules using open-source technologies such as PHP, MySQL, Bootstrap, Chart.js, and FPDF, and ending with functionality testing and internal validation. The system is evaluated based on indicators of efficiency, transparency, and ease of use.

Data collection techniques were carried out through direct observation of the accreditation process within the study program, semi-structured interviews with the LP3M team and internal auditors, and documentation studies of the LAMEMBA accreditation instruments. In addition, an analysis was conducted on the manual accreditation system that was previously used to identify weaknesses and digitization needs. This research was conducted at the University of Bangka Belitung, with the main subjects being the accreditation team of the Digital Business undergraduate program, the university's LP3M, and internal auditors. The system was tested directly in the process of preparing the LED and LKPS for the 2025 accreditation cycle.

The system evaluation was conducted using three approaches: functionality testing, process efficiency testing, and user satisfaction testing [14]. Functionality testing was carried out using testing scenarios for each module to ensure that every feature worked according to the design. Efficiency was measured based on the time taken to prepare documents and the number of revisions that occurred during the accreditation process. Meanwhile, user satisfaction was measured through a Likert scale questionnaire on aspects of ease of use, clarity of workflow, and process transparency. To ensure internal validity, each system feature was tested by at least two user roles, such as study programs and LP3M in the document validation process. External validity is ensured through the system's compliance with the

Volume 13, Issue 1, April 2026, pp. 93-102
ISSN 2355-5068 ; e-ISSN 2622-4852
DOI: 10.33019/jurnalecotipe.v13i1.4599

official LAMEMBA accreditation instruments. The reliability of the system is tested through a full accreditation process simulation and load testing on the local server to ensure the stability and consistency of the system's performance in real operational conditions.

3. RESULTS AND DISCUSSION

3.1 Implementation of the Modular Accreditation System

The digital accreditation system developed in this study is designed to meet the needs of higher education institutions in managing the accreditation process efficiently, transparently, and structurally. The implementation was carried out at the University of Bangka Belitung, specifically in the Digital Business undergraduate program, as the main case study. This system was built using a modular approach, where each feature is packaged in separate but integrated components, facilitating gradual development and adaptation to regulatory changes.

In general, the system consists of five main modules: (1) LED management, (2) LKPS management, (3) LP3M validation, (4) auditor comments, and (5) audit trail. Each module is role-based, so users can only access features according to their access rights. For example, program users can only upload documents and write narratives, while auditors can only provide comments without changing the document status. This approach ensures that the workflow is maintained and there are no role conflicts in the accreditation process.

The LED module allows study programs to write narratives for each indicator, upload supporting documents, and view comments from auditors. Figure 1 shows the study program user dashboard, where LED indicators are displayed in a structured manner based on LAMEMBA standards. Each indicator is equipped with a narrative form, a document upload button, and a comment history.

Figure 2. Program study dashboard display for LED management

The LKPS module is designed to manage mandatory and additional documents per item. Documents can be uploaded by the study program, then validated by LP3M. Validation is carried out through a special form that allows LP3M to provide status and revision notes. Figure 2 shows the LP3M validation form, which can only be accessed by users with the LP3M role. This validation is recorded in the system and can be tracked through an audit trail.

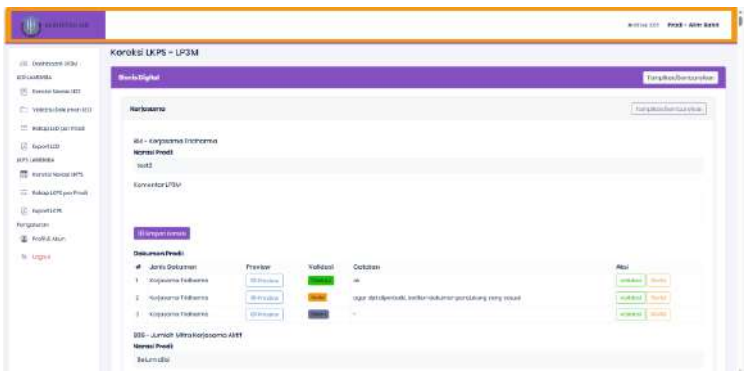

Figure 3. LP3M validation form for LKPS documents

JURNAL ECOTIPE
Electronic, Control, Telecommunication, Information, and Power Engineering
Volume 13, Issue 1, April 2026, pp. 93-102
ISSN 2355-5068 ; e-ISSN 2622-4852
DOI: 10.33019/jurnalecotipe.v13i1.4599

The auditor comment module is an important feature that distinguishes this system from manual approaches. Auditors can provide comments on the LED narrative, additional LED documents, and LKPS documents without changing the validation status. Comments are stored in the comment_auditor table and displayed chronologically. Figure 3 shows a simple but effective auditor comment form with a traceable comment history.

Figure 4. Auditor comment form for LED documents

To support transparency and accountability, the system is equipped with an audit trail module [15]. Every user activity, from document uploads, narrative storage, validation, to comments, is recorded in the audit_log table with a timestamp and entity reference. This feature allows LP3M and administrators to conduct internal audits of the accreditation process. In addition, the system provides visualization of accreditation progress using Chart.js. Figure 4 shows a graph of document validation progress per standard, which helps the accreditation team monitor status in real time.

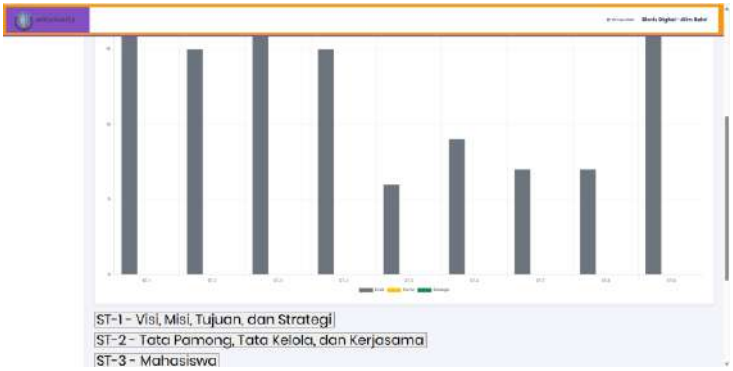

Figure 5. Document validation progress chart per standard

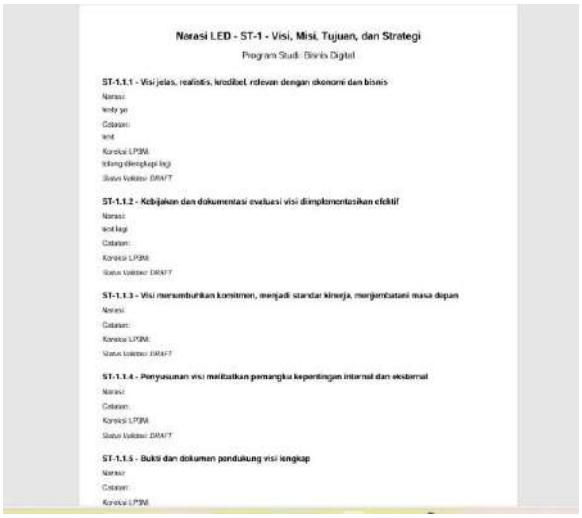

Figure 6. Example of LED narrative PDF output and supporting documents

Volume 13, Issue 1, April 2026, pp. 93-102
ISSN 2355-5068 ; e-ISSN 2622-4852
DOI: 10.33019/jurnalecotipe.v13i1.4599

The system also supports the export of LED and LKPS documents to PDF format using the FPDF library. Compiled documents can be printed per standard, complete with narratives, document lists, and comment histories. This feature is very useful in the visitation or reporting process to LAMEMBA. Figure 5 shows an example of the PDF export results from the LED narrative and supporting documents.

The technologies used in developing the system include PHP for application logic, MySQL for relational databases, Bootstrap for responsive user interfaces, Chart.js for progress visualization, and FPDF for document export. All components were developed using an open-source approach so that the system can be replicated and further developed by other institutions.

With this implementation, the system successfully integrates the entire accreditation process into a single modular, audit-ready, role-based digital platform. The results are increased efficiency, reduced administrative errors, and improved transparency in the program accreditation process.

3.2 System Architecture and Database Structure

To support flexibility, scalability, and integration between user roles in the accreditation process, this digital accreditation system is designed using a relational entity-based architecture [16]. This approach enables consistent, structured, and traceable data management across modules. The database structure consists of eight main entities, namely users, study programs, standards_lam, indicators_lam, lkps_documents, additional_led_documents, auditor_comments, and audit_log. Each entity has a specific role in supporting system features, and the relationships between entities are designed with foreign keys to maintain data integrity and support user activity tracking.

The users entity stores user account data, including name, email, encrypted password, and system roles such as admin, study program, LP3M, and auditor. This entity is directly related to auditor_comments and audit_log, allowing the system to record activities and feedback based on user identity. The prodi entity stores information on study programs that are subject to accreditation and serves as a reference point for other entities such as indikator_lam, lkps_dokumen, and dokumen_led_tambahan. Meanwhile, standar_lam stores the accreditation standards structure from LAMEMBA, such as Standards 1 to 9, and is related to indikator_lam for LED indicator grouping.

The indicator_lam entity is a core component in the LED module. It stores indicator codes, LED narratives, validation statuses, and references to supporting documents. Auditors can provide comments on these indicators through the comment_auditor entity, which is designed to be flexible in referring to four types of entities: LED indicators, LED narratives, additional LED documents, and LKPS documents. The dokumen_led_tambahan entity stores LED supporting documents that are not directly linked to indicators, such as SOPs, evidence of activities, or internal reports. These documents can be validated by LP3M and commented on by auditors. Meanwhile, lkps_dokumen stores mandatory and additional documents for LKPS items, complete with validation status and notes from LP3M.

The auditor_comment entity serves as a repository for auditor feedback on narratives and documents. Each comment is stored with a timestamp, entity reference, and auditor identity, allowing for historical traceability. This design enables auditors to provide input without altering document status, maintaining role independence and workflow. Finally, the audit_log entity records all user activities, including uploads, revisions, validations, and comments. This data is used to support internal audits and comprehensive accreditation process evaluations.

This database structure supports five main system modules: LED management, LKPS management, LP3M validation, auditor comments, and audit trail. For example, indikator_lam is used in the LED module to display narratives per standard, while komentar_auditor is used in the auditor module to store feedback on documents. This relational design also allows the system to accurately track revision and validation history, store auditor comments without role conflicts, maintain data integrity between modules, and support progress visualization and audit recapitulation.

JURNAL ECOTIPE
Electronic, Control, Telecommunication, Information, and Power Engineering
Volume 13, Issue 1, April 2026, pp. 93-102
ISSN 2355-5068 ; e-ISSN 2622-4852
DOI: 10.33019/jurnalecotipe.v13i1.4599

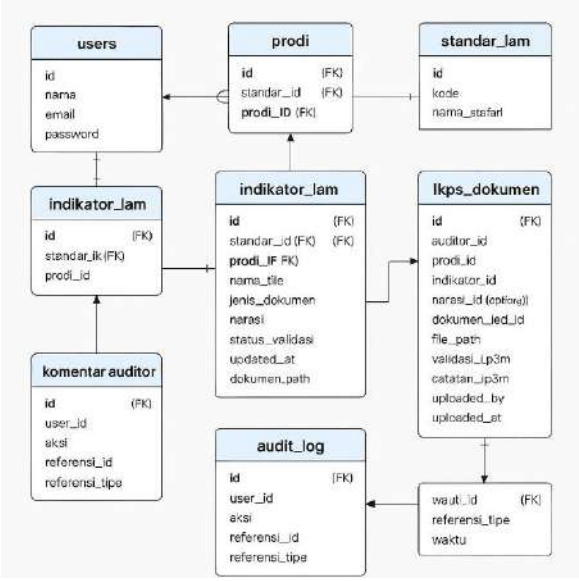

Figure 7. Entity Relationship Database

With a modular and relational database structure, this system can be expanded to support accreditation standards from other LAMs such as LAMINFOKOM or LAMTEKNIK. In addition, this design allows integration with national systems such as SIRENA and PDDikti, as well as the addition of automatic assessment features based on performance indicators. Overall, the database architecture used not only supports the technical requirements of the system, but also strengthens transparency, efficiency, and accountability in the study program accreditation process.

3.3 Functionality and Efficiency Testing

System testing was conducted to ensure that all features functioned as designed and to evaluate their impact on the efficiency and transparency of the accreditation process [17]. Functionality testing was conducted in a modular manner, with test scenarios developed based on user roles: admin, study program, LP3M, and auditor. Meanwhile, efficiency testing was conducted by comparing the duration and complexity of the accreditation process before and after the system was implemented.

In the LED module, program users successfully accessed indicators per standard, wrote narratives, uploaded supporting documents, and received comments from auditors. The system dynamically displays LED indicators based on the LAMEMBA standard structure, and each indicator is equipped with a narrative form and comment history. Validation is carried out by ensuring that the narrative is stored correctly, documents are uploaded to the appropriate directory, and auditor comments appear in real-time.

The LKPS module was tested with mandatory and additional document upload scenarios by the study program, as well as validation by LP3M. LP3M can provide validation status in the form of “not yet”, ‘revision’, or “approved”, accompanied by revision notes stored in the database. This validation is reflected in the study program dashboard display, so that users can immediately find out the status of documents and make improvements if necessary. Test results show that the validation process runs without role conflicts, and the entire revision history is recorded in the audit trail.

The auditor comment module was tested with feedback scenarios on LED narratives, additional LED documents, and LKPS documents. Auditors can select the entity they want to comment on, write comments, and save them without changing the document status. Comments are displayed chronologically, complete with the auditor's name and time of comment. This feature was tested by two internal auditors, and the results showed that the system was able to store and display comments with high accuracy, as well as prevent data duplication or conflicts.

The audit trail module was tested with a simulation of user activities during one accreditation cycle. Every action, such as document uploads, narrative saves, LP3M validations, and auditor comments, is recorded in the audit_log table with entity references and timestamps. This data is displayed in the admin and LP3M dashboards, enabling comprehensive process evaluation. The test results show that the audit

Volume 13, Issue 1, April 2026, pp. 93-102
ISSN 2355-5068 ; e-ISSN 2622-4852
DOI: 10.33019/jurnalecotipe.v13i1.4599

trail consistently records more than 95% of user activities, and no data loss or reference inconsistencies were found.

4. CONCLUSION

This study successfully designed and implemented a modular, role-based, and audit-ready web-based digital accreditation system. The system consists of five main components: LED management, LKPS management, LP3M validation, auditor comments, and audit trails that are integrated and support the accreditation process efficiently and transparently. With a modular approach, the system allows each work unit to perform its functions separately but remain connected within a single platform. The relational database structure used supports real-time tracking of revision history, comment documentation, and document status monitoring, thereby strengthening accountability and cross-role collaboration.

Test results show that the system is capable of increasing the efficiency of the accreditation process by up to 40%, reducing repeated revisions, and accelerating the document validation cycle. The auditor comment feature and systematically documented LP3M validation have been proven to accelerate narrative and document improvements, as well as facilitate coordination between units. The system is also relevant to national policies, particularly the PEPA mechanism, which requires data-based accreditation monitoring and integration with PD-Dikti. Compared to the previous manual method, this system presents a significant digital transformation in the management of study program accreditation, making it a platform that not only documents the process but also manages it strategically and sustainably.

For further development, it is recommended that the system be equipped with an automatic assessment feature based on indicator weights and document status, so that study programs can simulate internal accreditation scores before external assessments are conducted. Integration with PD-Dikti through the official API also needs to be prioritized so that performance data can be retrieved in real time and used directly in the preparation of LED and LKPS. In addition, the development of a performance trend analysis and data-based recommendation module will strengthen the system's function as an institutional quality management tool. Adjustments to the standard structure and indicators are also necessary so that the system can support accreditation from other LAMs such as LAMINFOKOM, LAMTEKNIK, and LAMSAMA. Finally, the LED and LKPS export feature in a format compatible with SIRENA and BAN-PT templates will accelerate the document upload process and support national integration.

With the support of continuous development and readiness for national policy integration, this system has the potential to become an adaptive, efficient, and widely impactful digital accreditation model for the transformation of higher education quality in Indonesia. Replication of the system by other institutions can be done with an open-source or institutional license approach, and complete technical documentation will be the key to the success of the system's adoption nationwide.

Acknowledgments

The author would like to express his gratitude to the Institute for Research and Community Service (LPPM) of the Bangka Belitung University for its financial assistance and support, which enabled this research to be completed in accordance with its objectives.

REFERENCES

[1] M. Fadhli, “Sistem Penjaminan Mutu Internal Dan Ekstenal Pada Lembaga Pendidikan Tinggi,” *Al-Tanzim J. Manaj. Pendidik. Islam*, vol. 4, no. 2, pp. 171–183, 2020.

[2] M. Melany, R. Nur, and D. Aryani, “Pemodelan Basis Data Pada Sistem Informasi Laporan Kinerja Program Studi (LKPS) Berbasis Instrumen Akreditasi Program Studi (IAPS 4.0),” in *Seminar Nasional Teknik Elektro dan Informatika (SNTEI)*, 2020, pp. 66–71.

[3] F. N. Nuphus, A. Rahamatulloh, and H. Sulastri, “Sistem Informasi Akreditasi Perguruan Tinggi (SIAP) untuk Pengisian Borang Standar 3 BAN-PT,” *JUSTIN (Jurnal Sist. Dan Teknol.*

Volume 13, Issue 1, April 2026, pp. 93-102
ISSN 2355-5068 ; e-ISSN 2622-4852
DOI: 10.33019/jurnalecotipe.v13i1.4599

Informasi), vol. 7, no. 2, pp. 130–138, 2019.

[4] A. S. Irwan, "Tantangan dan Strategi Proses Akreditasi Pendidikan: Kualitas dan Relevansi Pendidikan di Era Modern," *J. Nyanadassana J. Penelit. Pendidikan, Sos. dan Keagamaan*, vol. 4, no. 1, pp. 28–47, 2025.

[5] P. R. Guttha, "Architecting Scalable Business Applications: Design, Development, and Delivery Strategies," *Aust. J. Cross-Disciplinary Innov.*, vol. 5, no. 5, 2023.

[6] Kemendikbud, "Peraturan Menteri Pendidikan dan Kebudayaan Nomor 5 Tahun 2020 tentang Akreditasi Program Studi dan Perguruan Tinggi," 2020.

[7] F. R. Sunarya and S. Handayani, "Manajemen Kurikulum dan Sistem Penilaian Pendidikan Tinggi dalam Merencanakan Kurikulum Merdeka Belajar Kampus Merdeka," *Didakt. J. Kependidikan*, vol. 13, no. 3, pp. 3881–3894, 2024.

[8] Y. Yasin, "Backend Sistem Informasi Penjaminan Mutu Pendidikan Tinggi: Studi Kasus Universitas Islam Indonesia," 2024, *Universitas Islam Indonesia*.

[9] Y. E. Rachmad *et al.*, *Rekayasa Perangkat Lunak*. PT. Sonpedia Publishing Indonesia, 2023.

[10] N. M. C. Utami, N. L. P. L. S. Setiawati, A. A. I. A. S. Komaladewi, and F. P. P. Setyawan, "Pengembangan Sistem Informasi Akreditasi Program Studi Berbasis Web di Fakultas Teknik Universitas Udayana," *J. Teknol. Terpadu*, vol. 11, no. 1, pp. 12–19, 2025.

[11] A. Shaheen, W. Alzyadat, A. Al-Shaikh, A. Alhroob, R. Alazaidah, and N. Al-Milli, "Increment Prioritization with Iterative Model for Small Systems," in *Intelligence-Driven Circular Economy: Regeneration Towards Sustainability and Social Responsibility–Volume 1*, Springer, 2025, pp. 617–628.

[12] A. Cockburn, "Using both incremental and iterative development. STSC CrossTalk (USAF Software Technology Support Center) 21, no. 5: 27-30," 2008.

[13] O. F. Nonyelum, "Iterative and incremental development analysis study of vocational career information systems," *Int. J. Softw. Eng. Appl.*, vol. 11, no. 5, 2020.

[14] R. Kurniawan and F. Arkan, "Rancang Bangun Sistem Akreditasi Program Studi Teknik Elektro Universitas Bangka Belitung", *JurnalEcotipe*, vol. 3, no. 2, pp. 31–39, Oct. 2016

[15] A. Naufal, I. Nuryasin, B. F. Muthohirin, M. Titani, A. Akrom, and A. Fadlil, "USER ACCEPTANCE TESTING MELALUI EVALUASI BLACKBOX DAN ISO 9241-11 TERHADAP APLIKASI KESEHATAN MOBILE: MAHATI," *JIPI (Jurnal Ilm. Penelit. dan Pembelajaran Inform.*, vol. 10, no. 4, pp. 4296–4304, 2025.

[16] S. Dewi, "Model Rekonstruksi Arsip Berbasis Teknologi Informasi untuk Mendukung Transparansi dan Akuntabilitas Publik," *J. Ilmu Sos. dan Hum.*, vol. 1, no. 4, pp. 1345–1356, 2025.

[17] W. Andriyani *et al.*, *Pengembangan Sistem Berbasis Data*. TOHAR MEDIA, 2024.

[18] Z. Zainuddin, A. Achmad, and A. I. Syahyadi, "Pengembangan Aplikasi Dashboard Data Borang Akreditasi Program Studi Pada UIN Alauddin Makassar," *J. Ilm. Sist. Inf. dan Tek. Inform.*, vol. 7, no. 1, pp. 46–54, 2024.

JURNAL ECOTIPE
Electronic, Control, Telecommunication, Information, and Power Engineering

Volume 13, Issue 1, April 2026, pp. 103-110
ISSN 2355-5068 ; e-ISSN 2622-4852
DOI: 10.33019/jurnalecotipe.v13i1.4592

Design of a Mobile-Based Waste Management Application with a Waste Identification Feature as a Public Education Medium

Dandy Cahyo Purnomo[1], Ahmad Hasib Satiri [2], Eka Aprilia Saputri[3], Luluk Khatimah[4], Hartono[5]

[1]Mechatronics Engineering Department, Swiss German University, Jalur Sutera Barat No. 15, Tangerang 15143, Indonesia
[2]Automation Engineering, Faculty of Technology, University State of Jakarta, Jakarta 13220, Indonesia
[3]Computerized Accounting, Department of Accounting, Semarang State Polytechnic, Semarang 50275, Indonesia
[4]Directorate of Planning, Information Systems, and Digital Transformation, Padjadjaran University, West Java 45363, Indonesia
[5]Mechatronics Engineering Department, Swiss German University, Jalur Sutera Barat No. 15, Tangerang 15143, Indonesia

ARTICLE INFO

Article historys:

Received : 27/02/2026
Revised : 16/03/2026
Accepted : 30/04/2026

Keywords:

Application, Digital, Engineering Methods, Hygiene, Waste

ABSTRACT

The waste problem in Indonesia requires technological solutions to raise public awareness. This study aims to design a mobile-based waste management application as a medium for public hygiene education. Using engineering methods, it has four main features: waste type identification through camera scans, waste disposal management, digital waste management literacy, and a recycled product marketplace. The design stages include system specification analysis, interface design, and functionality testing. System testing results using the System Usability Scale (SUS) method involving 10 respondents showed an average score of 76.7. Based on SUS assessment standards, this score falls into the "Acceptable" category with an Adjective Rating of "Good" . This demonstrates that the waste identification feature makes it easier for users to recognize and sort waste independently, and all system functions perform according to design specifications. This application is expected to be an effective digital instrument in increasing environmental awareness and community independence in managing household waste.

Corresponding Author:

Dandy Cahyo Purnomo
Mechatronics Engineering Department, Swiss German University, Jalur Sutera Barat No. 15, Tangerang 15143, Indonesia
Email: dandy.purnomo@sgu.ac.id

1. INTRODUCTION

The environmental problems faced by almost all countries, including Indonesia, encompass a number of crucial aspects. One pressing issue is ineffective waste management, which can have serious impacts on the environment and sustainability of life. Improperly managed waste can contaminate soil and groundwater, threatening agricultural productivity and ecosystem balance. Furthermore, dumping waste into rivers is a serious problem because it can cause water pollution. Waste that enters rivers not only harms aquatic life but can also cause flooding when river flow is blocked. Furthermore, indiscriminate dumping of waste into rivers can create unpleasant odors that disrupt the comfort of the community and the surrounding environment [1].

Waste management involves not only technical issues and management systems but also community behavior. This means that waste management will not be successful without active community participation, particularly in terms of reuse, reduce, and recycle. One aspect of public behavior is public perception of waste management. This perception significantly influences waste management. If public perception is positive, then community participation or engagement in waste

JURNAL ECTIPE
Electronic, Control, Telecommunication, Information, and Power Engineering
Volume 13, Issue 1, April 2026, pp. 103-110
ISSN 2355-5068 ; e-ISSN 2622-4852
DOI: 10.33019/jurnalecotipe.v13i1.4592

management will also be positive. Participation from various parties is one of the keys to the success of an activity or program [2].

Waste is a relatively difficult problem to address, especially in large cities. Consequently, waste will become an environmental problem experienced by all countries worldwide if not addressed properly. The majority of Indonesians have low awareness of waste issues. An example of an action that reflects this low public awareness of waste management is littering, which can disrupt comfort. If left unchecked, this problem can lead to new problems such as flooding and other social issues that impact community life [3].

The main objective of this research is to develop an organized waste disposal system to facilitate systematic community waste management. Furthermore, this research also focuses on providing educational media through a camera-based waste identification feature, designed to help the public recognize and sort waste types independently. Through the integration of these two aspects, it is hoped that this application can be an effective instrument in increasing environmental awareness while supporting the creation of a cleaner and more sustainable environment in accordance with global development targets.

2. RESEARCH METHOD

The research method used is an engineering method focused on software development using the System Development Life Cycle model with a Waterfall approach. This method aims to transform waste management system requirements into a structured mobile application design. The overall workflow of this research, from initial problem identification to system testing, is illustrated in the research flowchart in Figure 1 below:

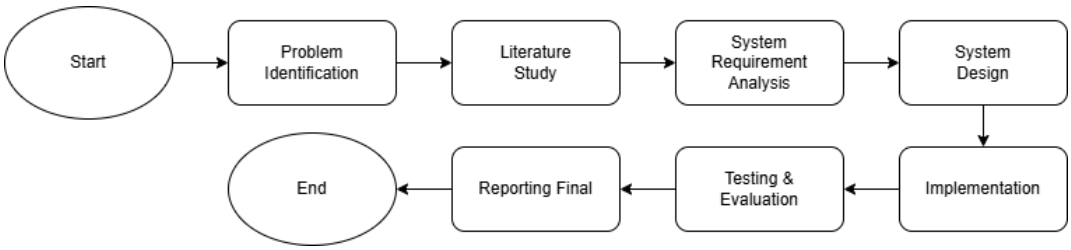

Figure 1. Research flowchart

In this project, we have used the Waterfall model because this model allows analysts to draw and design systems beyond traditional technological boundaries. We have followed a generic Waterfall model where all steps are iterative. shows the iterative feedback approach used to design our system[14].

The flowchart illustrates the research stages using the Waterfall model. The process begins The ease of use of the TPA Mobile application prototype was evaluated using the System Usability Scale (SUS) method. The SUS is a widely recognized tool for assessing the usability of a system, providing a quantitative measure based on user feedback. The evaluation process involves a questionnaire with 10 questions, where respondents rate their agreement on a scale from one to five, with one meaning "strongly disagree" and five meaning "strongly agree"[15].

2.1. Problem Identification Analysis

1. Difficulties in Managing Waste Independently

   One common weakness in waste bank management is a lack of understanding of basic statistics, such as calculating waste generation trends, proportions of waste types, average weights, and customer contribution patterns. These analytical skills are essential to support program planning, activity evaluation, internal policy formulation, and the preparation of accountability reports to stakeholders [4].

2. Lack of Waste Disposal Management

   Waste management, which still relies on landfills, requires the participation of the entire community. The public needs to be educated on how to manage waste effectively [13] The lack of an organized system to provide information on waste management, collection schedules, and

Volume 13, Issue 1, April 2026, pp. 103-110
ISSN 2355-5068 ; e-ISSN 2622-4852
DOI: 10.33019/jurnalecotipe.v13i1.4592

payment methods makes the waste management process inefficient. Furthermore, the lack of public awareness about the importance of separating organic and inorganic waste before disposal also exacerbates this problem [5].

2.2. System Requirements Analysis

System analysis and design is a step-by-step process for building or developing a quality information system [10]. At this stage, researchers systematically identify and analyze overall development needs, and formulate detailed functional and non-functional specifications that must be met. The analysis is conducted by examining problems related to household waste in the surrounding environment [6].

1. Functionality Requirements

   Functional requirements are statements of the system services that must be provided, how the system reacts to certain inputs and how the system behaves in certain situations. In a simpler sense, functional requirements are requirements that contain what processes/services the system must provide, including how the system must react to certain inputs and how the system behaves in certain situations [6].

Table 1. Functional requirements

Functionality Requirements	Function Description
User Authentication	The system must provide sign-up and login features to manage user identities and store user activity data.
Waste Identification	The system must be able to access the device's camera to capture images of waste objects and automatically provide waste classification information.
Waste Disposal Management	The system must provide reporting or scheduling features for waste disposal to make the disposal process more structured and documented.

2. Non-Functional Requirements

   Non-functional requirements are limitations on services or functions offered by the system, such as time constraints, process development constraints, standardization, etc. In other words, non-functional requirements are requirements that emphasize the behavioral properties possessed by the system [6].

Table 2. Non-functional requirements

Non Functionality Requirements	Function Description
Operating System	The application is designed to run on Android-based devices.
Security	User passwords in the authentication feature must be protected to ensure account privacy.
Interface Design	The interface uses a simple and intuitive user-centered design concept for ease of use by novice users.

2.3. UI/UX Design

A User Interface (UI) is an element designed to interact through a display screen on a device being used. Creating an effective UI involves creating wireframes, mockups, and prototypes. User Experience (UX) is an individual's perception and response to the product, system, or service they are using [7].

2.4. Usability Testing

The most important Usability characteristics to pay attention to are design and interface. Designing the interface is the main concern to produce a design and interface to meet user needs in accessing the application [12]. The System Usability Scale (SUS) is a usability testing tool developed by Brooke in 1986. The SUS consists of ten questions with a five-choice scale, from strongly disagree to strongly agree, with a rating scale from 0 to 10 [7].

JURNAL ECTIPE
Electronic, Control, Telecommunication, Information, and Power Engineering
Volume 13, Issue 1, April 2026, pp. 103-110
ISSN 2355-5068 ; e-ISSN 2622-4852
DOI: 10.33019/jurnalecotipe.v13i1.4592

Table 3. Usability testing questions

Num	Questions
1	I think I will use this app frequently.
2	I feel the app is too complicated, though it could be simplified.
3	I feel the features in the app are well integrated.
4	I feel others will quickly understand how to use the app.
5	I feel there are no obstacles to using the app.
6	I find the app easy to use.
7	I think I will need technical assistance to use the app.
8	I feel there are many inconsistencies in the app.
9	I find the app very confusing to use.
10	I need to get used to it before I become proficient.

3. RESULTS AND DISCUSSION

The results presented represent a solution to the identified problems of limited understanding of waste statistics and the lack of an organized waste management system. Using a Systems Development Life Cycle (SDLC) approach, the research output is a prototype application, which is then tested for effectiveness to ensure all user needs are met.

3.1. System Design Results

The previously identified functional and non-functional requirements were transformed into a systematic technical architecture model and visual design. These design results served as the primary blueprint for developing the application prototype, ensuring that each system component aligned with the solution to the waste management problem.

1. Logical Architecture

   Logical architecture provides a visualization of the workflow and interactions between actors and all functionality within the application. This design combines two main models: interaction modeling through Use Case Diagrams and procedural modeling through System Flowcharts.

2. Use Case Diagram

A use case diagram is a type of diagram used in software development methods to illustrate scenarios or activities that a system can perform. In the use case diagram of the system being created, there is one actor, namely the user. The following is an image of a use case diagram [8].

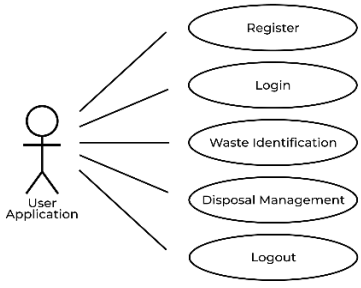

Figure 2. Use case diagram

Illustrates the interaction between user actors and the application's core functionalities to map the boundaries of the developed system. This diagram shows essential services such as user authentication, waste identification features, and waste disposal management integrated into a single platform.

3. Flowchart

   A flowchart is a symbolic representation of an algorithm or procedure for solving a problem. Using a flowchart makes it easier for the project team to check for missed points in the problem analysis. Furthermore, flowcharts are also useful as a communication tool between programmers working on a project team. Flowcharts help understand complex and lengthy logical sequences. They help communicate the program's flow to others [9].

JURNAL ECOTIPE
Electronic, Control, Telecommunication, Information, and Power Engineering
Volume 13, Issue 1, April 2026, pp. 103-110
ISSN 2355-5068 ; e-ISSN 2622-4852
DOI: 10.33019/jurnalecotipe.v13i1.4592

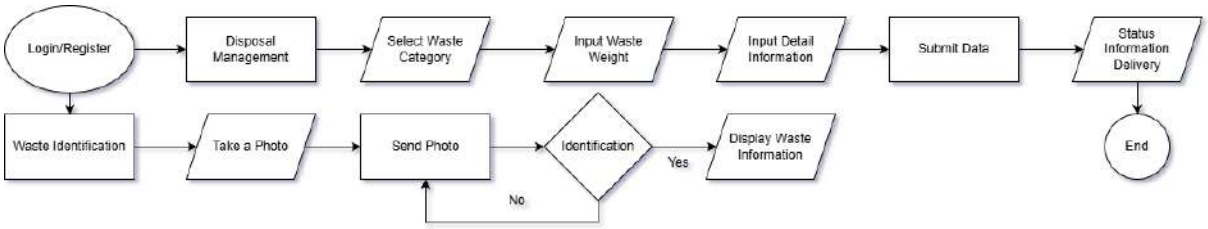

Figure 3. Application flowchart

Presents the system's procedural workflow, explaining the logical steps when users interact with the application. This flowchart visualizes how the system processes data from the initial input stage to generating documented waste classification information and disposal schedules.

3.2. User Interface Design Results

This stage produces a visual design (High-Fidelity Design) for the application using Figma software. The interface design is based on User-Centered Design principles, emphasizing layout simplicity to ensure the application's functionality is quickly understood by novice users.

1. Account Registration and Login Interface

The account registration and login interface is the first step for users to create a personal profile so that identified junk data can be permanently stored. This page is minimalistic in design, with a simple form to expedite the authentication process without confusing new users.

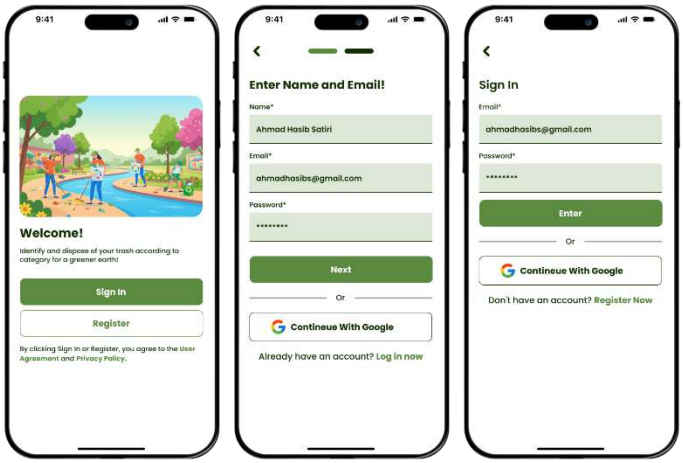

Figure 4. Login and Registration Application

Displays the interface design for registration and account login features, which function to manage user identities and activity data security. This design applies User-Centered Design principles with a simple layout so that application functionality can be immediately understood by novice users.

2. Waste Identification Interface

The waste identification interface is designed to make it easier for users to classify waste types through a live camera scan feature. This page provides clear visual cues to help users capture images correctly, enabling the system to provide accurate identification results.

Shows the primary camera, based waste identification feature that allows the system to perform automatic classification through object scanning. This interface is designed as a digital educational medium to increase community independence in recognizing and sorting waste types independently.

JURNAL ECOTIPE
Electronic, Control, Telecommunication, Information, and Power Engineering
Volume 13, Issue 1, April 2026, pp. 103-110
ISSN 2355-5068 ; e-ISSN 2622-4852
DOI: 10.33019/jurnalecotipe.v13i1.4592

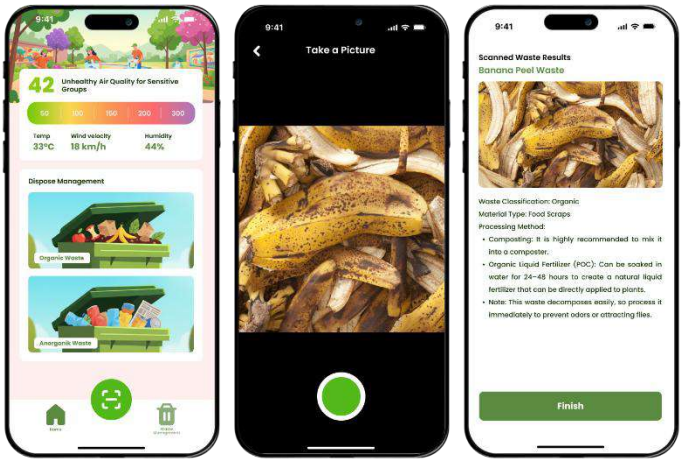

Figure 5. Identification waste application

3. Waste Management Interface

The waste management interface is designed to simplify the process of disposing of previously identified waste. Through this page, users can select a disposal method, specify a pickup location, or locate the nearest drop-off point so that waste can be properly distributed immediately.

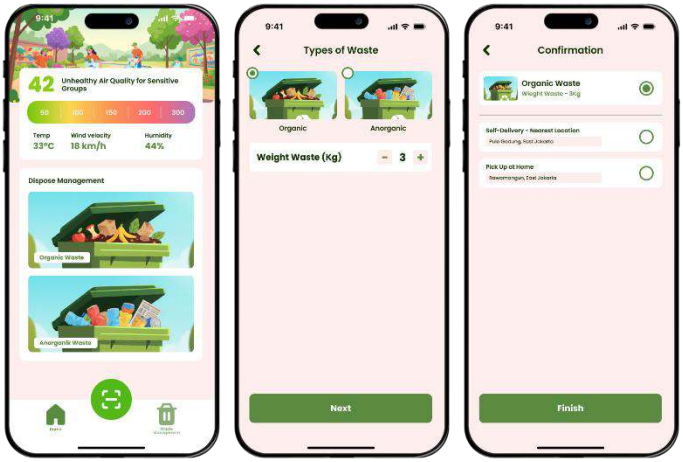

Figure 6. Disgase Management Application

Depicts the waste management interface, which provides structured waste disposal reporting and scheduling features. Through this display, the waste management process becomes more documented and efficient, supporting the goal of creating a cleaner and more sustainable environment.

3.3. User Interface Evaluation

Once the user interface design phase is complete, the next step is to conduct an evaluation to measure the extent to which the design meets user needs and provides usability. This evaluation aims to validate the effectiveness of the application's workflow and ensure that the implemented visual elements align with the principles of a good user experience.

1. System Usability Scale Score Analysis

Questionnaires are a well-known usability measurement and evaluation method among developers and researchers. Questionnaires are a type of form designed to obtain information and respondents [11]. The evaluation stage is carried out to measure the level of usability of the application interface design that has been created. This test involved 10 respondents by providing 10 standard SUS statement items covering aspects of ease, consistency, and system efficiency. Each respondent provided an assessment on a scale ranging from 1 Strongly Disagree to 5 Strongly

Volume 13, Issue 1, April 2026, pp. 103-110
ISSN 2355-5068 ; e-ISSN 2622-4852
DOI: 10.33019/jurnalecotipe.v13i1.4592

Agree, with the calculation (Q1-1) + (5–Q2) + (Q3-1) + (Q4-1) + (Q5-1) + (Q6-1) + (5-Q7) + (5-Q8) + (5-Q9) + (5-Q10).

Table 4. System Usability Scale Score Analysis

Respondents	Question Value	Total Value	Average Value
1	(5-1) + (5–2) + (5-1) + (5-1) + (5-1) + (5-1) + (5-2) + (5-1) + (5-1) + (5-1)	38	95
2	(5-1) + (5–2) + (4-1) + (4-1) + (5-1) + (5-1) + (5-1) + (5-1) + (5-2) + (5-3)	34	85
3	(4-1) + (5–2) + (3-1) + (3-1) + (3-1) + (3-1) + (5-3) + (5-3) + (5-3) + (5-3)	22	55
4	(4-1) + (5–4) + (4-1) + (5-1) + (5-1) + (5-1) + (5-2) + (5-1) + (5-2) + (5-2)	32	80
5	(4-1) + (5–3) + (4-1) + (5-1) + (3-1) + (5-1) + (5-4) + (5-2) + (5-2) + (5-3)	27	67.5
6	(4-1) + (5–1) + (3-1) + (5-1) + (4-1) + (5-1) + (5-1) + (5-2) + (5-1) + (5-3)	33	82.5
7	(4-1) + (5–1) + (4-1) + (4-1) + (4-1) + (5-1) + (5-2) + (5-1) + (5-1) + (5-2)	37	92.5
8	(4-1) + (5–2) + (5-1) + (5-1) + (3-1) + (5-1) + (5-5) + (5-3) + (5-3) + (5-5)	24	60
9	(4-1) + (5–3) + (4-1) + (4-1) + (4-1) + (4-1) + (5-2) + (5-3) + (5-2) + (5-3)	27	67.5
10	(4-1) + (5–2) + (4-1) + (5-1) + (5-1) + (4-1) + (5-2) + (5-2) + (5-2) + (5-1)	33	82.5
Overall Value		**307**	**76,7**

2. Discussion of Results and Feedback

After obtaining quantitative data through calculating System Usability Scale scores, the next step is to analyze the qualitative feedback provided by respondents. This section aims to align the numerical results with actual user experiences when interacting directly with the application interface, identifying which areas are optimal and which still need improvement.

Table 5. Respondent Feedback

Category	Respondent Feedback
Feature Development	Respondents expected additional fundamental features like "Forgot Password" and "Edit Profile" for account security and completeness.
Interaction & Visuals	Users suggested the use of more engaging animations and more efficient transitions to create a more modern user experience.
Technical Aspects	There was a need for advanced technical features like Focus Mode, app speed optimization, Dark Mode, and accessibility features for users with special needs.
User Satisfaction	Most respondents felt the current app was already very good and easy to understand, so drastic changes to its core functionality were not necessary.

4. CONCLUSION

Based on the design and evaluation results, it can be concluded that this research has successfully developed a mobile-based waste management application. Through its key features of camera-based waste identification and waste management, this application can serve as a digital educational tool that facilitates the community in identifying and sorting waste independently.

Testing results using the System Usability Scale method on 10 respondents showed an average score of 76,7. Based on the SUS assessment standards, this score falls into the Acceptable category with an Adjective Rating of Good. This demonstrates that the application interface meets the ease-of-use criteria and is well-received by potential users. However, qualitative feedback indicates the need for further development of authentication features such as forgot password, visual enhancements through animation, and technical optimizations such as dark mode support and accessibility.

Volume 13, Issue 1, April 2026, pp. 103-110
ISSN 2355-5068 ; e-ISSN 2622-4852
DOI: 10.33019/jurnalecotipe.v13i1.4592

This research is expected to be the first step in utilizing artificial intelligence technology for environmental management in the community. Recommendations for further study include fully functional implementation of the software and integration of a database system to support more organized and efficient waste management.

Acknowledgments

The authors acknowledge the financial support of Swiss German University through internal research funds program.

REFERENCES

[1] P. P. Saraswati, S. Suyeno, and L. R. Putra, "Implementation of waste management policy through regional regulation no. 07 of 2021 concerning waste management in Malang city (study at the Malang city environmental service)," *Public Response*, vol. 17, no. 12, pp. 55–65, 2023.

[2] P. Windiari and M. Salsabiela, "Public perception in waste management in Indramayu district," *Gema Wiralodra*, vol. 13, no. 2, pp. 363–380, 2022.

[3] E. B. Utoyo and S. Sudarti, "The potential of waste-to-energy power plants (PLTSa) as a solution to environmental and social problems in Indonesia," *CERMIN: Research Journal*, vol. 6, no. 2, pp. 337–347, 2022.

[4] K. Suryowati, et al., "Community empowerment through basic statistics training for independent waste management at the Anugerah 13 waste bank in Klitren village, Gondokusuman sub-district, Yogyakarta city," *Indonesian Community Service Journal*, vol. 6, no. 1, pp. 9–15, 2026.

[5] Maula, et al., "Optimization of waste management in Mendalo Indah village through the Reliji trash care platform," *Proficio*, vol. 6, no. 1, pp. 939–946, 2025.

[6] Mahesa, et al., "Analysis and design of information systems in the Lazada application," *Smart Techno (Smart Technology, Informatics and Technopreneurship)*, vol. 4, no. 1, pp. 1–6, 2022.

[7] J. A. Salsabila and A. Pramono, "User experience analysis for UI/UX development of ABC mobile application using user centered design method," *JATI (Journal of Informatics Engineering Students)*, vol. 8, no. 4, pp. 5914–5925, 2024.

[8] H. Hermansyah, R. F. Wijaya, and S. Wahyuni, "Design of a mobile-based mangrove love application in Kota Pari village using the waterfall method," *Senashtek 2024*, vol. 2, no. 1, pp. 42–48, 2024.

[9] T. Susanti, et al., "Development of a mobile statistics application for BPS Merangin regency," *Innovative: Journal of Social Science Research*, vol. 4, no. 3, pp. 17939–17949, 2024.

[10] E. F. Harahap, S. Adisuwiryo, and R. Fitriana, *Analysis and design of information systems*. Insight Science, 2022.

[11] T. Wahyuningrum, *Questionnaire reference book in usability measurement*. Deepublish, 2023.

[12] R. Fitria, *Usability testing on m-commerce with heuristic evaluation and UX test methods*. NEM Publisher, 2023.

[13] E. R. Simamora, et al., *Implementation of waste management in marketing management*. CV Eureka Media Aksara, 2025.

[14] M. N. Hasnine, M. K. H. Chayon, and M. M. Rahman, "A Cost Effective Approach to Develop Mid-size Enterprise Software Adopted the Waterfall Model," *International Journal of Computer and Information Engineering*, vol. 9, no. 5, pp. 1298–1302, 2015.

[15] M. V. P. Samsudin, M. Muslih, N. D. Arianti, M. Z. Saringat, and A. Ellahuuta, "Designing UI/UX for a Mobile TPA Application Using Design Thinking Method," *Engineering Proceedings*, vol. 107, no. 112, pp. 1–8, 2025.

JURNAL ECOTIPE
Electronic, Control, Telecommunication, Information, and Power Engineering
Volume 13, Issue 1, April 2026, pp. 111-120
ISSN 2355-5068 ; e-ISSN 2622-4852
DOI: 10.33019/jurnalecotipe.v13i1.4594

Design of an Automatic Relay-Based Switching System Using Battery and PV Voltage in Off-Grid Solar PV Lighting

Reza Satria Rinaldi[1], Afriyastuti Herawati[2], Mawardi[3], Ika Novia Anggraini[4]
[1,2,4]Electrical Engineering, University of Bengkulu, Bengkulu 38122, Indonesia
[3]Civil Engineering, University of Bengkulu, Bengkulu 38122, Indonesia

ARTICLE INFO

Article historys:

Received : 02/03/2026
Revised : 03/04/2026
Accepted : 30/04/2026

Keywords:

Automatic Switching; Backup Power; PV Off-grid Lighting; State Control Logic; SOL-ARSAT

ABSTRACT

The use of solar energy through off-grid photovoltaic (PV) systems to meet energy demands—particularly for DC lighting —still requires further development to address challenges such as weather variability and other limitations. Additionally, an effective control process for valve-regulated lead-acid (VRLA) batteries is crucial to prevent rapid degradation and shorten lifespan. This control ensures charging starts when the depth of discharge (DoD) limit is reached and prevents simultaneous charging and discharging. This study proposes an integrated off-grid PV lighting system with control features. The system uses a low-cost, relay-based automation approach, known as SOL-ARSAT (Solar PV Off-Grid Lighting System with Relay Switching Automation Technology). The system incorporates an AC power source as backup and applies three automatic switching controls based on battery and PV voltage. The results show that the system operates according to the designed control logic (logic 1 = active, 0 = inactive) and successfully manages power transfer between PV and AC sources. The control strategy prevents simultaneous charging and discharging, a prolonged low state of charge (SoC). As a result, the system improves lighting reliability and enhances battery protection, thereby extending the battery lifespan.

Corresponding Author:

Reza Satria Rinaldi
Electrical Engineering, University of Bengkulu, Kandang Limun, Bengkulu 38122, Indonesia
Email: reza_s_r@unib.ac.id.

1. INTRODUCTION

Solar PV (photovoltaic) energy in Indonesia has enormous technical, environmental, and economic potential, surpassing all other renewable energy sources. Its potential far exceeds current and future national energy needs if utilized optimally. With increasingly competitive costs, solar energy is a strategic solution for energy transition and long-term energy security [1].

The electrical energy generated by the PV module is highly dependent on weather conditions. The average electrical power generated during cloudy and overcast weather is much smaller than during sunny weather [2, 3]. Two 120 Wp PV modules were able to supply the daily electrical energy needs of the hallway lights of the PSTW of Bengkulu Province during sunny weather. When the weather is cloudy, these PV modules are unable to charge the battery sufficiently to meet the daily electrical energy needs of the hallway lights. In these conditions, a battery charger is used that utilizes PLN electricity sources to meet the daily electrical energy needs of the hallway lights [4]. Three 120 Wp PV modules are capable of charging a 100 Ah battery in sunny weather conditions. However, in cloudy weather

Volume 13, Issue 1, April 2026, pp. 111-120
ISSN 2355-5068 ; e-ISSN 2622-4852
DOI: 10.33019/jurnalecotipe.v13i1.4594

conditions, battery charging remains insufficient because the charging current stays below 10% of the battery capacity [5].

Besides weather conditions, the physical condition of the PV module can also affect the amount of electrical energy generated by the PV system. These conditions include the layout of the PV module, the area of the PV module, and shadows that block the surface of the PV module. The intensity of light received by the PV module depends on the input power per area, which means that the size of the PV module affects how much electrical energy can be generated. PV modules achieve their highest efficiency when solar irradiance is at its peak, typically between 09:00 and 12:00. In general, PV modules achieve their highest efficiency when solar irradiance is strongest, typically between 09:00 and 12:00. However, from 13:00 to 16:00, the intensity of sunlight decreases, leading to a corresponding decline in the efficiency of the PV [6].

The hybrid system of PLTS with PLN, equipped with an ATS (Automatic Transfer Switch), has been designed on a small scale as a prototype for the lamp load. This hybrid system is designed to reduce dependence on PLN electricity sources for household electricity needs. Solar energy captured by PV modules, serving as the main source of electrical energy, is connected to the SCC (Solar Charge Controller) and LVD (Low Voltage Disconnect). The LVD, which functions as a charge control mechanism to prevent overcharging or deep discharging, is utilized as the control component for an ATS. LVD provides a signal to the relay to change the power source to the PLN as a backup power source when the battery voltage drops to the predefined minimum threshold. The system automatically switches back to the battery once the voltage reaches the predefined maximum level [7].

The ATS panel was designed for an off-grid solar power system (PLTS) supplying a waterwheel motor load at the Vaname shrimp cultivation pond in Sungai Geniot Village, Dumai City. In this study, the ATS panel incorporates two power sources: the solar power system (PLTS) as the primary and the PLN grid as a backup power source. The system operated in two main operation modes. In the first mode, the system utilizes the primary power source, where electrical energy generated by the PLTS is stored in a battery and then converted into AC (alternating current) power by the inverter. The second mode uses AC power supplied entirely by the PLN electricity network as a backup source. This mode is set and used to maintain battery life. When the battery voltage drops below the minimum set-point configured on the LVD, the ATS panel will automatically switch the power source to the PLN network. When the battery position has reached the SoC (State of Charge) value of 100%, the ATS panel will switch the power source position back to the inverter position. [8].

An ATS system is designed to transfer the main power (PLN electricity source) to the backup power source (PLTS battery). This ATS system utilizes Inverter Standby Mode (ISM) and Inverter Off Mode (IOM) to automatically manage the switching process between the PLN and PLTS power sources. ISM is used to manage the distribution of electrical energy based on a switching mechanism, while Inverter Off Mode (IOM) functions to conserve battery power during inverter-based energy distribution. The switching technique is executed as quickly as possible to prevent potential damage to the equipment. The distribution of electrical energy from the inverter is regulated by the LVD so that when the battery cannot distribute electrical energy to the load, the ATS will switch to the PLN electricity source [9].

A study has examined the degradation mechanism of VRLA (Valve-Regulated Lead-Acid) batteries. Sulfation is a major challenge in the use of VRLA batteries. Heavy sulfation and water loss are the main causes of increased internal resistance (ohmic, charge-transfer, and mass-transport resistances). The capacity decrease is in line with the increase in internal resistance in all duty cycles, with the same general trend. Sulfation mitigation should be a top priority in VRLA battery management. VRLA batteries that are not promptly recharged after reaching their Depth of Discharge (DoD) limit and are left in a low SoC condition are at high risk of sulfation, which is a major cause of degradation and increased internal resistance [10, 11].

In a renewable energy system, VRLA batteries are an important component of an off-grid PV system. It acts as a component of electrical energy storage. If this system cannot properly manage the charging and discharging processes, it significantly accelerates battery degradation and reduces its service life. Therefore, an effective charging and discharging control method is essential to protect the battery and extend its lifespan [12].

Volume 13, Issue 1, April 2026, pp. 111-120
ISSN 2355-5068 ; e-ISSN 2622-4852
DOI: 10.33019/jurnalecotipe.v13i1.4594

A prototype control system that combines grid (PLN) and off-grid PV power sources has been designed to accelerate battery charging at the Base Transceiver Station (BTS). The grid serves as the primary power source for battery charging in this system. Meanwhile, the backup energy source is taken from the PV system. When the battery reaches the empty limit, it will be charged by a combination of PLN electricity and the off-grid PV system while the PLN electricity source is on. Conversely, when the PLN electricity source is off, the battery will be charged by the off-grid PV system [13].

Based on various research findings, the utilization of solar energy, particularly through off-grid PV systems, for meeting electricity demands requires further development to address any constraints. Moreover, VRLA batteries that are discharged to their deepest DoD and not quickly restored to an optimal SoC tend to undergo accelerated degradation, significantly shortening their cycle life. To prevent this, it is essential to implement a control process for the VRLA battery to ensure charging begins promptly once the DoD limit is attained, thereby preventing simultaneous charging and discharging operations. Based on these considerations, this research conceptually designs a solar PV off-grid DC lighting control system, governed by the voltage of the VRLA battery and the PV module, which uses a relay-based switching mechanism as an actuator, hereafter referred to as the SOL-ARSAT (Solar PV Off-Grid Lighting System with Relay Switching Automation Technology). The SOL-ARSAT is designed as an independent control unit that can be integrated with various types of backup power to increase battery life and ensure uninterrupted DC (direct current) lighting availability using a low-cost relay-based automation approach. The system also allows alternating VRLA battery charge-discharge control, so that the battery operates in only one mode at a time. Backup energy can be operated while the VRLA battery is charging, either to maintain a continuous power supply to DC lighting loads or to assist VRLA battery charging when PV energy is insufficient.

2. RESEARCH METHOD

This research is an applied study aimed at addressing practical, real-world problems—specifically, the implementation of automatic switching technology in the utilization of solar energy through off-grid PV systems for 12 V DC lighting applications. This research employs a conceptual system analysis and design method, focusing on developing a conceptual design for the SOL-ARSAT using a state control logic approach. The selection of energy sources for charging and discharging the VRLA battery is adaptively based on voltages of both the VRLA battery and the PV module. The research stages include system requirements analysis, block diagram design, flowchart design, wiring diagram design, and the SOL-ARSAT state tables based on implemented control logic.

The novelty of this research lies in the formulation of a finite-state control logic design that clearly separates the charging and discharging modes of the VRLA battery. The main contribution of this research is the design of the SOL-ARSAT control system that can maintain the operation of the VRLA battery by switching between charging and discharging modes in a coordinated manner, while ensuring the continuity of power supply to the off-grid PV DC lighting system and the VRLA battery charging through the integration of the external backup energy sources.

The SOL-ARSAT design comprises several subsystems, as illustrated in the block diagram in Figure 1. The SOL-ARSAT is a friendly energy source for the environment. It uses solar as the primary source, with a backup power activated when needed. In this research, the backup power source is a 220 V AC, operated automatically when solar energy is insufficient to meet the demands of battery charging and powering the 12 DC lighting system. This function is managed by switching automation through battery charging and load power supply controls to maintain continuity and operational efficiency of the off-grid PV system.

JURNAL ECOTIPE
Electronic, Control, Telecommunication, Information, and Power Engineering
Volume 13, Issue 1, April 2026, pp. 111-120
ISSN 2355-5068 ; e-ISSN 2622-4852
DOI: 10.33019/jurnalecotipe.v13i1.4594

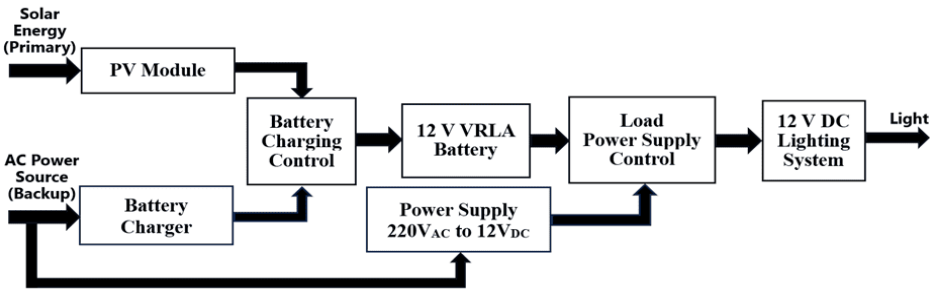

Figure 1. Block diagram design of the SOL-ARSAT with the AC backup power source

Furthermore, simultaneous charging and discharging should be avoided during VRLA battery operation, as this can accelerate degradation processes [14-16]. In this research, the SOL-ARSAT is designed to operate alternately in two distinct modes: discharge and charge. This alternating operation prevents the battery from undergoing charging and discharging processes simultaneously. In discharge mode, the system supplies electrical energy to the load (12 V DC lighting system) from the VRLA battery as the primary source or an AC backup power source, which does not undergo charging during this process. Conversely, in charge mode, the SOL-ARSAT charges the battery without connecting it to the load, using a power source to charge the VRLA battery from the PV off-grid system as a primary or an AC backup.

The SoC represents the usable battery capacity, and the DoD represents the used battery capacity. They are usually expressed as percentages, e.g., when a battery is fully charged, the SoC is 100%, and the DoD is 0%. Based on the recommendation from the VRLA batteries manufactory, the DoD is limited to 80% to preserve battery longevity. Nevertheless, experimental findings suggest that maintaining the DoD of approximately 60% offers more favorable conditions for prolonged battery life [17].

The work process algorithm of the SOL-ARSAT is presented in the flowchart in Figure 2. The value of SoC or DoD becomes the key control parameter in deciding the operating mode. In this process, SoC or DoD is represented by the battery voltage (V_B). It begins with V_B monitoring. As shown in the flowchart, when V_B exceeds the lower threshold voltage (V_{BL}), the system operates in discharge mode, indicating that the battery DoD is between 0% to 60%. Conversely, when V_B falls below V_{BL} and up to the upper threshold voltage (V_{BH}), the system switches to charge mode, corresponding to a battery SoC range of 40% to 100%. The transition between these operating modes is automatically regulated by the operation mode control subsystem, ensuring appropriate switching based on real-time battery conditions. The relationship between SoC and DoD values can be analyzed using Equations (1) and (2).

$$DoD\ (t) = 100\% - SoC\ (t) \quad (1)$$

$$SoC\ (t) = \frac{V_B - V_{Bmin}}{V_{Bmax} - V_{Bmin}} \cdot 100\% \quad (2)$$

Where V_B is battery voltage at t, V_{Bmin} is the minimum battery voltage when SoC is 0%, and V_{Bmax} is the maximum battery voltage when SoC is 100%.

JURNAL ECOTIPE
Electronic, Control, Telecommunication, Information, and Power Engineering
Volume 13, Issue 1, April 2026, pp. 111-120
ISSN 2355-5068 ; e-ISSN 2622-4852
DOI: 10.33019/jurnalecotipe.v13i1.4594

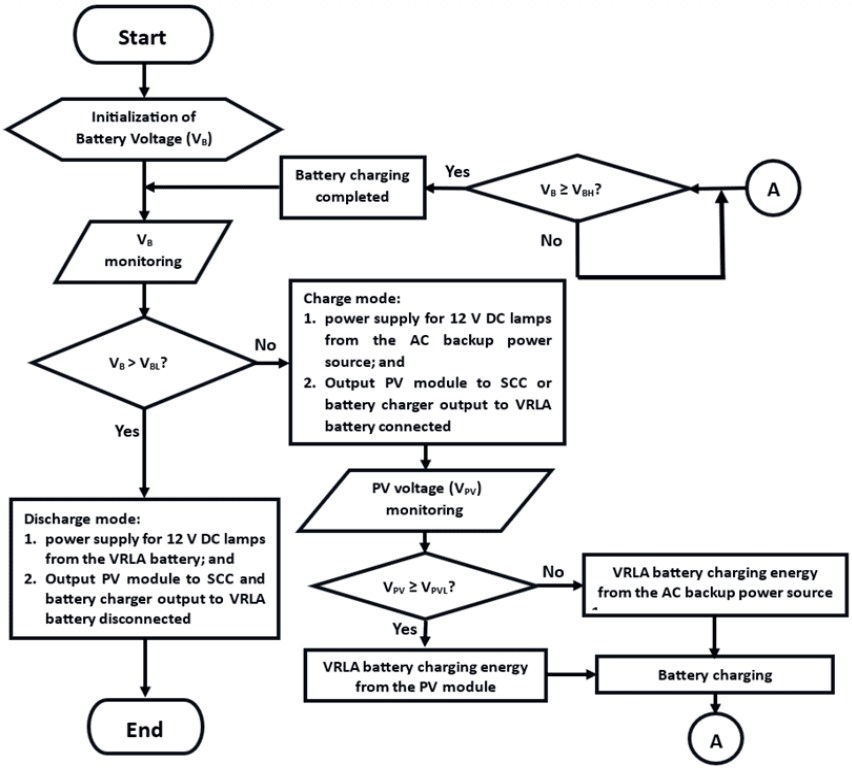

Figure 2. Flowchart of the SOL-ARSAT with the AC backup power source

Table 1. The state of the SOL-ARSAT operation mode control

State	VRLA Battery Voltage (V_B)	Control Logic	Operation Mode
State A1	Decreases from V_{BH} to > V_{BL}	1	Discharge mode
State A2	≤ V_{BL}	0	Discharge to Charge mode transition
State A3	Increases from ≤V_{BL} to < V_{BH}	0	Charge mode
State A4	≥ V_{BH}	1	Charge to Discharge mode transition

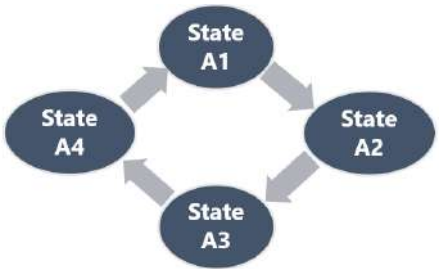

Figure 3. State cycle of the SOL-ARSAT operation mode control

Based on these SoC and DoD thresholds, the operation mode control is implemented using finite state control logic. In this approach, each operation condition of the SOL-ARSAT is represented as a distinct state, defined by specific voltage ranges corresponding to the battery's SoC and DoD levels. The operation mode control can be categorized into four state control logics, with the conditions of each state as in Table 1. This state of control logic condition establishes a repetitive operating cycle, as illustrated in Figure 3.

The control logic comprises four primary states: State A1, State A2, State A3, and State A4, each with clearly defined transition conditions to prevent overlap and unstable switching. State transitions are triggered when the battery voltage crosses predefined threshold values, the lowest V_B (V_{BL}) and the

Volume 13, Issue 1, April 2026, pp. 111-120
ISSN 2355-5068 ; e-ISSN 2622-4852
DOI: 10.33019/jurnalecotipe.v13i1.4594

highest V_B (V_{BH}). This formulation ensures deterministic mode selection and eliminates ambiguity in the control decision process.

The SOL-ARSAT is designed to operate in discharge mode when the V_B exceeds the specified V_{BL}, which occurs when the VRLA battery DoD is 0% to 60%. When operating in this mode, the load is supplied by the VRLA battery as the primary power source. To prevent the VRLA battery from being charged while in this mode, the PV module output to the SCC and the battery charger output to the VRLA battery are disconnected.

When the battery energy is insufficient for discharge, which occurs when V_B is lower than V_{BL} or the VRLA battery's DoD exceeds 60%, the SOL-ARSAT is designed to change to charge mode, and an AC backup power source is used to maintain power to the load. The AC power source is connected to a power supply unit that converts the 220 V_{AC} input into the 12 V_{DC} output, enabling it to power the load. To enable automatic switching between the battery and the backup power source, the load power supply control is implemented. This control system can be categorized into two state control logics: State A3 and A4, as in Table 2, which are the repetitive cycles.

Table 2. The state of the SOL-ARSAT load power supply control

State	VRLA Battery Voltage (V_B)	Control Logic	Load Power Supply Source
State A3	Decreases from V_{BH} to > V_{BL}	1	VRLA battery
State A4	Increases from ≤V_{BL} to < V_{BH}	0	AC Backup power supply

Table 3. The state of the SOL-ARSAT battery charge control

State	PV Module Voltage (V_{PV})	Control Logic	Battery Charge Source
State B1	Decreases from V_{PVH} to > V_{PVL}	1	PV module
State B2	≤ V_{PVL}	0	PV module to AC power source transition
State B3	Increases from ≤V_{PVL} to < V_{PVH}	0	AC Power Source
State B4	≥ V_{PVH}	1	AC Power Source to PV module transition

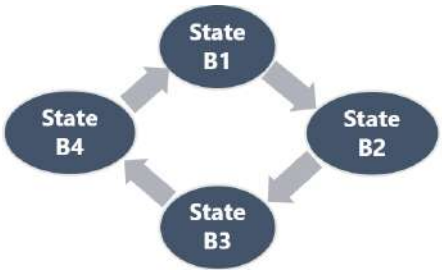

Figure 4. State cycle of battery charge control

In the charge mode of the SOL-ARSAT design, the primary power source to charge the VRLA battery is the PV module by SCC. When the PV module's energy is insufficient to charge the VRLA battery, which occurs when the PV module voltage (V_{PV}) is lower than the specified lowest V_{PV} (V_{PVL}), the AC backup power source is used. The AC power source is connected to a battery charger, which converts AC power into the required DC power to charge the VRLA battery. When the V_{PV} is above the specified highest V_{PV} (V_{PVH}), the primary source is back. The transition between the primary and backup power sources in the charge mode of the SOL-ARSAT is automatically controlled by the battery charge control, which is categorized into four control states as in Table 3. Figure 4 illustrates that the control condition establishes a repetitive operating cycle. To prevent the VRLA battery discharge while in this mode, the VRLA battery is disconnected from the load. Once the V_{BH} is reached, the SOL-ARSAT is designed to switch to discharge mode.

3. RESULTS AND DISCUSSION

The results of this research present a conceptual wiring diagram for the relay-based switching control actuator implementation of the proposed state control logic, as illustrated in Figure 5. The design

Volume 13, Issue 1, April 2026, pp. 111-120
ISSN 2355-5068 ; e-ISSN 2622-4852
DOI: 10.33019/jurnalecotipe.v13i1.4594

clearly separates the charging and discharging states of the VRLA battery, establishing voltage-dependent transition conditions based on the PV module and battery parameters. Unlike conventional PV charge control systems that typically rely on microcontroller-based architectures, the developed design adopts a purely electromechanical control strategy using LVDs and electromechanical relays.

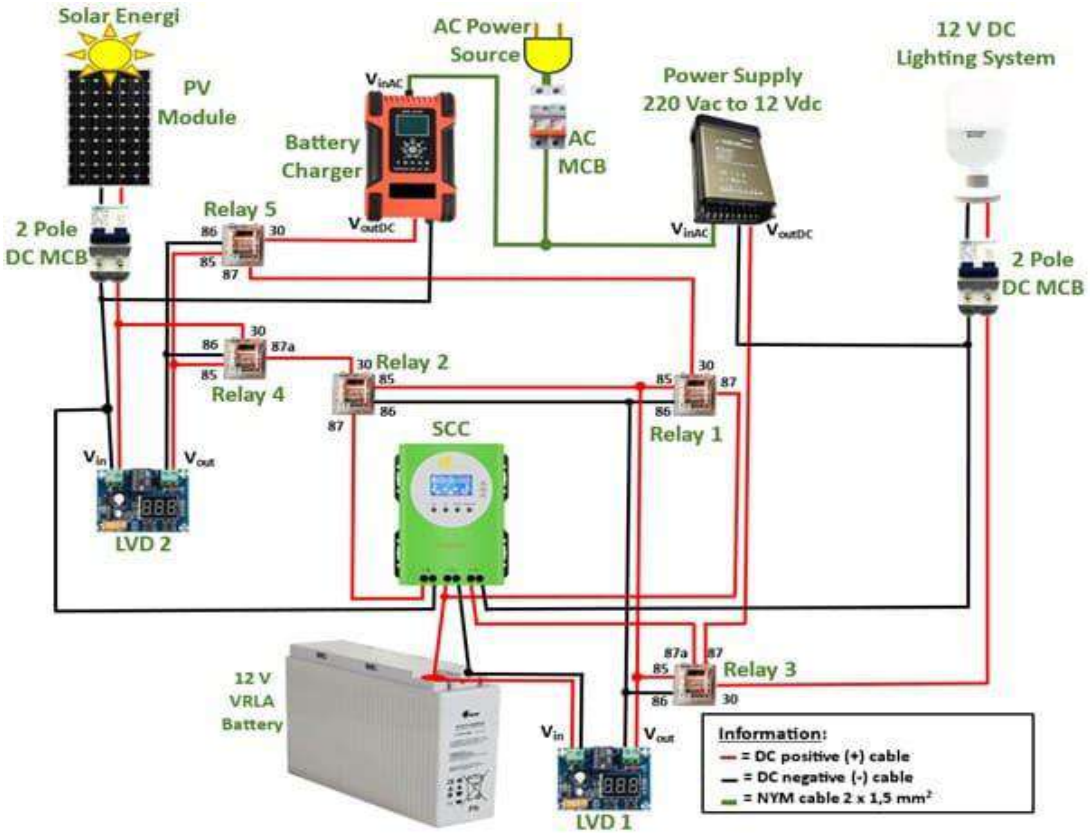

Figure 5. Wiring diagram of the SOL-ARSAT design with AC backup power source

LVDs are selected as the primary sensing elements because the control decision is based on voltage thresholds of the VRLA battery and PV module. Meanwhile, relays are used as switching devices due to their structural simplicity, inherent electrical isolation, high reliability in low-voltage DC applications, and suitability for cost-sensitive off-grid environments. This hardware realization enables state transitions control without requiring programmable control units, thereby reducing system complexity while maintaining operational robustness and power supply continuity for the load.

An LVD is an electronic module that operates based on the voltage at its input and output terminals (positive and negative). The LVD output voltage cuts off when the input voltage falls below the specified low limit, and is restored when the high voltage limit is reached. The LVD has a button to set the low and high voltage. The output voltage generated by the LVD matches the input provided. This LVD operating principle is very suitable for generating control logic in the design of SOL-ARSAT systems. In this design, two LVDs are used, namely LVD 1 and LVD 2, as shown in Figure 5.

LVD 1 functions as a VRLA battery voltage sensor for the operation mode control and the load power supply control. LVD 1 sets a low-voltage reference threshold corresponding to V_{BL} and a high-voltage reference threshold corresponding to V_{BH}. LVD 2 functions as a voltage sensor for the battery charge control, sensing the voltage generated by the PV module. LVD 2 sets a low-voltage reference threshold corresponding to V_{PVL} and a high-voltage reference threshold corresponding to V_{PVH}.

The SOL-ARSAT system is designed with 5 (five) relays to perform control operations based on control signals from the output voltage of LVD 1 and LVD 2. This control signal is the state control logic in the SOL-ARSAT system control logic design. In Figure 5, it can be seen that the relays consist of 3 (three) 4-pin relays (Relay 1, Relay 2, and Relay 5) and 2 (two) 5-pin relays (Relay 3 and Relay 4).

JURNAL ECOTIPE
Electronic, Control, Telecommunication, Information, and Power Engineering
Volume 13, Issue 1, April 2026, pp. 111-120
ISSN 2355-5068 ; e-ISSN 2622-4852
DOI: 10.33019/jurnalecotipe.v13i1.4594

The control signal is connected to pin 85 (positive) and pin 86 (negative). In the absence of a control signal at these pins, the relay remains in its default state: pin 87 is in a Normally Open (NO) position and disconnected from pin 30, whereas pin 87a is in a Normally Closed (NC) position and connected to pin 30. Conversely, when a control signal is applied, the relay switches state, pin 87 connects to pin 30, and pin 87a is disconnected. Relay 1, Relay 2, and Relay 3 receive control signals from LVD 1, while Relay 4 and Relay 5 receive control signals from LVD 2. Relay 1 and Relay 2 act as switching devices for the operation mode control, Relay 3 acts as a switching device for the operation mode and the load power supply control, Relay 4 and Relay 5 act as switching devices for the battery charge control.

Relay 1 prevents the battery charger output from connecting to the VRLA battery in discharge mode on the SOL-ARSAT. Pin 30 is connected to pin 87 when there is no control signal on Relay 1, so the battery charger output is only connected to the VRLA battery when the SOL-ARSAT is in charge mode. Similarly, Relay 2 prevents the PV module output from connecting to the VRLA battery via the SCC input in discharge mode on the SOL-ARSAT. Pin 30 is connected to pin 87 when there is no control signal on Relay 2, so the PV module output is only connected to the SCC input for battery charging when the SOL-ARSAT is in charge mode.

When the control signal is applied to Relay 3, pin 87a is connected to pin 30, thereby connecting the VRLA battery through the SCC output as the primary source of the load, thus putting the SOL-ARSAT operation in discharge mode. Conversely, when there is no control signal, pin 87 is connected to pin 30, the SOL-ARSAT operation changes to charge mode, and the AC backup power through the power supply becomes the load power source. Thus, the SOL-ARSAT can maintain the availability of the load power supply even though the VRLA battery power is insufficient. This functionality is made possible by the automatic switching mechanism for the load backup power source.

Pin 30 of Relay 4 is connected to the positive terminal of the PV module output, serving as the primary source of battery charging. Pin 87a of Relay 4 is connected to pin 30 of Relay 2 so that when SOL-ARSAT is in charge mode, and the PV module voltage is sufficient to charge the battery, the PV module is connected to the positive input of the SCC. In the opposite condition, the PV module will be disconnected from the SCC, and the backup power source will charge the VRLA battery.

Pin 30 of Relay 5 is connected to the positive pole of the battery charger output as a backup source for battery charging. Pin 87 of Relay 5 is connected to pin 30 of Relay 1 so that when SOL-ARSAT is in charge mode, and the PV voltage is insufficient to charge the battery, the backup source is connected to the positive input of the VRLA battery. In the opposite condition, the backup power source will be disconnected from the positive input of the VRLA battery because charging is done through the SCC.

Table 5. The SOL-ARSAT state based on implemented control logic

Control Logic		Operation Mode		Load Power Source		Battery Charge Source	
LVD 1	LVD 2	Discharge	Charge	Primary	Backup	Primary	Backup
0	0	0	1	0	1	0	1
0	1	0	1	0	1	1	0
1	0	1	0	1	0	0	0
1	1	1	0	1	0	0	0

The state of the SOL-ARSAT, successfully designed based on the control logic used in this research, is presented in Table 5. Logic 1 means active, and logic 0 means inactive. The SOL-ARSAT system, integrated with an AC backup power source, was successfully designed. This system automatically manages the power supply for battery charging and load power supply between the primary and backup power sources as needed. With the SOL-ARSAT managing battery charging and discharging, the battery is better protected, potentially extending its life cycle. It allows for avoiding simultaneous charging and discharging, as well as low SoC conditions, for extended periods.

4. CONCLUSION

This research successfully designed the SOL-ARSAT system, which uses an off-grid PV system as its primary energy source and incorporates an AC power supply as a backup. The SOL-ARSAT consists of three automatic switching control systems: the operation mode control, the battery charge control,

Volume 13, Issue 1, April 2026, pp. 111-120
ISSN 2355-5068 ; e-ISSN 2622-4852
DOI: 10.33019/jurnalecotipe.v13i1.4594

and the load power supply control. These are implemented using a control circuit comprising two LVDs and five electromechanical relays. The battery voltage serves as the basis for both the operation mode and the load power supply control. The battery charge control is based on the PV module voltage. Through the SOL-ARSAT control mechanism, which ensures that charging and discharging processes do not occur simultaneously and that the battery is not left in a low SoC. This research contributes to the development of control for battery protection. This conceptual design can be implemented easily and at a low cost. Furthermore, in off-grid PV lighting, it maintains the battery's lifespan. Therefore, the proposed system constitutes a feasible and scalable solution for rural and standalone applications, where reliability and cost efficiency are critical.

Acknowledgments

We would like to express our gratitude to the Faculty of Engineering, University of Bengkulu, for providing funding sources through the DIPA (Budget Implementation List) of the Faculty of Engineering, University of Bengkulu, with contract number 3046/UN30.13/PG/2024.

REFERENCES

[1] D. F. Silalahi, A. Blakers, M. Stocks, B. Lu, C. Cheng, and L. Hayes, 'Indonesia's Vast Solar Energy Potential', *Energies*, vol. 14, no. 17, 2021, doi: 10.3390/en14175424.

[2] B. Sugeng and R. H. Saputra, 'Estimasi State-Of-Charge Menggunakan Simulink Pada Baterai Pembangkit Listrik Tenaga Surya', *Jurnal ELTIKOM*, vol. 3, no. 1, pp. 1–8, 2019, doi: 10.31961/eltikom.v3i1.89.

[3] P. Gunoto and S. Sofyan, 'Perancangan Pembangkit Listrik Tenaga Surya 100 Wp untuk Penerangan Lampu di Ruang Selasar Fakultas Teknik Universitas Riau Kepulauan', *Sigma Teknika*, vol. 3, no. 2, pp. 96–106, 2020, doi: 10.33373/sigma.v3i2.2754.

[4] R. S. Rinaldi, A. Herawati, I. N. Anggraini, and Y. Rodiah, 'Instalasi Sistem Penerangan Menggunakan Panel Surya Pada Selasar Panti Sosial Tresna Werdha Pagar Dewa Bengkulu', *Abdi Reksa*, vol. 5, no. 1, pp. 36–41, 2024, doi: 10.33369/abdireksa.v5.i1.36-41.

[5] D. A. Efriansyah, A. Herawati, I. N. Anggraini, R. S. Rinaldi, and Y. Rodiah, 'Analisis Potensi Energi Matahari dan Pembangkitan Daya Pada PLTS Sebagai Sumber Rumah Energi Terbarukan Sederhana di Kota Bengkulu', *Serambi Engineering*, vol. 9, no. 1, pp. 8258–8267, 2024, [Online]. Available: http://jurnal.serambimekkah.ac.id/index.php/jse/article/view/960/714

[6] W. Kamisah, Rahmaniar, and Y. Andinata, 'Analysis of the Efficiency of Solar Power Plants (PLTS) Against Solar Irradiation Using a Solar Power Meter', *Jurnal Teknik Elektro dan Komputer*, vol. 12, no. 3, pp. 189–194, 2023, [Online]. Available: https://ejournal.unsrat.ac.id/index.php/elekdankom

[7] W. B. Rahmatulloh and A. H. Andriawan, 'Rancang Bangun PLTS Menggunakan Sistem Hybrid Pada Rumah Tangga untuk Menggurangi Ketergantungan Energi Listrik dari PLN', *Uranus: Jurnal Ilmiah Teknik Elektro, Sains dan Informatika*, vol. 2, no. 3, pp. 58–72, Jul. 2024, doi: 10.61132/uranus.v2i3.207.

[8] B. Demeianto *et al.*, 'Rancang Bangun Panel Automatic Transfer Switch (ATS) Pada Pembangkit Listrik Tenaga Surya sebagai Catu Daya Kincir Air Pada Tambak Perikanan', *Aurelia Journal*, vol. 4, no. 2, pp. 203–218, 2022.

[9] A. P. Putra and A. Mulyadi, 'Design an Automatic Transfer Switch for Solar Power Plant', *LOGIC: Journal of Engineering Design and Technology*, vol. 22, no. 1, pp. 9–12, 2022, doi: https://doi.org/10.31940/logic.v22i1.9-12.

[10] N. Shamim, V. V. Viswanathan, V. L. Sprenkle, E. C. Thomsen, G. Li, and D. M. Reed, 'Valve Regulated Lead Acid Battery Evaluation under Peak Shaving and Frequency Regulation Duty

Volume 13, Issue 1, April 2026, pp. 111-120
ISSN 2355-5068 ; e-ISSN 2622-4852
DOI: 10.33019/jurnalecotipe.v13i1.4594

Cycles', *Energies*, vol. 15, no. 9, 2022, doi: 10.3390/en15093389.

[11] P. T. Thong *et al.*, 'Cycle Performance Analysis of Lead–carbon Electrode Under High-load Conditions for Automotive Battery Applications', *Journal of Power Sources*, vol. 580, p. 233291, 2023, doi: 10.1016/j.jpowsour.2023.233291.

[12] E. Banguero, A. Correcher, Á. Pérez-Navarro, F. Morant, and A. Aristizabal, 'A review on battery charging and discharging control strategies: Application to renewable energy systems', *Energies*, vol. 11, no. 4, pp. 1–15, 2018, doi: 10.3390/en11041021.

[13] M. R. Sufandi and W. I. Rahayu, 'Pengembangan Sistem Pengisian Baterai Dengan Kombinasi Sumber Listrik Dari PLN dan Energi Surya', *Elkha*, vol. 10, no. 1, p. 27, 2019, doi: 10.26418/elkha.v10i1.25280.

[14] A. Kern, J. X. Johnson, and J. L. Mathieu, 'Environmental Impacts of Using Energy Storage Aggregations to Provide Multiple Services', *Proceedings of the 52nd Hawaii International Conference on System Sciences*, vol. 2019-Janua, pp. 3580–3589, 2019, doi: 10.24251/hicss.2019.433.

[15] M. Shabani, M. Shabani, F. Wallin, E. Dahlquist, and J. Yan, 'Smart and Optimization-based Operation Scheduling Strategies for Maximizing Battery Profitability and Longevity in Grid-connected Application', *Energy Conversion and Management: X*, vol. 21, no. December 2023, p. 100519, 2024, doi: 10.1016/j.ecmx.2023.100519.

[16] J. Vaicys, S. Gudzius, A. Jonaitis, R. Rackiene, A. Blinov, and D. Peftitsis, 'A Case Study of Optimising Energy Storage Dispatch: Convex Optimisation Approach with Degradation Considerations', *Journal of Energy Storage*, vol. 97, p. 112941, 2024, doi: 10.1016/j.est.2024.112941.

[17] H. R. Iskandar *et al.*, 'Analisis Performa Baterai Jenis Valve Regulated Lead Acid Pada PLTS Off-Grid 1 Kwp', *Jurnal Teknologi*, vol. 13, no. 2, pp. 129–140, 2021, doi: 10.24853/jurtek.13.2.129-140.

JURNAL ECOTIPE
Electronic, Control, Telecommunication, Information, and Power Engineering
Volume 13, Issue 1, April 2026, pp. 121-129
ISSN 2355-5068 ; e-ISSN 2622-4852
DOI: 10.33019/jurnalecotipe.v13i1.4595

Optimization of Oyster Mushroom Dough Mixing Machine Using Omron CP1E PLC Control

Saepul Rahmat[1], Arif Sumardiono[2], Purwiyanto[3]
[1,2,3]Electrical Engineering, Politeknik Negeri Cilacap, Jln. Dr. Soetomo No.1 Karangcengis Sidakaya, Kabupaten Cilacap, 53212, Indonesia

ARTICLE INFO

Article historys:

Received : 05/03/2026
Revised : 03/04/2026
Accepted : 30/04/2026

Keywords:

Growing Media Mixing; Oyster Mushroom; Omron CP1E Process Automation; PLC Control

ABSTRACT

Oyster mushroom cultivation is vital for providing the growing medium. Manually mixing the growing medium has several limitations, including time-consuming and inconsistent results. This paper objectives are to resolve growing medium oyster mushroom with mixing machine based on the Omron CP1E Programmable Logic Controller (PLC). The research methodology of mechanical and electrical of the machine was equipped with a single-phase AC motor, relay, control panel, and PLC-based control system to increases labor efficiency and ensures uniformity in the media mixture. This paper contribution research are to find the best composition of ingredients with PLC control to get homogenous media mixture by measuring the weight of the ingredients, mixing time, power consumption, and the homogeneity of the mixture. Based on the test results, the prototype is able to pack oyster mushroom growing media close to the initial mass, which is around 2975–3015 grams with an error of 1%, as well as decreasing power consumption due to the growing media mixture starting to become homogeneous so that the motor works lighter. The prototype of the oyster mushroom mixing machine has been successfully mix the media homogenous in 3minutes with the motor speed 70 rpm and power consumption 345 Watt.

Corresponding Author:

Saepul Rahmat
Electrical Engineering, Politeknik Negeri Cilacap,
Jln. Dr. Soetomo No.1 Karangcengis Sidakaya, Kabupaten Cilacap, 53212, Indonesia
Email: saepulrahmat@pnc.ac.id.

1. INTRODUCTION

Oyster mushrooms (Pleurotus ostreatus) are a type of edible mushroom that has high economic value and is rich in nutrients such as protein, fiber, and vitamin B[1]. Besides being easy to cultivate, oyster mushrooms have a delicious flavor and a texture similar to meat, making them a popular healthy food alternative. The demand for oyster mushrooms continues to rise, along with growing public awareness of the health benefits of ant-based foods[2]. Manual mixing of planting media ingredients is often an obstacle in large-scale production because it is inefficient and yields an inhomogeneous mixture. Therefore, technological innovations such as a planting media mixing machine are needed to speed up the production process and maintain the consistency of the planting media. This machine can help oyster mushroom farmers improve work efficiency and production quality[3]. Oyster mushroom planting media is a planting medium used to grow oyster mushrooms. This medium is made from sawdust mixed with other materials, such as bran, corn flour, lime, and water; the sawdust is usually derived from hardwoods such as sengon or mahogany. This mixture is then compacted and placed in

JURNAL ECOTIPE
Electronic, Control, Telecommunication, Information, and Power Engineering
Volume 13, Issue 1, April 2026, pp. 121-129
ISSN 2355-5068 ; e-ISSN 2622-4852
DOI: 10.33019/jurnalecotipe.v13i1.4595

sterile plastic bags. After that, the planting media are sterilized to kill organisms that can interfere with mushroom growth. After sterilization, the mushroom spawn is planted into the oyster mushroom growing medium [4,5]. The growing medium is then stored in a humid, temperature-controlled environment suitable for oyster mushroom growth. A good growing medium will produce high-quality oyster mushrooms that can be harvested multiple times until the medium is exhausted.

To make oyster mushroom growing medium, a press machine is needed to compress the mixture to an appropriate density, neither too dense nor too soft (28–29%)[6,7]. A PLC allows for precise adjustment of raw material dosages (sawdust, rice bran, lime, etc.). The PLC can be programmed to automatically control the speed and duration of mixing the raw materials, resulting in a homogeneous, uniform mixture, which is essential for uniform mushroom growth. By using a PLC, oyster mushroom growing medium producers can increase production efficiency, produce growing medium with consistent quality, and reduce operational costs, making the PLC the right choice for oyster mushroom growing medium mixing machines[8].

2. RESEARCH METHOD

The design process begins with the design of the desired tool. The next step is the manufacturing process, which involves constructing the frame of the oyster mushroom growing media mixer according to the predetermined design, followed by assembling the electrical circuit to meet the requirements. If the tested circuit does not work, repair it by reassembling it until it does. If the assembled circuit works well, proceed to the next stage: data collection and processing, and finally, report preparation.

2.1. Block Diagram

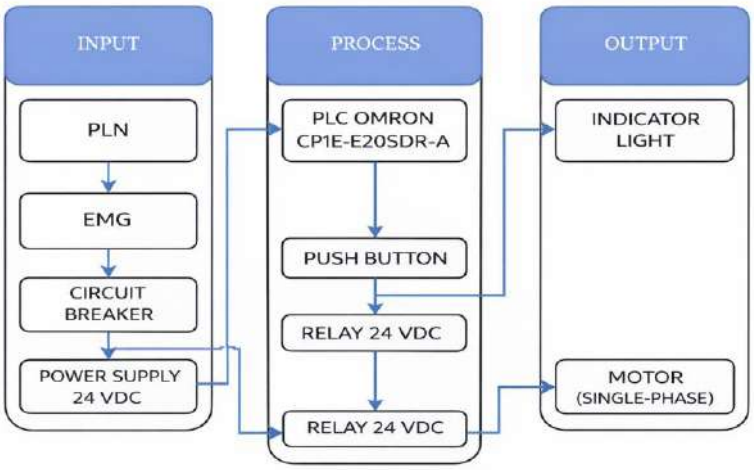

Figure 1. Block diagram

In Figure 1, the block diagram of the PLN energy source control system for the oyster mushroom growing media mixer machine begins with the main PLN electricity source, which powers the AC electric motor. This electrical power is then distributed to various components in the panel. From the panel, the outputs of these components are connected to a power supply that converts the voltage to supply other electrical components that require a lower voltage, such as the PLC. In this system, the Omron CP1E PLC requires a 24 VAC input, so a power supply is required. After that, the PLC will process data from the ladder diagram to control the AC electric motor as needed.

2.2. Flowchart

The process begins with preparing the ingredients for oyster mushroom growing media, as shown in Figure 2. The operator prepares ingredients such as sawdust, bran, lime, and water according to the measurements, then adds them one by one into the mixing machine tube[9]. After all the ingredients are added, the mixing machine starts automatically and runs for 120 seconds (2 minutes) to ensure homogeneity. In the middle of the process (at the 60th second), an alarm will sound as a halfway indicator, providing the operator with information. After 120 seconds, the valve at the bottom of the mixing machine opens automatically. The perfectly mixed dough will fall onto the turntable or container

JURNAL ECOTIPE
Electronic, Control, Telecommunication, Information, and Power Engineering
Volume 13, Issue 1, April 2026, pp. 121-129
ISSN 2355-5068 ; e-ISSN 2622-4852
DOI: 10.33019/jurnalecotipe.v13i1.4595

for further processes such as printing or packaging. After the valve opens, the mixing machine continues to rotate for 60 seconds to ensure no dough remains, and it is ready to be repeated for the next batch.

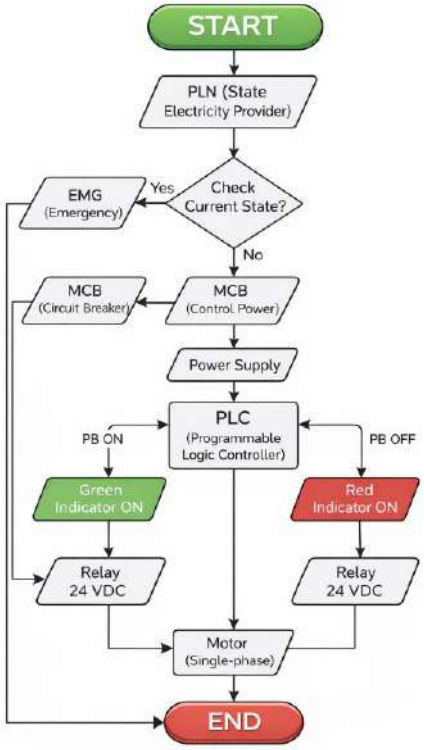

Figure 2. Flowchart system

2.3. Prototype Design

The prototype oyster mushroom media mixer machine is equipped with mechanical and electrical designs based on the CP1E-E20SDR-A control. The mechanical design uses SolidWorks software to determine dimensions and requirements, as shown in Figure 3. The mechanical design of the oyster mushroom media mixer machine consists of an electric motor, V-belt drive, gearbox, primary and secondary gears, press bars, stopper, printing plate, and electrical panel box.

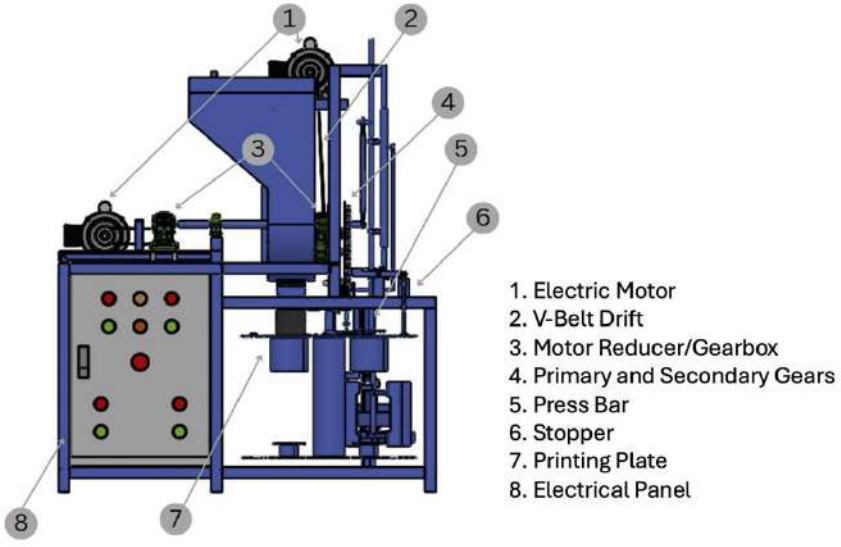

Figure 3. Mechanical design

JURNAL ECTIPE
Electronic, Control, Telecommunication, Information, and Power Engineering
Volume 13, Issue 1, April 2026, pp. 121-129
ISSN 2355-5068 ; e-ISSN 2622-4852
DOI: 10.33019/jurnalecotipe.v13i1.4595

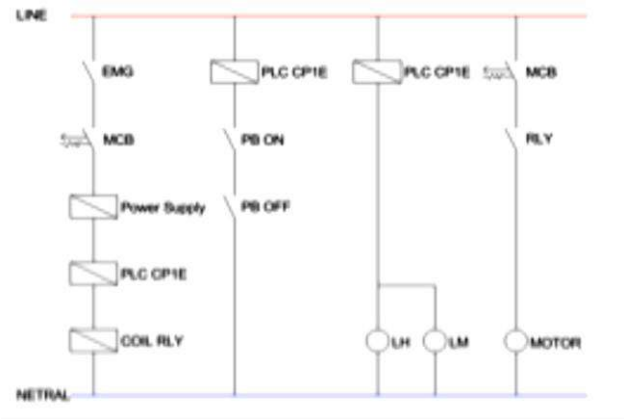

Figure 4. Control wiring installation

Figure 4 shows a diagram of a PLC-based control system installation. From the PLN (State Electricity Company) source, electricity flows to the MCB (Miniature Circuit Breaker) and then to the Power Supply. From the Power Supply, the DC power flows to the PLC I/O terminals and indicator lights. A ground is connected from the Power Supply to the PLC and other circuit components. For equipment requiring a 220 V supply, an AC neutral line is used.

The automated system for the oyster mushroom growing media mixer is powered by a 220 V supply from the PLN, protected by an MCB. The Power Supply converts the 220 V AC power to 24 V DC. The Power Supply powers the PLC and other control components. The operator presses the start and stop buttons. The PLC then processes the signals according to the ladder diagram. The resulting output is sent to the indicator lights and motor, which then illuminate according to the process conditions. This device is also equipped with an MCB and grounding to protect the system from electrical hazards.

3. RESULTS AND DISCUSSION

Figure 5(a) shows the main frame of the machine, which is made of 40x40 mm hollow iron, with the mixing container or tube being a 3 mm-thick stainless steel plate with a capacity of about 5 kg , used to mix planting media materials such as sawdust, bran, lime, and water. For the drive, a 0.5 HP motor is installed to rotate the stirrer via a pulley and a reducer gearbox with a 1:20 reduction[10], [11]. This machine is designed to mix planting media such as sawdust, bran, and lime homogeneously at adjustable stirring times and speeds, with the capacity of each bag is 1 kg as shown in Figure 5(b). The PLC system serves as a control center, regulating the drive motor and stirring duration according to a predetermined program, enabling the mixing process to run automatically and consistently. This machine is equipped with the main components: a single-phase AC motor, a relay, and a control panel, which support efficient and safe operation. With a PLC-based control system, this machine not only increases time and labor efficiency but also ensures uniformity in the planting media mixture, which is optimal for oyster mushroom growth. In addition, safety features are included to minimize the risk of accidents during the mixing process [12].

(a) (b)

Figure 5. Oyster mushroom mixer machine prototype

JURNAL ECOTIPE
Electronic, Control, Telecommunication, Information, and Power Engineering
Volume 13, Issue 1, April 2026, pp. 121-129
ISSN 2355-5068 ; e-ISSN 2622-4852
DOI: 10.33019/jurnalecotipe.v13i1.4595

3.1. Electrical and Automation Design

The electrical system for the oyster mushroom growing media mixer is designed to control the mixing process automatically and more efficiently. Using the Omron CP1E PLC as the main control enables the system to operate according to the program and with high precision, thereby reducing human error and increasing the speed of growing media production. Before implementation in the tool prototype, configuration, control, automatic circuits, and ladder programming for the Omron CP1E PLC were carried out using the CX-Programmer software [13]. The goal is to create a simulation of a control logic circuit that regulates the working sequence of components, such as motors and indicator lights, that show the on/off status of the Omron CP1E PLC. The Omron CP1E PLC circuit can be used in two modes, namely Manual Mode. The operator can turn the motor on and off directly using the on/off push button. Meanwhile (Automatic Mode), the PLC can execute automatic logic, such as mixing time, pauses, and motor working sequence, according to the ladder program [14].

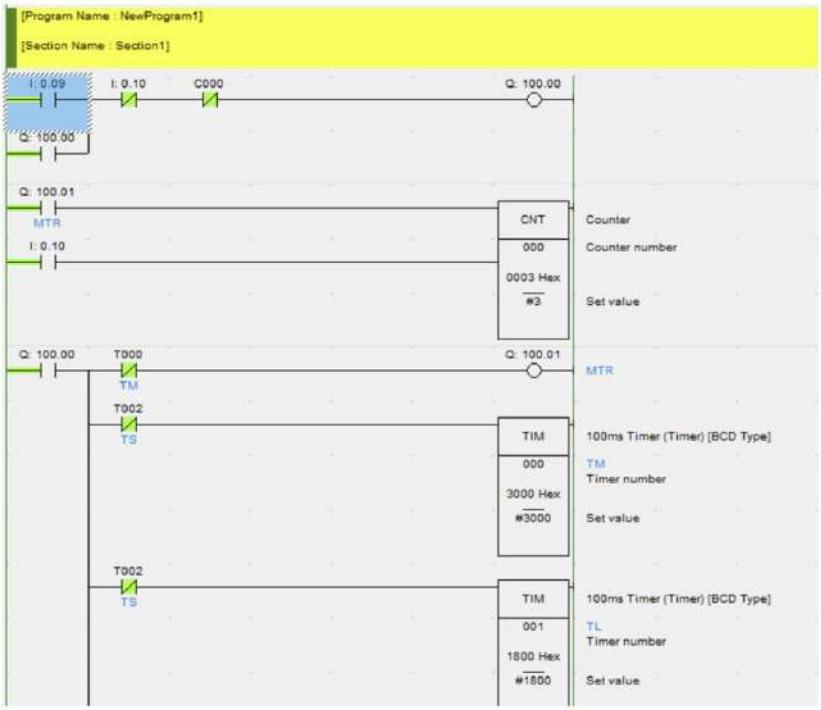

Figure 6. Ladder diagram of PLC

The PLC ladder diagram in Figure 6 shows a system ready to operate upon receiving the initial input. A combination of counters and timers controls the process, limiting the number of cycles and regulating the working time and pauses between cycles. Using a latch, counter, and two sequential timers, the system can run automatically and regularly, stopping after reaching a predetermined number of repetitions, thereby making it efficient and meeting process requirements [15]. When the mixer control alarm sounds, the mixer timer (T001) triggers an active interlock, which activates the press machine control program, as indicated by an NC contact (I:0.08) and a green line showing the contact is connected. The press machine can be activated at any time by pressing the on button. The ladder diagram in the ON/active state shows that the system operates automatically and is structured according to the timers' time sequence. Timers T0, T1, and T2 regulate the working duration of each process, while outputs Q100.01 to Q100.04 are activated sequentially. After all stages are completed, the process will return to the beginning via trigger T002, allowing the system to run repeatedly and efficiently according to the predetermined working cycle.

3.2. Testing of Material Mixture

Testing the oyster mushroom growing medium includes several parameters. The following are raw material parameters. The first parameter is raw materials, including weighing and mixing sawdust, bran,

Volume 13, Issue 1, April 2026, pp. 121-129
ISSN 2355-5068 ; e-ISSN 2622-4852
DOI: 10.33019/jurnalecotipe.v13i1.4595

lime, and water according to the specified measurements. The second parameter is material mixing, which is performed to assess the mixture's homogeneity, both visually and by sampling several points. The third parameter is mass and power, which measure the mass of the processed material and the electrical power consumed during the process, respectively, to assess the machine's efficiency. The last parameter is Initial and Final Mass Error, which compares the mass before and after mixing to determine the level of material loss during the process.

Table 1 presents the test results for the material mixing process using a mixer at a constant rotation speed of 70 rpm and a mixed mass of 3 kg. The test was conducted three times, with each trial having a different process duration: 1 minute, 2 minutes, and 3 minutes. The parameter observed at each process time was the quality of the mixing results, which was categorized into three levels: inhomogeneous, fairly homogeneous, and homogeneous.

In the first trial, mixing results at 1 and 2 minutes showed inhomogeneity, but after 3 minutes, the mixing quality became fairly homogeneous. Similarly, in the second trial, mixing remained inhomogeneous for the first minute but became fairly homogeneous at the 2nd and 3rd minutes. In the third trial, the improvement was more notable. In the first minute, results were still inhomogeneous; by the second minute, they were nearly homogeneous; and in the third minute, the mixing quality had achieved a homogeneous level.

Table 1. Material mixture test data

No of Experiment	Speed (Rpm)	Mass (Kg)	Time (Minutes)	Quality
1	70	3	1	not homogeneous
			2	not homogeneous
			3	almost homogeneous
2	70	3	1	not homogeneous
			2	almost homogeneous
			3	almost homogeneous
3	70	3	1	not homogeneous
			2	almost homogeneous
			3	homogeneous

3.3. Electrical power usage testing

Based on the data in Table 2, the results of testing the Omron CP1E PLC-based oyster mushroom growing media mixer machine under two conditions: no-load and loaded. The first to third columns show the parameters for no-load conditions, while the fourth to seventh columns show the parameters when the machine is loaded with a dough mass of 3000 grams. Meanwhile, under loaded conditions with a dough weighing 3000 grams, the rotational speed is maintained at 70 rpm, but the electric current increases consistently to 1.7 A for each test. The required power is also higher, ranging from 382 to 407 Watts. This increase in power reflects the additional energy required to handle the workload during mixing.

Table 2. Electrical power usage testing

No of Experiment	On-load condition			Load-free condition		
	Speed (Rpm)	Current (Ampere)	Power (Watt)	Speed (Rpm)	Current (Ampere)	Power (Watt)
1	70	1,7	406	70	1,5	345
2	70	1,7	406	70	1,6	347
3	70	1,7	407	70	1,6	349
4	70	1,7	382	70	1,6	353
5	70	1,7	389	70	1,7	353

Based on Table 2, the test results indicate that the machine can maintain a fairly stable dough mass, despite small fluctuations between the initial and final masses. The error value ranges from 1% to 1.1%, which remains within reasonable tolerances. This mass difference is likely due to several factors, including dough residue on the tool, minor spills, humidity, and weighing variations. These results

Volume 13, Issue 1, April 2026, pp. 121-129
ISSN 2355-5068 ; e-ISSN 2622-4852
DOI: 10.33019/jurnalecotipe.v13i1.4595

indicate that the mixer machine operates well and is suitable for making dough for oyster mushroom growing media.

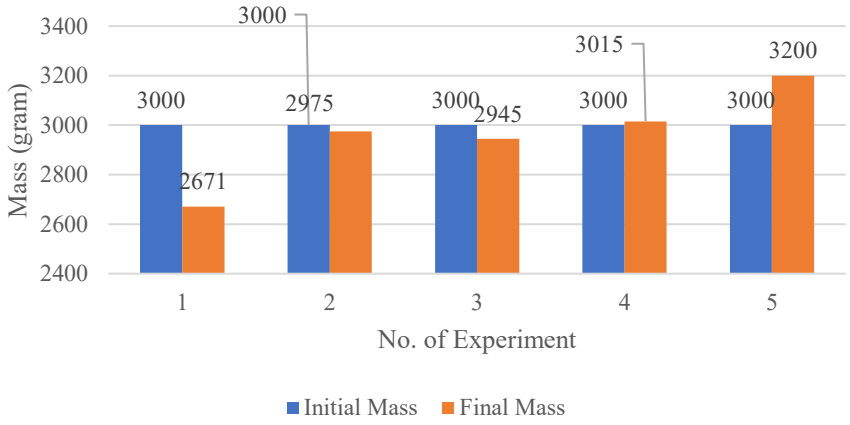

Figure 7. The mass of the planting media mixture graph

In Figure 7, the initial mass for all experiments was constant at 3000 grams. This shows that the material input was kept constant to maintain the test's validity. The final mass of Experiment 1 was lower (2671 grams), with the highest error at 1.1%. Experiments 2–4 showed a final mass close to the initial mass, ranging from 2975 to 3015 grams, with an error of 1%. Experiment 5 even showed a final mass greater than the initial mass (3200 grams), as the remaining dough stuck to the tool and small spills occurred.

4. CONCLUSION

The prototype of the oyster mushroom growing media mixing machine has been successfully designed with an automatic programming system using the Omron CP1E PLC, which supports a mechanical load of 3000 grams of growing media. This paper's contribution is to identify the optimal ingredient composition using PLC control to achieve a homogeneous media mixture by measuring ingredient weights, mixing time, power consumption, and the homogeneity of the mixture. Based on the test results, the prototype is able to pack oyster mushroom growing media close to the initial mass, which is around 2975–3015 grams, with an error of 1%, as well as decreasing power consumption due to the growing media mixture starting to become homogeneous, so that the motor works lighter. This research has a limitation in the value of the press mixture from the machine due to mechanical factors. To guide further research, the author suggests identifying the maximum pressure for media mixing and optimizing the packaging of oyster mushroom growing media to reduce production time. Based on the test results, the final mass in experiment 1 was lower (2671 grams), with the highest error of 1.1%. Experiments 2–4 showed a final mass close to the initial mass, ranging from 2975 to 3015 grams, with an error of 1%. The 5th experiment even showed a final mass greater than the initial mass (3200 grams of remaining dough stuck to the tool, a small spill, higher power required than without a load, which was around 406–407 watts in the 1st to 3rd tests). Power decreased to 382 watts in the 4th test and increased slightly to 389 watts in the 5th test. This decrease in power can be caused by the mixture of planting media becoming more homogeneous, so that the motor operates more lightly, or by external factors such as voltage and temperature fluctuations. In conclusion, the prototype oyster mushroom mixing machine has successfully homogeneously mixed the media in 3 minutes at a motor speed of 70 rpm and a power consumption of 345 watts.

REFERENCE

[1] N. A. Mardianti, S. Saadah, R. A. Nadja, and …, "Strategi pemasaran efektif untuk meningkatkan produksi dan pendapatan usaha jamur tiram (studi kasus PT Timur Mushroom Farm Desa

Volume 13, Issue 1, April 2026, pp. 121-129
ISSN 2355-5068 ; e-ISSN 2622-4852
DOI: 10.33019/jurnalecotipe.v13i1.4595

Kuajang Kecamatan …," *JIA (Jurnal Ilmiah …*, 2024, [Online]. Available: https://ejournal.agribisnis.uho.ac.id/index.php/JIA/article/view/965

[2] K. E. Wahyudi, M. A. Aziz, A. A. Putri, and …, "Pemberdayaan masyarakat dalam melakukan pembudidayaan jamur tiram di Desa Laweyan," *Jurnal …*, 2023, [Online]. Available: https://azramediaindonesia.azramediaindonesia.com/index.php/abdimasberkarya/article/view/604

[3] I. Badarina, E. Sulistyowati, Z. Efendi, and …, "Pelatihan membuat bibit jamur tiram putih dari bahan lokal bersama kelompok petani pengusaha jamur di Desa Suro Ilir Kabupaten Kepahiang," *Panrita Abdi-Jurnal …*, 2023, [Online]. Available: http://journal.unhas.ac.id/index.php/panritaabdi/article/view/18711

[4] N. A. Pratiwi, H. Alfi, B. Warman, and E. Syafri, "Review Media Tanam dan Hasil Jamur Tiram putih (Pleurotus ostreotus)," *Agroteknika*, 2025, [Online]. Available: https://agroteknika.id/index.php/agtk/article/view/476

[5] N. A. Elhany, D. Indriyani, C. Handayani, and ..., "Pelatihan Pembuatan Produk Jamur Tiram Sebagai Upaya Untuk Meningkatkan Pendapatan Ibu-Ibu PKK Paaraman Kelurahan Dawuhan Kabupaten Situbondo," *GUNAVATTA: Jurnal …*, 2025, [Online]. Available: https://unars.ac.id/ojs/index.php/GUNAVATTA/article/view/6872

[6] M. Risal and A. Firmanzah, "Pelatihan Budidaya Jamur Tiram Untuk Mendorong Minat Berwirausaha Bagi Mahasiswa Magister Manajemen Universitas Muhammadiyah Kalimantan Timur," *Jurnal Abdimas Sang Buana*, 2024, [Online]. Available: https://jurnal.usbypkp.ac.id/index.php/Abdimas_Sang_Buana/article/view/3541

[7] Y. Mulyanto, F. Idifitriani, E. S. Susanto, and S. Sulastri, "Implementasi Sistem Monitoring Berbasis Internet Of Things (IoT) pada Rumah Budidaya Jamur Tiram," *Digit. Transform. Technol*, 2024.

[8] B. J. Tiram, *Budidaya Jamur Tiram Dalam Upaya Peningkatan Pendapatan Keluarga Di Nagari Tanjung Alai*. pdfs.semanticscholar.org, 2023. [Online]. Available: https://pdfs.semanticscholar.org/2901/fa53aa42f9fb5e11838ebd6dc9d5919bc456.pdf

[9] N. Kusumadewi, N. Hernita, A. Rusdiana, and ..., "Pendampingan Labeling Dan Packaging Dalam Upaya Membangun Branding Ukm Jamur Tiram Desa Ujungberung Kabupaten Majalengka," *Bernas: Jurnal …*, 2023, [Online]. Available: https://www.researchgate.net/profile/Alan-Rusdiana-2/publication/375575808_Pendampingan_Labeling_Dan_Packaging_Dalam_Upaya_Membangun_Branding_UKM_Jamur_Tiram_Desa_Ujungberung_Kabupaten_Majalengka/links/654f8f3ab1398a779d7d6138/Pendampingan-Labeling-dan-PA

[10] A. Anggraeni, S. Salmi, R. Robika, and ..., "Optimalisasi usaha budidaya jamur tiram di desa teru melalui kemandirian pengadaan media tumbuh dan penanaman bibit jamur," *Jurnal Pengabdian …*, 2023, [Online]. Available: http://jurnal.borneo.ac.id/index.php/jpmb/article/view/2998

[11] E. W. Fatmawati, I. Y. Astuti, and ..., "Pemberdayaan masyarakat melalui kewirausahaan budidaya jamur tiram sebagai sumber pendapatan alternatif," *Jurnal Abdimas Bina …*, 2025, [Online]. Available: http://www.jabb.lppmbinabangsa.id/index.php/jabb/article/view/1693

[12] N. A. Elhany, U. B. Husnudin, A. M. A. Nuriyante, and ..., "Sosialiasasi Budidaya Jamur Tiram dan Pelatihan Penanaman Jamur Tiram bagi BEM Fakultas Pertanian, Sains dan Teknologi Unars," *INTEGRITAS: Jurnal …*, 2023, [Online]. Available: https://unars.ac.id/ojs/index.php/integritas/article/view/3800

[13] A. Anugrah, G. A. Tanan, I. Jamaluddin, and ..., "Pengembangan Mesin Pencampur Bahan Media Tanam Jamur Tiram," *Jurnal Teknik Mesin …*, 2024, [Online]. Available: https://jurnal.poliupg.ac.id/index.php/Sinergi/article/view/4765

Volume 13, Issue 1, April 2026, pp. 121-129
ISSN 2355-5068 ; e-ISSN 2622-4852
DOI: 10.33019/jurnalecotipe.v13i1.4595

[14] I. Mayada, *Analisis Usahatani Jamur Tiram di Gampong Panggoi Kecamatan Muara Dua Kota Lhokseumawe (Studi Kasus: Usahatani Jamur Tiram Bapak Safwandi)*. rama.unimal.ac.id, 2024. [Online]. Available: https://rama.unimal.ac.id/id/eprint/617/

[15] D. Subali and A. T. Hartanti, "Pelatihan Pembuatan Bibit Jamur Tiram dan Kuping Untuk Keberlangsungan Budi Daya Jamur di Papua," *Abdimas Galuh*, 2024, [Online]. Available: https://jurnal.unigal.ac.id/abdimasgaluh/article/view/14032

JURNAL ECOTIPE
Electronic, Control, Telecommunication, Information, and Power Engineering

Volume 13, Issue 1, April 2026, pp. 130-139
ISSN 2355-5068 ; e-ISSN 2622-4852
DOI: 10.33019/jurnalecotipe.v13i1.4591

Optimized PID Tuning in Pyrolysis Temperature Control Using Genetic Algorithm and Particle Swarm Optimization

Hartono[1], Yunita Umniyati[2], Eka Budiarto[3], Henry Nasution[4], Mulyadi[5]
[1,2]Mechatronics Engineering Department, Swiss German University, Jalur Sutera Barat No. 15, Tangerang 15143, Indonesia
[3]Information Technology Department, Swiss German University, Jalur Sutera Barat No. 15, Tangerang 15143, Indonesia
[4]Renewable Energy Engineering Technology, Bung Hatta University, Jl. Sumatera Ulak Karang Utara, Padang 25133, Indonesia
[5]Mechatronics Engineering Technology Department, Caltex Riau Polytechnic, Umbansari Street - Rumbai, Pekanbaru, 28265, Indonesia

ARTICLE INFO

Article historys:

Received : 28/02/2026
Revised : 06/04/2026
Accepted : 30/04/2026

Keywords:

Genetic Algorithm; Particle Swarm Optimization; PID Tuning; Pyrolysis Temperature Control

ABSTRACT

Temperature control is crucial for maintaining stable and effective thermal treatment in pyrolysis system. For this application, Proportional-Integral-Derivative (PID) controller is frequently utilized due to its ease of use and efficiency. This study aims to evaluate and compare the performance of classical and metaheuristic tuning methods for PID controllers in pyrolysis temperature control. This work compares conventional Ziegler-Nichols (ZN) and Cohen-Coon (CC) methods with metaheuristic optimization techniques, specifically Genetic Algorithm (GA) and Particle Swarm Optimization (PSO), for tuning PID controller parameters. The main contribution of this research is the demonstration of improved control performance and computational efficiency using PSO-based PID tuning for pyrolysis applications. Simulation results show that PID controllers that the parameters tuned by GA and PSO achieve faster and smoother responses, with small overshoot, compared to classical methods. From both methods, PSO provides balanced performance with the shortest rise time (30.66 s), fastest settling time (50.80 s), and lowest overshoot (1.15%). Although both GA and PSO can maintain the set point of 500 °C with satisfactory transient response, PSO also shows better convergence efficiency, with smaller iteration numbers and lower computational effort. The results indicate that PSO-tuned PID is suitable for pyrolysis temperature control applications.

Corresponding Author:

Hartono
Mechatronics Engineering Department, Swiss German University, Jalur Sutera Barat No. 15, Tangerang 15143, Indonesia
Email: har.tono@sgu.ac.id

1. INTRODUCTION

Pyrolysis process is a thermochemical method that converts plastic waste into useful biofuels by decomposing polymers in an oxygen-limited environment [1]. Due to its potential to reduce environmental pollution and provide renewable energy, pyrolysis has become popular solution for managing plastic waste and supporting green energy initiatives [2−3]. The efficiency and quality of the products produced by pyrolysis process are highly influenced by precise temperature control in the process [4]. Therefore, an appropriate temperature controller is required to ensure stable thermal conditions, improve process efficiency, and optimize energy usage.

There are numerous studies related to temperature control in pyrolysis systems. Due to its simplicity, intuitive design, and good performance in linear systems, Proportional-Integral-Derivative (PID) controller become the most popular control strategy in temperature control system [5−7]. PID

Volume 13, Issue 1, April 2026, pp. 130-139
ISSN 2355-5068 ; e-ISSN 2622-4852
DOI: 10.33019/jurnalecotipe.v13i1.4591

parameters can be tuned using classical methods, such as manual tuning, Ziegler–Nichols (ZN), and Cohen–Coon (CC), which rely on reaction curves [8−10]. However, when applied to systems with slow dynamics and large time constants, these methods frequently lead to high overshoot, oscillatory responses, and sub-optimal results [11−13]. Optimization-based algorithm, such as Genetic Algorithm (GA) and Particle Swarm Optimization (PSO), aim to minimize control error for improved performance based on certain objective function [14]. Furthermore, frequency-domain approaches ensure robustness, while modern techniques including metaheuristic optimization and fuzzy logic adapt to nonlinear or complex systems [15].

In this paper, PID parameters will be selected by comparing conventional ZN and CC methods with metaheuristic optimization techniques, namely GA and PSO. The contribution of this paper is to provide insight into how these advanced tuning methods can improve temperature control performance in pyrolysis heater systems by analyzing their transient and steady state responses while considering optimization effort. Finally, the best approach among them will be selected as optimized tuning method for PID temperature control of pyrolysis process.

2. RESEARCH METHOD

This paper presents simulation-based investigation to compare the performance of PID tuning methods, specifically classical approaches with metaheuristic optimization. This research focus on tuning techniques from the conventional ZN and CC methods to the more modern GA and PSO. The behavior of each controller is analyzed by evaluating its step response, with analysis centered on their ability to reach and maintain desired set point in pyrolysis heater temperature control.

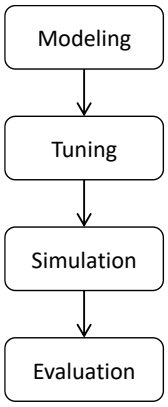

Figure 1. Research flow diagram

Figure 1 shows general flow of the research, which has four main steps: modeling, tuning, simulation, and evaluation. This study starts with the redefinition of mathematical model for thermal system of pyrolysis reactor, refering previous literature. After that, classical and metaheuristic methods are used to adjust the PID parameters. Subsequently, these parameters are used in the simulation to see how the system reacts to the inputs. Then, the performance is evaluated by comparing the response characteristics of each tuning method to see how well they kept the temperature stable and accurate.

2.1. Pyrolysis System

Pyrolysis is a thermochemical process in which organic materials are decomposed at high temperatures in the absence of oxygen environment. This process can be used to produce char, liquid biofuel, and gases. Product quality is highly dependent on reactor temperature treatment so that proper temperature control becomes essential. It can be seen from pyrolysis process diagram in Figure 2 that an extruder moves the feedstock into pyrolysis reactor. Inside, it is heated by a heater in nitrogen atmosphere to ensure an oxygen-free environment. The substance decomposes thermally under these conditions, producing solid residue and vapors. A cyclone is used to remove the solid char, and catalytic reactor is used to further enhance the vapor phase. The resulting vapors are then condensed to obtain liquid biofuel as the main product, while the produced gas is sent back to the heater as fuel [16].

JURNAL ECTIPE
Electronic, Control, Telecommunication, Information, and Power Engineering
Volume 13, Issue 1, April 2026, pp. 130-139
ISSN 2355-5068 ; e-ISSN 2622-4852
DOI: 10.33019/jurnalecotipe.v13i1.4591

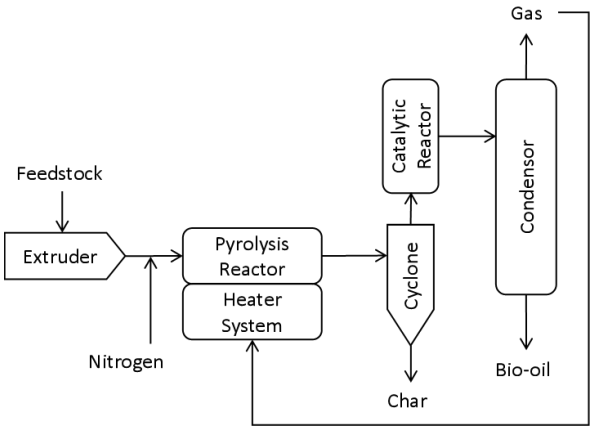

Figure 2. Pyrolysis process diagram

From temperature control perspective, the heater system consists of the pre-heater process, main heater, and second heater stage. This study will be focused on the main heater stage, which governs the temperature dynamics. This stage is modeled as second-order transfer function and is used for step-response simulations to evaluate PID tuning performance in terms of rise time, overshoot, settling time, and steady-state accuracy. The plant model used in this study is adopted from Muharto *et al*. [17] based on real heater model to allow consistent performance comparison. The system dynamics are represented by the following transfer function:

$$G(s) = \frac{1.737 \times 10^{-5}}{s^2 + 0.004285s + 6.179 \times 10^{-7}} \quad (1)$$

2.2. Temperature Control

For effective and consistent thermal treatment in the pyrolysis process, the temperature of reactor must be controlled as temperature directly influences reaction process and product quality. In this system, the error signal for PID controller is produced by comparing the measured reactor temperature with reference set point.

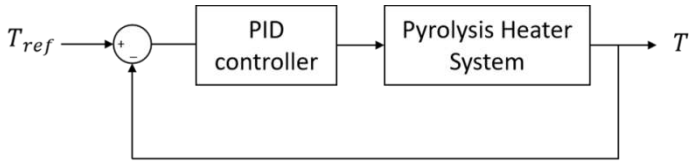

Figure 3. Pyrolysis temperature control block diagram

Figure 3 shows the closed loop temperature control structure applied in this work. The output of the controller adjusts the pyrolysis heater system and the heat input is changed to respond to dynamics of the system in order to hold the system at the desired operating temperature. The main controller used in this system is PID due to its proven effectiveness and simplicity in industrial thermal systems, and a step-response analysis is used to define system behavior for different settings of the PID controller.

2.3. PID Tuning and Optimization

The control performance of PID controller is affected by its parameters, namely proportional gain (Kp), integral time (Ti), and derivative time (Td). Therefore, this paper analyzes the classical tuning methods, Ziegler-Nichols (ZN) and Cohen-Coon (CC), and compares them with the metaheuristic methods, Genetic Algorithm (GA) and Particle Swarm Optimization (PSO). While the classical methods tune the PID parameters using system reaction curves, or ultimate gain and offer a simple rules of thumb approach, GA and PSO aim to tune the PID parameters by minimizing a predetermined cost function, typically relating to control errors, to achieve an improved system response speed and smoothness.

JURNAL ECOTIPE
Electronic, Control, Telecommunication, Information, and Power Engineering
Volume 13, Issue 1, April 2026, pp. 130-139
ISSN 2355-5068 ; e-ISSN 2622-4852
DOI: 10.33019/jurnalecotipe.v13i1.4591

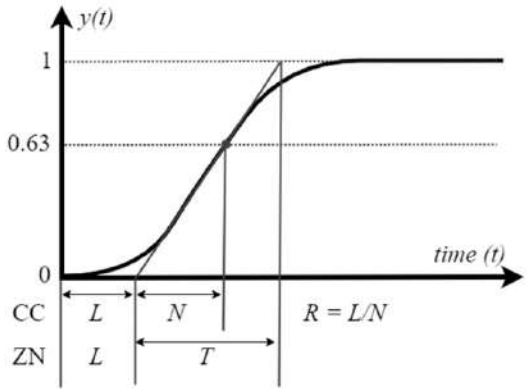

Figure 4. S-curve of ZN and CC tuning methods

The application of the ZN and CC tuning methods in this study are illustrated in Figure 4 and Table 1, respectively. Both methods are used in setting the PID controller parameters based on the process reaction curve from an open-loop step response. From the S-curve response, parameters of process delay and time constant are used to calculate the proportional, integral, and derivative parameters according to specific tuning rules. The parameter L is used to quantify the apparent process delay (dead time) and is defined as the time span between the step input is applied and the point where the tangent at the inflection point intersects the time axis. The parameter N reflects the speed of the process response to the input change and describes the slope of the tangent line at the inflection point, while the ratio R=L/N is used in CC method to characterize the process further for controller parameter calculation.

Table 1. ZN and CC PID tuning rule

Tuning Method	K_p	T_i	T_d
ZN	$1.2\frac{T}{\mathrm{L}}$	$2L$	$0.5L$
CC	$\frac{P}{\mathrm{NL}}\left(1.33+\frac{R}{4}\right)$	$L\left(\frac{30+3R}{9+20\mathrm{R}}\right)$	$\frac{4L}{11+2\mathrm{R}}$

The performance of the PID controller in the optimization process is evaluated using the objective function. In the present study, the controller parameters are introduced as a vector $\theta = [K_p, T_i, T_d]$. The optimizer seeks to reduce the ITAE (Integral of Time-weighted Absolute Error), which is used to measure tracking error within the limits of a defined acceptable transient performance. In the case of a unit step input, the tracking error is defined as $\mathrm{e(t)} = [1 - \mathrm{y(t)}]$. The objective function is formulated under an overshoot constraint as follows

$$J(\theta) = \begin{cases} \int_0^{t_s} t|e(t)|dt, & OS \leq 0.02 \\ \int_0^{t_s} t|e(t)|dt + 10^6(OS - 0.02), & OS > 0.02 \end{cases} \quad (2)$$

where t_s refers to simulation time and OS refers to maximum overshoot. A penalty term is added to the overshoot > 2% to force the optimized controller to meet the transient response specification.

Table 2 shows the optimization settings for GA and PSO techniques applied to tune the PID parameters. For each controller optimization, three control parameters are considered as decision variables. To define a feasible and stable search space, parameter limits. are constrained to a lower and upper range of [0, 100, 50] and [20, 1000, 200] respectively. These limits are designed to prevent the search from unreasonable control parameters but are still effective to provide the desired convergence towards the optimal solution.

JURNAL ECTIPE
Electronic, Control, Telecommunication, Information, and Power Engineering
Volume 13, Issue 1, April 2026, pp. 130-139
ISSN 2355-5068 ; e-ISSN 2622-4852
DOI: 10.33019/jurnalecotipe.v13i1.4591

Table 2. GA and PSO Optimization Parameters

Algorithm	Parameter	Value
GA	Population size (*N*)	20
	Maximum generation (*Gen*)	50
	Number of variables (*nvars*)	3
	Crossover probability (*Pc*)	0.8
	Mutation probability (*Pm*)	0.1
PSO	Number of particles (*m*)	20
	Maximum iteration (*Iter*)	50
	Number of variables (*k*)	3
	Inertia weight (*w*)	0.7
	Cognitive coefficient (c_1)	1.5
	Social coefficient (c_2)	1.5
	Maximum velocity (*vmax*)	0.1 x (ub-lb)

Procedure of GA applied in this study is provided in Table 3. The algorithm processes population candidates of potential solutions through selection, crossover, and mutation using fitness evaluation. The evolutionary process is repeated until the stopping criterion is met and results in optimal controller parameters. Furthermore, the fitness function is created to reduce error in the system and enhance the control performance. Therefore, the GA provides a structured way of investigating the search space and obtaining strong and near optimal controller parameters.

Table 3. Genetic Algorithm (GA) Pseudocode

Step	Algorithm
1	Define GA parameters: population size (*N*), maximum generation (*Gen*), crossover probability (*Pc*), mutation probability (*Pm*), and objective function f.
2	Randomly initialize population of candidate solutions within predefined search bounds.
3	Evaluate fitness value *f(xi)* for each individual.
4	Initialize iteration counter n=0.
5	While $g < Gen$ do
6	Perform selection process based on fitness value.
7	Apply crossover operation with probability *Pc*.
8	Apply mutation operation with probability *Pm*.
9	Evaluate fitness value of the new offspring population.
10	Replace population with newly generated individuals.
11	Determine the best individual solution.
12	Increase generation counter $g = g + 1$.
13	End While
14	Output optimal solution representing controller parameters.

The following Table 4 provides the PSO algorithm utilized in this study as pseudocode. This table describes the sequential order to be followed during the optimization process, which consists of particle initialization, fitness evaluation, and the iterative updates of velocity and position of the particles based on the personal best and the global best solutions. This pseudocode describes the optimization process to determine the controller parameters and the iterative search process the swarm performs until a stopping criterion is met.

Table 4. Particle Swarm Optimization (PSO) Pseudocode

Step	Algorithm
1	Define PSO parameters: number of particles (*m*), maximum iteration (*Iter*), dimension (*k*), inertia weight (*w*), cognitive coefficient (c_1), social coefficient (c_2), and objective function *f*.
2	Randomly initialize particle positions pi and velocities vi within predefined search bounds.
3	Evaluate the fitness value $f(p_i)$ of each particle.

Volume 13, Issue 1, April 2026, pp. 130-139
ISSN 2355-5068 ; e-ISSN 2622-4852
DOI: 10.33019/jurnalecotipe.v13i1.4591

Step	Algorithm
1	Define PSO parameters: number of particles (m), maximum iteration (*Iter*), dimension (k), inertia weight (w), cognitive coefficient (c_1), social coefficient (c_2), and objective function f.
4	Set individual best position pbesti=pi and determine global best position gbest.
5	Initialize iteration counter n=0.
6	While $n < Iter$ do
7	For each particle $i = 1,2,\ldots,m$:
8	Update particle velocity: $v_{ij} = wv_{ij} + c_1\gamma_1(pbest_{ij} - p_{ij}) + c_2\gamma_2(gbest_{ij} - p_{ij})$
9	Update particle position: $f(p_i) = p_{ij} + v_{ij}$
10	Evaluate updated fitness value $f(p_i)$.
11	Update *pbesti* if a better solution is obtained.
12	Update global best position *gbest*.
13	Increase iteration counter $n=n+1$.
14	End While
15	Output optimal solution represented by *gbest*.

3. RESULTS AND DISCUSSION

To evaluate the performance of the PID controller under different tuning methods, step response simulations were conducted using MATLAB. In these simulations, classical tuning methods (ZN and CC) and metaheuristic optimization techniques (GA and PSO) were applied to determine the PID parameters. The performance of each method is compared using performance metrics such as rise time, settling time, overshoot, and steady-state error, which describe how quickly and accurately the system reaches the desired temperature.

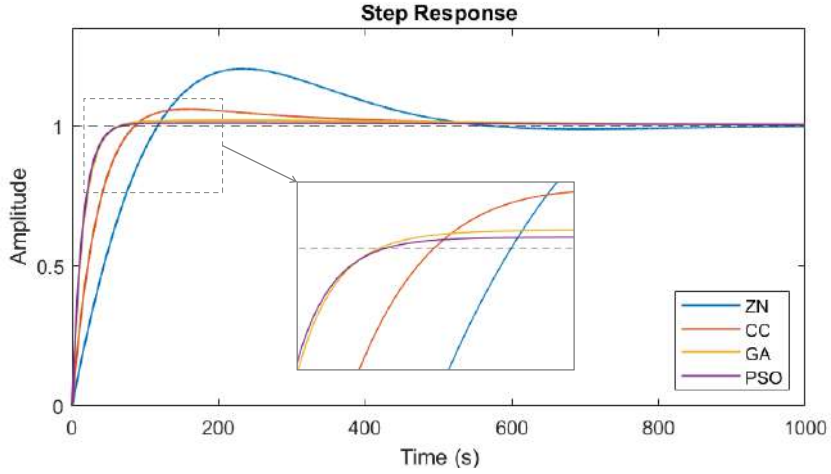

Figure 5. Cost function of GA and PSO

Figure 5 represents step responses of the PID controlled system using ZN, CC, GA, and PSO tuning methods. The ZN-tuned response shows the largest overshoot and the slowest convergence, indicating oscillatory and less stable behavior. The CC method has better transient response but still requires long time to fully achieve steady state. On other hand, GA and PSO significantly produce faster and smoother responses with minimal overshoot. It can be seen that GA and PSO have very close responses but GA shows slightly higher overshoot. Among them, PSO achieves the fastest and most stable convergence to the reference value, showing the best control performance for the system.

JURNAL ECTIPE
Electronic, Control, Telecommunication, Information, and Power Engineering
Volume 13, Issue 1, April 2026, pp. 130-139
ISSN 2355-5068 ; e-ISSN 2622-4852
DOI: 10.33019/jurnalecotipe.v13i1.4591

Table 5. Comparison of step responses for different tuning methods

Tuning Method	PID Parameters			Step Response Performance			
	K_p	T_i	T_d	Rise Time (s)	Settling Time (s)	Overshoot (%)	Steady-State Error
ZN	8.54	366.00	92.00	88.57	508.60	20.50	0.0013
CC	13.89	974.00	129.00	56.29	428.48	6.10	0.0059
GA	20.00	556.91	189.08	31.93	51.35	1.99	0.0045
PSO	20.00	950.92	200.00	30.66	50.80	1.15	0.0055

Table 5 provides the performance comparison of four PID tuning methods, namely ZN, CC, GA, and PSO. The comparison is based on rise time, settling time, overshoot, and steady-state error, which describe how well the temperature control system responds to a step change. The ZN method shows relatively the worst performance. Although its steady-state error is small, it produces very long settling time (508.60 s) and high overshoot (20.50%), indicating excessive oscillations and slow stabilization. This behavior is not suitable for pyrolysis temperature control system, which require stable and smooth operation. While, the CC method improves the response compared to ZN, reducing the overshoot to 6.10% and shortening the rise time. However, the settling time is still high (428.48 s), describing the system needs long time to reach steady conditions.

In contrast, the GA-based tuning provides much faster and more stable response. The rise time decreases to 31.93 s and the settling time to 51.35 s, while the overshoot is limited to 1.99%, indicates that GA can effectively balance speed and damping. The PSO method produces the best performance, achieves the shortest rise time and settling time of 30.66 s and 50.80 s respectively, with the lowest overshoot of 1.15%. Although the steady-state error produced by PSO is slightly higher than GA, the difference is very small and still acceptable for real practical performance.

Overall, the results show that metaheuristic optimization methods, in this case GA and PSO, outperform classical ZN and CC tuning. Among them, PSO provides the most balanced response, suitable for pyrolysis temperature control. These two optimization methods can therefore be applied to PID controllers for pyrolysis temperature control, as provided by simulation result in Figure 6.

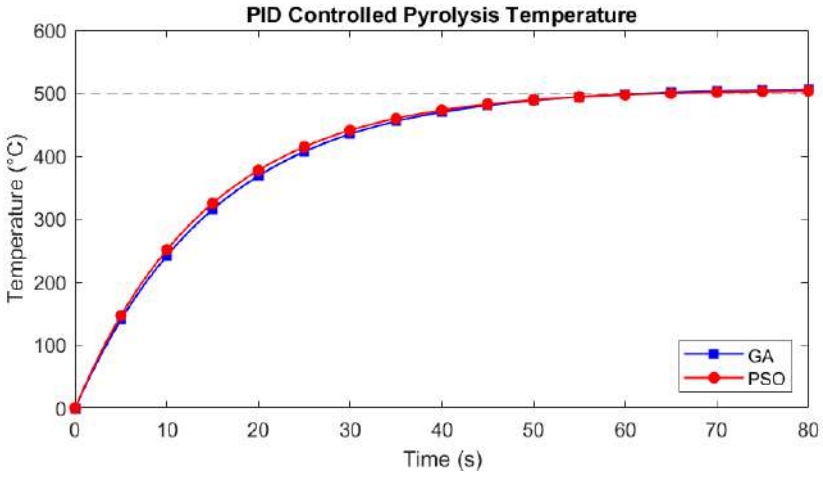

Figure 6. PID Controlled Pyrolysis Temperature

The comparison of PID controllers tuned by GA and PSO for pyrolysis temperature control shows some differences between the two methods. As shown in the temperature graph, both techniques are capable to control the system to targeted set point of 500 °C with acceptable transient response. The responses of PID controllers tuned by GA and PSO have similar rise times and settling time patterns, indicating that both algorithms can find controller parameters that deliver satisfactory closed-loop performance without overshoot for the heater temperature of pyrolysis process, which contributes to reduced thermal energy loss. While, small differences in time response and steady-state accuracy show that the methods can maintain the required thermal conditions for the pyrolysis system effectively.

JURNAL ECTIPE
Electronic, Control, Telecommunication, Information, and Power Engineering
Volume 13, Issue 1, April 2026, pp. 130-139
ISSN 2355-5068 ; e-ISSN 2622-4852
DOI: 10.33019/jurnalecotipe.v13i1.4591

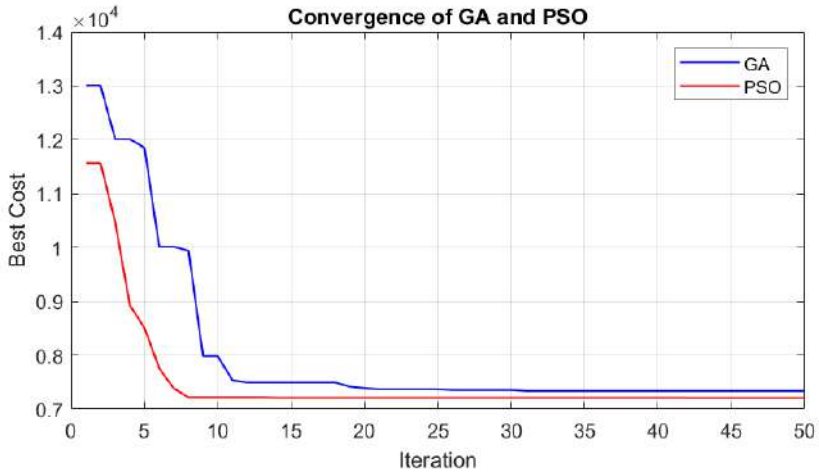

Figure 7. Cost function of GA and PSO

Although the control performances are similar, it can be observed that PSO has better advantage in terms of optimization efficiency as shown in the convergence characteristics of both methods. The convergence graph in Figure 7 shows that PSO reduces the cost function faster and with smaller iteration numbers than GA, meaning lower computational effort during parameter searching. This behavior indicates shorter processing times and reduced computational resources when finding optimal PID parameters. Since the control performance is similar, PSO is preferable primarily for its computational efficiency. In practical applications, where PID tuning may need to be repeated under varying operating conditions, the lower computational load of PSO provides more advantage without compromising control performance.

4. CONCLUSION

This study demonstrates the effectiveness of PID parameters selection using metaheuristic optimization methods, particularly GA and PSO, that provide better performance for pyrolysis temperature control compared to classical tuning methods. The simulation results represent that both GA and PSO achieve faster and smoother responses with minimal overshoot compared to ZN and CC, however PSO offers the most balanced performance, resulting the shortest rise time, fastest settling time, and lowest overshoot. The main contribution of this study is the quantitative demonstration that PSO-based PID tuning significantly improves both dynamic response and optimization efficiency compared to classical methods for pyrolysis temperature control. In addition, PSO shows higher convergence efficiency, requiring only fewer iterations and lower computational effort. These findings indicate that PSO-tuned PID controller is well suited for maintaining stable and effective thermal conditions in pyrolysis systems. Practically, the proposed approach can be implemented in real pyrolysis systems to achieve more stable temperature regulation, reduced energy loss, and improved process reliability under varying operating conditions.

Acknowledgments

The authors thank Academic Research and Community Service (ARCS) of Swiss German University for supporting this work through Faculty Research Fund 2026 program.

Volume 13, Issue 1, April 2026, pp. 130-139
ISSN 2355-5068 ; e-ISSN 2622-4852
DOI: 10.33019/jurnalecotipe.v13i1.4591

REFERENCES

[1] Ren-X. Yang, K. Jan, C.-T. Chen, W.-T. Chen, and K. C.-W. Wu, "Thermochemical Conversion of Plastic Waste into Fuels, Chemicals, and Value-Added Materials: A Critical Review and Outlooks," *ChemSusChem*, vol. 15, no. 11, pp. e202200171, Jun. 2022.

[2] N. Ungureanu, N.-V. Vlăduț, S.-Ș. Biriș, N.-E. Gheorghiță, and M. Ionescu, "Biomass pyrolysis pathways for renewable energy and sustainable resource recovery: A critical review of processes, parameters, and product valorization," *Sustainability*, vol. 17, no. 17, 2025.

[3] S. K. Lodhi et al., "Renewable energy technologies: Present patterns and upcoming paths in ecological power production," *Global Journal of Universal Studies*, vol. 1, no. 1, pp. 108–131, Jun. 2024.

[4] D. Aboelela, H. Saleh, A. M. Attia, Y. Elhenawy, T. Majozi, and M. Bassyouni, "Recent advances in biomass pyrolysis processes for bioenergy production: Optimization of operating conditions," *Sustainability*, vol. 15, no. 14, p. 11238, 2023.

[5] A. A. Jamil, W. F. Tu, S. W. Ali, Y. Terriche, and J. M. Guerrero, "Fractional-Order PID Controllers for Temperature Control: A Review," Energies, vol. 15, no. 10, Art. no. 3800, 2022.

[6] R. P. Borase, D. K. Maghade, S. Y. Sondkar, and A. et al., "A review of PID control, tuning methods and applications," *International Journal of Dynamics and Control*, vol. 9, pp. 818–827, 2021.

[7] M. Ouyang, Y. Wang, F. Wu, and Y. Lin, "Continuous reactor temperature control with optimized PID parameters based on improved sparrow algorithm," *Processes*, vol. 11, no. 5, 2023.

[8] N. H. Sahrir and M. A. Mohd Basri, "Modelling and manual tuning PID control of quadcopter," in *Control, Instrumentation and Mechatronics: Theory and Practice*, vol. 921. Singapore: Springer, 2022.

[9] A. D. M. Africa, J. O. Q. Chua, and J. L. H. Solis, "PID tuning of speed controller using Ziegler–Nichols and manual method DC motor," in *Proc. 2023 IEEE 15th Int. Conf. on Humanoid, Nanotechnology, Information Technology, Communication and Control, Environment, and Management (HNICEM)*, Philippines, 2023, pp. 1–6.

[10] L. Bhardwaj, A. Mishra, and D. Asija, "Parameter optimisation of PID controller utilised for speed control of DC motor with Ziegler-Nichols and Cohen-Coon tuning method," in *Intelligent and Sustainable Power and Energy Systems*, 1st ed. Boca Raton, FL, USA: CRC Press, 2025, pp. 1–9.

[11] K. S. Kula, "Tuning a PI/PID controller with direct synthesis to obtain a non-oscillatory response of time-delayed systems," *Applied Sciences*, vol. 14, no. 13, 2024.

[12] H. Hartono, E. Budiarto, and H. Nasution, "Design of PID controller using LQR-based parameter selection for DC motor position control," *Jurnal Ecotipe*, vol. 12, no. 1, pp. 11–19, Apr. 2025.

[13] L. Bhardwaj, A. Mishra, and D. Asija, "Parameter optimisation of PID controller utilised for speed control of DC motor using Ziegler–Nichols and Cohen–Coon tuning method," *Advances in Smart Communication and Imaging Systems*, Boca Raton, FL, USA: CRC Press, 2023.

[14] F. Z. M. Ridha, W. S. Hacham, and M. H. O. Ajam, "Optimizing indoor temperature control using genetic algorithm for PID tuning," *NTU Journal of Renewable Energy*, vol. 9, no. 1, pp. 1–11, Jul. 2025.

[15] P. Chotikunnan, R. Chotikunnan, A. Nirapai, A. Wongkamhang, P. Imura, and M. Sangworasil, "Optimizing Membership Function Tuning for Fuzzy Control of Robotic Manipulators Using PID-Driven Data Techniques", *Journal of Robotics and Control (JRC)*, vol. 4, no. 2, pp. 128–140, Mar. 2023.

Volume 13, Issue 1, April 2026, pp. 130-139
ISSN 2355-5068 ; e-ISSN 2622-4852
DOI: 10.33019/jurnalecotipe.v13i1.4591

[16] D. Gahane, D. Biswal, and S. A. Mandavgane, "Life cycle assessment of biomass pyrolysis," *BioEnergy Research*, vol. 15, pp. 1387–1406, Sep. 2022.

[17] B. Muharto, F. R. Saputro, W. Prabowo, T. Anggoro, A. B. Adiprabowo, I. Masfuri, and B. B. Irawan, "Pyrolysis process control: Temperature control design and application for optimum process operation," *International Journal of Electrical and Computer Engineering (IJECE)*, vol. 14, no. 2, pp. 1473–1485, Apr. 2024.

JURNAL ECOTIPE
Electronic, Control, Telecommunication, Information, and Power Engineering

Volume 13, Issue 1, April 2026, pp. 140-149
ISSN 2355-5068 ; e-ISSN 2622-4852
DOI: 10.33019/jurnalecotipe.v13i1.4584

Energy Audit and Optimization of Energy Consumption in the Electronics Manufacturing Industry based on ISO 50001:2018

Abudhiya Harits Ulhaq Hadyan [1], Chairul Gagarin Irianto [2], Syah Alam [3]
[1,2,3]Electrical Engineering Departement, Universitas Trisakti, Jl. Kyai Tapa no.1, Jakarta, Indonesia

ARTICLE INFO

Article historys:

Received : 13/01/2026
Revised : 10/02/2026
Accepted : 30/04/2026

Keywords:

Electronics Manufacturing Industry; Energy Consumption Intensity (IKE); Energy Management System; Energy Saving Opportunities (PHE); ISO 50001:2018

ABSTRACT

The development of modern science and technology, especially in the field of industry. Currently, It will grow every year in line with the increasing demand for electricity. The increase will be directly proportional to the increasing needs and production targets in the Electronics Industry. Industries that have a land area of 25.552,76$m2$. In 2022 the total energy consumption of PT XYZ amounted to 8,133.08 MWh with an average of 677.75 MWh per month and is expected to increase by 2% in 2023. This research will focus on computer loads as the most widely used loads in the Electronics Manufacturing Industry. PT XYZ management motivated to optimize and improve the efficiency of energy use with increasing energy demand. Therefore, this research method will determine the value of Energy Consumption Intensity (IKE) and determine Energy Saving Opportunities (PHE) based on ISO 50001: 2018 and using Power Server Application to facilitate assessments, decisions, and quick actions of relevant parties in saving electrical energy in order to minimize waste of electrical energy in accordance with the principles of energy management.. The savings generated by this application reach 77,839 kWh/m² per year and potential electricity cost savings of around Rp 170,780,234.63 per year.

Corresponding Author:

Syah Alam
Electrical Engineering Department, Universitas Trisakti, Jl. Kyai Tapa no. 1, Jakarta, Indonesia
Email: syah.alam@trisakti.ac.id.

1. INTRODUCTION

The development of modern science and technology, especially in the industrial sector, continues to experience significant growth every year. A variety of new discoveries can provide competitive advantages and alternatives for increasing productivity. Along with this technological advancement, the need for electrical energy also increases. This increase is directly correlated with the increasing demand and production targets of the electronics industry. This includes, for example, the addition of DC power supplies, lighting, inspection machines, and air conditioners. The growing demand for energy resources and industrial products worldwide creates serious challenges for the sustainable development in many sectors [1].

High energy consumption is often caused by the use of inappropriate equipment and poor energy management, therefore an energy audit must be conducted to address the problem [2]. To achieve continuous improvement in energy performance, companies need to implement a systematic approach that includes the preparation and implementation of standards and structured energy management processes. As a comprehensive global framework, the ISO 50001 standard is an Energy Management

Volume 13, Issue 1, April 2026, pp. 140-149
ISSN 2355-5068 ; e-ISSN 2622-4852
DOI: 10.33019/jurnalecotipe.v13i1.4584

System published on June 15, 2011. ISO 5001 provides technical and strategic guidelines for companies in optimizing energy use.

An energy audit is a systematic procedure designed to evaluate energy flows within an industry, identify potential savings, and formulate strategies to improve energy efficiency without sacrificing productivity [3]. The ISO 50001:2018 Energy Management System framework can be implemented with several regulations that serve as references related to energy management, one of which is the Regulation of the Minister of Energy and Mineral Resources No. 13 of 2012 concerning Energy Management Savings, which also regulates a standard value for Energy Consumption Intensity (IKE).

Energy Consumption Intensity (IKE) is an indicator used to measure the amount of electrical energy used by a company in a building. By knowing the value of Energy Consumption Intensity (IKE), strategic steps can be taken to save and optimize energy performance [4] . Energy Saving Opportunities (PHE) are the potential for reducing energy consumption that can be identified through analysis of Energy Consumption Intensity (IKE). By comparing the IKE value with applicable standards, the potential savings that can be achieved can be identified. It should be noted that efforts to save energy should not only focus on reducing energy consumption alone, but must also consider aspects of comfort and productivity in the workplace [5].

Referring to Deny Satyagraha's research which discusses the implementation of ISO 50001:2018 in the tire manufacturing industry, it examines efforts to optimize energy use at Plant X, a tire production facility owned by PT. Ban Indonesia which faces the challenge of inefficient energy consumption. The method used in analyzing the data is in the form of requirements referring to the ISO 50001:2018 standard and the calculation of energy consumption intensity (IKE) and specific consumption (KS). Plant X has a high level of energy consumption but low efficiency due to unutilized power and over-supply. This encourages the need for an energy audit to identify opportunities for savings and optimization [6].

In this study, PT. XYZ is a manufacturing industry that produces electronic products and will use a quantitative method based on the ISO 50001:2018 framework in companies that consume fossil energy from PLN sources. The industry has a land area of 25,552.76 m^2.. In 2022, the amount of energy consumption of PT. XYZ is 8,133.08 MWh with an average of 677.75 MWh per month, and is estimated to increase by 2% in 2023. PT. PLN as the main source of electricity provides electrical energy with a power contract of 3,465 kVA at a 20 kVA substation. Therefore, analysis and optimization of electrical energy use are needed for the implementation of energy management based on the ISO 5001:2018 system.

Some companies, as part of their environmental policies and commitments, set goals to reduce energy consumption. However, due to various factors (lack of indicators, a methodology that does not adapt to the production method, among others), the stated objective is not achieved. Despite its benefits, energy efficiency can encounter barriers in various areas, including behavioural, financial, economic, political, regulatory, awareness, information, and organizational [7]. PT XYZ management is motivated to optimize and improve energy efficiency with increasing energy needs. To do these two things, an energy audit and management are needed [8].

2. RESEARCH METHOD

2.1. Energy Audit

An energy audit is the first step in implementing energy management. Identifying potential energy waste in energy-using systems, planning, analyzing, evaluating, and suggesting actions to improve energy efficiency are all part of an energy audit.

Research methodology in energy management involves a systematic approach to understanding, analyzing, and managing energy use in an organization. Figure 1 below show energy audit research flowchart.

JURNAL ECOTIPE
Electronic, Control, Telecommunication, Information, and Power Engineering
Volume 13, Issue 1, April 2026, pp. 140-149
ISSN 2355-5068 ; e-ISSN 2622-4852
DOI: 10.33019/jurnalecotipe.v13i1.4584

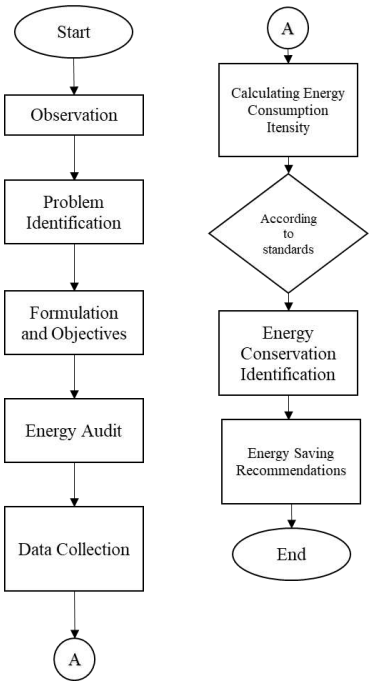

Figure 1. Energy audit research flowchart

This research applied a systematic methodology to evaluate energy use and propose improvements based on the principles of the ISO 50001:2018 Energy Management System Standard. The study began with field observation to understand the company's operational conditions and identify existing energy-related issues. The main problem identified was the absence of an ISO 50001:2018–based Energy Management System, which potentially causes inefficient energy use and higher electricity costs. Based on this problem, the research objectives were formulated to design a more efficient energy management approach. An energy audit was then conducted in an electronics manufacturing industry located in Karawang, covering a total building area of 25,552.76 m². Data were collected using documentation tools such as Microsoft Word and Microsoft Excel, supported by relevant literature as references for analysis. The collected data were used to calculate energy consumption intensity based on building area according to applicable regulatory standards. Furthermore, the audit results were analyzed to identify potential energy conservation opportunities in each room or operational area. Finally, recommendations were proposed to improve energy efficiency and support the implementation of an effective energy management system.

2.2. Energy Management System ISO5001 : 2018

A systematic and comprehensive method for using energy effectively, efficiently, and rationally without sacrificing the quantity or quality of a building's primary activities is known as energy management. Monitoring, assessing, and regulating a system's energy consumption to achieve maximum energy efficiency is the primary goal of energy management. Energy efficiency plays a crucial role in a clean energy transition of the industrial sector [9] The implementation of energy management is crucial given the recent rise in energy costs [10] . The following are some programs that can be applied in management:

1. Increase energy efficiency through audits energy
2. Collect and analyze energy usage data At the moment
3. Save energy
4. Prepare the energy sources needed in the energy budget

2.3. Electrical Energy Consumption Itensity (IKE)

The regulation issued by the Government regarding Energy Consumption Intensity (IKE) is contained in the Minister of Energy and Mineral Resources Regulation Number 13 of 2012. This regulation aims to serve as a basis for planning, monitoring, and evaluation. The ECI value is an

JURNAL ECOTIPE
Electronic, Control, Telecommunication, Information, and Power Engineering
Volume 13, Issue 1, April 2026, pp. 140-149
ISSN 2355-5068 ; e-ISSN 2622-4852
DOI: 10.33019/jurnalecotipe.v13i1.4584

indicator for measuring energy efficiency in a room. ECI parameters can be categorized into four categories, namely very efficient, efficient, fairly efficient, and wasteful, as shown in Table 2 below [11].

Table 1. Category of IKE parameters

Class	Room with AC (Kwh/m2/month)	Room Non AC (Kwh/m2/month)
Very Efficient	< 8.5	< 3.4
Efficient	8.5 - 14	3.4 – 5.6
Quite Efficient	14 – 18.5	5.6 – 7.4
Inefficient	>18.5	>7.4

Energy Consumption Intensity (IKE) to calculate Electrical Energy Consumption Intensity (IKE) is the ratio of electrical energy consumption over a certain period of time to the amount of time required. IKE is usually calculated over a period of one year using building area units. This formula can also be used to write it, in equation (1) [12]:

$$IKE = \frac{kWh}{m^2} \quad (1)$$

Information:
IKE = Energy Consumption Intensity. (kWh /m^2) .
kWh = Consumption energy (kWh).
m^2= unit of area (m^2)

2.4. Energy Saving Opportunities (PHE)

Particularly, energy saving is considered the most economical energy source since it can provide, at a cheap cost, a great reduction in CO2 emissions and save investments on infrastructures and new energy sources [13]. This implies that the potential or opportunity increases as the price of energy intensity achieved relative to the target energy intensity. The target achieved must be in accordance with the standard. Thus, the Energy Consumption Intensity analysis produces potential energy savings, which are then compared with the current applicable standard using SNI. The following calculation offers savings opportunities if the IKE value is higher than the general IKE, in equation (2) [14].

$$\text{PHE:} \frac{\Delta\, IKE \text{ x total area x tarif listrik}}{12\ bulan\ /tahun} \quad (2)$$

Information :
PHE = Energy Saving Opportunity (kWh)
Δ *IKE* = IKE value obtained – IKE value obtained targeted
kWh = Consumption energy (kWh).

PHE value is a parameter in carrying out opportunity programs. To optimize energy savings and increase electrical efficiency, we have carried out various stages of energy audits, from the most basic to in-depth analysis [15].

2.5. Power Server Application

PT. XYZ is a manufacturing industry electronics with use automation system in the process . The automation system uses computer (PC) with Power around 300W. The number of PCs used in industry manufacturing the is 447.

It used the high load on computers, the high number of operating hours, and the fluctuating energy consumption, energy-saving processes are necessary. One opportunity is the development of power server applications .

JURNAL ECOTIPE
Electronic, Control, Telecommunication, Information, and Power Engineering
Volume 13, Issue 1, April 2026, pp. 140-149
ISSN 2355-5068 ; e-ISSN 2622-4852
DOI: 10.33019/jurnalecotipe.v13i1.4584

Power Server application is designed to conserve energy when the computer is idle *during* employee breaks. The total idle time per day is 60 minutes. It works by automatically putting the computer to sleep when not in use, maximizing the potential of idle time. The following is a screenshot of the Power Server application, as shown in Figure 2.

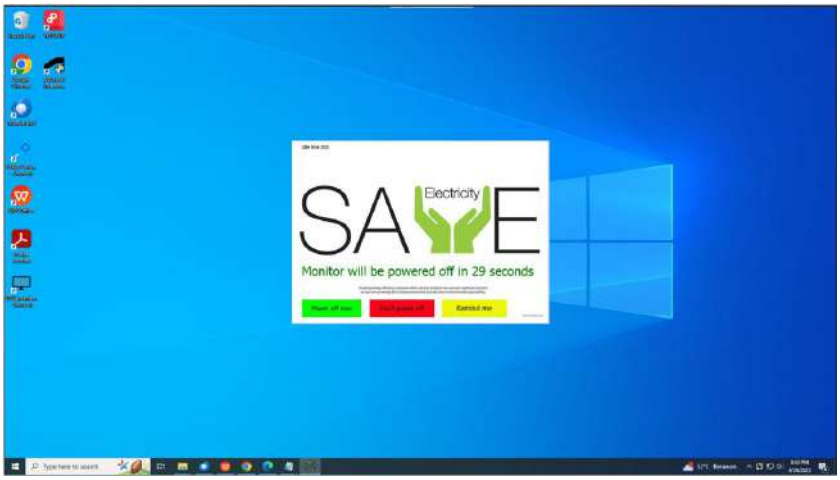

Figure 2. Power server application

The PHE calculation from the savings value using the Power Server application can be obtained from the PHE equation (2.3):

$$\text{PHE computer} = Kc1 - Kc2 \quad (3)$$

$Kc1$ = (Total power consumption in running mode)
$Kc2$ = (Total power consumption in running mode - idle power + Total power in sleep mode power mode)

3. RESULTS AND DISCUSSION

The Following is energy audit results from use PT. XYZ's load before implementing the energy audit method in table 3 .

Table 2. Energy audit

No	Rooms Name	Lenght (mm)	Widht (mm)	Area (m2)	Power Consumption (Kwh)	IKE Before	Type	Category
1	Pantry	5650	5600	31.64	5.690	3.956	AC	Very Efficient
2	Laboraturium 1	5740	5600	32.144	0.904	0.619	Non-AC	Very Efficient
3	Meeting Room 1	3775	5850	22.0838	15.297	15.239	AC	Quite Efficient
4	Meeting Room 2	3400	5850	19.89	15.306	16.930	AC	Quite Efficient
5	Customer Service Room	8750	8046	70.4025	76.141	23.793	AC	Inefficient
6	Laboraturium 2	8750	3350	29.3125	0.824	0.619	Non-AC	Very Efficient
7	Rest Room 1	8750	19200	168	20.460	2.679	AC	Very Efficient
8	Bank	4025	2180	8.7745	14.467	36.272	AC	Inefficient
9	Main Office	15250	53500	815.875	565.208	15.241	AC	Quite Efficient
No	**Rooms Name**	**Lenght**	**Widht**	**Area**	**Power**	**IKE**	**Type**	**Category**

Volume 13, Issue 1, April 2026, pp. 140-149
ISSN 2355-5068 ; e-ISSN 2622-4852
DOI: 10.33019/jurnalecotipe.v13i1.4584

		(mm)	(mm)	(m2)	Consumption (Kwh)	Before		
10	Clinic	8750	4300	37.625	16.574	9.691	AC	Efficient
11	Coating Room	8750	5814.94	50.8807	8.226	3.557	AC	Very Efficient
12	RnD Room 1	8750	5501.32	48.1366	10.522	4.809	Non-AC	Very Efficient
13	RnD Room 2	15250	6350	96.8375	36.114	8.205	AC	Very Efficient
14	Quality Control Room 1	8750	11850	103.688	133.584	28.343	AC	Inefficient
15	Part Storage Room 1	8416	8678	73.034	13.224	3.983	AC	Very Efficient
16	Workshop Room 1	13450	17200	231.34	27.026	2.570	Non-AC	Very Efficient
17	Workshop Room 2	13450	11600	156.02	10.836	1.528	Non-AC	Very Efficient
18	Part Storage Room 2	8416	23500	197.776	200.592	22.313	AC	Inefficient
19	Logistic Room 1	17450	10647	185.79	17.633	2.088	Non-AC	Very Efficient
20	Logistic Room 2	17450	6954	121.347	27.774	5.035	AC	Very Efficient
21	Logistic Room 3	8416	5703	47.9964	13.938	6.389	Non-AC	Very Efficient
22	Logistic Room 4	8416	5647	47.5252	1.337	0.619	Non-AC	Very Efficient
23	Driver Room	5812	6150	35.7438	1.005	0.619	Non-AC	Very Efficient
24	Production 1	75250	92796	6982.9	6451.496	20.326	AC	Inefficient
26	General Storage	75250	35500	2671.38	75.132	0.619	Non-AC	Very Efficient
27	Measurement Room	6700	6700	44.89	1.263	0.619	Non-AC	Very Efficient
28	Quality Control Room 2	26925	6700	180.398	152.874	18.643	AC	Inefficient
29	Part Storage Room 3	44750	119500	5347.63	2705.604	11.131	AC	Efficient
30	Meeting Room VIP 1	5250	3900	20.475	28.992	31.151	AC	Inefficient
31	Meeting Room VIP 2	5250	4550	23.8875	11.054	10.181	AC	Efficient
32	Lobby	13750	20350	235.45	64.404	6.018	AC	Very Efficient
33	Musholla	8500	3050	25.925	36.229	30.744	AC	Inefficient
34	Meeting Room VIP 3	7150	10097	72.1936	24.288	7.401	AC	Very Efficient
35	Part Storage Room 4	7150	20350	145.503	27.648	4.180	AC	Very Efficient
36	Production 2	119500	44150	5234.89	5667.686	23.819	AC	Inefficient
38	General Storage 2	5700	11700	66.69	1.876	0.619	Non-AC	Very Efficient
39	Production Storage 2	5700	11700	66.69	1.876	0.619	Non-AC	Very Efficient
40	Building Storage	5700	11700	66.69	1.876	0.619	Non-AC	Very Efficient
41	IT	14600	8750	127.75	147.047	25.323	AC	Inefficient
42	Meeting Room 3	6150	6900	42.435	33.072	17.146	AC	Quite Efficient

Volume 13, Issue 1, April 2026, pp. 140-149
ISSN 2355-5068 ; e-ISSN 2622-4852
DOI: 10.33019/jurnalecotipe.v13i1.4584

No	Rooms Name	Lenght (mm)	Widht (mm)	Area (m2)	Power Consumption (Kwh)	IKE Before	Type	Category
43	Meeting Room 4	8750	6900	60.375	33.206	12.100	AC	Efficient
44	Production Storage 1	17500	23500	411.25	11.340	0.607	Non-AC	Very Efficient
45	Hall	17450	35650	622.093	4.423	0.156	AC	Very Efficient
46	Meeting Room 5	6599	2750	18.1473	8.646	10.482	AC	Efficient
47	Meeting Room 6	6599	2750	18.1473	8.646	10.482	AC	Efficient
48	Meeting Room 7	6599	2750	18.1473	8.646	10.482	AC	Efficient
49	Meeting Room 8	6599	2698	17.8041	8.646	10.684	AC	Efficient
50	Meeting Room 9	8448	5500	46.464	8.356	3.956	AC	Very Efficient
51	Meeting Room 10	6599	5500	36.2945	4.480	2.716	AC	Very Efficient
52	Meeting Room 11	5350	11400	60.99	50.430	18.191	AC	Quite Efficient
53	Director Room	5350	5600	29.96	24.030	17.646	AC	Quite Efficient
54	Secretary Room	5350	3050	16.3175	7.146	9.635	AC	Efficient
55	Training Room 1	8900	10400	92.56	0.868	0.206	AC	Very Efficient
56	Training Room 2	8900	13100	116.59	1.093	0.206	AC	Very Efficient

Result of energy audit data collection and analysis show that there are 10 rooms with IKE value that is still categorized as wasteful so that required the existence of a savings program energy in the room.

Table 3. Sample of audit computer in CS room using power server application

No	Dept	Room Name	Type	Brand	*OS Version*	Power (W)	Time (h)	Power Consumption (Wh)	*Power Sleep Mode* (W)	*Sleep Mode* Time (h)	*Power Sleep Mode* (wh)	*Power Idle Mode* (wh)
1	CS	Ruang Customer Service	Laptop	Dell Latitude 3480	win 10	42	4	168	-	-	-	-
2	CS	Ruang Customer Service	Laptop	Dell Inspiron 3459	win 10	65	4	260	-	-	-	-
3	CS	Ruang Customer Service	Laptop	Dell Inspiron 3459	win 10	65	4	260	-	-	-	-
4	CS	Ruang Customer Service	Laptop	Lenovo Thinkpad E14	win 10	45	4	180	-	-	-	-
5	CS	Ruang Customer Service	Computer	Dell OptiPlex 3010	win 10	250	9	2250	1.77	1	1.77	250
6	CS	Ruang Customer Service	Computer	Dell OptiPlex 3070	win 11	200	9	1800	1.62	1	1.62	200
7	CS	Ruang Customer Service	Computer	Dell OptiPlex 3060	win 11	200	9	1800	1.14	1	1.14	200
8	CS	Ruang Customer Service	Computer	Dell OptiPlex 3080	win 11	200	9	1800	1.62	1	1.62	200
9	CS	Ruang Customer Service	Computer	Dell OptiPlex 3060	win 11	200	9	1800	1.14	1	1.14	200

Volume 13, Issue 1, April 2026, pp. 140-149
ISSN 2355-5068 ; e-ISSN 2622-4852
DOI: 10.33019/jurnalecotipe.v13i1.4584

No	Dept	Room Name	Type	Brand	*OS Version*	Power (W)	Time (h)	Power Consumption (Wh)	*Power Sleep Mode* (W)	*Sleep Mode* Time (h)	*Power Sleep Mode* (wh)	*Power Idle Mode* (wh)
10	CS	Ruang Customer Service	Computer	Dell OptiPlex 3080	win 11	200	9	1800	1.62	1	1.62	200
11	CS	Ruang Customer Service	Computer	Dell Optiplex 3010	win 10	250	9	2250	1.77	1	1.77	250
12	CS	Ruang Customer Service	Computer	Dell Optiplex 790	win 11	240	9	2160	2.27	1	2.27	240
13	CS	Ruang Customer Service	Computer	Dell OptiPlex 3060	win 11	200	9	1800	1.14	1	1.14	200
14	CS	Ruang Customer Service	Computer	HP 280 G1 MT	win 10	280	9	2520	1.43	1	1.43	280
15	CS	Ruang Customer Service	Laptop	Dell Latitude 3400	win 10	42	4	168	-	-	-	-
16	CS	Ruang Customer Service	Laptop	Lenovo Thinkpad x13	win 10	45	4	180	-	-	-	-
17	CS	Ruang Customer Service	Laptop	Lenovo Thinkpad E14	win 10	45	4	180	-	-	-	-
	Total					**2569**		**21376**	**15.52**		**15.52**	**2220**

Electricity savings on computer loads using the Power Server application in equation (3) resulted in CS Room savings.

$Kc1$ = 21.376 Kwh
$Kc2$ = (21.376 – 2.220 + 0.01552) Kwh
PHE computer = 21.376 – 19.171 = 2.205 Kwh

The electricity savings in the CS room is 2,205 Kwh per day, so the total savings per month is 48.51Kwh as 1 month as 22 work day. The IKE is :

IKE = 48.51 Kwh / 70.4025 m^2 = 0.689

The following are the results of energy consumption savings generated by *the power server application* in table 4.

Table 4. Energy consumption savings

No	Rooms Name	Area (m^2)	Power Consumption (Kwh)	IKE Before	IKE After	Δ IKE
1	Customer Service	70.4025	76.141	23.793	23.104	0.689
2	Laboraturium 2	29.3125	0.824	0.619	0.484	0.135
3	Bank	8.7745	14.467	36.272	35.276	0.996
4	Main Office	815.875	565.208	15.241	14.815	0.426
5	Clinic	37.625	16.574	9.691	9.441	0.250
6	RnD 1	48.13655	10.522	4.809	4.355	0.454
7	RnD 2	96.8375	36.114	8.205	7.925	0.280
8	Quality Control 1	103.6875	133.584	28.343	27.852	0.491
9	Part Storage 1	73.034048	13.224	3.983	3.789	0.195
10	Workshop 1	231.34	27.026	2.570	2.357	0.213
11	Workshop 2	156.02	10.836	1.528	1.430	0.098
12	Part Storage 2	197.776	200.592	22.313	22.156	0.157

JURNAL ECTIPE
Electronic, Control, Telecommunication, Information, and Power Engineering
Volume 13, Issue 1, April 2026, pp. 140-149
ISSN 2355-5068 ; e-ISSN 2622-4852
DOI: 10.33019/jurnalecotipe.v13i1.4584

No	Rooms Name	Area (m^2)	Power Consumption (Kwh)	IKE Before	IKE After	Δ IKE
13	Logistic 1	185.79015	17.633	2.088	1.928	0.160
14	Logistic 2	121.3473	27.774	5.035	4.803	0.232
15	Logistic 3	47.996448	13.938	6.389	5.760	0.628
16	Production 1	6982.899	6451.496	20.326	20.147	0.179
17	Quality Control 2	180.3975	152.874	18.643	18.389	0.254
18	Part Storage 3	5347.625	2705.604	11.131	11.111	0.020
19	Part Storage 4	145.5025	27.648	4.180	4.039	0.141
20	Production 2	5234.885	5667.686	23.819	23.705	0.114
21	IT	127.75	147.047	25.323	24.948	0.375
Total		**20,243.01**	**16316.814**	**274.302**	**267.815**	**6.487**

Table 5. Total Energy consumption savings

Area (m2)	Electric Rate (Rp)	Δ IKE year (kWh /m^2)	PHE (Rp)
20,243.01	1300.6	77.839	170,780,234.63

The Δ IKE year calculate is :
Δ IKE year = 6.487 x 12 months =77.839 kWh /m^2
The PHE year calculate is :
PHE = (20,243.01 x 1300.6 x 77.839)/12 = Rp. 170,780,234.63

Overall, this table shows that with a reduction in energy consumption of 77,839 kWh/m² per year in an area of 20,243.01 m², potential electricity cost savings of around Rp 170,780,234.63 per year can be achieved.

4. CONCLUSION

The Result of energy audit and optimization data collection and analysis show could saving energy that there are 21 rooms from 56 rooms with IKE value that is still categorized as that required the existence of a savings program energy in the room.

Computer load is one of the most widely used energy sources at PT. XYZ, with 447 PCs in use, necessitating an audit of the computer load usage. The Power server application is an application developed by PT. XYZ to save energy in computer use. The savings generated by this application reach 77,839 kWh/m² per year and potential electricity cost savings of around Rp 170,780,234.63 per year.

REFERENCES

[1] P. Zlateva, A. Terziev, N. Kolev, M. Ivanov, M. Murzova, and M. Vasilev, "Methods for Enhancing Energy and Resource Efficiency in Sunflower Oil Production : A Case Study from Bulgaria," *MDPI*, vol. 6, no. 195, pp. 1–20, 2025.

[2] D. Almanda and B. Kusuma, "Audit energi listrik pabrik," *Resist. (Elektronika Kendali Telekomun. Tenaga List. Komputer)*, vol. 1, no. 1, p. 25, 2018, doi: 10.24853/resistor.1.1.25-34.

[3] W. Gunawan, "Mengurangi konsumsi energi dengan audit dan manajemen energi pada ruang kendali," *J. Ind. Serv.*, vol. 4, no. 1, 2018, doi: 10.36055/jiss.v4i1.4099.

[4] P. T. Helena Hutabarat and M. Fitra Zambak, "Penghematan konsumsi energi melalui analisa ike di kampus 2 efarina pematangsiantar," *Jesce*, vol. 5, no. 1, p. 2021, 2021, [Online]. Available: http://ojs.uma.ac.id/index.php/jesce

[5] W. Gunawan, T. Zakaria, and M. A. Ridlo, "Audit energi listrik pt. niaga nusa abadi dengan

Volume 13, Issue 1, April 2026, pp. 140-149
ISSN 2355-5068 ; e-ISSN 2622-4852
DOI: 10.33019/jurnalecotipe.v13i1.4584

menggunakan metode intensitas konsumsi energi (ike) dan peluang hemat energi (phe)," *J. Intent (Jurnal Ind. dan Teknol. Terpadu)*, vol. 7, no. 1, pp. 41–49, 2024, doi: 10.47080/intent.v7i1.3533.

[6] D. Satyagraha, S. Abduh, and I. Kasim, "Manajemen energi di industri: optimasi sisi utiliti pada industri ban," *Jetri J. Ilm. Tek. Elektro*, vol. 17, no. 2, pp. 191–204, 2020, doi: 10.25105/jetri.v17i2.5362.

[7] L. Vargas-gurrola, Q. Aguilar-virgen, and S. Balderas-lópez, "PDCA-Based Methodology for the Evaluation of Energy Efficiency in the Industrial Sector," *MDPI*, vol. 15, no. 12530, pp. 1–17, 2025.

[8] M. . Catur Trimunandar', Dr. Ir Dian Retno Sawitri, M.T, Herwin Suprijono, ST, "Audit energi untuk efisiensi listrik di gedung b universitas dian nuswantoro semarang," *Techno.Com*, pp. 1–7, 2015, [Online]. Available: http://eprints.dinus.ac.id/17544/1/jurnal_16391.pdf

[9] M. Piccioni, F. Martini, C. Martini, and C. Toro, "Evaluation of Energy Performance Indicators and Energy Saving Opportunities for the Italian Rubber Manufacturing Industry," *MDPI*, vol. 17, no. 1584, pp. 1–24, 2024.

[10] R. H. Salim Nur Rohman, Z. Abidin, and M. I. Arsyad, "Energy audit of lighting system, air conditioning system and medical equipment in yarsi pontianak general hospital," *Telecommun. Comput. Electr. Eng. J.*, vol. 1, no. 2, p. 150, 2023, doi: 10.26418/telectrical.v1i2.72005.

[11] S. N. Illahi, E. Priatna, and N. Hiron, "Analisis konservasi energi pada sistem pencahayaan dan sistem pendingin di kantor sekretaris daerah kabupaten garut," *J. Energy Electr. Eng.*, vol. 1, no. 2, pp. 29–36, 2020, doi: 10.37058/jeee.v1i2.820.

[12] S. Alim, "Audit energi sistem pencahayaan dan sistem tata udara pada gedung admin pltu tanjung jati b unit 3 & 4," *J. DISPROTEK*, vol. 12, no. 2, pp. 78–84, 2022, doi: 10.34001/jdpt.v12i2.2638.

[13] G. Bruni, C. Martini, F. Martini, and M. Salvio, "On the Energy Performance and Energy Saving Potential of the Pharmaceutical Industry : A Study Based on the Italian Energy Audits," *MDPI*, vol. 11, no. 1114, pp. 1–29, 2023.

[14] F. S. Desky, S. Hardi, and M. Harahap, "Intensitas konsumsi energi listrik dan analisa peluang hemat energi pada gedung a, b Dan m di kampus universitas pembangunan panca budi," *RELE (Rekayasa Elektr. dan Energi) J. Tek. Elektro*, vol. 4, no. 2, pp. 104–108, 2022, doi: 10.30596/rele.v4i2.9532.

[15] P. K. Hanawati, B. Minto Basuki, and E. S. Wirateruna, "Audit dan rancangan implementasi manajemen energi listrik berbasis iso 50001 di gedung utsman bin affan (b) universitas islam malang," *Sci. Electro*, vol. 07, no. 07, pp. 1–6, 2023.

JURNAL ECOTIPE
Electronic, Control, Telecommunication, Information, and Power Engineering
Volume 13, Issue 1, April 2026, pp. 150-160
ISSN 2355-5068 ; e-ISSN 2622-4852
DOI: 10.33019/jurnalecotipe.v13i1.4604

Design and Development of an Android-Based Application for Employee Leave and Absence Management at the Faculty of Science and Engineering, Bangka Belitung University

Ulpa Yulita[1], Fardhan Arkan[2], Rudy Kurniawan[3]
[1,2,3] Electrical Engineering Department, Bangka Belitung University, Indonesia

ARTICLE INFO

Article historys:

Received : 28/03/2026
Revised : 10/04/2026
Accepted : 30/04/2026

Keywords:

Absence Management and Employee Leave; Android Application, Application Programming Interface; Bangka Belitung University; MySQL Database

ABSTRACT

The process of submitting leave and absence management for employees of the Faculty of Science and Engineering, Bangka Belitung University, is still carried out manually using paper forms, potentially causing delays in information, recording errors, and difficulties in data archiving. This study aims to design and implement an Android- and web-based leave and absence management application system to improve the efficiency of personnel administration. The system development method used includes the stages of needs analysis, system design, implementation, and testing. The Android application was developed using Flutter, while the web-based system uses PHP with a MySQL database and Application Programming Interface (API) integration for real-time data measurement. This system provides features for submitting leave and permits, application history, verification and approval stages by superiors, employee data management, and application status notifications. The results of functional testing indicate that most features run according to system requirements, although there is one date logic validation test that does not meet expectations. Overall, the system developed is able to improve the efficiency of the administrative process, minimize recording errors, and support more structured, transparent, and integrated personnel data management.

Corresponding Author:

Rudy Kurniawan
Electrical Engineering Department, Bangka Belitung University, Indonesia
Email: rudy14k@gmail.com

1. INTRODUCTION

Applying for leave is an official application process carried out by an employee or worker to a superior or authorized party to obtain permission to be absent from work for a certain period of time for legitimate reasons such as personal needs, health, pregnancy, family matters, worship, and for other purposes regulated in employment regulations or internal policies of an agency or company.

In general, employee leave and absence requests at the Faculty of Science and Engineering at Bangka Belitung University are still processed manually, namely by filling out paper forms and submitting them directly to superiors or the personnel department. However, this process often causes problems such as complicated and time-consuming processes, the risk of losing or damaging physical documents, a lack of transparency in application status, documentation that is not centralized and difficult to find, susceptibility to administrative errors, lack of efficiency and delays in approval, and difficulties in automatically monitoring and summarizing remaining leave. Therefore, utilizing

JURNAL ECOTIPE
Electronic, Control, Telecommunication, Information, and Power Engineering
Volume 13, Issue 1, April 2026, pp. 150-160
ISSN 2355-5068 ; e-ISSN 2622-4852
DOI: 10.33019/jurnalecotipe.v13i1.4604

technology such as Android-based applications can streamline the process of requesting leave and absence from work, making it quick, transparent, and integrated. This not only simplifies employee leave and absence requests but also assists the HR department in monitoring, recording, and reporting employee leave and absence data accurately and in real time.

Based on initial observations and literature review, several key issues were identified that prompted the development of this application. These include the manual process for submitting leave and permits, which is prone to delays and data loss. The lack of notifications makes it difficult for employees to monitor the status of applications. Furthermore, the lack of a digital system makes recapitulation and auditing inefficient. Access is also limited due to the lack of a mobile application, especially for employees outside the office. The lack of integration with the personnel system leads to data duplication and potential input errors.

2. RESEARCH METHOD

In this research, several stages and methods were used, such as: problem identification, literature study, system development methods, tools and materials used, information system design, system testing methods.

2.1. Problem Identification and Literature Study

The results of the problem identification are as follows:

1. A personnel information system is a system used to manage personnel data such as employee attendance, leave, and permits in a structured and integrated manner.
2. Leave and permit management is part of human resource management that must be effective to avoid disrupting the institution's operations. Procedures for submission, approval, and data recapitulation are crucial aspects of this system.
3. With the advancement of technology, Android application development has become a practical solution that provides easy access anytime and anywhere. Android, as an open and flexible mobile operating system, allows the integration of notification features, electronic forms, and real-time status tracking.
4. To ensure application functionality meets user requirements, black box testing is used. This testing focuses on system input and output without addressing internal code, making it ideal for testing functionality such as login, leave requests, and approval notifications.

2.2. System Development Methods

In this research, the system development method used is the Software Development Life Cycle (SDLC) with the waterfall model. This model was chosen because it has systematic, structured, and sequential stages, thus meeting the needs of academic research, which requires clear documentation at each stage of development.

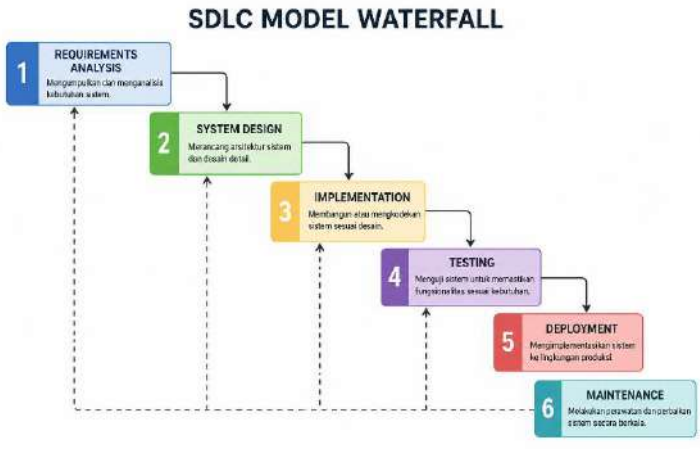

Figure 1. SDLC model waterfall

JURNAL ECOTIPE
Electronic, Control, Telecommunication, Information, and Power Engineering
Volume 13, Issue 1, April 2026, pp. 150-160
ISSN 2355-5068 ; e-ISSN 2622-4852
DOI: 10.33019/jurnalecotipe.v13i1.4604

2.3. Research Procedures

The research procedure is described using a flow diagram as shown in Figure 2.

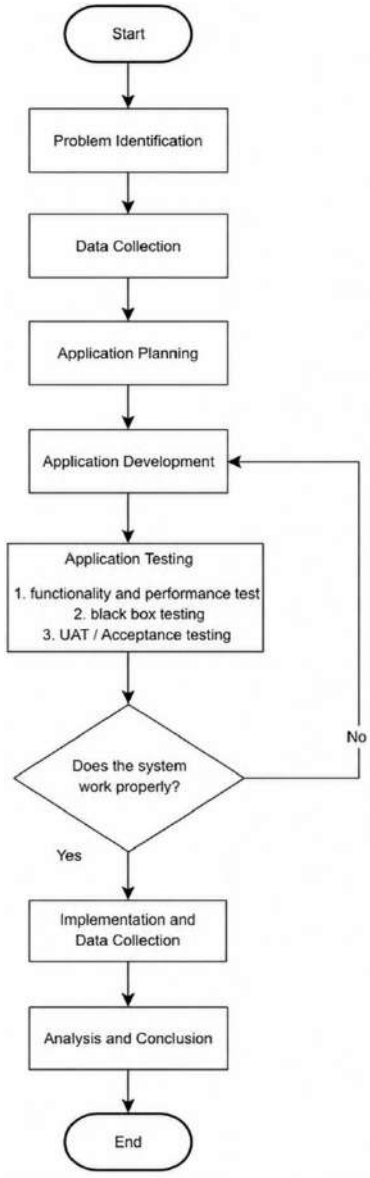

Figure 2. The research procedure

2.4. Information System Design

1. Information System Architecture

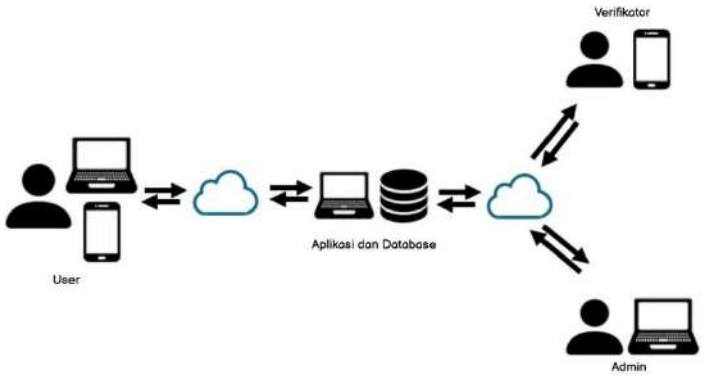

Figure 3. Employee leave and absence management application system architecture

JURNAL ECOTIPE
Electronic, Control, Telecommunication, Information, and Power Engineering
Volume 13, Issue 1, April 2026, pp. 150-160
ISSN 2355-5068 ; e-ISSN 2622-4852
DOI: 10.33019/jurnalecotipe.v13i1.4604

2. Use Case Diagram Design

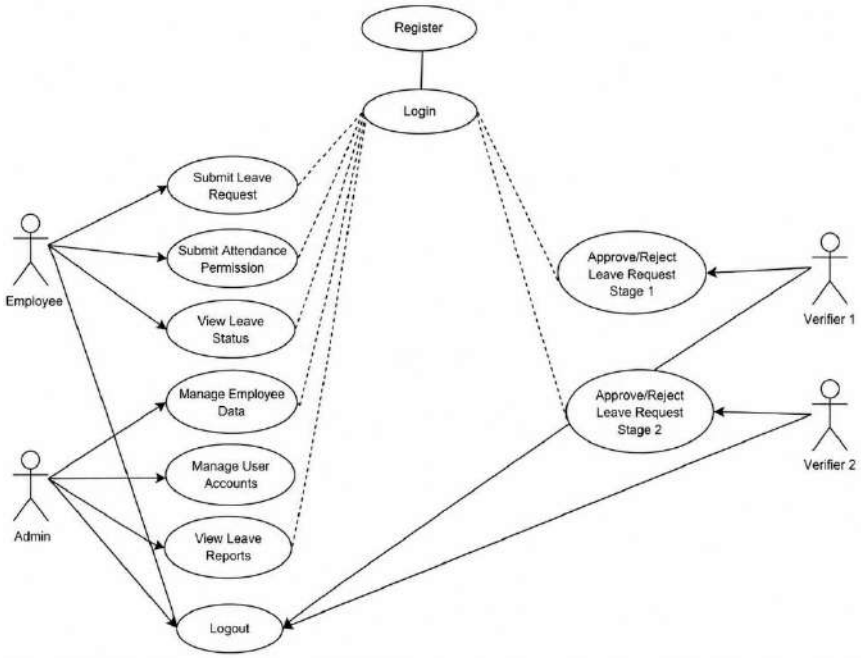

Figure 4. Use case diagram

3. Entity Relationship Diagram (ERD) Design

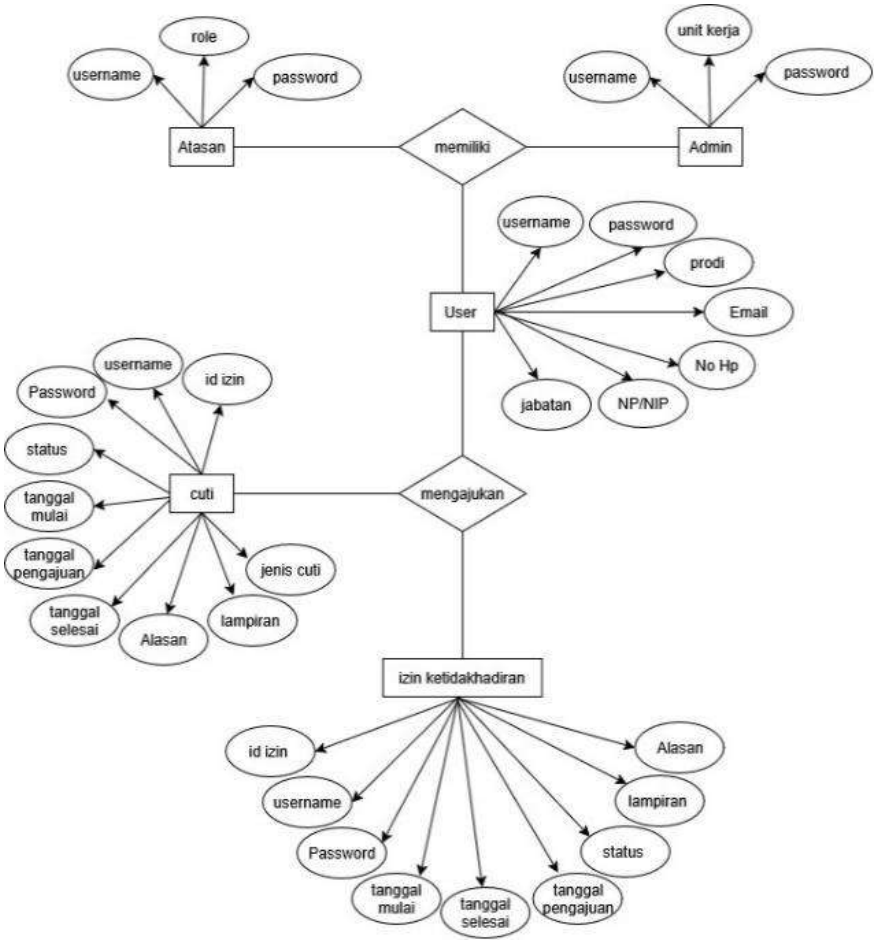

Figure 5. ERD for leave applications and employee absence permits

JURNAL ECOTIPE
Electronic, Control, Telecommunication, Information, and Power Engineering
Volume 13, Issue 1, April 2026, pp. 150-160
ISSN 2355-5068 ; e-ISSN 2622-4852
DOI: 10.33019/jurnalecotipe.v13i1.4604

4. System Database Design

The database tables in this system consist of: user table, admin table, leader table, leave table, absence permit table, and reason table. The database tables are as shown in Tables 1, 2, 3, 4, 5, and 6.

Table 1. User table

No	Field Name	Type	Keterangan
1.	Id_user (pk)	INT	Primary Key, Auto increment
2.	Username	VARCHAR (50)	unik
3.	Password	VARCHAR (100)	Terenkripsi
4.	Nama	VARCHAR (100)	
5.	Jabatan	VARCHAR (100)	
6.	prodi	VARCHAR (50)	
7.	Email	VARCHAR (50)	
8.	No_hp	VARCHAR (100)	
9.	NIP/NP	VARCHAR (15)	Nomor induk pegawai
10.	role	VARCHAR (30)	Hak akses

Table 2. Admin table

No	Field Name	Type	keterangan
1.	Id_admin(pk)	INT	PK
2.	Id_user(fk)	INT	FK ke User
3.	Unit_kerja	VARCHAR (50)	

Table 3. Leader table

No	Field Name	Type	keterangan
1.	Id_atasan(pk)	INT	PK
2.	Id_user(fk)	INT	FK ke User
3.	Jabatan	VARCHAR (50)	

Table 4. Leave table

No	Field Name	Type	Keterangan
1.	Id_cuti	INT	PK Auto increment
2.	Id_user	INT	FK ke User
3.	Tanggal_pengajuan	DATE	
4.	Tanggal_mulai	DATE	
5.	Tanggal_selesai	DATE	
6.	Jenis_cuti	VARCHAR (50)	
7.	Alasan	TEXT	
8.	lampiran	VARCHAR (255)	Path file
9.	Status	ENUM (‘diajukan’,’ disetujui’,’ditolak’)	Default diajukan

Table 5. Absence permit table

No	Field Name	Type	Keterangan
1.	Id_izin(PK)	INT	PK Auto increment
2.	Id_user(FK)	INT	FK ke User
3.	Tanggal_pengajuan	DATE	
4.	Tanggal_mulai	DATE	
5.	Tanggal_selesai	DATE	
6.	alasan	TEXT	
7.	lampiran	VARCHAR (255)	Path file
8.	status	ENUM (‘diajukan’,’disetujui’,’ ditolak’)	Default diajukan`

JURNAL ECOTIPE
Electronic, Control, Telecommunication, Information, and Power Engineering
Volume 13, Issue 1, April 2026, pp. 150-160
ISSN 2355-5068 ; e-ISSN 2622-4852
DOI: 10.33019/jurnalecotipe.v13i1.4604

Table 6. Reason table (optional if you want to separate)

No	Field Name	Type	Keterangan
1.	Id_alasan(PK)	INT	PK
2.	keterangan	TEXT	

5. Flutter Framework Design
   In developing this application, Flutter is used as a forwarder, displaying the user interface and managing user interactions. The system is designed using a client-server architecture with the following components:
   a. Client (Flutter application) : displays the user interface (UI), manages user input, sends and receives data via API.
   b. Backend (web service/API) : manages business processes, manages leave application data, connects the application to the database.
   c. Connects the application to the database : database (MySQL), stores employee data, stores leave and permit application data, stores approvals and application history.

6. Application User Interface (UI) Display Design
   This stage involves the design and planning of the application. The following is the user interface design, as follows:
   a. Employee User Interface Design; This design consists of several displays, including: login page, registration page, dashboard page, profile page, leave information page, leave status page, permit status page, leave history page, permit history page, leave application form page, permit application form page.
   b. Admin User Interface Design; This design consists of several displays, including: login page, employee list page, employee leave data page, admin profile page, leave status page, permission status page, leave history page, permission history page, leave application page, permission application page.
   c. Design of the Leadership User Interface; This design consists of several displays, including: leadership login page, dashboard view, leave application page view, leave approval page view, permit application page view, permit approval page view.

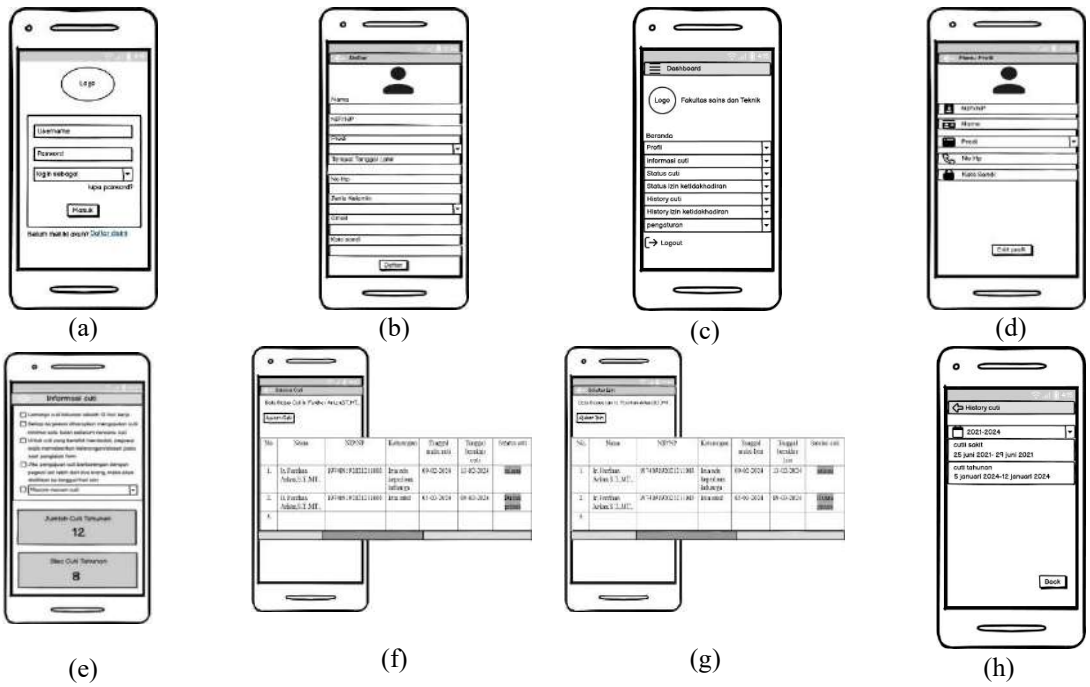

Figure 6. Employee user interface design : (a) login page, (b) registration page, (c) dashboard page, (d) profile page, (e) leave information page, (f) leave information page, (g) leave status page, (h) permit status page

JURNAL ECOTIPE
Electronic, Control, Telecommunication, Information, and Power Engineering
Volume 13, Issue 1, April 2026, pp. 150-160
ISSN 2355-5068 ; e-ISSN 2622-4852
DOI: 10.33019/jurnalecotipe.v13i1.4604

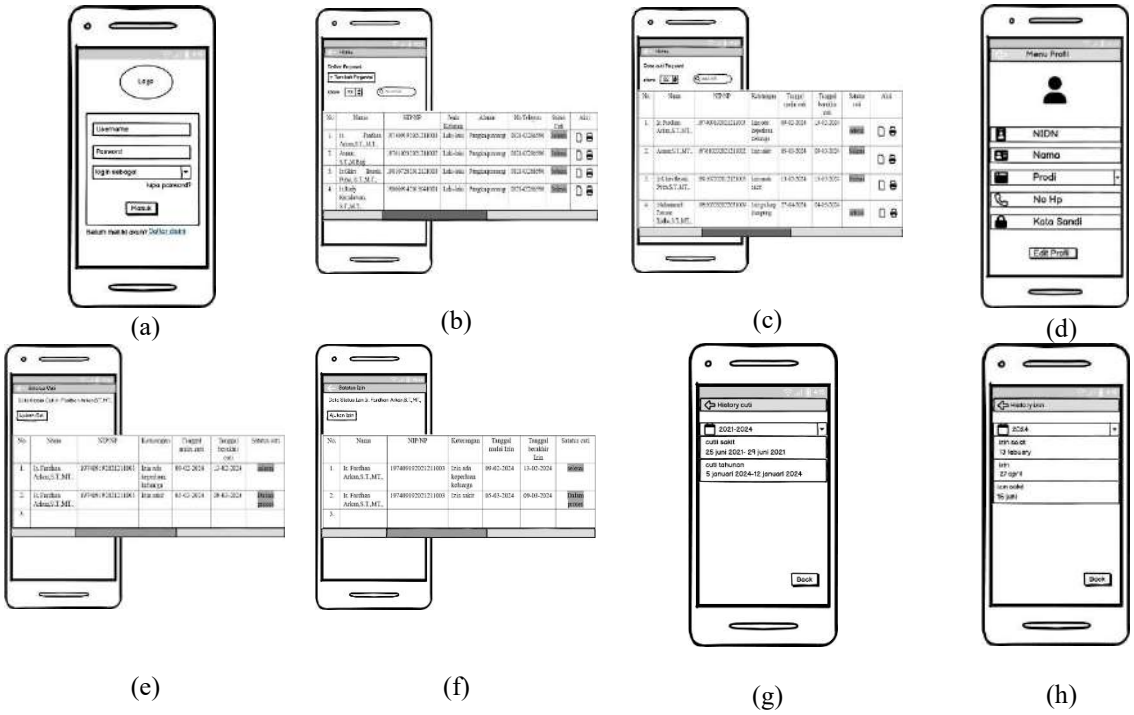

Figure 7. Admin user interface design : (a) login page, (b) employee list page, (c) employee leave data page, (d) admin profile page, (e) leave status page, (f) permission status page, (g) leave history page, (h) permission history page

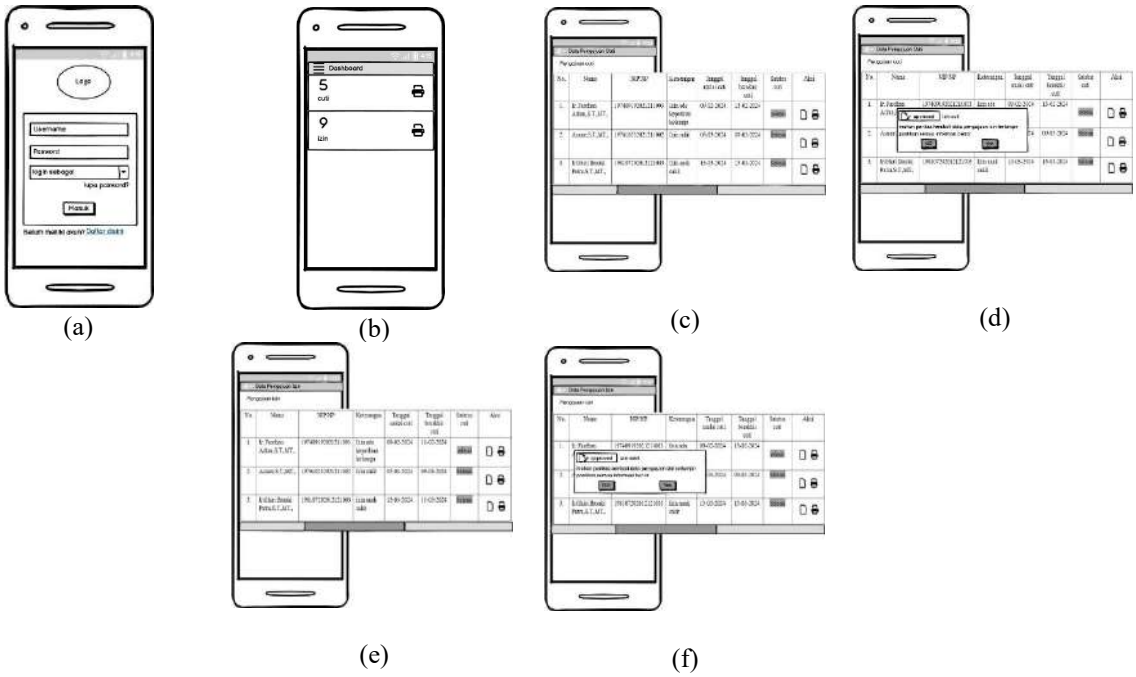

Figure 8. Design of the leadership user interface : (a) leadership login page, (b) dashboard view, (c) leave application page view, (d) leave approval page view, (e) permit application page view, (f) permit approval page view

7. User Experience (UX) Design
   UX design is carried out by paying attention to several aspects, namely:

Volume 13, Issue 1, April 2026, pp. 150-160
ISSN 2355-5068 ; e-ISSN 2622-4852
DOI: 10.33019/jurnalecotipe.v13i1.4604

a. Ease of access (Usability); the application is designed with simple navigation so that users can easily log in, apply for leave or permits, and monitor the status of applications without experiencing any difficulties.
b. Process efficiency; the application process is structured in several steps, from filling out the form to submitting the data, saving users time compared to manual systems.
c. Clarity of information (feedback system); the system provides notifications and real-time application status information so employees can know whether the application has been approved or rejected.
d. Consistency; the interface design is consistent on every page, in terms of layout, color, and action buttons, thus enhancing the app's usability.

8. Application and System Testing Methods
The testing methods in this study are divided into several stages, namely:
a. System functionality and performance testing (test each feature created)
b. System suitability testing (black box testing)
c. System User Acceptance Test (UAT)/Questionnaire

3. RESULTS AND DISCUSSION

This chapter explains several results and discussions which include: results of application implementation on the user page, results of web-based system implementation, and system testing results.

3.1. Result of Application Implementation on the User Page

In the result of application implementation on the user page, several display results are explained, such as: User Login Page, User Profile Page, User Dashboard Page, Leave Application Form Page, Permit Application Form Page, Leave Application Status and History Page, Permit Application Status and History Page. The display results of several of these pages can be seen in Figure 9.

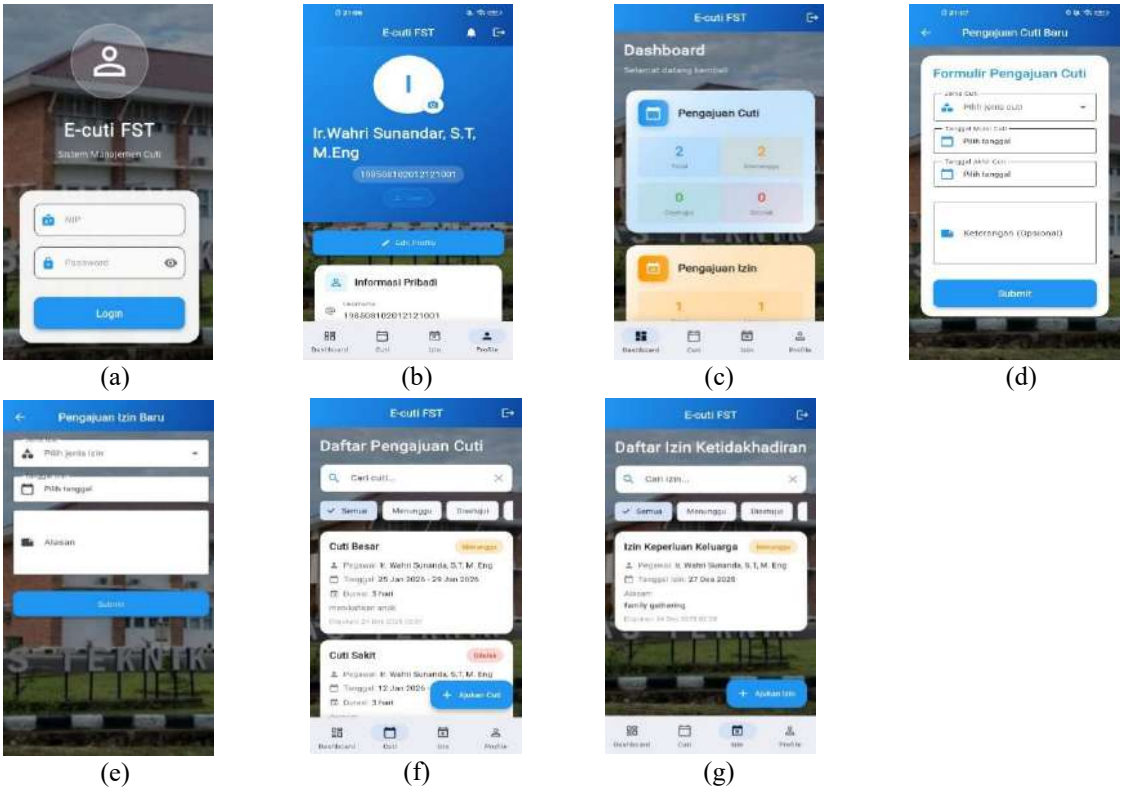

(a) (b) (c) (d)

(e) (f) (g)

Figure 9. Application implementation results on the user page: (a) user login page, (b) user profile page, (c) user dashboard page, (d) leave application form page, (e) permit application form page, (f) leave application status and history page, (g) permit application status and history page

JURNAL ECOTIPE
Electronic, Control, Telecommunication, Information, and Power Engineering
Volume 13, Issue 1, April 2026, pp. 150-160
ISSN 2355-5068 ; e-ISSN 2622-4852
DOI: 10.33019/jurnalecotipe.v13i1.4604

3.2. Results of Web-Based System Implementation

The results of the web-based system implementation show several display results, such as: Admin Login and Approval Pages, Admin and Leader Dashboard Pages, Employee Data Management Pages, Leave Approval Pages, and Absence Permit Approval Pages. The display results of these several pages can be seen in Figure 10.

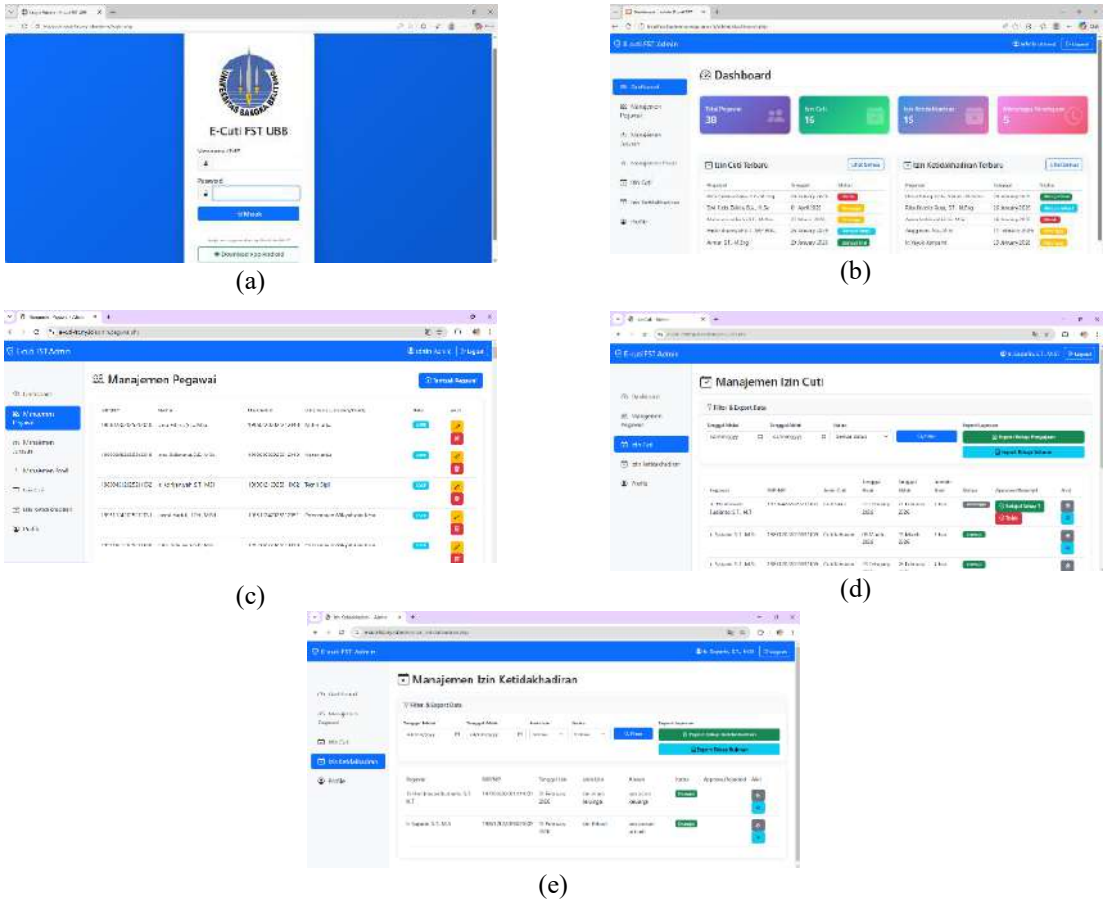

Figure 10. Application implementation results on the user page: (a) admin login and approval pages, (b) admin and leader dashboard pages, (c) employee data management pages, (d) leave approval pages, (e) absence permit approval pages

3.3. System Test Results

The system testing results show several test results, such as: System Functionality and Performance Test Results (Functionality Test Results and System Performance Test Results), Black Box Testing Results on the Application, User Acceptance Test (UAT)/Questionnaire System Test Results.

1. System Functionality and Performance Test Results

   The results of the system's functionality and performance tests showed results that met expectations and achieved a 90% success rate. Meanwhile, the system performance tests met expectations and demonstrated satisfactory application access times.

2. Black Box Testing Results

Table 7. Black Box Testing results on applications

No.	Submission scenario	Description	Results
1.	Enter the login page	Can display login page on all user levels	☑ accepted ☐ ditolak
2.	Open the home page	Can display various types of information on the home menu for each user	☑ accepted ☐ rejected
3.	Submitting a leave application	Can display the leave page and can submit leave requests based on the superior who will approve them	☑ accepted ☐ rejected

Volume 13, Issue 1, April 2026, pp. 150-160
ISSN 2355-5068 ; e-ISSN 2622-4852
DOI: 10.33019/jurnalecotipe.v13i1.4604

No.	Submission scenario	Description	Results
4.	Submitting an absence request	Can display the absence permit page for the permit application based on the superior who will be approved	☑ accepted ☐ rejected
5.	Opening the history page	Can display a summary of leave or permits that have been approved or rejected	☑ accepted ☐ rejected
6.	Approving leave	Can display the leave approval page and make approvals or rejections	☑ accepted ☐ rejected
7.	Conduct permit approval	Can display the permission approval page and make approvals or rejections	☑ accepted ☐ rejected
8.	Open the leave status page	Can display leave status approved, rejected or in process	☑ accepted ☐ rejected
9.	Open the permission status page	Can display the permit status approved, rejected or in process	☑ accepted ☐ rejected
10.	*Logout*	Can end the user session and redirect the user back to the login page so that the account cannot be re-logged in.	☑ accepted ☐ rejected

3. User Acceptance Test (UAT)/Questionnaire System Test Results

Based on the UAT/Questionnaire results by giving several questions to 22 respondents and the results of the recapitulation and calculation of the actual score and the calculation of the maximum score, the UAT results obtained a value of 93.27% which is in the very appropriate category. This indicates that the Android-based employee leave and absence application application has been very well received by users, both in terms of ease of use, interface appearance, and system functionality.

4. CONCLUSION

Based on the results of the requirements analysis, system design, Android application implementation, and testing, the following conclusions were drawn:

1. The Android-based leave and absence application can be implemented successfully and is capable of running all features, such as application, history, and approval, effectively in real time.
2. The system's functionality and performance tests yielded a 90% success rate, black box testing revealed no system failures, and the UAT/Questionnaire test, which included questions from 22 respondents, yielded a score of 93.27%, categorizing it as highly appropriate.

REFERENCES

[1] A. Kadir, “Pemrograman Android dan Database”, Elex Media Komputindo, Jakarta, 2018.

[2] Ahmad Mahdiyan and Perani Rosyani, “Rancang Bangun Aplikasi Pengajuan Cuti Karyawan Berbasis Android pada PT. Surya Toto Indonesia Tbk.”, Biner, Vol.1 No.1, pp.10-16, 2022.

[3] A. K. Ramadhani, "Rancang Bangun Aplikasi Android Absensi dan Manajemen Penugasan Karyawan Berbasis React Native (Studi Kasus: PT. Queen Network Nusantara)." (2023).

[4] H. H. Muzakkir and B. A, Herlambang “Rancang Bangun Aplikasi E-cuti Berbasis *Web* di CV. Sumber Bahagia CTCP”, Proceeding Science and Engineering National Seminar, vol. 7, no. 1. 2022.

[5] I. Ulumudin, N. M. Faizah, and W. Nurcahyo. "Aplikasi Sistem Presensi Pegawai PT. Berkah Pena Ilmu dengan Metode Location Based Service (LBS) Berbasis Android Menggunakan Firebase." *Design Journal* 1, no. 1 (2023): 89-98.

[6] K. Pamungkas, S. Tri, and R. A. Muhammad. "Rancang Bangun Sistem Presensi Berbasis Web-Mobile Menggunakan Metode Prototype (Studi Kasus: Klinik Pratama Dokter Yanti)." PhD diss., Universitas Jambi, 2025.

[7] M. Arijal and I. Hermawan. "Rancang Bangun Sistem Pengajuan Cuti dan Izin Berbasis Website Studi Kasus Unit Kepegawaian PT. XYZ." *MULTINETICS* 7, no. 1 (2021): 92-103.

Volume 13, Issue 1, April 2026, pp. 150-160
ISSN 2355-5068 ; e-ISSN 2622-4852
DOI: 10.33019/jurnalecotipe.v13i1.4604

[8] R. Kurniawan and F. Arkan, “Rancang Bangun Sistem Akreditasi Program Studi Teknik Elektro Universitas Bangka Belitung”, *JurnalEcotipe*, vol. 3, no. 2, pp. 31–39, Oct. 2016

[9] R. Kurniawan, T. H. Budianto, and W. Yandi, “Rancang Bangun Aplikasi Presensi Dosen dan Mahasiswa Berbasis Android dan Cloud Server”, *JurnalEcotipe*, vol. 9, no. 1, pp. 96–101, Apr. 2022, doi: 10.33019/jurnalecotipe.v9i1.2971.

[10] R. Kurniawan, M. Y. Puriza, and F. Arkan. "Membangun Sistem Informasi Desa Untuk Pelayanan Publik Prima Berbasis Cloud Server Di Desa Pagarawan Kabupaten Bangka." *Panrita Abdi-Jurnal Pengabdian pada Masyarakat* 5, no. 2 (2021): 193-200.

[11] N.M. Aznawi, S. D. Fachroza, and D. J. Ritonga. "Penerapan Waterfall SDLC pada Perancangan Sistem Pengelolaan Izin Keluar Kantor di KanReg VI BKN Medan." *Journal of Software Engineering and Information System (SEIS)* (2026): 1-7.

[12] T. Kurniawan, "Implementasi Firebase Dalam Pengembangan Platform Sewa Sarana Olahraga Berbasis Android." *Universitas Islam Negeri Sumatera Utara* (2021).

Volume 13, Issue 1, April 2026
ISSN 2355-5068
e-ISSN 2622-4852

Publisher Address :

Electrical Engineering Department
Faculty of Science and Engineering - Bangka Belitung University
Balunijuk, Kab. Bangka, Prov. Kep. Bangka Belitung
University Phone : (0717) 422145, 422965 Fax. (0717) 421303
Faculty Phone : (0717) 4260033 ext. 2122, 2124
Website : https://ecotipe.ubb.ac.id/index.php/ecotipe
E-mail : jurnalecotipe@ubb.ac.id / jurnal.ecotipe@yahoo.com